

**THE UNIVERSITY OF MANCHESTER - APPROVED ELECTRONICALLY
GENERATED THESIS/DISSERTATION COVER-PAGE**

Electronic identifier: 15500

Date of electronic submission: 26/06/2015

The University of Manchester makes unrestricted examined electronic theses and dissertations freely available for download and reading online via Manchester eScholar at <http://www.manchester.ac.uk/escholar>.

This print version of my thesis/dissertation is a TRUE and ACCURATE REPRESENTATION of the electronic version submitted to the University of Manchester's institutional repository, Manchester eScholar.

A molecular pentafoil knot and related circular helicates

A thesis submitted to the University of Manchester for the degree of Doctor of
Philosophy

In the faculty of Engineering and Physical Sciences

2015

Jean-François Ayme

School of Chemistry

Contents

Abstract.....	7
Declaration and copyright statement.....	8
Acknowledgements.....	9
Abbreviations.....	10
Chapter I: "Template synthesis of molecular knots".....	12
1.1. Synopsis.....	13
1.2. Introduction.....	14
1.3. Knots in biopolymers.....	15
1.3.1. Naturally occurring molecular knots.....	15
1.3.2. Synthetic knots constructed from biopolymers.....	16
1.4. Knots in synthetic polymers.....	18
1.5. Template routes to molecular knots.....	19
1.5.1. Generating crossing points with linear metal helicates.....	20
1.5.2. Applications and limitations of the linear metal helicate approach.....	26
1.5.3. Generating crossing points through hydrogen bond motifs.....	28
1.5.4. Trefoil knots assembled about a single metal ion template.....	30
1.5.5. Active template synthesis of a trefoil knot.....	31
1.5.1. Other synthetic strategies to molecular trefoil knots and related structures.....	32
1.5.2. Reversible covalent bond formation as a means of 'error-checking' during synthesis.....	37
1.5.3. Routes, and potential routes, to higher molecular knots: cyclic helicates and grids.....	39
1.6. Recent updates.....	43
1.7. Conclusions.....	44
1.8. Notes and references.....	45
Chapter II: "A synthetic molecular pentafoil knot".....	50
2.1. Synopsis.....	51
2.2. Introduction.....	52
2.3. Results and discussion.....	54
2.4. Conclusion.....	62
2.5. Experimental Section.....	63
2.5.1. Synthesis.....	63
2.5.1.1. Synthesis of dialdehyde 1.....	63
2.5.1.2. Synthesis of bis(imino) ligands S8 and S9.....	71
2.5.1.3. Synthesis of cyclic helicates.....	73
2.5.1.4. Discussion of stereochemistry assignment of helicate [3g]Cl(PF ₆) ₉	85
2.5.2. Knot assembly process: additional data.....	88
2.5.2.1. Monitoring of crude reaction mixture of [6](Cl) ¹⁰⁺	88
2.5.2.2. Effect of reaction stoichiometry on knot yield.....	89
2.5.3. X-Ray crystal structure of [6]Cl(PF ₆) ₉ ·xSolvent.....	90
2.5.3.1. Experimental details.....	90
2.5.3.2. Additional X-ray structure pictures.....	91
2.5.3.3. Crystal packing diagrams.....	92
2.5.4. Comparison with Lehn's cyclic helicate.....	93
2.6. Notes and References.....	94

Chapter III: "Pentameric Circular Iron(II) Double Helicates and a Molecular Pentafoil Knot"	97
3.1. Synopsis	98
3.2. Introduction	99
3.3. Cyclic Helicates and Their Potential for Molecular Knot Synthesis	100
3.4. Results and Discussion	101
3.5. Structural Requirements for Pentameric Cyclic Helicate Assembly	104
3.6. Probing the Reaction Conditions of Pentameric Cyclic Helicate Assembly	106
3.6.1. Reactant Stoichiometry	107
3.6.2. Influence of Anions	108
3.6.3. Role of Chloride Ions	109
3.6.4. Solvent and Concentration	111
3.6.5. Rate of Pentameric Circular Helicate Formation	112
3.6.6. X-ray Crystal Structure of Pentameric Cyclic Helicate [3bCl](PF ₆) ₉	113
3.7. Controlling the Helix Stereochemistry of Pentameric Cyclic Helicates	115
3.8. Assembly of a Molecular Pentafoil Knot	118
3.9. Conclusion	123
3.10. Experimental section	125
3.10.1. Synthesis	125
3.10.1.1. Synthesis of dialdehyde 1	125
3.10.1.2. Synthesis of bis(imino) ligands S8 and 4	125
3.10.1.3. General synthesis of pentameric circular helicates	126
3.10.1.4. Synthesis of circular helicates	126
¹ HNMR (CD ₃ CN, 500 MHz) of circular helicates	129
3.10.2. Formation of linear triple helicate [Fe ₃ (S8) ₃](PF ₆) ₆	139
3.10.3. Failed synthesis of circular helicates with various amines	142
3.10.4. Monitoring reaction kinetics	143
3.10.4.1. Formation of circular helicate ([3hCl]Cl ₉) from dialdehyde 1 and hexylamine (2h)	143
3.10.4.2. Formation of circular helicate ([3hCl]Cl ₉) from pre-formed ligand 4	144
3.10.4.3. Formation of pentafoil knot ([7Cl]Cl ₉) from dialdehyde 1 and diamine 6	145
3.10.5. Reaction stoichiometry	146
3.10.5.1. Effect of Fe(II):dialdehyde/amine ratio on hexylamine pentameric circular helicate (3h) yield	146
3.10.5.2. Effect of amine:dialdehyde/Fe(II) ratio on hexylamine circular pentameric helicate (3h) yield	147
3.10.5.3. Effect of diamine:dialdehyde/Fe(II) ratio on pentafoil knot [7Cl](PF ₆) ₉ yield	148
3.10.5.4. Effect of Fe(II):diamine/dialdehyde ratio on pentafoil knot [7Cl](PF ₆) ₉ yield	149
3.10.5.5. Effect of diamine (6):FeCl ₂ ratio on pentafoil knot [7Cl](PF ₆) ₉ yield	150
3.10.5.6. Effect of chloride on the yield of pentameric cyclic helicate [3hCl](PF ₆) ₉ and pentafoil knot [7Cl](PF ₆) ₉	152
3.10.6. Diastereoselective pentameric circular helicates	155
3.10.6.1. Synthesis of diastereoselective pentameric circular helicate [R/S-3jCl](PF ₆) ₉	155
3.10.6.2. Synthesis of diastereoisomers of pentameric circular helicate [(R)-3kCl](PF ₆) ₉	157

3.10.6.3. Discussion of stereochemistry assignment of pentameric circular helicate R-[3j]Cl(PF ₆) ₉ , S-[3j]Cl(PF ₆) ₉ and the major diastereoisomer of R-[3k]Cl(PF ₆) ₉	159
3.10.7. X-ray crystal structure experimental	160
3.10.7.1. X-Ray crystal structure of [3bCl](PF ₆) ₉ ·xSolvent	160
3.10.7.2. X-Ray crystal structure of [7Cl](PF ₆) ₉ ·xSolvent	164
3.11. Notes and references.....	165
Chapter IV: "The Self-Sorting Behavior of Circular Helicates and Molecular Knots and Links"	
.....	172
4.1. Synopsis.....	173
4.2. Introduction	174
4.3. Results and Discussion	175
4.4. Conclusion.....	183
4.5. Experimental section	184
4.5.1. Open Systems	184
4.5.1.1. Experimental Procedure for the Self-Sorting of Cyclic Helicates 4 and 5.....	184
4.5.1.2. Experimental Procedure to Determine the Effects of Mixing on the Relative Yields of Cyclic Helicates 4 and 5	185
4.5.1.3. Experimental Procedure to Determine the Effects of Concentration on the Self-Sorting of Helicates 4 and 5	187
4.5.1.4. Thermodynamic Investigations of the Self-Sorting of Helicates 4 and 5	189
4.5.1.5. Experimental Procedure for the Thermodynamic Investigations of the Self-Sorting of Helicates 4 and 5	190
4.5.2. Closed Systems	193
4.5.2.1. Experimental Procedure for the Self-Sorting of Solomon Link 7 and Pentafoil Knot 8.....	193
4.5.2.2. Experimental Procedure to Determine the Effects of Mixing on the Relative Yields of Solomon Link 7 and Pentafoil Knot 8	197
4.5.2.3. Experimental Procedure to Determine the Effects of Concentration on the Self-Sorting of Closed Topologies 7, 8 9 and 10.....	199
4.5.2.4. Experimental Procedure For the Thermodynamic Investigations of the Self-Sorting of Closed Topologies 7, 8, 9 and 10.....	202
4.6. Notes and references.....	204
Chapter V: "Probing the Dynamics of Pentameric Circular Helicates and Pentafoil Knots" .	208
5.1. Synopsis.....	209
5.2. Introduction	210
5.3. Results and Discussion	210
5.4. Conclusion.....	221
5.5. Experimental Section	223
5.5.1. Amine Exchange on Pentameric Circular Helicates	223
5.5.1.1. Experimental Procedure for the Thermodynamic Investigations of Amine Scrambling.....	223
5.5.1.2. ¹ HNMR Analysis for the Thermodynamic Investigations of Amine Scrambling	225
5.5.2. Aldehyde Exchange on Pentameric Circular Helicate 2	226
5.5.2.1. Synthesis of labeled aldehyde 1-D ₈	226
5.5.2.2. Experimental Procedure for the Synthesis of Helicate 2-D ₄₀	227
5.5.2.3. Experimental Procedure for the Thermodynamic Investigations of Aldehyde Scrambling on Helicates 2 and 2-D ₄₀	229

5.5.3. Aldehyde Exchange on Pentafoil Knot 6.....	231
5.5.3.1. Experimental Procedure for the Synthesis of Pentafoil Knot 6-D ₄₀	231
5.1.1.1. Experimental Procedure for the Thermodynamic Investigations of Aldehyde Scrambling on Pentafoil Knots 6 and 6-D ₄₀	232
5.6. Notes and References	235
Chapter VI: "Strong and Selective Anion Binding within the Central Cavity of Molecular Knots and Links"	238
6.1. Synopsis.....	239
6.2. Introduction	240
6.3. Results and Discussion	241
6.4. Conclusion.....	247
6.5. Experimental Section	248
6.5.1. Synthetic Procedures and Characterization Data	248
6.5.1.1. Solomon link [1](PF ₆) ₈	248
6.5.1.2. Pentafoil knot [2•Cl](PF ₆) ₉	249
6.5.1.3. Pentafoil knot [2](PF ₆) ₁₀	250
6.5.1.4. Star of David catenane [3](PF ₆) ₁₂	252
6.5.1.5. Calix[4]bipyrrole S1	253
6.5.2. Derivation of the expressions used to determine K ₁	254
6.5.2.1. Derivation of the equation for competitive binding studies of pentafoil knot [2] for Cl ⁻ using AgPF ₆	254
6.5.2.2. Derivation of the fraction of occupied host as a function of total guest concentration via ¹ H NMR integrals in the case of the 1:1 binding at [2] + I ⁻ in slow exchange	256
6.5.2.3. Derivation of the fraction of occupied host as a function of total guest concentration via NMR chemical shift in the case of a 1:1 binding event in fast exchange	257
6.5.3. Binding studies.....	258
6.5.3.1. Solomon link [1](PF ₆) ₈	258
6.5.3.2. Pentafoil knot [2](PF ₆) ₁₀	266
6.5.3.3. Star of David catenane [3](PF ₆) ₁₂	274
6.6. Notes and References	282
Outlook	287

Abstract

A molecular pentafoil knot and related circular helicates

A thesis submitted to the University of Manchester for the degree of Doctor of Philosophy
In the faculty of Engineering and Physical Sciences

Jean-François Ayme
School of Chemistry
University of Manchester

2015

Knots are being discovered with increasing frequency in both biological and synthetic macromolecules and have been fundamental topological targets for chemical synthesis for the past two decades. However, only few synthetic molecular knots have been prepared to date and their properties remain largely unexplored. This thesis reports the synthesis of the most complex non-DNA molecular knot prepared to date: the self-assembly of five bis-aldehyde and five bis-amine building blocks around five metal cations and one chloride anion forms a 160-atom-loop molecular pentafoil knot (five crossing points).

Chapter I aims to give the reader an overview of the current state of research in the field of template synthesis of molecular knots.

Chapter II reports the synthesis and full characterisation of the most complex non-DNA molecular knot prepared to date, a pentafoil knot.

Chapter III describes the synthesis of eleven pentameric cyclic double helicates derived from the scaffold of a pentafoil knot and presents an extensive study of the factors influencing the assembly process.

Chapter IV reports the study of the self-sorting behaviour of a molecular Solomon link and a molecular pentafoil knot and their related non-interlocked systems.

Chapter V the dynamic nature of pentameric circular helicates and a pentafoil knot is investigated, bringing insights on the subtle balance of thermodynamic and kinetic parameters involved in their self-assembly process.

Chapter VI describes the halide binding properties of a synthetic molecular knot and doubly- and triply-entwined [2]catenanes based on circular Fe(II)-double-helicate scaffolds.

Declaration and copyright statement

Unless otherwise stated at the beginning of each chapter, the work referred to in the thesis has not been submitted in support of an application for another degree or qualification of this or any other university or other institute of learning.

- i. The author of this thesis (including any appendices and/or schedules to this thesis) owns certain copyright or related rights in it (the “Copyright”) and he has given The University of Manchester certain rights to use such Copyright, including for administrative purposes.
- ii. Copies of this thesis, either in full or in extracts and whether in hard or electronic copy, may be made only in accordance with the Copyright, Designs and Patents Act 1988 (as amended) and regulations issued under it or, where appropriate, in accordance with licensing agreements which the University has from time to time. This page must form part of any such copies made.
- iii. The ownership of certain Copyright, patents, designs, trademarks and other intellectual property (the “Intellectual Property”) and any reproductions of copyright works in the thesis, for example graphs and tables (“Reproductions”), which may be described in this thesis, may not be owned by the author and may be owned by third parties. Such Intellectual Property and Reproductions cannot and must not be made available for use without the prior written permission of the owner(s) of the relevant Intellectual Property and/or Reproductions.
- iv. Further information on the conditions under which disclosure, publication and commercialisation of this thesis, the Copyright and any Intellectual Property and/or Reproductions described in it may take place is available in the University IP Policy (see <http://documents.manchester.ac.uk/DocuInfo.aspx?DocID=487>), in any relevant Thesis restriction declarations deposited in the University Library, The University Library’s regulations (see <http://www.manchester.ac.uk/library/aboutus/regulations>) and in The University’s policy on Presentation of Theses.

Acknowledgements

Firstly, I would like to thank Dave for giving me the opportunity to work within his group for the last five years. It has been a great experience.

I would like to thank everyone in the Leigh's group (past and present) for their help, advice, support and tolerance over the past several years.

This thesis could not have been completed without the guidance and help of Jon, Chris, Gus and Guzmann.

Thanks to Sau Yin and Valerie for making the laboratory run so smoothly.

Finally, I couldn't have completed this PhD without the support of my wife, friends and family.

Jean-François

Abbreviations

aq.	aqueous
BINAP	(2,2'-bis(diphenylphosphino)-1,1'-binaphthyl)
bpy	bipyridine
calcd.	calculated
CD	circular dichroism
CuAAC	copper(I)-catalysed azide alkyne cycloaddition
Da	Dalton
DCM	Dichloromethane
dec.	decomposition
DNA	desoxyribonucleic acid
δ	chemical shift
COSY	correlation spectroscopy
CSD	Cambridge Structural Database
equiv., eq.	equivalents
ESI	electrospray ionisation
Et₂O	diethylether
Et₃N	triethylamine
equiv.	equivalent
EtOAc	ethyl acetate
EtOH	ethanol
DMF	N,N'-dimethylformamide
DMSO	Dimethylsulfoxide
HPLC	high performance liquid chromatography
HRMS	high resolution mass spectrometry
Hz, MHz	Hertz, megahertz
LRMS	low resolution mass spectrometry
m/z	mass-to-charge ratio
m.p.	melting point
MeCN	acetonitrile
MeOH	methanol
min	minutes
MLCT	metal to ligand charge transfert
MS	mass spectrometry
NMR	nuclear magnetic resonance
ppm	part per million
RCM	ring closing metathesis
RNA	ribonucleic acid
ROSEY	rotating-frame nuclear Overhauser effect correlation spectroscopy

RT, r.t.	room temperature
satd.	saturated
TBA, Bu₄N	butylammonium
tBu	tetrabutyl
THF	tetrahydrofuran
TLC	thin layer chromatography
tpy	terpyridine
UV	ultraviolet (light)

Chapter I: “Template synthesis of molecular knots”

Published as "Template synthesis of molecular knots", J.-F. Ayme, J. E. Beves, C. J. Campbell and D. A. Leigh, Chem. Soc. Rev., **2013**, 42, 1700-1712.

Acknowledgements

The presented work was a joint effort between the authors.

1.1. Synopsis

This chapter aims to give the reader an overview of the current state of research in the field of template synthesis of molecular knots. After a short historical background on the origin of knots in science, the scope of this chapter is narrowed to the study of the diversity and properties of knots in biological and man-made systems, before focusing on an exhaustive review of the different template strategies that chemists have employed to synthesise knotted molecular topologies. Metal ion coordination, hydrogen bonding and aromatic donor–acceptor interactions have all been used to direct the formation of well-defined crossing points for molecular strands. Along these template synthesis strategies, advances in the methods used to covalently capture the interwoven structures are highlighted, including the active metal template strategy in which metal ions both organise crossing points and catalyse the bond forming reactions that close the loop to form the topologically complex product. Although most non-trivial knots prepared to date from small-molecule building blocks have been trefoil knots, the synthesis of the most complex knot to date, the first pentafoil knot is included in this chapter. Finally, recent updates and possible future directions and strategies in the rapidly evolving area of chemical topology are discussed.

1.2. Introduction

When Werner proposed the structural basis of coordination complexes at the end of the 19th century,¹ he surely could not have foreseen the tremendous impact and influence they would have on other, apparently disparate, areas of chemistry. A dramatic example is the now widespread use of the well-defined geometries of metal ions as templates for the rational synthesis of macrocycles, cavitands, cages, knots and links.^{2,3} Unfortunately Werner did not live to see the impact of his work on chemical topology; the first synthesis of a catenane utilising a metal template was not published until 64 years after his death.⁴ However, he may well have been aware of the field's origins. During Werner's youth a series of papers⁵ was published by the Edinburgh chemist and mathematician Peter Guthrie Tait, who inspired by Lord Kelvin's flawed theory that atoms might be knotted vortices in the aether,⁶ set about characterising and tabulating the different knots that could be formed within a closed loop. He classified the knots by their crossing number, later including an additional identifier, the order of the knot.⁷ In collaboration with Kirkman, all prime knots⁸ up to and including those with a crossing number of ten were tabulated and, somewhat remarkably, drawn out by hand⁹ (for an extract of one of these tables see Figure 1).¹⁰ Tait was also aware of many of the properties that prime knots possess. For example, each has a non-superimposable mirror image, although they are not all chiral as some knots are able to be deformed into their mirror image. Tait termed such knots ‘amphichiral’ (for example, knot 4A in Figure 1). Subsequently Tait applied a similar analysis to links,¹¹ which are interlocked structures featuring two or more closed loops.

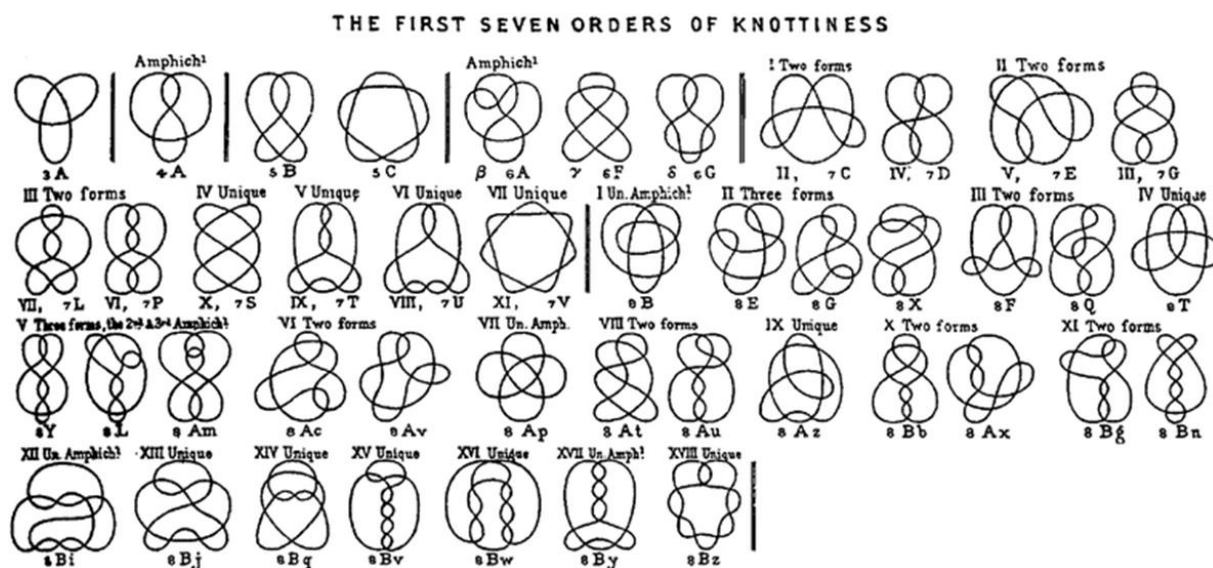


Figure 1. Extract from Tait's table of ‘The first seven orders of knottiness’. Prime knots with up to eight crossing points are shown, knots marked with ‘two/three forms’ are topologically identical but are represented in different ways. Reproduced by permission of the Royal Society of Edinburgh from *Transactions of the Royal Society of Edinburgh* volume 32 (1883–1884), pp. 327–342.

Knot theory has subsequently become a well-established branch of mathematics, with over six billion prime knots tabulated thus far.¹² Even today, however, the knots depicted in Tait's tables represent extraordinarily ambitious targets for synthetic chemistry, requiring the development of increasingly sophisticated strategies and tactics² for their efficient assembly.

1.3. Knots in biopolymers

1.3.1. Naturally occurring molecular knots

Molecular knots are found throughout biology. Catenated DNA superstructures were first isolated in 1967 from the mitochondria of HeLa cells¹³ and human leukaemic leucocytes.¹⁴ The molecules were imaged using electron microscopy, showing

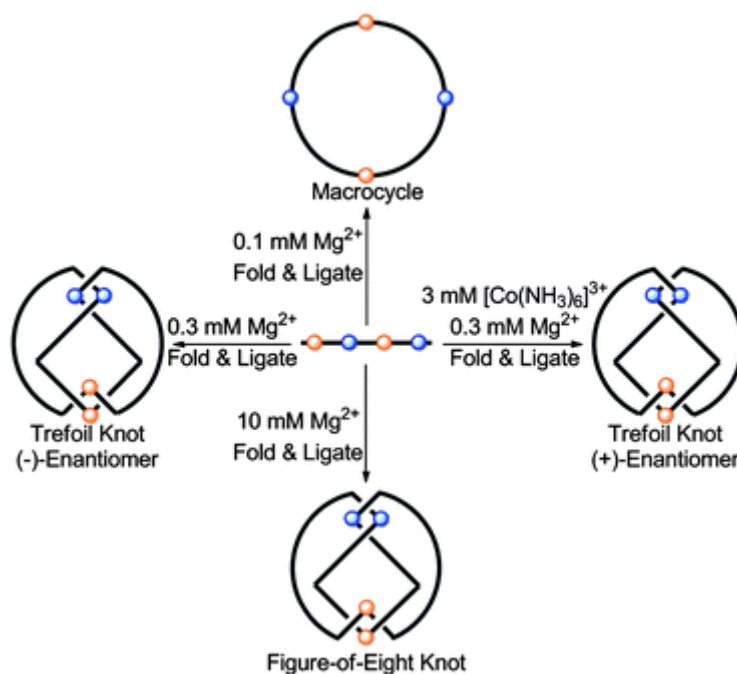
unambiguously the interwoven nature of the biopolymers. Numerous knotted DNA structures have since been identified, ranging from simple trefoil knots to complex higher order and composite knots.¹⁵ DNA topoisomerases are responsible for the formation of these structures as they control the coiling and entwinement of the double helical backbone.¹⁶

Entwined and threaded structures have also been found within proteins.^{17,18} These are best classified as ‘open knots’ as the end groups are not connected to form a closed loop. A number of remarkable examples have been identified in which the knotted section is deeply embedded¹⁹ within the overall structure of the protein. Despite it not being clear exactly why or how these entangled structures are formed, their presence—often in close proximity to an active site—can have significant effects, possibly as a result of the rigidity and chirality of the knotted section of the protein backbone.¹⁷

1.3.2. Synthetic knots constructed from biopolymers

Knots have also been introduced into synthetic biopolymers.^{20–27} Seeman pioneered the synthesis of complex molecular topologies based on single-stranded DNA.²⁰ DNA sequences can be designed that fold in a prescribed manner, generating well-defined crossing points. Subsequent ligation can join the ends of strands to generate closed-loop knotted macromolecules. Under certain conditions (high ionic strength or the presence of cationic effectors) the helicity of particular DNA sequences can be inverted, which is required for the synthesis of knots with differing +/- crossings.²¹ In this way Seeman was able to synthesise the first two prime knots (namely the trefoil (3^1) and figure-of-eight (4^1) knots).²⁰ In a carefully constructed experiment, a single strand of DNA was prepared that was able to cyclise under different conditions to form either a macrocycle (topologically an

‘unknot’), a trefoil knot (either enantiomer) or a figure-of-eight knot (Scheme 1).²² This strategy was subsequently extended to prepare Borromean rings,²³ Solomon links (a doubly-interlocked [2]catenane)²⁴ and the 5_2 and 7_4 prime knots.²⁵



Scheme 1. A single strand of DNA with complementary base pairing regions highlighted in orange and green. Depending on the conditions the molecule can fold to give different numbers of crossing points and handedness. Ligation connects the ends of the strand generating the entwined closed loop.²²

Remarkably, a trefoil knot analogous to that shown in Scheme 1 has also been synthesised using single stranded RNA,²⁶ a far more challenging undertaking as a result of its instability relative to DNA and the lack of suitable ligation enzymes necessary to connect the ends of the strand together.

Yeates and co-workers have recently designed a protein that undergoes folding into an open trefoil knot.²⁷ Their strategy involved connecting the two components of an entwined, but unknotted, protein homodimer, resulting in a single chain knotted topology. X-Ray

crystallography confirmed the interlocked nature of the protein backbone. Folding was found to be reversible but twenty times slower than for a similar unknotted control protein.²⁷

1.4. Knots in synthetic polymers

Knots are known to form spontaneously in the backbones of long flexible polymer chains as they are synthesised.²⁸ The probability of knot formation is influenced by a number of characteristics of the polymer, most importantly its length and stiffness.^{29,30} Studies indicate that these factors can also influence the complexity of the knots formed.^{29,31} Work in this area has usually first been predicted computationally and then later confirmed by experimental work.

The presence of knots within polymer backbones can be detrimental to polymer stability. In 1999 Wasserman carried out calculations that showed that the strain induced in a polymer strand upon knotting is localised at the entrance to the knot (Figure 2).³² This was confirmed experimentally later that year. Optical tweezers were used to tie simple open knots in the backbones of strands of DNA or actin, strain could then be induced by applying a force to either end of the biopolymers.³³ When the more rigid actin molecule was knotted and pulled, the strand was observed to break at the entrance to the knot, indicating that the knot had substantially weakened the thread. Using the more flexible strand of DNA the knot formed was observed to tighten but no breakage occurred.³³

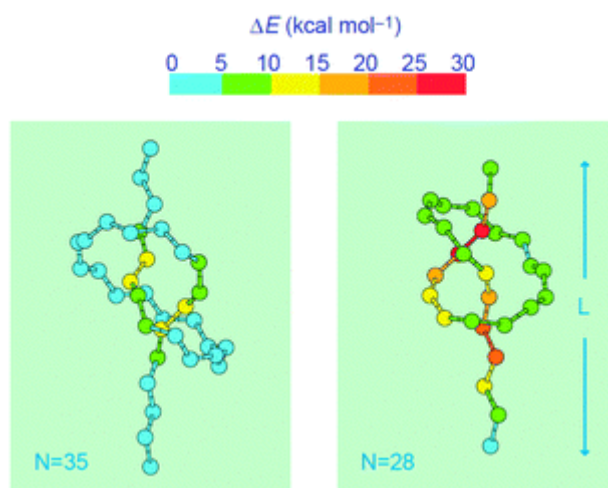


Figure 2. The presence of knots within polymers weakens the strands. The polyethylene chain on the left is relatively strain free. However, upon tightening the knot (by reducing the length of the backbone from 35 to 28 carbons; right) calculations show that strain is induced in the molecule at the entrance to the knot (red and orange regions). Reprinted by permission from Macmillan Publishers Ltd: Nature, 399, 46–48 (1999), copyright 1999.

The presence of knots in the backbones of polymers on a molecular level is known to influence the overall bulk mechanical properties of the polymer³⁴ and it is quite possible that a certain degree of polymer failure may be attributed to knotting on a molecular level.

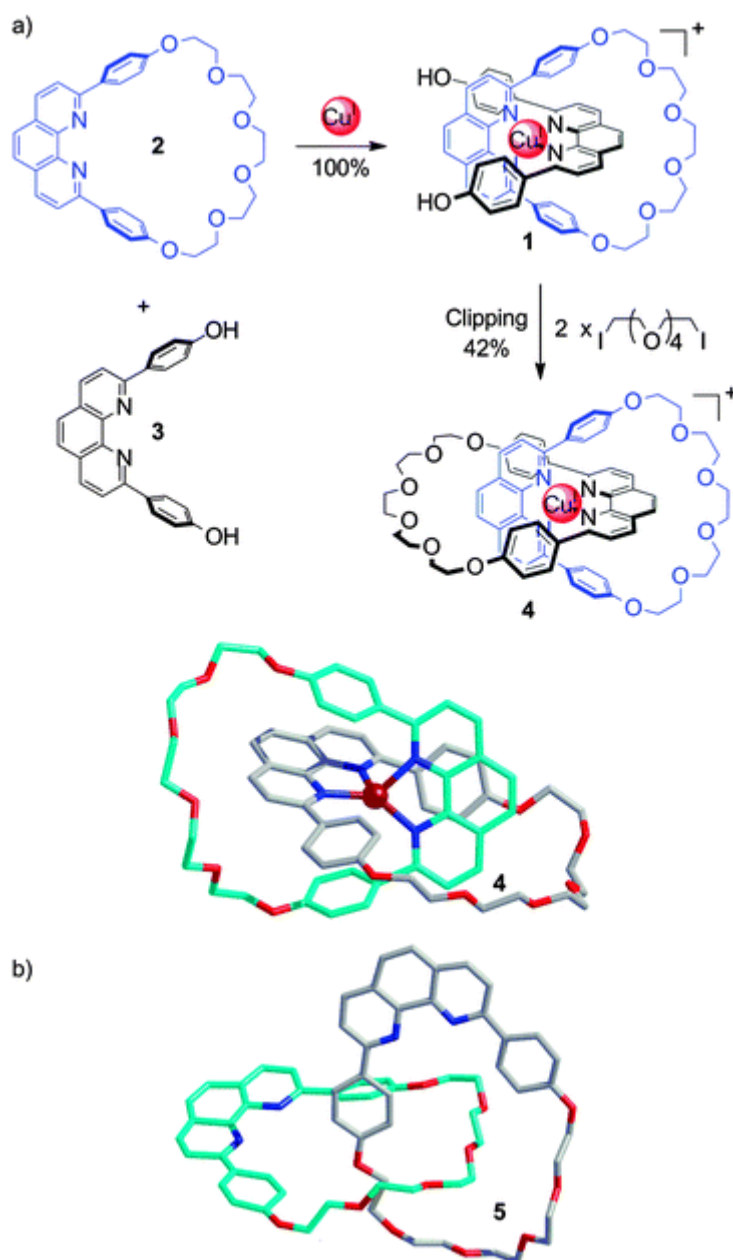
1.5. Template routes to molecular knots

Despite the examples of molecular knots formed using biological polymers (DNA base pairs, tertiary structure of proteins), and their template-free statistical formation in synthetic polymers, template synthesis is the most efficient and versatile approach to form molecular knots from small molecule building blocks. The key factors to be considered when designing a route to molecular knots are the generation of crossing points, their connectivity and the method used to form the closed loop. Hydrogen bonding, donor–acceptor interactions and metal ion templates have all been successfully used to generate the required crossing points. A relatively small collection of reactions have been used as

methods to covalently capture the entwined architectures: amide couplings, Williamson ether synthesis, ring-closing olefin metathesis, copper(I)-catalysed azide–alkyne cycloaddition (the CuAAC ‘click’ reaction³⁵) and reversible imine bond formation. The following sections detail how these methods have been employed and highlight the benefits and potential drawbacks of each approach.

1.5.1. Generating crossing points with linear metal helicates

In 1983 Sauvage introduced the use of metal ions as templates for interlocked molecular structures with the first high yielding [2]catenane synthesis.⁴ This pioneering strategy² used the tetrahedral coordination geometry of a copper(I) ion to hold two bidentate 1,10-phenanthroline (phen) based ligands in an orthogonal arrangement to form the necessary crossing-points (Scheme 2a).⁴ Hydroxyl groups on the ligands were positioned to favour intraligand (rather than intermolecular) Williamson ether macrocyclisation reactions. Complex **1** was formed quantitatively from macrocycle **2** and ligand **3**, and the [2]catenane **4** subsequently generated in 42% yield (Scheme 2a). This was a spectacular accomplishment compared with the statistical and multistep directed synthesis routes of the time³⁶ that generated catenanes in less than 1% overall yield and typically took 6–20 steps to complete. The copper ion could be removed quantitatively from catenane **4** with potassium cyanide to afford metal-free catenane **5** (the X-ray crystal structure of which is shown in Scheme 2b). Sauvage extended this approach to multiple metal centres, using the helical repeat unit of the assemblies to form additional crossing points (see Section 4.2).



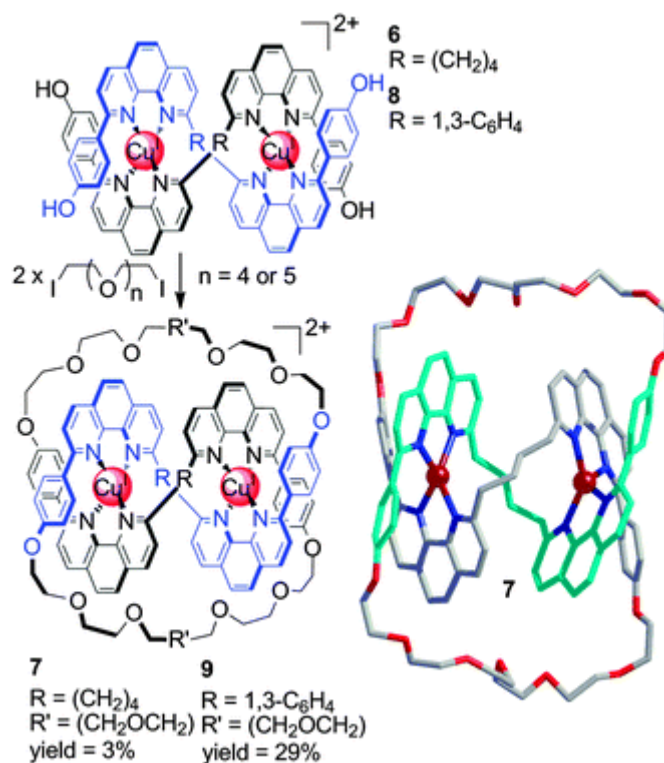
Scheme 2. (a) Sauvage's original use of a metal template to synthesise an interlocked molecule.⁴ The copper(I) bis(phenanthroline) template motif formed the basis of subsequent multinuclear helicates used to prepare molecular trefoil knots. (b) Catenate **4** could be demetallated to give catenand **5**. Both compounds were characterised by X-ray crystallography.³⁷ All of the cap-and-stick structures shown in this Review are X-ray crystal structures produced from coordinates taken from the Cambridge Structural Database (CSD).

The first synthetic molecular knot was reported in 1989 using a dicopper(I) double-stranded helicate **6** (Scheme 3)³⁸ and Williamson ether synthesis to generate the entwined closed loop **7** in 3% yield. The molecular topology was supported by a variety of analytical techniques and later established unambiguously by X-ray crystallography (structure shown in Scheme 3).³⁹ The ¹H NMR spectrum of the helicate **6** indicated a significant amount of the mononuclear copper(I) complex was present; that is, the ligand was able to fold and act as a tetradentate ligand for a single copper(I) centre. To prevent this undesired coordination mode, different spacers were introduced between the phenanthroline groups to induce a tighter wound helicate (*e.g.* **8**) leading to yields of 29% for trefoil knot **9** (Scheme 3) with a rigid 1,3-phenylene spacer.⁴⁰ Detailed studies of this series of molecular trefoil knots examined the expression of their chirality, the binding of other metal ions, kinetics of demetallation and electrochemical properties.⁴¹

The development of efficient catalysts for ring-closing olefin metathesis (RCM) marked a major practical advance for the preparation of interlocked structures by substantially increasing the yield of macrocyclisation reactions. Sauvage and co-workers used RCM to prepare trefoil knot **10** in 74% yield,⁴² the highest yield reported for a synthetic molecular knot to date (Scheme 4a).

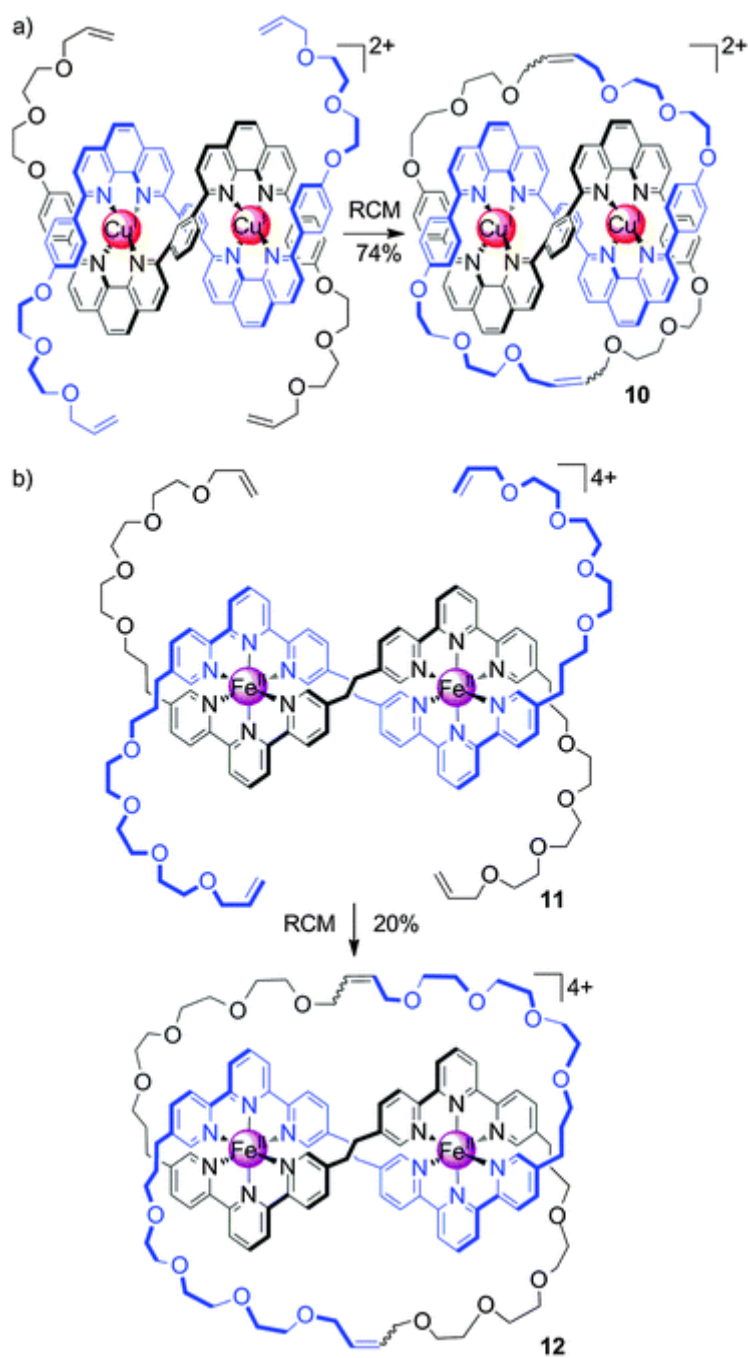
The success of tetrahedral copper(I) templates for forming trefoil knots prompted an extension to the use of octahedral metal ions as templates (Scheme 4b).⁴³ The bidentate phen ligands were replaced with tridentate 2,2':6',2''-terpyridine (tpy) groups which strongly bind octahedral metal ions. The use of iron(II) salts generated double-stranded dinuclear helicate **11**, analogous to the copper(I)–phen ligand intermediates (*e.g.* **6** and **8**, Scheme 3). The yield of RCM to form the trefoil knot **12** was a modest 20%, perhaps due to the

conformation adopted by the complex ligands not favouring macrocyclisation as effectively as the Cu(I)–phen systems.⁴³

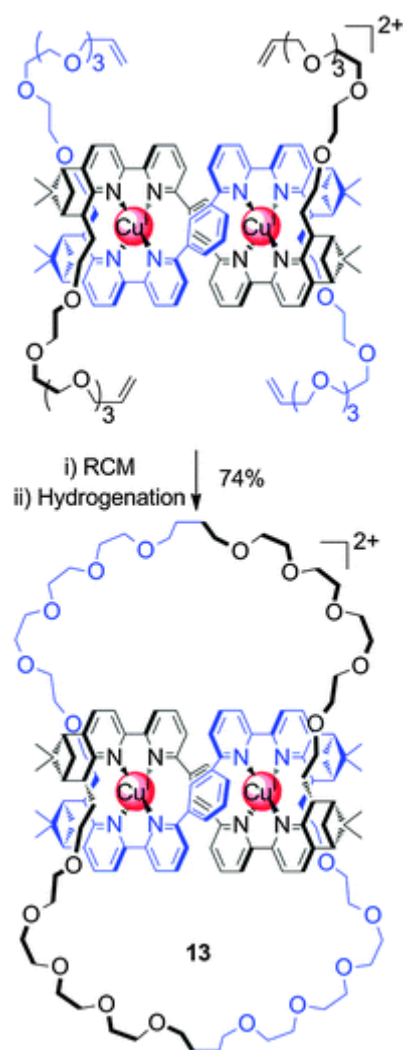


Scheme 3. The first molecular trefoil knot prepared by Sauvage using a metal-template strategy.³⁸ The synthesis of trefoil knots with different spacer groups *via* Williamson ether synthesis gave yields of up to 29%.^{39–41} The X-ray crystal structure shows the distorted geometry of the four-coordinate Cu(I) centres in the trefoil knot metal complex **7**.³⁹

By using chiral groups fused to a 2,2'-bipyridine ligand, the groups of von Zelewsky and Sauvage were able to control the handedness of the chiral dinuclear copper(I) helicate and thus the stereochemistry of the resulting trefoil knot (Scheme 5).⁴⁴ Trefoil knot **13** was the first diastereospecific molecular knot to be synthesised⁴⁴ (an earlier trefoil knot was resolved by crystallisation using a chiral counter-ion⁴⁵). The handedness of the knot was established by circular dichroism.



Scheme 4. Sauvage's formation of trefoil knots *via* RCM with (a) tetrahedral copper(I) ion templates⁴² and (b) octahedral iron(II) ion templates.⁴³



Scheme 5. Diastereoselective synthesis of a chiral molecular trefoil knot by von Zelewsky, Sauvage and co-workers.⁴⁴

The simplest composite knots (knots formed by connecting prime knots) are derived from the sum of two trefoil knots. This addition can take place in one of two ways: If two trefoil knots of the same handedness are combined a granny knot is formed, which is topologically chiral, whereas if two trefoil knots of opposite handedness are combined a *meso* species, a square knot, is produced. Sauvage and co-workers synthesised molecular composite knots by linking linear helicates, isolating both granny and square knots in low yields (2.5%).⁴⁶

1.5.2. Applications and limitations of the linear metal helicate approach

The strategy of linking linear helicates to form topologically complex species was extended to three metal centres (generating four crossing-points) to form doubly-interlocked [2]catenanes (Solomon links, Figure 3).⁴⁷ The apparent limit of the linear helicate approach was reached when helicates containing four or five metal centres were successfully prepared, but attempts to use them to generate a pentafoil knot or a Star of David proved unsuccessful (Figure 3).⁴⁸ This is probably due to the large separation between the end-groups of each of the ligand strands which disfavours the intramolecular reaction to form the interlocked structure. Instead other intra- and intermolecular reactions, which form undesired side products, likely dominate.

The linear metal helicate approach is also limited by the types of topologies that are inherently accessible by this strategy. A linear helicate with three crossing points can form the basis of only three different topologies from intramolecular reactions that connect various pairs of end-groups (Figure 4). A similar situation arises with all other linear helicates: the number of possible intramolecular products is never greater than three (unless a linker with intrinsic additional crossing points is used) and subsequently the types of prime knots which can be formed by this approach are somewhat limited. Only 8% of knots with fewer than eight crossing points are theoretically accessible through a linear helicate strategy, and all of them are torus knots¹² (knots whose topologies can be drawn on an unknotted torus—a donut without any crossing points). Alternative synthetic strategies that could allow more and different types of knots to be realised, as well as other complex topologies, are introduced in Section 4.8.

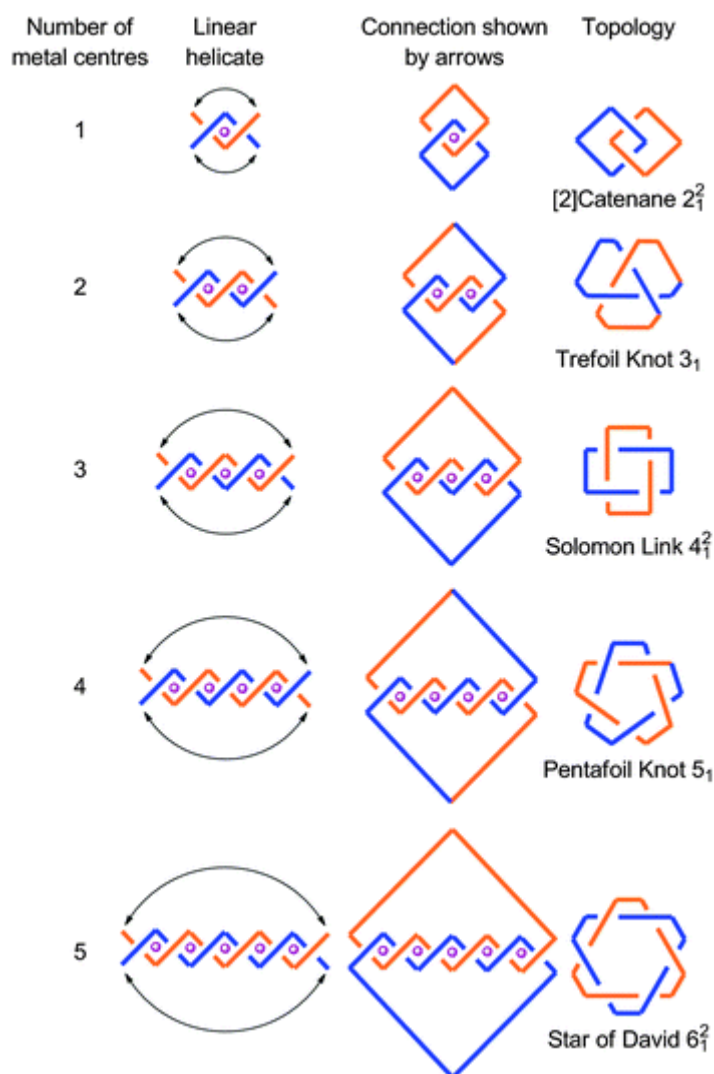


Figure 3. The linear helicate strategy to interlocked molecules introduced by Sauvage.⁴⁸ To date the first three entries of this table have been realised experimentally using this strategy, generating catenanes,⁴ trefoil knots³⁸ and doubly-interlocked[2]catenanes (Solomon links)⁴⁷ using one, two and three metal centres, respectively. The synthesis of a pentafoil knot or triply-interlocked [2]catenane (the 'Star of David' topology) from a linear helicate has thus far proved unsuccessful.⁴⁸

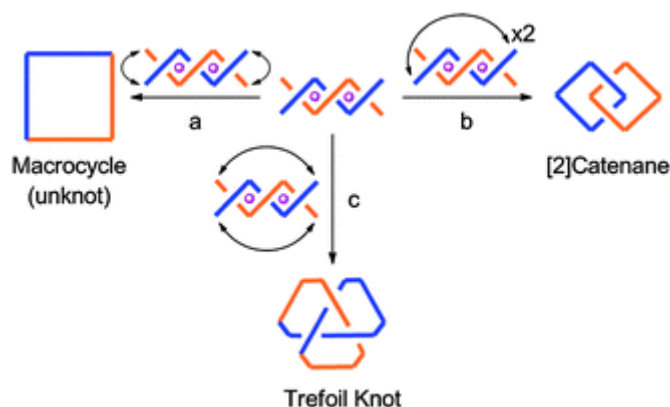
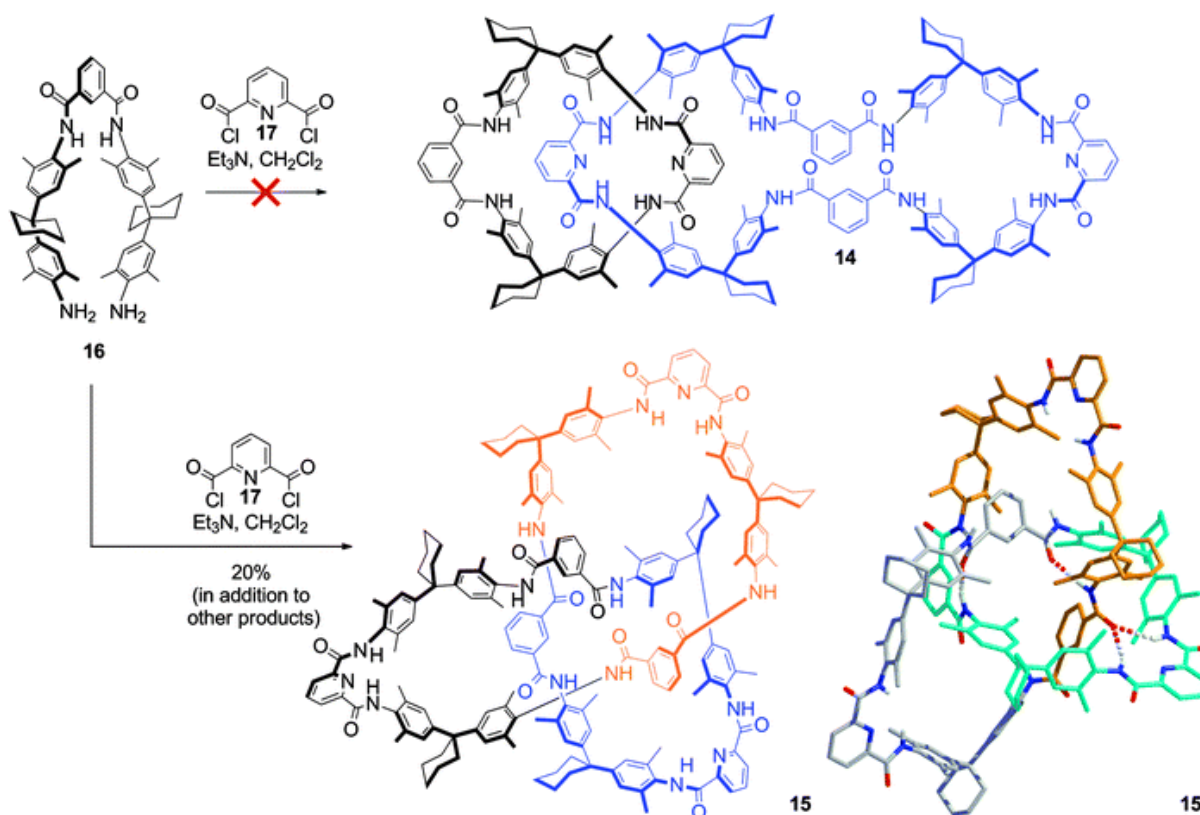


Figure 4. Topologies that can arise from connecting pairs of end-groups of a linear metal helicate with three crossing points. A linear double helicate can, in principle, be cyclised in one of three ways: connecting the closest end-groups of the blue and orange strands (pathway a) gives a topologically-trivial ‘unknot’ macrocycle. Connecting end-groups of the same colour gives a [2]catenane (pathway b). Connecting different coloured strands via the end-groups that are furthest from each other (pathway c), the route employed in Schemes 3–5, generates a trefoil knot.

1.5.3. Generating crossing points through hydrogen bond motifs

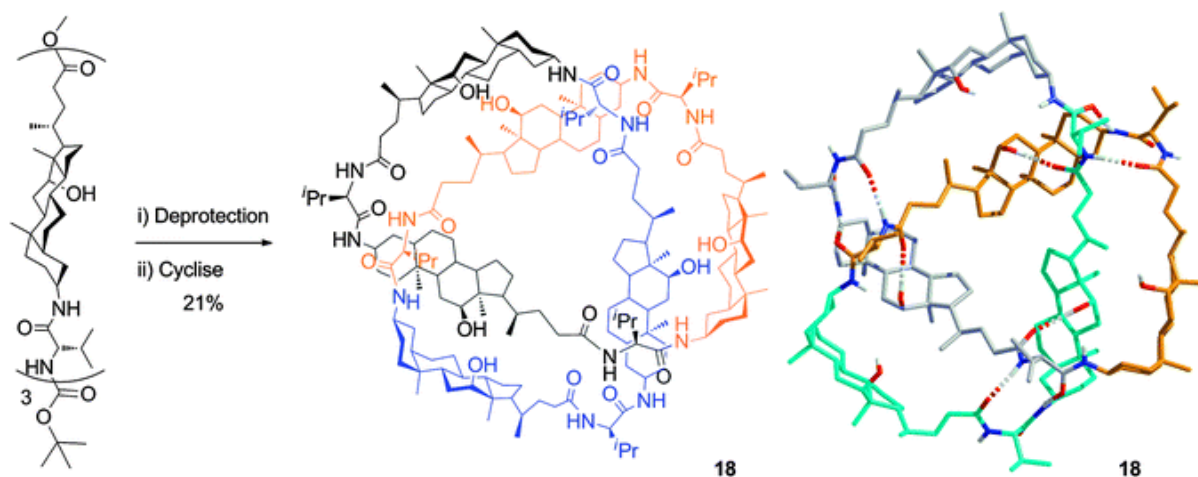
In the early 1990's amide–amide hydrogen bonding interactions were found to be able to direct the assembly of [2]catenanes.^{49–52} Whilst investigating the effect of replacing some of the isophthalamide hydrogen bonding groups with 2,6-dicarboxamide-5-pyridine units (Scheme 6), Hunter isolated an unusual high molecular weight compound that he characterised as a [2]catenane, **14**, with one large macrocycle and one smaller macrocycle.⁵³ A few years later, Vögtle's group repeated this synthesis, obtained single crystals suitable for X-ray diffraction, and found that Hunter's earlier compound was, in fact, a trefoil knot⁵⁴ (**15**, Scheme 6). The knot is assembled in 20% (Vögtle⁵⁴) or 29% yield (Hunter⁵³) from three equivalents of diamine **16** and three equivalents of diacyl chloride **17**. The role of hydrogen bonding in the formation of the knot and a possible mechanism for its formation have been discussed.⁵⁵ Trefoil knots bearing different substituents were

synthesised and in several instances both enantiomers of the knot could be separated by chiral HPLC.⁵⁵



Scheme 6. The formation of a molecular trefoil knot directed by amide–amide hydrogen bonding. The reaction between diamine **16** and diacyl chloride **17** was originally thought to produce [2]catenane **14**.⁵³ However, several years later X-ray crystallography showed that the product was actually the isomeric trefoil knot **15**.⁵⁴

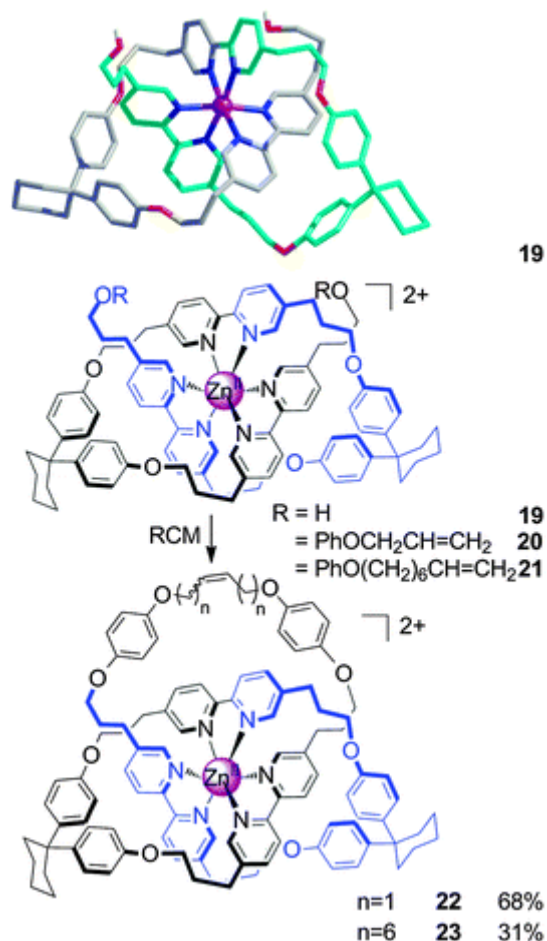
One other synthesis of a trefoil knot promoted by amide–amide hydrogen bonding interactions has been reported.⁵⁶ Feigl and co-workers found that trefoil knot **18** was unexpectedly formed in 21% yield during the amide coupling reaction of 3- α -aminodeoxycholic acid with L-valine (Scheme 7). The topology of the knot was determined by X-ray crystallography. As the architecture of the trefoil knot and both building blocks of the knot are chiral, two diastereomers of the knot could potentially be formed, but only the (+)-isomer was detected in the reaction mixture.



Scheme 7. An alternative hydrogen bonding template for trefoil knot formation was discovered by Feigel and co-workers.⁵⁶ The X-ray crystal structure shows an extensive array of hydrogen bonds that would have been difficult to predict prior to discovery.

1.5.4. Trefoil knots assembled about a single metal ion template

An interesting example of an ‘open-knotted’ structure assembled about an octahedral metal centre was described by Hunter and co-workers in 2001 (Scheme 8).⁵⁷ An octahedral zinc(II) template was used to wrap a single ligand containing three bipyridyl units into an open knot conformation (**19**) and the structure confirmed by X-ray crystallography (Scheme 8, top). The folding process was shown to be fully reversible. Addition of a chloride ion regenerated the free ligand, and subsequent addition of silver salts (precipitating the chloride ion as AgCl) reassembles the open knot complex. A decade after the initial report, it was demonstrated that the open knot could be closed to form a trefoil knot through either a bis-esterification reaction of the two terminal alcohols in **19**, or by ring closing metathesis from **20/21** to form **22/23**.⁵⁸



Scheme 8. Hunter's 'open knot' **19**,⁵⁷ derivatives of which (**20/21**) were cyclised to produce trefoil knots **22/23**.⁵⁸ Removal of the zinc(II) template from **23** was achieved with Li₂S to generate the free trefoil knot.

1.5.5. Active template synthesis of a trefoil knot

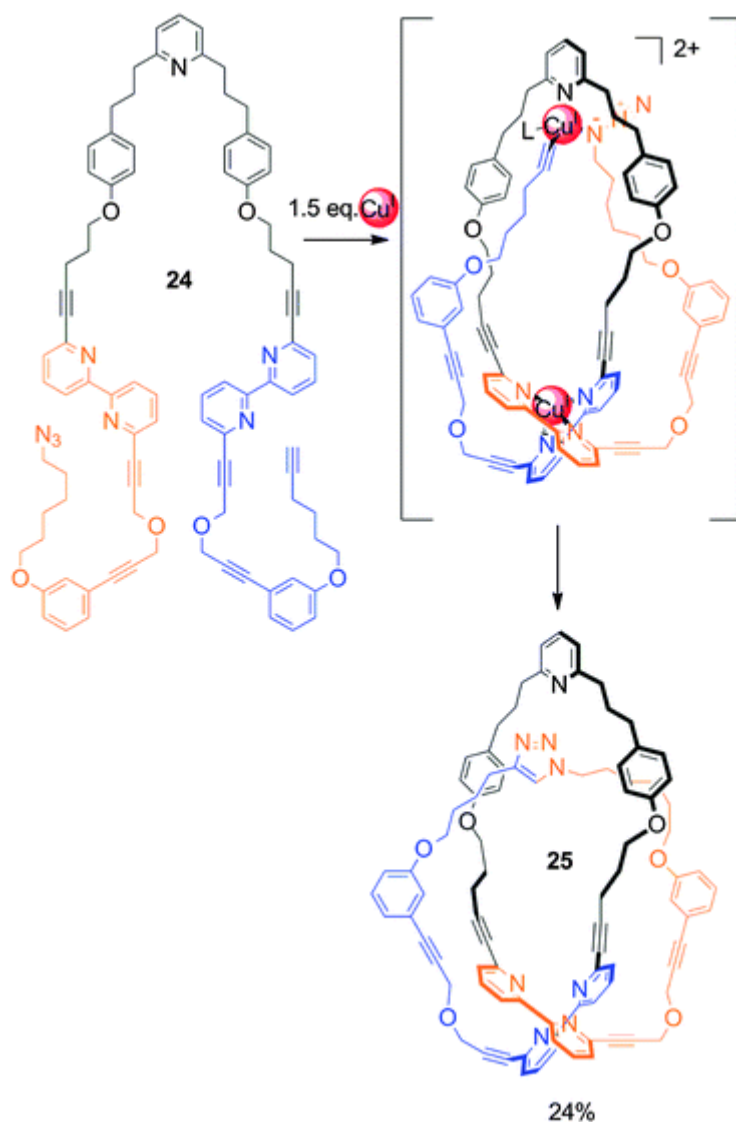
A recent development in the synthesis of interlocked compounds has been the introduction of active metal template strategies.⁵⁹ In this approach, the metal ion plays a dual role during the assembly process, acting simultaneously as a structural element able to assemble the various building blocks in the desired orientation, and as a reagent—or even a catalyst—for the covalent capture of the entanglement. This approach has allowed the synthesis of interlocked compounds using catalytic amounts of a transition metal (instead of the usual stoichiometric quantities used in passive metal strategies).⁵⁹ Significantly, permanent

recognition motifs on each component of the entanglement are no longer required, allowing the assembly to be traceless. The most recent innovation using an active metal template strategy has been the synthesis of the smallest molecular trefoil knot to date (a 76 atom long closed loop) from the reaction of a substoichiometric (relative to the number of available binding sites) amount of copper(I) and a single polypyridyl thread terminated with two reactive units, an azide and an alkyne (**24**, Scheme 9).⁶⁰

The process actually relies on the cooperation of two different kinds of templates. The coordination of a tetrahedral copper(I) ion—a passive template—to the two bipyridine units of **24** generates a loop in the strand. A second copper(I) ion—an active template—is bound in an endocyclic fashion to the pyridine unit in the loop and subsequently gathers the two functional end groups from opposite sides of the loop, catalysing the CuAAC cycloaddition to covalently capture the entwined topology. The knot **25** (Scheme 9) was isolated in a 24% yield and characterized by ¹H and ¹³C NMR spectroscopy, mass spectrometry, and by drift tube ion mobility mass spectrometry (DT IM-MS).

1.5.1. Other synthetic strategies to molecular trefoil knots and related structures

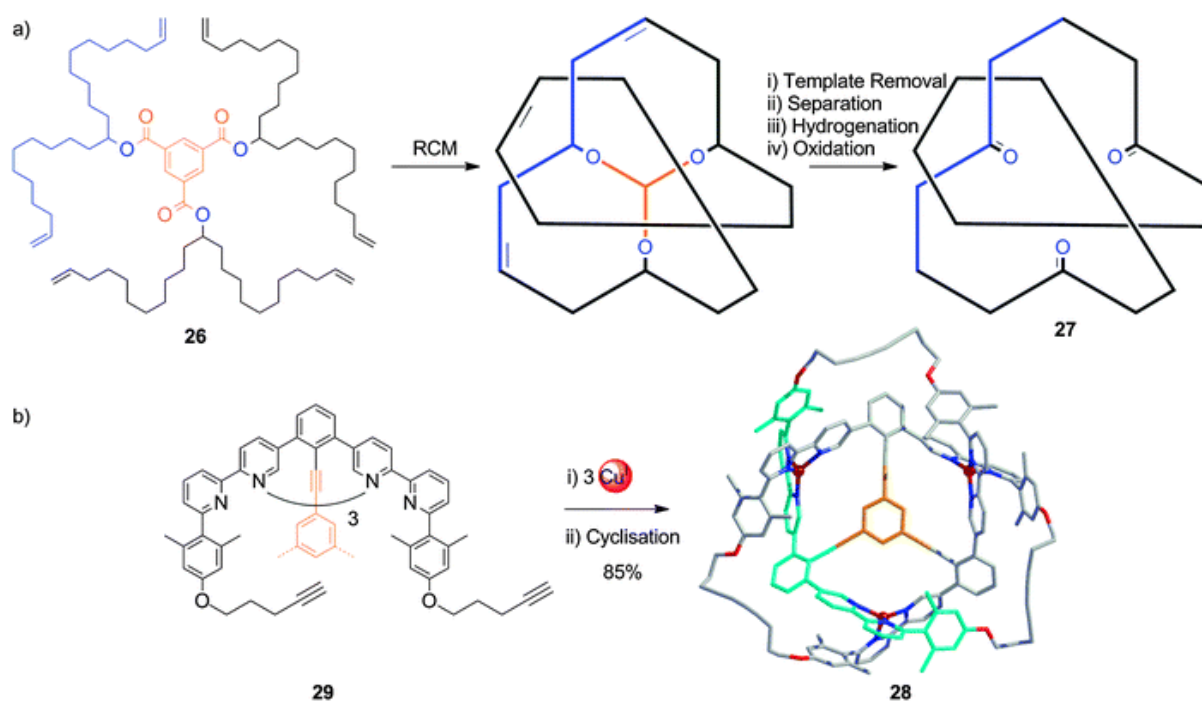
Several other synthetic strategies to molecular trefoil knots have been proposed and, in some cases, experimentally investigated. Donor–acceptor interactions have been used to prepare a trefoil knot, albeit in low yield.⁶¹ The trefoil knot was formed as a mixture with its macrocyclic isomer and was isolated by HPLC. The poor efficiency of this approach perhaps contributed to this strategy not being further explored.



Scheme 9. Synthesis of trefoil knot **25** by the cooperative action of passive and active copper(I) templates.⁶⁰ The trefoil knot is formed in addition to the macrocyclic ‘unknot’ isomer. The more compact knot was distinguished from the macrocycle and thread (**24**) isomers through drift tube ion mobility mass spectrometry.

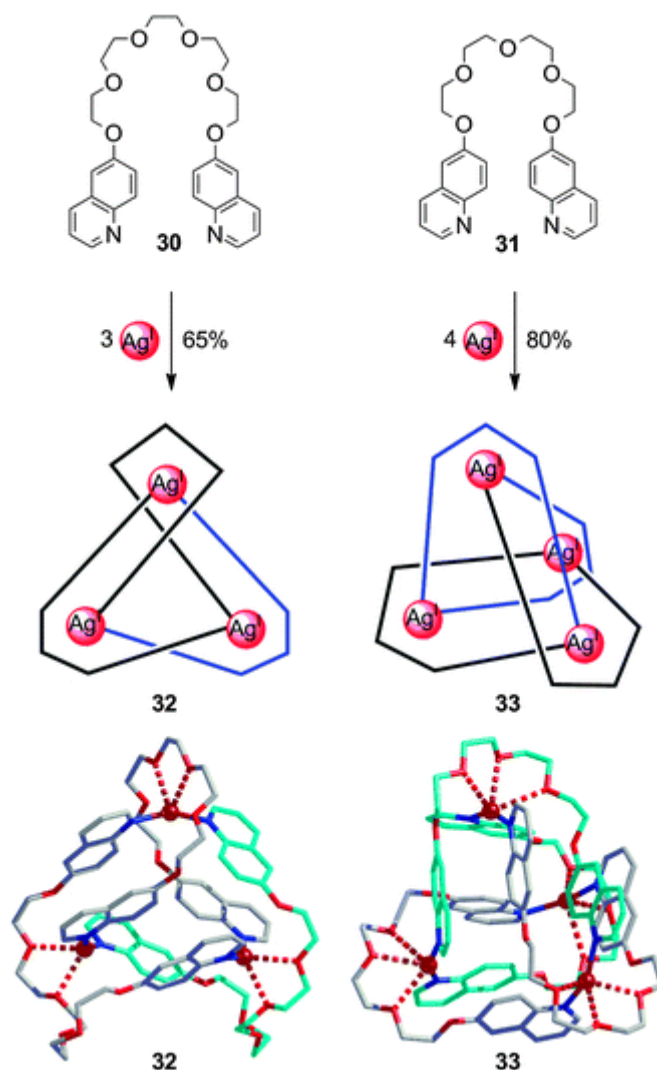
Fenlon has reported the synthesis of an almost entirely hydrocarbon trefoil knot. Hexa-alkene **26** (Scheme 10a), utilising a 1,3,5-tri substituted benzene template reminiscent of directed synthetic strategies,⁴¹ can be cyclised under RCM conditions, generating a number of possible cyclic products.⁶² One of the products obtained was tentatively assigned as being trefoil knot **27** based on chiral shift reagent NMR studies. Using a related 1,3,5-

trisubstituted benzene template in combination with copper(I) binding to control the positions of overlap of the ligand 'arms', Siegel was able to synthesise an interwoven trefoil knot precursor **28** (Scheme 10b).^{63,64} Ligand **29** binds to copper(I) generating the three crossing points required for a trefoil knot. Using Glaser couplings the open structure was cyclised in 85% yield, the excellent yield presumably resulting from the high degree of preorganisation present in the copper complex of **29**. The metal template could be removed from **28** by treatment with KCN. However, the final step required to produce a formal trefoil knot, removal of the organic template, has yet to be achieved.⁶⁴



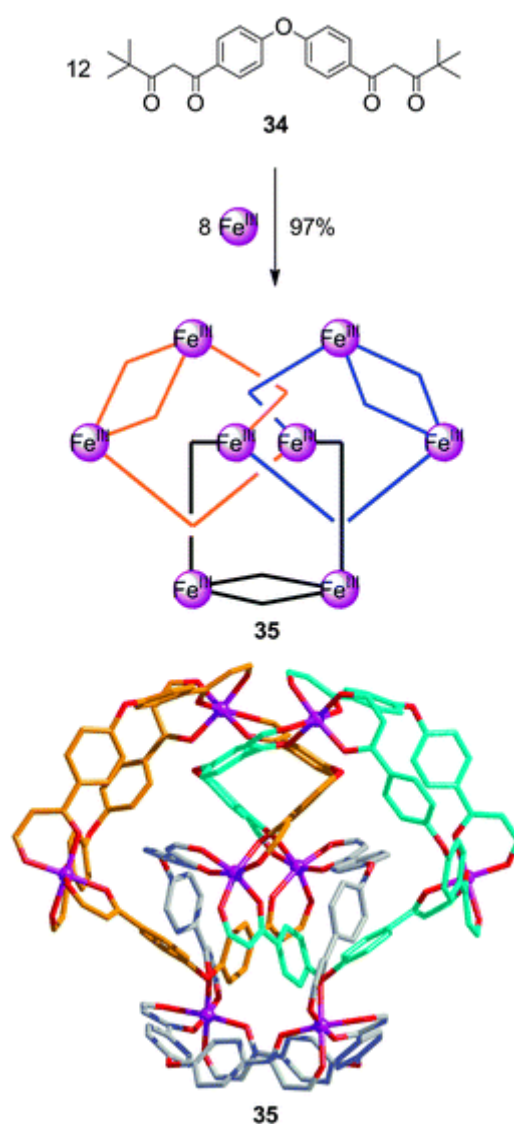
Scheme 10. Synthesis of interlocked molecules using a 1,3,5-trisubstituted benzene template: (a) Fenlon's synthesis of trefoil knot **27** using RCM.⁶² (b) Siegel's synthesis of trefoil knot precursor **29**, utilising both a covalently connected organic template and metal coordination to position crossing points. Removal of the central template should lead to the formation of a trefoil knot.⁶⁴

Hosseini has prepared two interwoven 'metallaknots' in which metal–ligand coordination bonds are part of the knot backbone. These metal–organic structures are based on bisquinoline ligands bound to silver(I) ions (Scheme 11). Small variations in the length of the linker connecting the two quinoline units lead to either tri-(using the longer linker **30**) or tetra-(using the shorter linker **31**) metal-centre compounds, **32** and **33**, respectively.⁶⁵



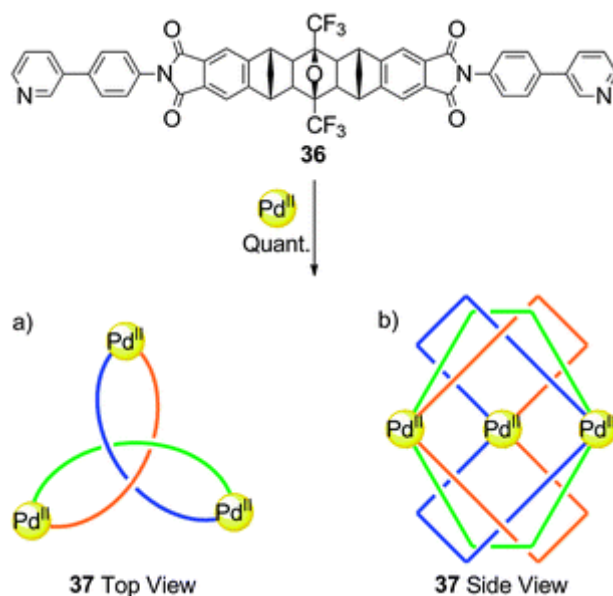
Scheme 11. Hosseini's 'metallaknots': tri- and tetra-nuclear complexes **32** and **33** formed by coordination of ligands **30** and **31** to silver(I) ions. Weak interactions between the metal centres and oxygens of the glycol linkers (shown by dashed bonds in the X-ray structure) aid the self-assembly process.⁶⁵

Ravels⁶⁶ are closely related to knots and links. Their structure is interwoven but contains nodes with more than two connections, making them a type of 'branched' knot. Lindoy and co-workers found that when a bis- β -diketone ligand, **34**, was mixed with an iron(III) template a 20-component self assembly process takes place over the course of three months to generate such a molecular ravel (**35**, Scheme 12).⁶⁷ The $[\text{Fe}_8\text{34}_{12}]$ complex (**35**) was formed in 97% yield and found to have the connectivity of a 'universal 3-ravel' by X-ray crystallography.



Scheme 12. Lindoy's 'universal 3-ravel': reaction of ligand **34** with FeCl_3 over the course of three months led to the formation of **35** in near quantitative yield. For clarity, the tBu groups are not shown in the X-ray structure.⁶⁷

Recently, Clever and co-workers have reported the synthesis of what appears to be another type of ravel composed of two trefoil knots that form the faces of a cage-like structure (Scheme 13).⁶⁸ The rigid ligand **36** forms a complex with palladium(II) with the formula $[\text{Pd}_3\text{36}_6]$ in quantitative yield. The non-trivial topology of product **37** was deduced from detailed NMR studies and molecular modelling.⁶⁸



Scheme 13. A double trefoil knot cage structure, the second example of a molecular ravel, synthesised by Clever and co-workers.⁶⁸ Connectivity shown from (a) top view, (b) side view.

1.5.2. Reversible covalent bond formation as a means of ‘error-checking’ during synthesis

A range of complex molecular architectures, including macrocycles, cavitands, cages, knots and links, have been assembled using metal ion templates and reversible covalent bond formation. For synthetic strategies that require the joining of multiple building blocks with the correct connectivity, the use of a reversible process can be particularly useful. It provides a mechanism for correcting ‘mistakes’ in connectivity that occur during the

covalent-capture step of mechanical bond formation, often by designing the desired product to be the most thermodynamically stable.² Over a decade ago reversible imine bond formation, and reversible metal ion coordination of the resulting imine ligand, was introduced as an effective means of assembling [2]catenanes⁶⁹ and [2]rotaxanes⁷⁰ under thermodynamic control, a tactic² that has subsequently been used to assemble other interlocked structures such as Borromean rings,⁷¹ Solomon links⁷² and a pentafoil knot⁷³ (see Section 4.8).

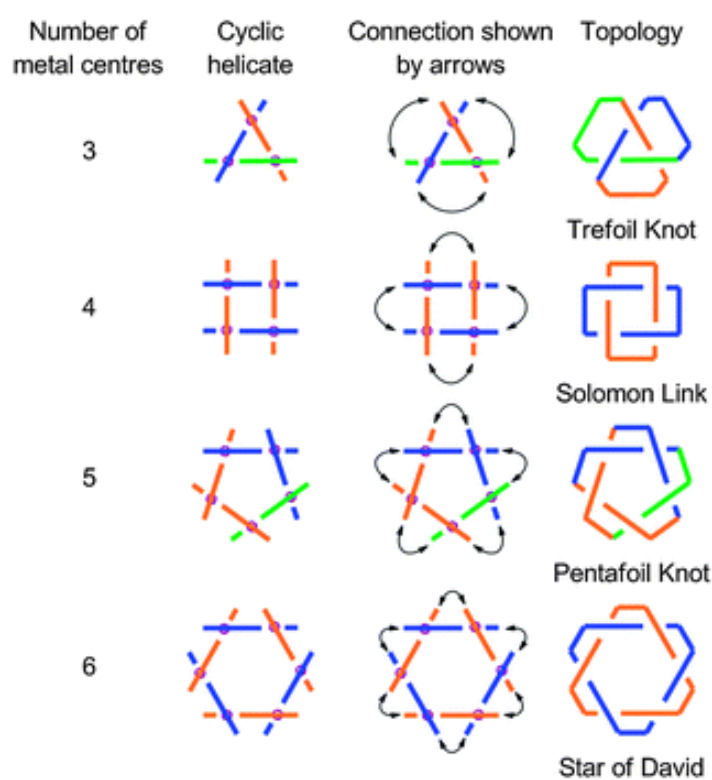


Figure 5. The potential of circular metal helicates to form molecular knots and links by connecting adjacent end-groups. To date only a pentafoil knot has been prepared through this strategy.⁷³

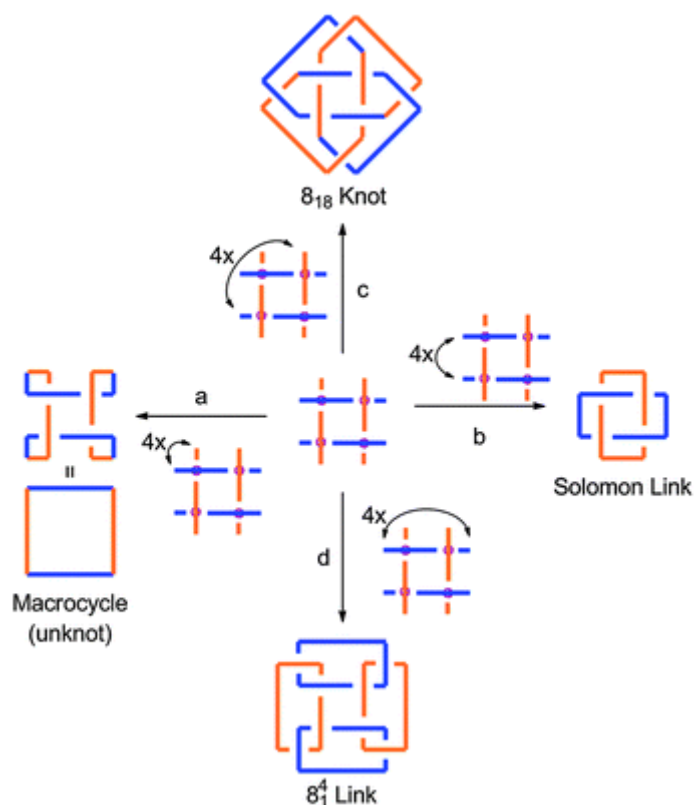


Figure 6. Different topologies that could in principle arise from a tetrameric cyclic metal helicate comprised of four metal centres and four ligands generating four crossing points. Many different topologies are possible by joining different pairs of end-groups, even for such a simple structure: Joining together corner end-groups of different coloured strands generates a simple macrocycle (pathway a). Connecting different strands of the same colour by end-groups closest to each other gives a Solomon link (pathway b). By connecting different coloured strands through joining end-groups that are opposite each other on the grid (generating an additional four crossing points) an 8_{18} knot would be formed (pathway c), whereas cyclising each strand in a similar manner would give rise to a cyclic [4]catenane (an 8_1^4 link, pathway d).

1.5.3. Routes, and potential routes, to higher molecular knots: cyclic helicates and grids

Over the past thirty years, Sauvage's linear metal helicate strategy (Figure 3) has been spectacularly successful for the rational synthesis of [2]catenanes, trefoil knots and a Solomon link. However, as discussed in Section 4.2, it has limits both experimentally and in terms of the topologies that can be theoretically accessed. Cyclic metal helicates and

interwoven molecular grids are alternative types of scaffold through which it may be possible to assemble higher order knots and other difficult-to-access molecular topologies.⁷⁴ With these systems the required crossing points can be generated using a double helix assembled by metal ion chelation (as with the linear metal helicate examples in Section 4.1) but they offer the opportunity to form a much wider range of topologies if the connectivities of the end-groups can be controlled using geometrical restrictions, non-covalent interactions and stereochemical control. Examples of the simplest interwoven structures that can be formed from cyclic helicates where adjacent end-groups are connected are shown in Figure 5. Other topologies that could be possible using these scaffolds through different connection combinations are shown in Figure 6 and 7.

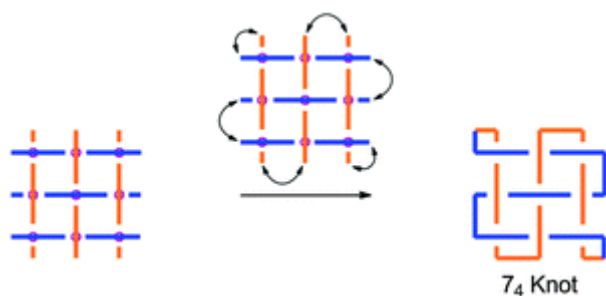
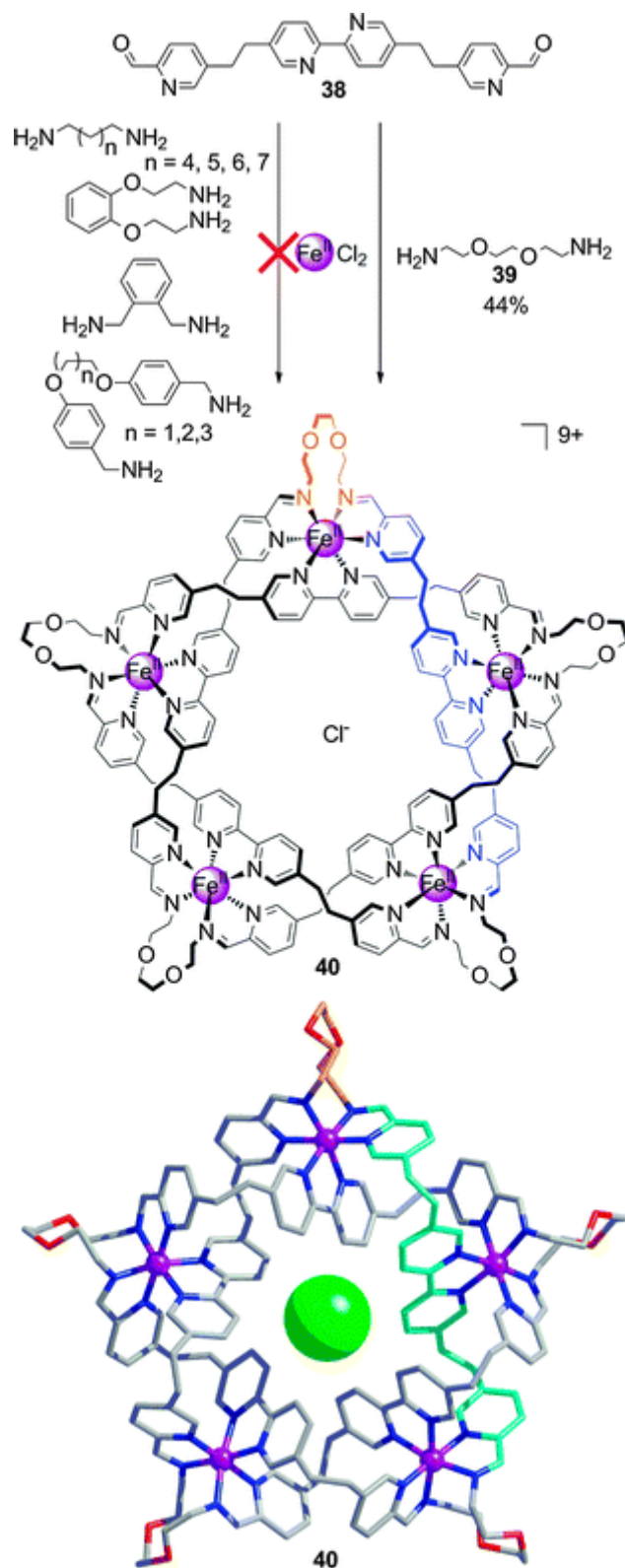


Figure 7. An interwoven $[3 \times 3]$ grid (not a grid composed of distinct layers of ligands) comprised of nine metal centres and six ligands generates nine crossing points. By connecting adjacent end-groups to form a closed loop, one possible outcome is a 7_4 , or ‘endless’, knot (shown). Note that two crossing points are lost by joining the two sets of adjacent corner end-groups.

Inspired by Lehn's seminal work on cyclic double helicates formed with iron(II) salts,⁷⁵ this strategy was recently applied to form pentameric cyclic helicates⁷⁶ and a molecular pentafoil knot.⁷³ With a cyclic helicate the distance between the end-groups can be relatively short in comparison to a linear metal helicate, increasing the probability of connections occurring in the desired manner. However, with a pentameric cyclic helicate

ten end-groups have to be joined (compared to the four required for a linear metal helicate; entry 4, Figure 3). Lehn's original ligand system was therefore modified to allow for imine-bond formation (see Section 4.7) with amine building blocks during the assembly process (**38**, Scheme 14). The presence of chloride ions in the reaction mixture (through the use of FeCl_2) selectively formed the pentameric cyclic helicate, which has the required number of crossing points (five) for pentafoil knot formation. The use of diamine **39**, which features a glycol spacer that allows for a low energy turn because of multiple gauche effects, produced the desired knot **40** in 44% yield (Scheme 14). The importance of the structure of the connecting loop is apparent from the observation that other diamines led to oligomers and polymers rather than pentafoil knot formation. The pentafoil knot was characterised by mass spectroscopy, NMR spectrometry and X-ray crystallography, which revealed the chloride ion is bound at the centre of the knot by ten $\text{CH}\cdots\text{Cl}^-$ hydrogen bonds (Scheme 14).

By changing the connectivity of the end-groups of cyclic helicates, many more topological products become theoretically possible. For example, from a basic tetrameric cyclic helicate core, a Solomon link, an 8_{18} prime knot, cyclic [4]catenane (an 8^4_1 link) or an unknot macrocycle are all possible outcomes by altering which of the end-groups are linked together (Figure 6). Clearly a significant degree of synthetic control would be required to synthesise any of these structures selectively. Learning how to control the sequence of crossing point connectivity is one of the key challenges for this field over the next few years.



Scheme 14. The formation of a molecular pentafoil knot via reversible imine bond formation between building blocks **38**($\times 5$) and **39** ($\times 5$), coordination to five octahedral geometry iron(II) ions, use of a chloride template to select the correct size of cyclic helicate, and conformational preferences of the linker groups to favour knot formation.⁷³ In the X-ray crystal structure part

of the knot originating from one molecule of **38** is shown in light blue and from one diamine linker **39** in orange.

A further, as yet unrealised experimentally, extension of the cyclic helicate strategy would be to employ interwoven molecular grids as the template system. The tetrameric cyclic helicate (Figure 6) can be considered an interwoven $[2 \times 2]$ grid. A $[3 \times 3]$ interwoven grid opens up even more possibilities for topological products (Figure 7)—and perhaps just as many synthetic challenges!

1.6. Recent updates

Recent updates in the field of molecular knots mainly include new strategies towards molecular trefoil knots with the exception of one new knot: a figure of eight knot.

Relying on the hydrophobic effect, Sanders *and al.*^{77,78} were able to obtain an impressive library of topologically complicated macrocycles. In fact, by carefully tuning the hydrophobicity/hydrophilicity, rigidity/flexibility and chirality of naphthalenediimide-based building blocks, it was possible to self-assemble in water a disulfide dynamic combinatorial library containing either an enantiomerically pure trefoil knot, an achiral meso figure of eight knot or a mixture of enantiomerically pure and racemic Solomon links depending on the building blocks used.

Trabolsi *and al.*⁷⁹ reported another example of dynamic covalent chemistry (DCC) applied to the synthesis of topologically non trivial objects. DCC of imine ligands was combined with zinc (II) metal templates to yield the one pot synthesis of a [2]catenane, a trefoil knot and a Solomon link, when diaminobipyridine and diformylpyridine were mixed with zinc acetate.

Following the earliest published idea proposed by Sokolov for a template synthesis of a trefoil knot, Leigh *and al.*⁸⁰ used ring closing metathesis to form a 81-atom-loop trefoil knot from three 2,6-pyridinedicarboxamide ligands entwined around a lutetium (III) ion.

1.7. Conclusions

The past thirty years have seen considerable advances in the field of chemical topology, including the invention and execution of increasingly sophisticated synthetic strategies, enabled by progress in the control of reactivity, conformation and supramolecular structure. Nevertheless, the control of molecular topology remains an almost entirely unconquered challenge for synthetic chemistry. Of the six billion prime knots known to mathematics only three—the unknot (*i.e.* a macrocycle), trefoil knot and pentafoil knot—have been synthesised to date using small-molecule building blocks. The use of cyclic metal helicates and interwoven grids as templates and scaffolds for complex molecular topologies (Section 4.8) is ongoing in our laboratory.

Alfred Werner began the field of coordination chemistry with investigations of the stereochemistry of relatively simple metal–ligand complexes. A hundred years after the award of his Nobel Prize coordinated transition metal centres lie at the heart of the most complex molecular knots prepared to date.

1.8. Notes and references

1. G. B. Kauffman, *Alfred Werner. Founder of Coordination Chemistry*, Springer-Verlag, Berlin, **1966**.
2. J. E. Beves, B. A. Blight, C. J. Campbell, D. A. Leigh and R. T. McBurney, *Angew. Chem., Int. Ed.*, **2011**, *50*, 9260–9327.
3. R. S. Forgan, J.-P. Sauvage and J. F. Stoddart, *Chem. Rev.*, **2011**, *111*, 5434–5464.
4. C. O. Dietrich-Buchecker, J.-P. Sauvage and J. P. Kintzinger, *Tetrahedron Lett.*, **1983**, *24*, 5095–5098.
5. Tait was instrumental in the foundation of knot theory and published widely on the subject. Early publications relating to his and others' work on knot theory can be accessed via <http://www.maths.ed.ac.uk/~aar/knots/index.htm>.
6. W. Thomson, *Proc. R. Soc. Edinburgh*, **1867**, *6*, 94–105.
7. For example a trefoil knot, the simplest non-trivial knot, has three crossing points and is denoted 3_1 . With links the number of components is also included. For example a [2]catenane, the simplest non-trivial link, has two components and two crossing points and is denoted 2^2_1 . This notation was introduced by Alexander and Briggs, see: J. W. Alexander and G. B. Briggs, *Ann. Math.*, **1926–1927**, *28*, 562–586.
8. Knots are classified as prime if they cannot be produced by connecting together two or more simpler knots (in the same way that prime numbers cannot be generated by the product of smaller numbers), whereas knots formed from two or more prime knots are termed composite knots. The simplest composite knot can be derived from the addition of two trefoil knots (as described in Section 4.1).
9. P. G. Tait, *Trans. – R. Soc. Edinburgh*, **1884–1885**, *32*, 493–506.
10. P. G. Tait, *Trans. – R. Soc. Edinburgh*, **1883–1884**, *32*, 327–342.
11. P. G. Tait, *Proc. R. Soc. Edinburgh*, **1876–1877**, *9*, 321–332.
12. J. Hoste, in *Handbook of Knot Theory*, ed. W. Menasco and M. Thistlethwaite, Elsevier, **2005**, pp. 209–232.
13. B. Hudson and J. Vinograd, *Nature*, **1967**, *216*, 647–652.
14. D. A. Clayton and J. Vinograd, *Nature*, **1967**, *216*, 652–657.
15. F. B. Dean, A. Stasiak, T. Koller and N. R. Cozzarelli, *J. Biol. Chem.*, **1985**, *260*, 4975–4983.

16. J. J. Champoux, *Annu. Rev. Biochem.*, **2001**, *70*, 369–413.
17. W. R. Taylor, *Comput. Biol. Chem.*, **2007**, *31*, 151–162.
18. A. L. Mallam, *FEBS J.*, **2009**, *276*, 365–375.
19. W. R. Taylor, *Nature*, **2000**, *406*, 916–919.
20. N. C. Seeman, *Angew. Chem., Int. Ed.*, **1998**, *37*, 3220–3238.
21. A positive (+) crossing point (or node) gives rise to a right-handed helix whilst a negative (–) crossing point will give rise to a left-handed helix.
22. S. M. Du, B. D. Stollar and N. C. Seeman, *J. Am. Chem. Soc.*, **1995**, *117*, 1194–1200.
23. C. Mao, W. Sun and N. C. Seeman, *Nature*, **1997**, *386*, 137–138.
24. T. Ciengshin, R. Sha and N. C. Seeman, *Angew. Chem., Int. Ed.*, **2011**, *50*, 4419–4422.
25. A. Bucka and A. Stasiak, *Nucleic Acids Res.*, **2002**, *30*, e24.
26. H. Wang, G. R. J. Di and N. C. Seeman, *Proc. Natl. Acad. Sci. U. S. A.*, **1996**, *93*, 9477–9482.
27. N. P. King, A. W. Jacobitz, M. R. Sawaya, L. Goldschmidt and T. O. Yeates, *Proc. Natl. Acad. Sci. U. S. A.*, **2010**, *107*, 20732–20737.
28. M. Schappacher and A. Deffieux, *Angew. Chem., Int. Ed.*, **2009**, *48*, 5930–5933.
29. M. D. Frank-Kamenetskii, A. V. Lukashin and A. V. Vologodskii, *Nature*, **1975**, *258*, 398–402.
30. C. Micheletti, D. Marenduzzo and E. Orlandini, *Phys. Rep.*, **2011**, *504*, 1–73.
31. D. M. Raymer and D. E. Smith, *Proc. Natl. Acad. Sci. U. S. A.*, **2007**, *104*, 16432–16437.
32. A. M. Saitta, P. D. Soper, E. Wasserman and M. L. Klein, *Nature*, **1999**, *399*, 46–48.
33. Y. Arai, R. Yasuda, K.-I. Akashi, Y. Harada, H. Miyata, K. Kinoshita, Jr. and H. Itoh, *Nature*, **1999**, *399*, 446–448.
34. R. K. Bayer, *Colloid Polym. Sci.*, **1994**, *272*, 910–932.
35. K. D. Hänni and D. A. Leigh, *Chem. Soc. Rev.*, **2010**, *39*, 1240–1251.
36. G. Schill and A. Lüttringhaus, *Angew. Chem., Int. Ed. Engl.*, **1964**, *3*, 546–547.
37. M. Cesario, C. O. Dietrich-Buchecker, J. Guilhem, C. Pascard and J.-P. Sauvage, *J. Chem. Soc., Chem. Commun.*, **1985**, 244–247.
38. C. O. Dietrich-Buchecker and J.-P. Sauvage, *Angew. Chem., Int. Ed. Engl.*, **1989**, *28*, 189–192.

39. C. O. Dietrich-Buchecker, J. Guilhem, C. Pascard and J.-P. Sauvage, *Angew. Chem., Int. Ed. Engl.*, **1990**, *29*, 1154–1156.
40. C. O. Dietrich-Buchecker, J.-P. Sauvage, A. De Cian and J. Fischer, *J. Chem. Soc., Chem. Commun.*, **1994**, 2231–2232.
41. J.-P. Sauvage and C. O. Dietrich-Buchecker, in *Molecular Catenanes, Rotaxanes and Knots*, ed. J. -P. Sauvage and C. O. Dietrich-Buchecker, Wiley-VCH, Weinheim, **1999**.
42. C. Dietrich-Buchecker, G. Rapenne and J.-P. Sauvage, *Chem. Commun.*, **1997**, 2053–2054.
43. G. Rapenne, C. Dietrich-Buchecker and J.-P. Sauvage, *J. Am. Chem. Soc.*, **1999**, *121*, 994–1001.
44. L.-E. Perret-Aebi, A. von Zelewsky, C. Dietrich-Buchecker and J.-P. Sauvage, *Angew. Chem., Int. Ed.*, **2004**, *43*, 4482–4485.
45. G. Rapenne, C. Dietrich-Buchecker and J.-P. Sauvage, *J. Am. Chem. Soc.*, **1996**, *118*, 10932–10933.
46. R. F. Carina, C. Dietrich-Buchecker and J.-P. Sauvage, *J. Am. Chem. Soc.*, **1996**, *118*, 9110–9116.
47. J.-F. Nierengarten, C. O. Dietrich-Buchecker and J.-P. Sauvage, *J. Am. Chem. Soc.*, **1994**, *116*, 375–376.
48. C. Dietrich-Buchecker, B. Colasson, D. Jouvenot and J.-P. Sauvage, *Chem.–Eur. J.*, **2005**, *11*, 4374–4386.
49. C. A. Hunter, *J. Am. Chem. Soc.*, **1992**, *114*, 5303–5311.
50. F. Vögtle, S. Meier and R. Hoss, *Angew. Chem., Int. Ed. Engl.*, **1992**, *31*, 1619–1622.
51. D. A. Leigh, R. J. Pritchard and M. D. Deegan, *Angew. Chem., Int. Ed. Engl.*, **1995**, *34*, 1209–1212.
52. A. G. Johnston, D. A. Leigh, L. Nezhat, J. P. Smart and M. D. Deegan, *Angew. Chem., Int. Ed. Engl.*, **1995**, *34*, 1212–1216.
53. F. J. Carver, C. A. Hunter and R. J. Shannon, *J. Chem. Soc., Chem. Commun.*, **1994**, 1277–1280.
54. O. Safarowsky, M. Nieger, R. Fröhlich and F. Vögtle, *Angew. Chem., Int. Ed.*, **2000**, *39*, 1616–1618.
55. O. Lukin and F. Vögtle, *Angew. Chem., Int. Ed.*, **2005**, *44*, 1456–1477.

56. M. Feigel, R. Ladberg, S. Engels, R. Herbst-Irmer and R. Fröhlich, *Angew. Chem., Int. Ed.*, **2006**, *45*, 5698–5702.
57. H. Adams, E. Ashworth, G. A. Breault, J. Guo, C. A. Hunter and P. C. Mayers, *Nature*, **2001**, *411*, 763–763.
58. J. Guo, P. C. Mayers, G. A. Breault and C. A. Hunter, *Nat. Chem.*, **2010**, *2*, 218–222.
59. J. D. Crowley, S. M. Goldup, A.-L. Lee, D. A. Leigh and R. T. McBurney, *Chem. Soc. Rev.*, **2009**, *38*, 1530–1541.
60. P. E. Barran, H. L. Cole, S. M. Goldup, D. A. Leigh, P. R. McGonigal, M. D. Symes, J. Wu and M. Zengerle, *Angew. Chem., Int. Ed.*, **2011**, *50*, 12280–12284.
61. P. R. Ashton, O. A. Matthews, S. Menzer, F. M. Raymo, N. Spencer, J. F. Stoddart and D. J. Williams, *Liebigs Ann./Recl.*, **1997**, 2485–2494.
62. E. E. Fenlon, *Eur. J. Org. Chem.*, **2008**, 5023–5035.
63. C. R. Woods, M. Benaglia, S. Toyota, K. Hardcastle and J. S. Siegel, *Angew. Chem., Int. Ed.*, **2001**, *40*, 749–751.
64. K. I. Arias, E. Zysman-Colman, J. C. Loren, A. Linden and J. S. Siegel, *Chem. Commun.*, **2011**, 9588–9590.
65. J. Bourlier, A. Jouaiti, N. Kyritsakas-Gruber, L. Allouche, J.-M. Planeix and M. W. Hosseini, *Chem. Commun.*, **2008**, 6191–6193.
66. T. Castle, M. E. Evans and S. T. Hyde, *New J. Chem.*, **2008**, *32*, 1484–1492.
67. F. Li, J. K. Clegg, L. F. Lindoy, R. B. Macquart and G. V. Meehan, *Nat. Commun.*, **2011**, *2*, 205.
68. D. M. Engelhard, S. Freye, K. Grohe, M. John and G. H. Clever, *Angew. Chem., Int. Ed.*, **2012**, *51*, 4747–4750.
69. D. A. Leigh, P. J. Lusby, S. J. Teat, A. J. Wilson and J. K. Y. Wong, *Angew. Chem., Int. Ed.*, **2001**, *40*, 1538–1543.
70. L. Hogg, D. A. Leigh, P. J. Lusby, A. Morelli, S. Parsons and J. K. Y. Wong, *Angew. Chem., Int. Ed.*, **2004**, *43*, 1218–1221.
71. K. S. Chichak, S. J. Cantrill, A. R. Pease, S. H. Chiu, G. W. V. Cave, J. L. Atwood and J. F. Stoddart, *Science*, **2004**, *304*, 1308–1312.
72. C. D. Pentecost, K. S. Chichak, A. J. Peters, G. W. V. Cave, S. J. Cantrill and J. F. Stoddart, *Angew. Chem., Int. Ed.*, **2007**, *46*, 218–222.

73. J. F. Ayme, J. E. Beves, D. A. Leigh, R. T. McBurney, K. Rissanen and D. Schultz, *Nat. Chem.*, **2012**, *4*, 15–20.
74. T. J. Hubin and D. H. Busch, *Coord. Chem. Rev.*, **2000**, *200*, 5–52.
75. B. Hasenknopf, J.-M. Lehn, B. O. Kneisel, G. Baum and D. Fenske, *Angew. Chem., Int. Ed. Engl.*, **1996**, *35*, 1838–1840.
76. J. F. Ayme, J. E. Beves, D. A. Leigh, R. T. McBurney, K. Rissanen and D. Schultz, *J. Am. Chem. Soc.*, **2012**, *134*, 9488–9497.
77. N. Ponnuswamy, F. B. L. Cougnon, J. M. Clough, G. D. Pantoş and J. K. M. Sanders, *Science*, **2012**, *338*, 783–785.
78. N. Ponnuswamy, F. B. L. Cougnon, G. D. Pantoş and J. K. M. Sanders, *J. Am. Chem. Soc.*, **2014**, *136*, 8243–8251.
79. T. Prakasam, M. Lusi, M. Elhabiri, C. Platas-Iglesias, J.-C. Olsen, Z. Asfari, S. Cianférani-Sanglier, F. Debaene, L. J. Charbonnière and A. Trabolsi, *Angew. Chem., Int. Ed.*, **2013**, *52*, 9956–9960.
80. J.-F. Ayme, G. Gil-Ramírez, D. A. Leigh, J.-F. Lemonnier, A. Markevicius, C. A. Muryn and G. Zhang, *J. Am. Chem. Soc.*, **2014**, *136*, 13142–13145.

Chapter II: “A synthetic molecular pentafoil knot”

Published as "A Synthetic Molecular Pentafoil Knot", J-F Ayme, J E Beves, D A Leigh, R T McBurney, K Rissanen & D Schultz, *Nature Chem.*, **2012**, *4*, 15-20.

Acknowledgements

Dr. D.Schultz and Dr. R. T. McBurney are gratefully acknowledged for their contribution to this chapter: D.S. and R.T.McB. had performed the synthesis of the knot $[\mathbf{6Cl}](\text{PF}_6)_9$ prior to the other authors arrival in Edinburgh. In a joint effort J.F.A. and J.E.B. scaled up the synthesis of $[\mathbf{6Cl}](\text{PF}_6)_9$ and obtained its full characterisation prior to studying the assembly process of the knot $[\mathbf{6Cl}](\text{PF}_6)_9$ and its corresponding circular double helicates. K. Rissanen is acknowledged for solving the crystal structure of the knot $[\mathbf{6Cl}](\text{PF}_6)_9$.

2.1. Synopsis

Knots are being discovered with increasing frequency in both biological and synthetic macromolecules and have been fundamental topological targets for chemical synthesis for the past two decades. This chapter reports the synthesis of the most complex non-DNA molecular knot prepared to date, a pentafoil knot. Building on the attempt of J.-P. Sauvage towards a pentafoil knot, a novel strategy based on Lehn's circular double helicates is presented. The self-assembly of five bis-aldehyde and five bis-amine building blocks around five metal cations and one chloride anion forms a 160-atom-loop molecular pentafoil knot (five crossing points). The structure and topology of the knot is established by NMR spectroscopy, mass spectrometry and X-ray crystallography, revealing a symmetrical closed-loop double helicate with the chloride anion held at the centre of the pentafoil knot by ten $\text{CH}\cdots\text{Cl}^-$ hydrogen bonds. In addition to the knot synthesis, the versatility of cyclic-helicate-forming-reactions is tested via the synthesis of five non-interlocked derivatives of the knot and the chloride template is removed from the knot using a large excess of a silver salt. The one-pot self-assembly reactions presented feature an exceptional number of different design elements—some well precedented and others less well known within the context of directing the formation of (supra)molecular species. It is anticipated that the strategies and tactics used here can be applied to the rational synthesis of other higher-order interlocked molecular architectures.

2.2. Introduction

Knots are important structural features in DNA¹, are found in some proteins^{2,3,4,5} and are thought to play a significant role in the physical properties of both natural and synthetic polymers^{6,7}. Although billions of prime knots are known to mathematics⁸, to date the only ones to have succumbed to chemical synthesis using building blocks other than DNA are the topologically trivial unknot (that is, a simple closed loop without any crossing points) and the next simplest knot (featuring three crossing points), the trefoil knot^{9,10}. A pentafoil knot—also known as a cinquefoil knot or Solomon's seal knot (the 5_1 knot in Alexander–Briggs notation¹¹)—is a torus knot¹² with five crossing points, is inherently chiral, and is the fourth prime knot (following the unknot, trefoil knot and figure-of-eight knot) in terms of number of crossing points and complexity^{8,11,12}.

Sauvage reported the first molecular knot synthesis¹³, using a linear metal helicate¹⁴ to generate the three crossing points required for a trefoil knot. Although other syntheses of trefoil knots have been reported^{15,16,17,18,19,20,21,22} (as have composites of trefoil knots²³ and other molecular topologies such as catenanes^{24,25,26,27,28} and Borromean links²⁹), higher-order molecular knots remain elusive. Here, we report on the synthesis of a molecular pentafoil knot that combines the use of metal helicates to create crossover points³⁰, anion template assembly to form a cyclic array of the correct size^{31,32,33}, and the joining of the metal complexes by reversible imine bond formation^{34,35,36,37} aided by the gauche effect³⁸ to make the continuous 160-atom-long covalent backbone of the most complex non-DNA molecular knot prepared to date.

So far, attempts to make molecular knots with more than three crossing points by extending the linear helicate strategy of Sauvage to ligands with more coordination sites have proved

unsuccessful³⁰, probably because joining the ends of each strand with the required connectivity becomes increasingly difficult as helicate length increases. An alternative way to use helicates (which generate the necessary crossing points) to make higher-order topologies could be to use cyclic structures or grids, where there is no requirement for there to be long distances between the ends of the strands that are to be connected. To generate the five crossing points required for a pentafoil knot, we modified a motif for generating cyclic metal helicates discovered by Lehn in the mid-1990s^{31, 32, 33}. Lehn found that double-stranded circular helicates of various sizes could be obtained using Fe(II) or Ni(II) ions with tris(bipyridine) ligands with very short inter-bipyridine spacers that destabilized the normally preferred three-metal-ion linear triple helicate. The presence of chloride ions in the reaction mixture led to the selective formation of the five-metal-ion cyclic double helicate. To have the potential to covalently connect the organic ligands to form a knot, we envisioned replacing two of the three bipyridine groups in Lehn's original building blocks with formylpyridine groups, then use their reversible reaction with amines to form imines and generate tris(bidentate) ligand strands. A decade ago we introduced reversible metal–imine bond coordination as an effective means of assembling mechanically interlocked molecules under thermodynamic control^{34, 35}. This provides a mechanism for correcting ‘mistakes’ in connectivity that occur during the covalent-capture step of mechanical bond formation and has been widely adopted for this purpose ever since^{10, 29, 36, 37}.

The reaction conditions (ethylene glycol, 170 °C)^{31, 32, 33} used to form cyclic helicates with tris(bipyridine) ligands are not compatible with imine bond formation. Because the product distribution between cyclic double helicate, linear triple helicate and polymer is a delicate thermodynamic balance that could change significantly depending on the structure

of the building blocks, reaction conditions, solvent and the nature and stoichiometry of the metal and anions, we first investigated whether it was possible to translate the self-assembly chemistry of the tris(bipyridine) ligands to an imine system.

2.3. Results and discussion

Treatment of bis-aldehyde **1** with 1-aminohexane **2a** in the presence of FeCl₂ in *d*₆-dimethylsulfoxide (CD₃SOCD₃, Figure 1) afforded a purple solution with an initially complex ¹H NMR spectrum (see Supplementary Information), indicative of the presence of a range of different monomeric, oligomeric and polymeric species. However, on heating at 60 °C, the ¹H NMR spectrum of the reaction mixture gradually simplified until, after 24 h, only a single, highly symmetrical species appeared to be present in solution. The thermodynamically driven change in product distribution can occur at relative low temperature (60 °C as opposed to the 170 °C used with tris(bipyridine)ligand strands^{31–33}) because of the reversible formation of the imine bonds and the relatively labile coordination of the iminopyridine groups, both of which promote dynamic exchange between the various reaction products and intermediates.

After cooling to room temperature, treatment with a saturated aqueous KPF₆ solution (to exchange chloride anions for hexafluorophosphates) produced a purple precipitate, which was collected by filtration and isolated in 63% yield (Figure 1). Electrospray ionization mass spectrometry (ESI-MS) showed that this material had a molecular mass and isotope pattern consistent with a supramolecular complex comprising five ligand strands, five Fe(II) cations, nine PF₆⁻ anions and one chloride anion that had not been substituted for hexafluorophosphate, [**3a**]Cl(PF₆)₉ (see Supplementary Information). The symmetry of

the ^1H NMR spectrum (Figure 2c) suggested that the pentameric complex was cyclic and the diastereotopic protons of the $\text{CH}_2\text{-Ar}$ groups (the two protons of the methylene group experience different environments) confirmed the chiral (racemic) helicate geometry shown for $[\mathbf{3a}]^{10+}$ in Figure 1. The H^a resonances of the bipyridyl ligand are deshielded by 1.42 ppm compared to $[\text{Fe}(\text{2,2}'\text{-bipyridine})_3](\text{PF}_6)_2$ (ref. 39), suggesting C–H hydrogen bonding to an electron-rich atom or ion.

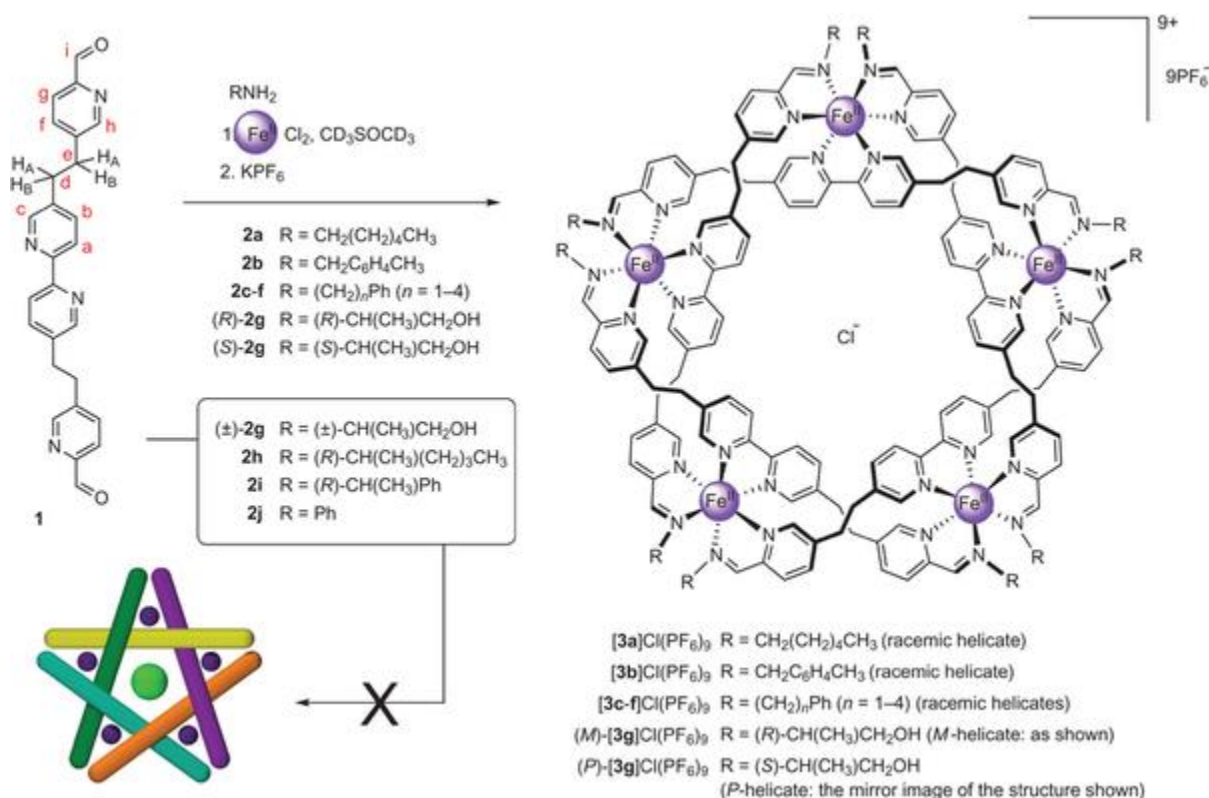


Figure 1: Chloride-template assembly of pentameric iron(II) cyclic double helicates $[\mathbf{3a-g}]\text{Cl}(\text{PF}_6)_9$. Reaction conditions: 1. d_6 -dimethylsulfoxide, 60 °C, 24 h (48 h for the formation of *(M)*-**3g** and *(P)*-**3g**Cl(PF₆)₉). 2. Excess saturated aqueous KPF₆. Yields: **[3a]Cl(PF₆)₉** (63%), **[3b]Cl(PF₆)₉** (56%), **[3c]Cl(PF₆)₉** (30%), **[3d]Cl(PF₆)₉** (43%), **[3e]Cl(PF₆)₉** (55%), **[3f]Cl(PF₆)₉** (52%), *(M)*-**3g**Cl(PF₆)₉ (34%), *(P)*-**3g**Cl(PF₆)₉ (34%). Primary amines (for example, **2a-2f**) are generally well tolerated by the cyclic-helicate-forming reaction, whereas most secondary amines (for example, **2h** and **2i**) and anilines (for example, **2j**) are not. The chiral secondary amine 2-amino-1-propanol (*(R)*-**2g** or *(S)*-**2g**) is an interesting exception; not only does it form the cyclic pentameric helicate (*(M)*-**3g** or *(P)*-**3g**Cl(PF₆)₉), but it does so diastereoselectively with the handedness of the helix dependent on the chirality of the amine used.

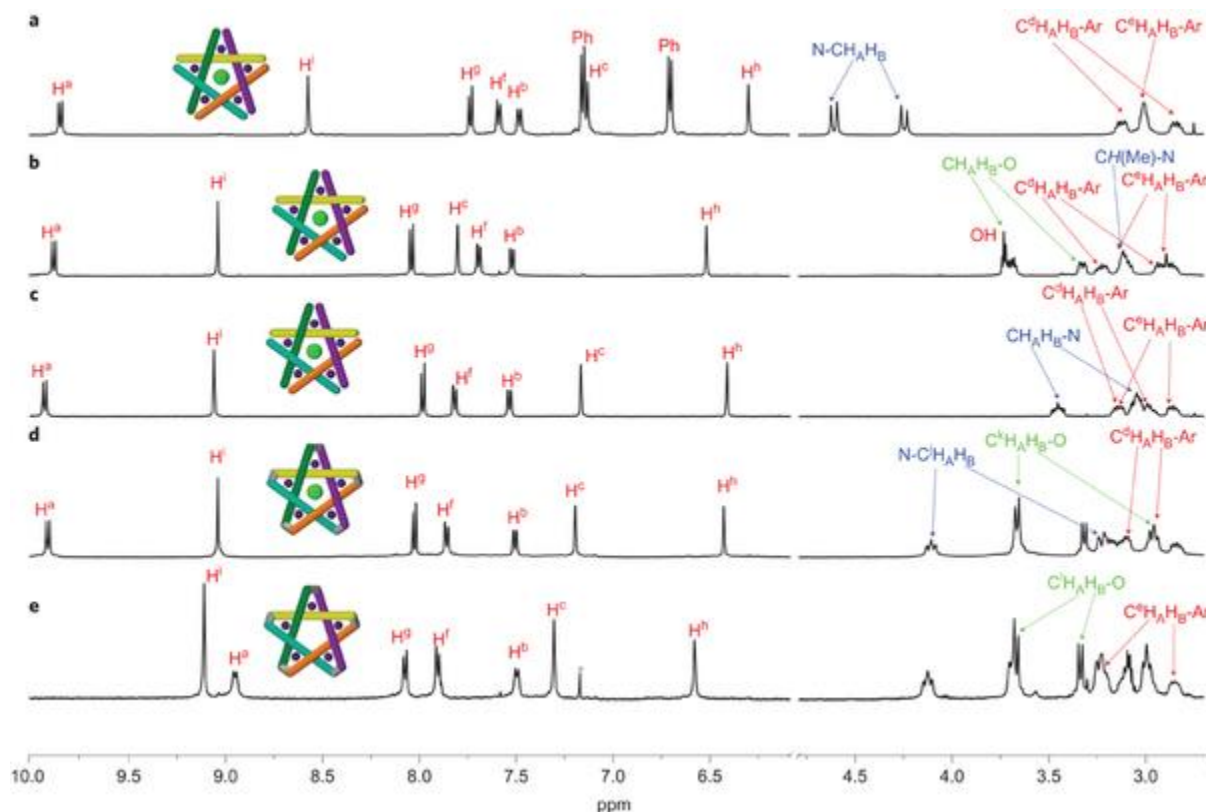


Figure 2: Partial ^1H NMR spectra (500 MHz, CD_3CN , 298 K) of cyclic double helicates and the chloride-complexed and 'empty cavity' pentafoil knot.

a, 4-Methylbenzylamine-derived pentameric cyclic helicate $[\mathbf{3b}]\text{Cl}(\text{PF}_6)_9$. b, (*R*)-2-amino-propanol-derived pentameric cyclic helicate of single handedness (*M*)- $\mathbf{3g}\text{Cl}(\text{PF}_6)_9$. c, Hexylamine-derived pentameric cyclic helicate $[\mathbf{3a}]\text{Cl}(\text{PF}_6)_9$. d, Pentafoil knot $[\mathbf{6}]\text{Cl}(\text{PF}_6)_9$. e, 'Empty cavity' pentafoil knot $[\mathbf{6}](\text{PF}_6)_{10}$ in the presence of excess AgPF_6 . The simplicity of each spectrum is indicative of a symmetrical, cyclic (no endgroups) molecular structure. The AB systems observed for certain resonances (for example, $\text{N}-\text{CH}_2\text{H}_\text{B}$) are characteristic of methylene groups in asymmetric environments (as conferred by a helix). The differences between the chemical shifts of H^f , H^g and H^h in some of the helicates probably reflect small changes in geometry at the metal centres with the different ligands. The absence of chloride in the 'empty cavity' pentafoil knot $[\mathbf{6}](\text{PF}_6)_{10}$ is signalled by the large shift in H^a (e) compared to the other complexes (a–d) in which the H^a protons are involved in strong $\text{CH}\cdots\text{Cl}^-$ hydrogen bonding. The proton assignments correspond to the lettering shown in Figs 1 and 3.

The cyclic-helicate-forming reaction proved to be tolerant to other sterically unhindered primary amines (for example, **2b–2f**, Figure 1). Use of 4-methylbenzylamine (**2b**) generated the corresponding pentameric helicate $[\mathbf{3b}]\text{Cl}(\text{PF}_6)_9$ in 56% yield. Differences in the chemical

shifts of several protons in the iminopyridyl rings (H^f , H^g and H^h) of **3a** and **3b** (Figure 2c and 2a) show that changes in the nature of the amine can influence the detailed conformation adopted by the cyclic helicate, presumably through small coordination geometry changes at the iron centres.

Anilines (for example, **2j**, Figure 1) and amines with two substituents on the amine-bearing carbon atom (for example, **2h** and **2i**, Figure 1) were generally not tolerated by the cyclic-helicate-forming reaction. However, each enantiomer of 2-amino-1-propanol (**2g**) formed the corresponding pentameric cyclic helicate in 34% yield. In this case, the helicates are formed with complete diastereoselectivity (for circular dichroism spectra see Supplementary Information), with the handedness of the cyclic helicate determined by the enantiomer of the amine used⁴⁰, suggesting that it may ultimately be possible to form topologically chiral single enantiomer knots using this assembly system. The selectivity of the particular handedness of the cyclic helicate appears to be due to favourable $CH\cdots O$ interactions between the H^c protons (shifted by 0.63 ppm relative to **2a** in the 1H NMR spectrum, Figure 2b) and the hydroxyl group of the chiral amine. Even intrinsically weak interactions such as these can have a major effect on the product distribution of the cyclic-helicate-forming reaction (in this case, one handedness of helix being significantly thermodynamically favoured over the other), because ten such interactions are present per pentameric helicate complex. However, the driving force for helix formation is not sufficiently strong to bring about ‘self-sorting’^{41, 42, 43}: racemic **2g** forms a mixture of oligomers and polymers rather than the two (*M*)-**3g** and (*P*)-**3gCl**(PF₆)₉ cyclic helicates (Figure 1).

Using the reaction conditions established for pentameric cyclic double helicate formation (Figure 1), we investigated replacing the monoamine starting material with a diamine (Figure 3). Although simple alkyl chain diamines of various lengths (**4**) gave complex mixtures of oligomers and polymers under these conditions, the use of diamine **5** led to the formation of a molecular pentafoil knot, $[\mathbf{6}]\text{Cl}(\text{PF}_6)_9$ (Figure 3). The ^1H NMR spectrum of the reaction mixture took longer to simplify than with most monoamines, but after two days showed the presence of essentially a single low-molecular-weight species (although some polymers are probably also present, consistent with the broad uneven baseline of the ^1H NMR spectrum of the crude reaction mixture, see Supplementary Information). After anion exchange and workup, $[\mathbf{6}]\text{Cl}(\text{PF}_6)_9$ was isolated in 44% yield. The yield of the knot is very sensitive to the stoichiometry of reactants used, with the best results obtained using a 1:1.1:1.1 ratio of **1**:**5**: FeCl_2 . Using strictly equimolar amounts of iron and diamine is particularly important, with even a 10% excess of amine decreasing the yield of the knot by up to half (see Supplementary Information).

Many of the signals in the ^1H NMR spectrum of pristine $[\mathbf{6}]\text{Cl}(\text{PF}_6)_9$ (Figure 2d) occur at very similar chemical shifts to the equivalent protons in the hexylamine-derived helicate **3a**¹⁰⁺ (Figure 2c), suggesting that the knot and this helicate are structurally very similar about the iron centres. ESI-MS revealed a series of m/z fragments corresponding to $[(\text{Fe}_5\text{L})\text{Cl}][\text{PF}_6]_n^{(9-n)+}$ (where L is the organic framework pentafoil knot) for $n = 2, 3, 4, 5$ and 6 , indicating that signals are observed for the molecular knot losing between two and six PF_6^- ions in the mass spectrum (see Supplementary Information).

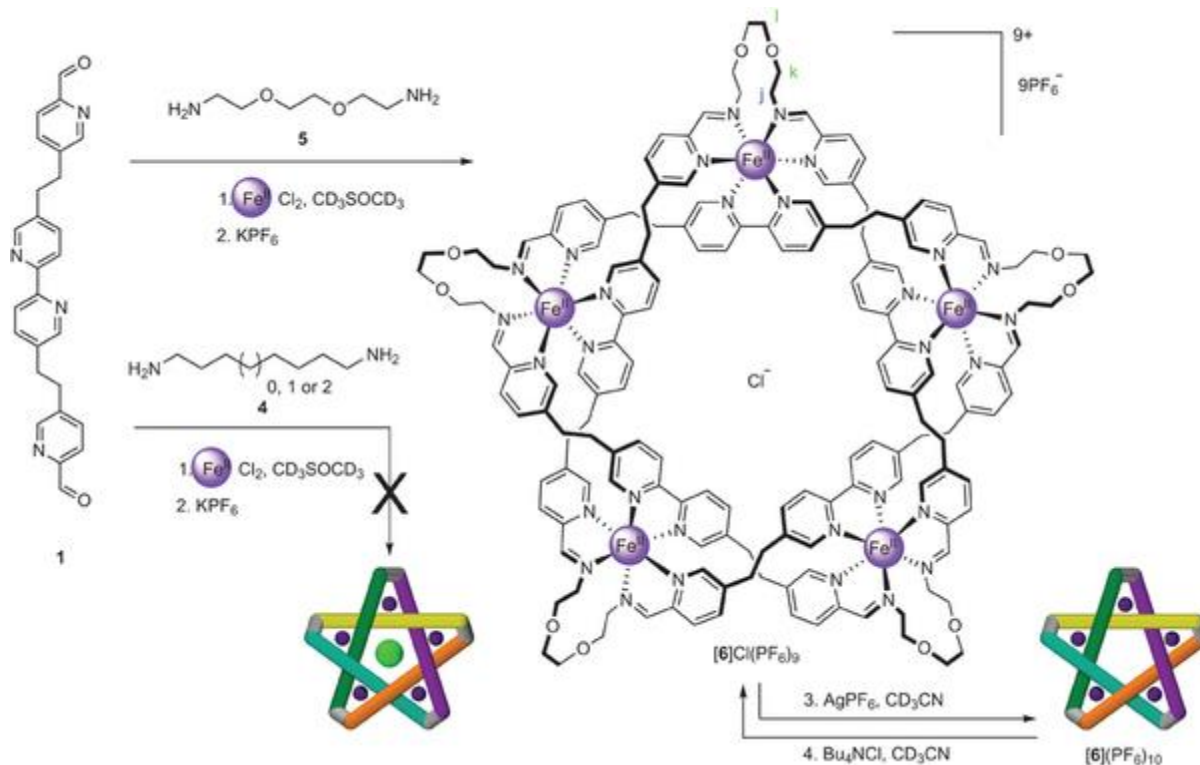


Figure 3: Synthesis of molecular pentafoil knot [6]Cl(PF₆)₉ and 'empty cavity' pentafoil knot [6](PF₆)₁₀. Reaction conditions: 1. *d*₆-dimethylsulfoxide, 60 °C, 48 h. 2. Excess saturated aqueous KPF₆. Yield of [6]Cl(PF₆)₉ from **1**, 44%. 3. AgPF₆ (90 equiv.), CD₃CN, 30 min (>98%). 4. Bu₄NCl (1 equiv.), CD₃CN, 5 min (>98%).

Single crystals of [6]Cl(PF₆)₉ were obtained by slow diffusion of diethyl ether vapour into a solution of the knot in acetonitrile:toluene (3:2) and the solid-state structure was determined by X-ray crystallography using the Diamond synchrotron source (see Supplementary Information). The crystal structure (Figure 4) confirms the topology and symmetry of the molecular pentafoil knot. The single organic ligand weaves a continuous path about the five co-planar iron centres, the loop passing over and under itself each time it wraps around a metal ion. At the centre of the structure is the chloride anion, held in place by ten CH...Cl⁻ hydrogen bonds that are presumably responsible for it not being exchanged during treatment with KPF₆ (Figure 4a). Interestingly, the chloride anion is displaced by ~1.30 Å from the least-squares plane defined by the five Fe(II) ions (Figure 4b).

Given the symmetry of the ^1H NMR spectrum, in solution the chloride anion must oscillate rapidly on the NMR timescale between the different sides of the molecular knot, accompanied by significant conformational changes in the overall framework of the structure.

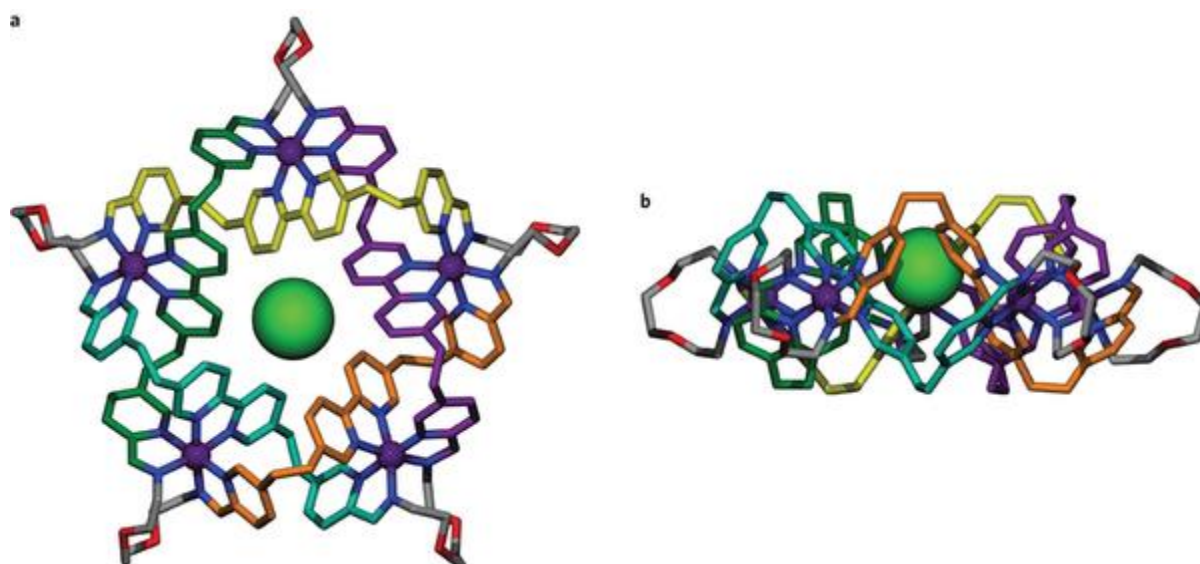


Figure 4: X-ray crystal structure of molecular pentafoil knot $[6]\text{Cl}(\text{PF}_6)_9$. Iron ions shown at 50% van der Waals radius. Chloride anion shown at 100% van der Waals radius. All other atoms shown in framework representation: nitrogen atoms, blue; oxygen atoms, red; carbon atoms originating from the diamine building block (**5**), grey; carbon atoms originating from the five dialdehyde building blocks (**1**), yellow, orange, dark green, purple and turquoise. PF_6^- anions, solvent molecules and hydrogen atoms are omitted for clarity. **a**, View from above the plane of the five octahedral Fe(II) ions, showing the symmetry and topology of the 160-atom-loop pentafoil knot with the chloride ion at the centre. $\text{CH}^a \cdots \text{Cl}^-$ distances (\AA): 2.70, 2.69, 2.71, 2.70, 2.76, 2.76, 2.71, 2.70, 2.69, 2.76. $\text{C}-\text{H}^a-\text{Cl}^-$ angles (deg): 177, 176, 176, 172, 179, 173, 176, 170, 177, 170. $\text{O}-\text{C}-\text{C}-\text{O}$ torsion angles (deg): 77(2), 64(3), 60(3), 56(3), 57(3). **b**, Side view showing the displacement of the chloride ion above the plane of the Fe(II) ions and the interwoven double helix of the ligand. Crystallographic data and experimental details of the structural refinement for $[6]\text{Cl}(\text{PF}_6)_9$ are provided in the Supplementary Information.

The conformations of the groups used to link the metal centres suggest why the pentafoil knot is not favoured using simple alkyl chain diamines (Figure 4a). To connect each metal

centre to the next, the bis-amine spacer must form a loop that allows its two amine groups to form imine bonds that coordinate to the same metal ion. Sequences of $-\text{CH}_2-$ groups prefer antiperiplanar arrangements of carbon atoms (that is, 180° C–C–C–C torsional angles), and forcing a chain to turn back on itself brings some of the C–H groups into pseudo-1,3-diaxial steric clashes. In contrast, the lowest energy conformation of $-\text{XCH}_2\text{CH}_2\text{O}-$ ($\text{X}=\text{O}, \text{N}$) units has the carbon-heteroatom bonds at 60° to each other, a gauche conformation that is favoured for stereoelectronic reasons³⁸, producing a low-energy turn. The lack of hydrogen atoms on the oxygen atoms also minimizes the steric interactions that occur as a consequence of the turn. Although the energetic cost of each of these effects may be individually small, multiplying them fivefold, as would be required to assemble a molecular pentafoil knot from alkyl chain diamines, is sufficient to tip the thermodynamic balance away from the cyclic-helicate knot to other oligomeric and polymeric products.

Treatment of $[\mathbf{6}]\text{Cl}(\text{PF}_6)_9$ with a large excess (90 equiv.) of AgPF_6 in CD_3CN (298 K, 30 min, Figure 3) caused significant changes in parts of the ^1H NMR spectrum (Figure 2e). The H^a protons, heavily deshielded in $[\mathbf{6}]\text{Cl}(\text{PF}_6)_9$ due to $\text{CH}\cdots\text{Cl}^-$ hydrogen bonding (Figure 2d), were shifted to 8.95 ppm (Figure 2e), indicating that the final chloride anion had been exchanged for hexafluorophosphate (confirmed by mass spectrometry), generating the empty cavity pentafoil knot $[\mathbf{6}](\text{PF}_6)_{10}$ (Figure 3). Treatment of $[\mathbf{6}](\text{PF}_6)_{10}$ with Bu_4NCl smoothly regenerates $[\mathbf{6}]\text{Cl}(\text{PF}_6)_9$ (Figure 3), but the ^1H NMR spectrum of the empty pentafoil knot shows no changes upon addition of other tetrabutylammonium salts (for example, Bu_4NBr , and Bu_4NI), demonstrating that $[\mathbf{6}](\text{PF}_6)_{10}$ is a selective cavitand for the chloride ion.

2.4. Conclusion

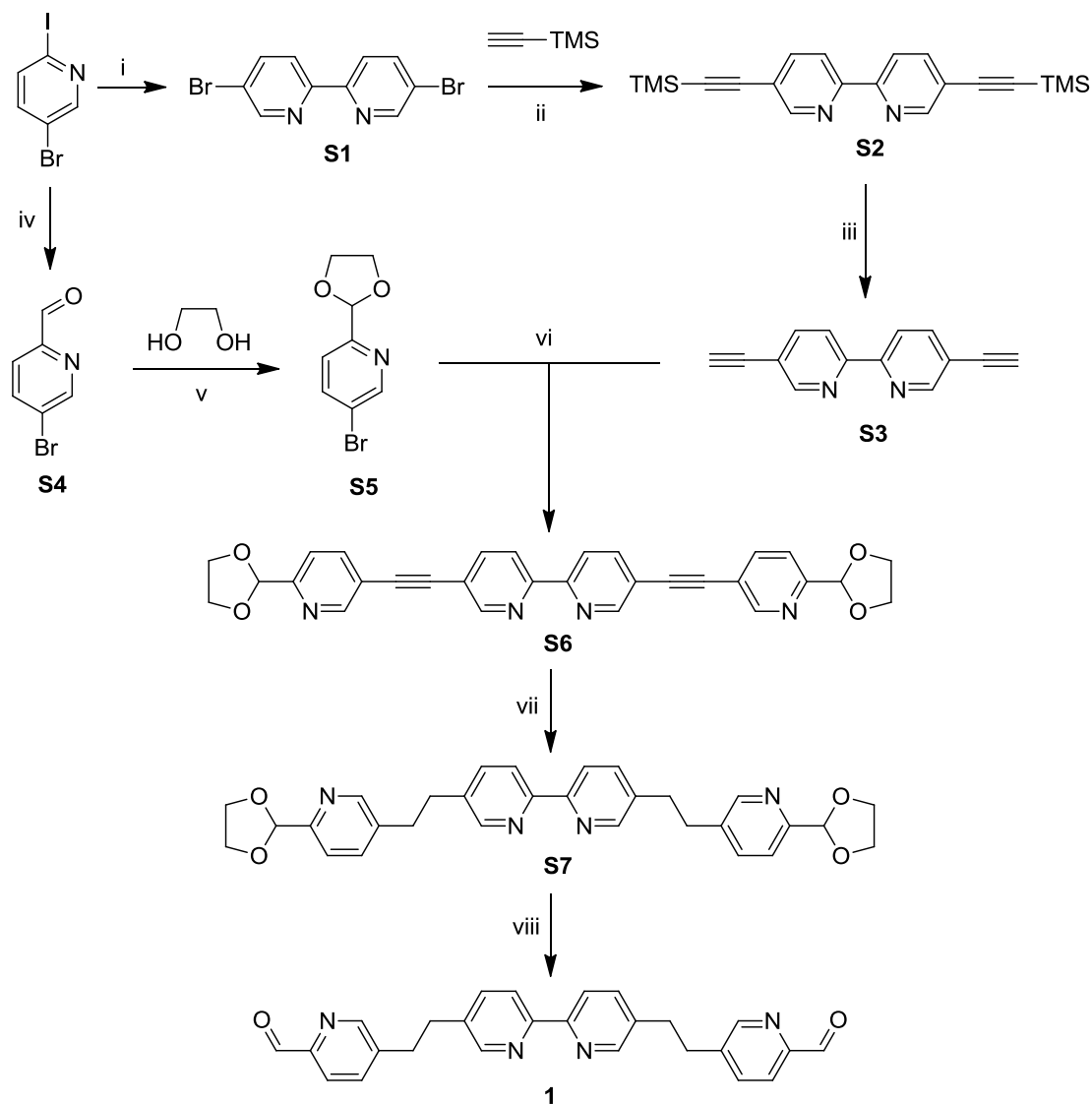
The one-step synthesis of molecular pentafoil knot $[6]Cl(PF_6)_9$ assembles five metal cations, five bis-aldehyde and five bis-amine building blocks about one chloride anion, in 44% isolated yield. The number of different design features that are combined to assemble the knot is exceptional: the system uses octahedral metal-ion helicate formation to generate entwined ligand strands, short linkers between chelating groups to favour cyclic double helicates over linear triple helicates, anion template synthesis to select the correct number of crossing points, and reversible imine bond formation to join the complexes with the required strand-to-strand connectivity. Macrocyclization to form the covalent backbone of the pentafoil knot makes use of stereoelectronic effects to favour the required turns in the linking units and ligand–ligand interactions to promote mechanical bond formation over polymer formation. The symmetry of the cyclic helicate structures means that even individually rather weak interactions can significantly perturb the product distribution in the reaction mixture, in some cases usefully (for example, to form cyclic helicates of a particular handedness) and in others detrimentally (for example, to disfavour knot formation).

The pentafoil knot has symbolic significance in many ancient and modern cultures and religions (as does its two-dimensional projection, the pentagram) and features as the central emblem on the present-day flags of both Morocco and Ethiopia. The practical significance of its preparation in molecular form includes the lessons learned from the multitude of different structural design features¹⁰ used in its assembly and the potential for the synthesis of higher-order structures with precisely defined knotted architectures that may enable the role of entanglements in molecular materials to be elucidated and exploited.

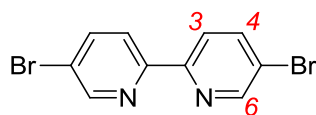
2.5. Experimental Section

2.5.1. Synthesis

2.5.1.1. Synthesis of dialdehyde **1**

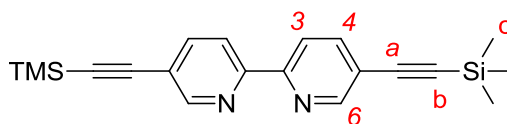


Scheme 1. Preparation of dialdehyde **1**. Reagents and conditions: (i) $\text{Pd}(\text{PPh}_3)_4$, $n\text{-Bu}_6\text{Sn}_2$, toluene, $125\text{ }^\circ\text{C}$, 3 days, 74%; (ii) $\text{Pd}(\text{PPh}_3)_4$, CuI , toluene, NEt_3 , $50\text{ }^\circ\text{C}$, overnight, 87%; (iii) K_2CO_3 , MeOH , THF , overnight, 85%; (iv) a) $i\text{-PrMgCl}$, THF , $-10\text{ }^\circ\text{C}$, 1 hour, b) DMF , $-10\text{ }^\circ\text{C}$, 1 hour, 90%; (v) $p\text{-TsOH}$, toluene, reflux, 44h, 97%; (vi) $\text{Pd}(\text{PPh}_3)_4$, THF , NEt_3 , $60\text{ }^\circ\text{C}$, 2d, 58%; (vii) H_2 , $\text{Pd}(\text{OH})_2/\text{C}$, $\text{THF}/\text{methanol}$, 48h, 80%; (viii) 10% HCl , reflux, 1 hour, 82%.

**S1**

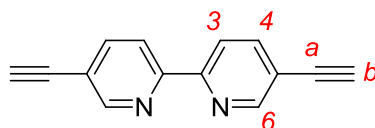
S1 was prepared by a modified literature procedure.⁴⁴

5-Bromo-2-iodopyridine (6.60 g, 23.2 mmol) was dissolved in anhydrous toluene (120 mL) and N₂ was bubbled through the solution for 15 min. Pd(PPh₃)₄ (0.72 g, 0.62 mmol) and *n*-Bu₆Sn₂ (7.25 g, 12.5 mmol) were added and the solution was degassed. The mixture was stirred at reflux for 3 days. The reaction mixture was cooled down and diethylether (about 200 mL) was added. The white-brown precipitate that formed was filtered and washed consecutively with distilled water and diethylether. The precipitate was dissolved in CHCl₃ and the solution was washed with brine, dried (MgSO₄) and concentrated under reduced pressure to afford **S1** as a colorless solid (2.71 g, 8.6 mmol, 74%). NMR in agreement with literature. ¹H NMR (500 MHz, CDCl₃) δ 8.71 (d, *J* = 2.2 Hz, 2H, H⁶), 8.29 (d, *J* = 8.5 Hz, 2H, H³), 7.94 (dd, *J* = 8.5, 2.4 Hz, 2H, H⁴). ¹³C NMR (126 MHz, CDCl₃) δ 153.8 (C²), 150.4 (C⁶), 139.8 (C⁴), 122.4 (C³), 121.6 (C⁵). HREI-MS: *m/z* = 312.8974, C₁₀H₇N₂Br₂ requires 312.8971 *m/z*. m.p. 212–214 °C, literature⁴⁵ 224–225 °C).

**S2**

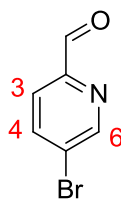
Trimethylsilylacetylene (4 mL, 28.1 mmol) was added to a degassed solution of **S1** (3.0 g, 9.5 mmol) in a mixture of toluene (200 mL) and NEt₃ (75 mL) and N₂ was bubbled through the

solution for 5 min. Pd(PPh₃)₄ (1.11 g, 0.96 mmol, 10%) and CuI (0.27 g, 1.42 mmol, 15%) were added and the solution was degassed again. The mixture was stirred at 60 °C overnight under nitrogen. The solution was concentrated under reduced pressure, the residue dissolved in CH₂Cl₂ and washed with an aqueous saturated solution of NH₄Cl, then brine, dried (MgSO₄) and absorbed onto SiO₂ and the solvent removed. Flash chromatography (SiO₂, CH₂Cl₂:MeOH 100:0 to 99:1) afforded **S2** as a pale yellow solid (2.9 g, 8.3 mmol, 87%). NMR in agreement with literature.⁴⁶ ¹H NMR (400 MHz, CDCl₃) δ 8.72 (dd, *J* = 2.0, 0.7 Hz, 2H, H⁶), 8.35 (dd, *J* = 8.3, 0.7 Hz, 2H, H³), 7.86 (dd, *J* = 8.3, 2.1 Hz, 2H, H⁴), 0.28 (s, 18H, H^c). ¹³C NMR (101 MHz, CDCl₃): δ = 154.3 (C²), 152.2 (C⁶), 139.9 (C⁴), 120.6 (C³), 120.5 (C⁵), 101.9 (C^{a/b}), 99.6 (C^{a/b}), -0.02 (C^c). HRESI-MS: *m/z* = 349.1552 [M+H]⁺ (calcd. for C₂₀H₂₅N₂Si₂ 349.1551). m.p. 162-164 °C, literature⁴⁷ 176-8 °C.

**S3**

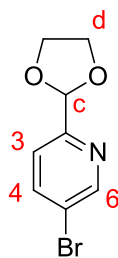
S2 (2.9 g, 8.3 mmol) was dissolved in methanol : THF (1:1, 150 mL) and powdered K₂CO₃ (1 g, 7 mmol) was added. The mixture was stirred overnight at room temperature and the solvent reduced to 50 mL, CH₂Cl₂ (150mL) was added and the mixture was washed with brine (2 x 100 mL). The organic fraction was treated with activated charcoal, dried over MgSO₄ and the solvent was removed under reduced pressure. Flash chromatography (CH₂Cl₂:EtOH 100:0 to 95:5) afforded **S3** as a beige solid (1.4 g, 7.0 mmol, 85%). ¹H NMR (400 MHz, CDCl₃) 8.77 (d, *J* = 1.5 Hz, 2H, H⁶), 8.39 (d, *J* = 8.2 Hz, 2H, H³), 7.91 (dd, *J* = 8.2, 2.1

Hz, 2H, H⁴), 3.31 (s, 2H, H^b). ¹³C NMR (100 MHz, CDCl₃) δ =154.7 (C²), 152.4 (C⁶), 140.2 (C³), 120.7 (C⁴), 119.6 (C⁵), 81.8 (C^{a/b}), 80.7 (C^{a/b}). NMR assignments differ from literature.^{46,47}

**S4**

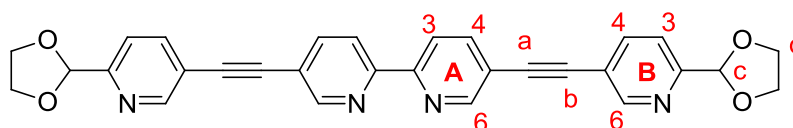
S4 was prepared by a literature procedure.⁴⁸

In a 250 mL, two-neck, round-bottom flask 10 g (35 mmol) of 5-bromo-2-iodopyridine was dissolved in 60 mL of THF. The solution was cooled to -10 °C and 2 M *i*-PrMgCl (19 mL, 38 mmol) was added over 30 min at a rate to maintain the temperature below 0 °C. The reaction mixture became a brown suspension. After the reaction mixture was stirred between -15 to 0 °C for 1 h, anhydrous DMF (4 mL, 51 mmol) was slowly (temperature maintained below 0 °C). The reaction mixture was stirred at 0 °C for 30 min and allowed to warm to room temperature over 1 h. The reaction mixture was then cooled to 0 °C, and 2M HCl (40 mL) was added with the internal temperature maintained below 25 °C and stirred for 30 min. The pH was adjusted to pH 6-7 by addition of 2 M NaOH. The organic phase was separated and the aqueous phase was extracted with CH₂Cl₂ (3x 100 mL). The combined organic phases were washed with water (2x 100 mL), dried over MgSO₄ and the solvent removed to give **S4** as a brownish-yellow solid (5.9 g, 31 mmol, 90% yield) which was used in the subsequent step without further purification.

**S5**

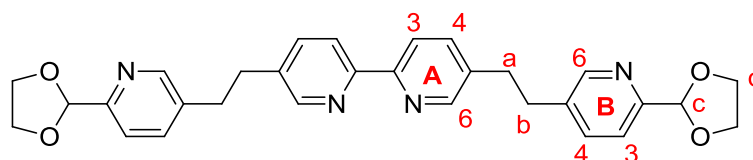
S5 was prepared by a modified procedure.⁴⁹

S4 (1.1 g, 5.9 mmol) and ethylene glycol (0.66 mL, 11.8 mmol) were dissolved in toluene (60 mL) and TsOH (0.12 g, 0.63 mmol) was added. The mixture was stirred under reflux using a Dean-Stark for 44 hours. A 1% aqueous solution of Na₂CO₃ (60 mL) was added and the two phases were separated. The aqueous layer was extracted with CHCl₃ and the organic phases were combined, dried (MgSO₄) and concentrated under reduced pressure. Flash chromatography (petroleum ether : EtOAc 95:5 to 80:20) afforded **S5** as a colorless solid (1.33 g, 5.8 mmol 97%). ¹H NMR (500 MHz, CDCl₃) δ 8.67 (dd, *J* = 2.3, 0.5 Hz, 1H, H⁶), 7.85 (dd, *J* = 8.3, 2.3 Hz, 1H, H⁴), 7.43 (d, *J* = 8.3 Hz, 1H, H³), 5.81 (s, 1H, H^c), 4.20–3.99 (m, 4H, H^d). ¹³C NMR (126 MHz, CDCl₃) δ 155.8 (C²), 150.6 (C⁶), 139.5 (C⁴), 122.2 (C³), 121.2 (C⁵), 103.2 (C^c), 65.7 (C^d). HRESI-MS: *m/z* = 229.9815 [M+H]⁺ (calcd. for C₈H₉O₂N₁Br, 229.9811). m.p. 50-52 °C.

**S6**

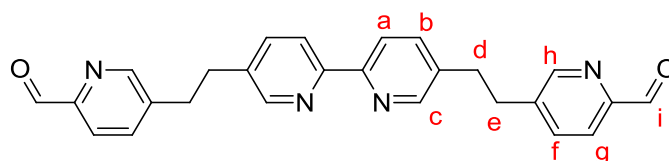
S3 (1.25 g, 6.1 mmol) and **S5** (3.08 g, 13.4 mmol) were dissolved in a mixture of THF (150 mL) and NEt₃ (30 mL). Then N₂ was bubbled through the solution for 10 minutes and

$\text{Pd}(\text{PPh}_3)_4$ (2.82 g, 2.4 mmol, 40%) was added and the solution was degassed again for 10 minutes. The solution was stirred at 60 °C for 2 days and then cooled down to room temperature. Activated carbon was added and the mixture was filtered over celite. The filtrate was absorbed onto SiO_2 and flash chromatography ($\text{CH}_2\text{Cl}_2:\text{CH}_3\text{OH}$ 100:0 to 96:4, product fluorescent blue under UV light) afforded crude **S6** as a slightly yellow solid which was dissolved in a minimum of CH_2Cl_2 and petroleum ether (100 mL) added to precipitate pure **S6** as a colorless solid (1.80 g, 3.5 mmol, 58%). ^1H NMR (400 MHz, CDCl_3): δ 8.84 (d, J = 1.5 Hz, 2H, H^{A6}), 8.81 (d, J = 1.4 Hz, 2H, H^{B6}), 8.47 (d, J = 8.3 Hz, 2H, H^{A3}), 7.98 (dd, J = 8.3, 2.1 Hz, 2H, H^{A4}), 7.91 (dd, J = 8.1, 2.0 Hz, 2H, H^{B4}), 7.57 (d, J = 8.1 Hz, 2H, H^{B3}), 5.89 (s, 2H, H^{C}), 4.24 – 4.06 (m, 8H, H^{d}). ^{13}C NMR (101 MHz, CDCl_3) δ 156.6 (C^{B2}), 154.6 (C^{A2}), 152.0 x 2 (C^{A6} , C^{B6}), 139.7 (C^{A4}), 139.5 (C^{B4}), 120.9 (C^{B3}), 120.4 (C^{A3}), 120.2 (C^{B5}), 120.0 (C^{A5}), 103.4 (C^{C}), 90.3 (C^{b}), 90.0 (C^{a}), 65.8 (C^{d}). HRESI-MS: m/z = 503.1706 $[\text{MH}]^+$ (calcd. for $\text{C}_{30}\text{H}_{23}\text{N}_4\text{O}_4$, 503.1714). m.p. 264-266 °C (dec.).

**S7**

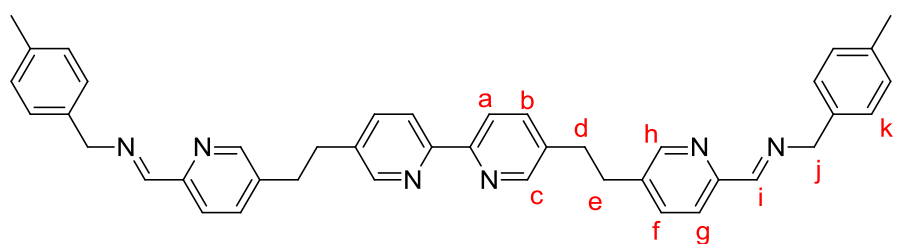
S6 (1.80 g, 3.5 mmol) was dissolved in THF:MeOH 2:1 (300 mL) and 20% w/w $\text{Pd}(\text{OH})_2/\text{C}$ (0.51 g) was added. The mixture was stirred under H_2 for 48 hours. The mixture was filtered through Celite and the residue washed with CH_2Cl_2 . The filtrate fractions were combined and the solvent removed under reduced pressure. The resulting yellow solid was purified by flash chromatography (SiO_2 , $\text{CH}_2\text{Cl}_2:\text{CH}_3\text{OH}:\text{NEt}_3$ 100:0:0 to 95:4:1) to yield to **S7** as a colorless solid (1.47 g, 2.8 mmol, 80%). ^1H - NMR (500 MHz, CDCl_3) δ 8.47 (d, J = 1.7 Hz, 2H, H^{B6}), 8.46 (d, J = 2.0 Hz, 2H, H^{A6}), 8.26 (d, J = 8.1 Hz, 2H, H^{A3}), 7.57 (dd, J = 8.1, 2.3 Hz, 2H,

H^{A4}), 7.49 (dd, $J = 8.0, 2.2$ Hz, 2H, H^{B4}), 7.44 (d, $J = 8.0$ Hz, 2H, H^{B3}), 5.84 (s, 2H, H^c), 4.24 – 4.03 (m, 8H, H^d), 2.99 (s, 8H, H^{a+b}). ^{13}C NMR (126 MHz, $CDCl_3$) δ 155.2 (C^{B2}), 154.5 (C^{A2}), 149.7 (C^{B6}), 149.4 (C^{A6}), 137.1 (C^{A4}), 136.9 (C^{B4}), 136.6 (C^{B5}), 136.1 (C^{A5}), 120.8 (C^{A3}), 120.6 (C^{B3}), 103.7 (C^c), 65.7 (C^d), 34.5 ($C^{a/b}$), 34.4 ($C^{a/b}$). HRESI-MS: $m/z = 511.2335$ [$M+H$] $^+$ (calcd. for $C_{30}H_{31}N_4O_4$, 511.2340). m.p. 278–280 °C (dec.).

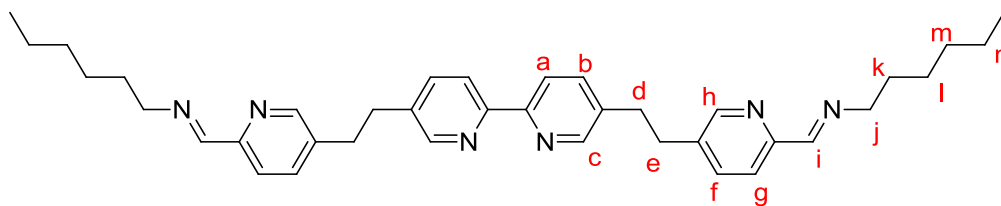
**1**

S7 (1.06 g, 2.1 mmol) was dissolved in 10% aqueous HCl (250 mL) and refluxed for 1 hour, cooled to room temperature and neutralized by slow addition of solid $NaHCO_3$. The mixture was extracted with CH_2Cl_2 and the organic fraction was washed with brine, dried over $MgSO_4$ and concentrated under reduced pressure. Flash chromatography (SiO_2 , CH_2Cl_2 to $CH_2Cl_2 : CH_3OH : NEt_3$ 94:4:2) afforded **1** as a colorless solid (0.727 g, 1.7 mmol, 82%). 1H NMR (500 MHz, $CDCl_3$) δ 10.05 (d, $J = 0.7$ Hz, 2H, H^i), 8.58 (d, $J = 1.6$ Hz, 2H, H^c), 8.43 (d, $J = 1.8$ Hz, 2H, H^h), 8.27 (d, $J = 8.1$ Hz, 2H, H^a), 7.89 (dd, $J = 7.9, 0.6$ Hz, 2H, H^g), 7.63 (dd, $J = 7.9, 1.6$ Hz, 2H, H^f), 7.56 (dd, $J = 8.1, 2.3$ Hz, 2H, H^b), 3.27 – 2.85 (m, 8H, H^{d+H^e}). 1H NMR (500 MHz, CD_3CN) δ 9.96 (d, $J = 0.7$ Hz, 2H, CHO), 8.60 (d, $J = 1.6$ Hz, 2H, H^c), 8.42 (d, $J = 1.9$ Hz, 2H, H^h), 8.27 (d, $J = 8.1$ Hz, 2H, H^a), 7.85 (dd, $J = 7.9, 0.6$ Hz, 2H, H^g), 7.78 (dd, $J = 7.9, 1.7$ Hz, 2H, H^f), 7.67 (dd, $J = 8.1, 2.3$ Hz, 2H, H^b), 3.14–3.00 (m, 10H, H^{d+H^e}). 1H NMR (500 MHz, $DMSO-d_6$) δ 9.94 (d, $J = 0.7$ Hz, 2H, C^c), 8.68 (d, $J = 1.4$ Hz, 2H, H^c), 8.49 (d, $J = 1.7$ Hz, 2H, H^h), 8.25 (d, $J = 8.1$ Hz, 2H, H^a), 7.92 (dd, $J = 7.9, 1.6$ Hz, 2H, H^f), 7.87 (dd, $J = 7.9, 0.7$ Hz, 2H, H^g), 7.79 (dd, $J = 8.2, 2.3$ Hz, 2H, H^b), 3.13–3.02 (m, 8H, H^{d+H^e}). ^{13}C NMR (126 MHz, $CDCl_3$) δ

193.2 (Cⁱ), 154.6 (N-C-C^g), 151.5 (N-C-C^a), 150.6 (C^c), 149.4 (C^h), 141.3 (C^f-C-C^h), 137.1 x 2 (C^b + C^f), 135.6 (C^c-C-C^b), 121.7 (C^g), 120.8 (C^a), 34.7 (C^d/C^e), 34.1 (C^d/C^e). HRESI-MS: $m/z = 423.1812$ [M+H]⁺ (calcd. for C₂₆H₂₃N₄O₂, 423.1816). m.p. 212-214 °C.

2.5.1.2. Synthesis of bis(imino) ligands **S8** and **S9****S8**

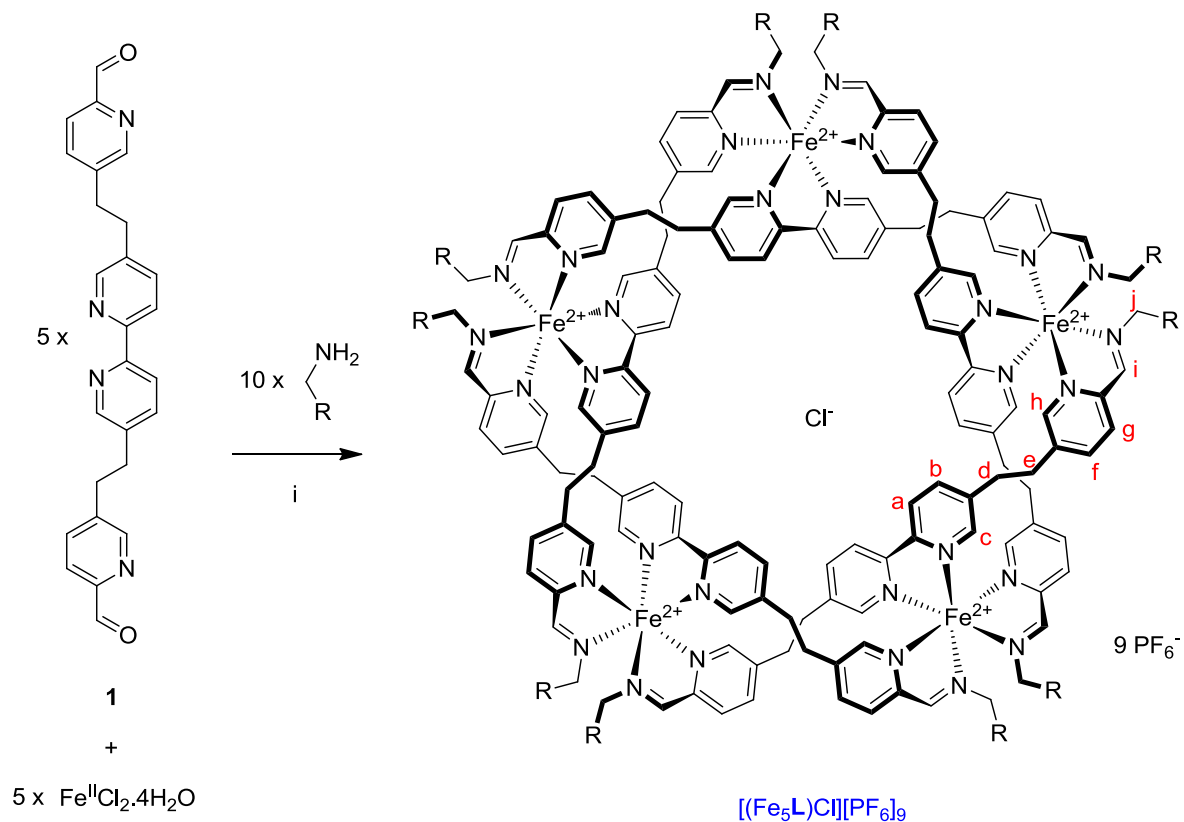
Dialdehyde **1** (50 mg, 120 μmol) was dissolved in hot MeOH (20 mL) and two drops of glacial acetic acid were added. 4-Methylbenzylamine (30 μL) was added and the mixture was refluxed for 3h. The solution was cooled to room temperature and the white precipitate was collected and washed with EtOH (\sim 2mL) to give **S8** as a colorless powder (55 mg, 87 μmol , 74%). ^1H NMR (400 MHz, CDCl_3) δ 8.48–8.38 (m, 6H, $\text{H}^c + \text{H}^h + \text{H}^i$), 8.25 (d, $J = 8.1$ Hz, 2H, H^a/H^b), 7.96 (d, $J = 8.1$ Hz, 2H, H^a/H^b), 7.55 (dd, $J = 8.1, 2.2$ Hz, 2H, H^b/H^f), 7.50 (dd, $J = 8.1, 2.1$ Hz, 2H, H^b/H^f), 7.23 (d, $J = 7.9$ Hz, 4H, H^k/H^l), 7.16 (d, $J = 7.9$ Hz, 4H, H^k/H^l), 4.82 (s, 2H, H^j), 3.01 (s, 4H, H^d+H^e), 2.34 (s, 6H, CH_3). ^1H NMR (500 MHz, DMSO) δ 8.52–8.45 (m, 4H, H^c+H^h), 8.42 (s, 2H, H^i), 8.24 (d, $J = 8.1$ Hz, 2H, H^a/H^b), 7.89 (d, $J = 8.1$ Hz, 2H, H^a/H^b), 7.76 (m, 4H, H^b+H^f), 7.21 (d, $J = 8.0$ Hz, 4H, H^k/H^l), 7.15 (d, $J = 7.9$ Hz, 4H, H^k/H^l), 4.77 (s, 4H, H^j), 3.01 (s, 4H, H^d+H^e), 2.28 (s, 3H, CH_3). ^{13}C NMR (101 MHz, CDCl_3) δ 162.5 (C^i), 154.5 ($\text{N}-\underline{\text{C}}-\text{C}^a/\text{N}-\underline{\text{C}}-\text{C}^b$), 153.0 ($\text{N}-\underline{\text{C}}-\text{C}^a/\text{N}-\underline{\text{C}}-\text{C}^b$), 149.6 (C^c/C^h), 149.4 (C^c/C^h), 137.6 ($\text{C}^c-\underline{\text{C}}-\text{C}^b/\text{C}^f-\underline{\text{C}}-\text{C}^h$), 137.1 (C^b/C^f), 136.9 ($\text{C}^c-\underline{\text{C}}-\text{C}^b/\text{C}^f-\underline{\text{C}}-\text{C}^h$), 136.8 (C^b/C^f), 135.9 ($\text{C}^k-\underline{\text{C}}-\text{C}^l/\underline{\text{C}}-\text{Me}$), 135.7 ($\text{C}^k-\underline{\text{C}}-\text{C}^l/\underline{\text{C}}-\text{Me}$), 129.4 (C^l), 128.3 (C^k), 121.2 (C^a/C^b), 120.8 (C^a/C^b), 64.8 (C^j), 34.6 (C^d/C^e), 34.4 (C^d/C^e), 21.3 (CH_3). HRESI-MS: $m/z = 629.3382$ [$\text{M}+\text{H}$] $^+$ (calcd. for $\text{C}_{42}\text{H}_{41}\text{N}_6$, 629.3387). m.p. 224–226 $^\circ\text{C}$

**S9**

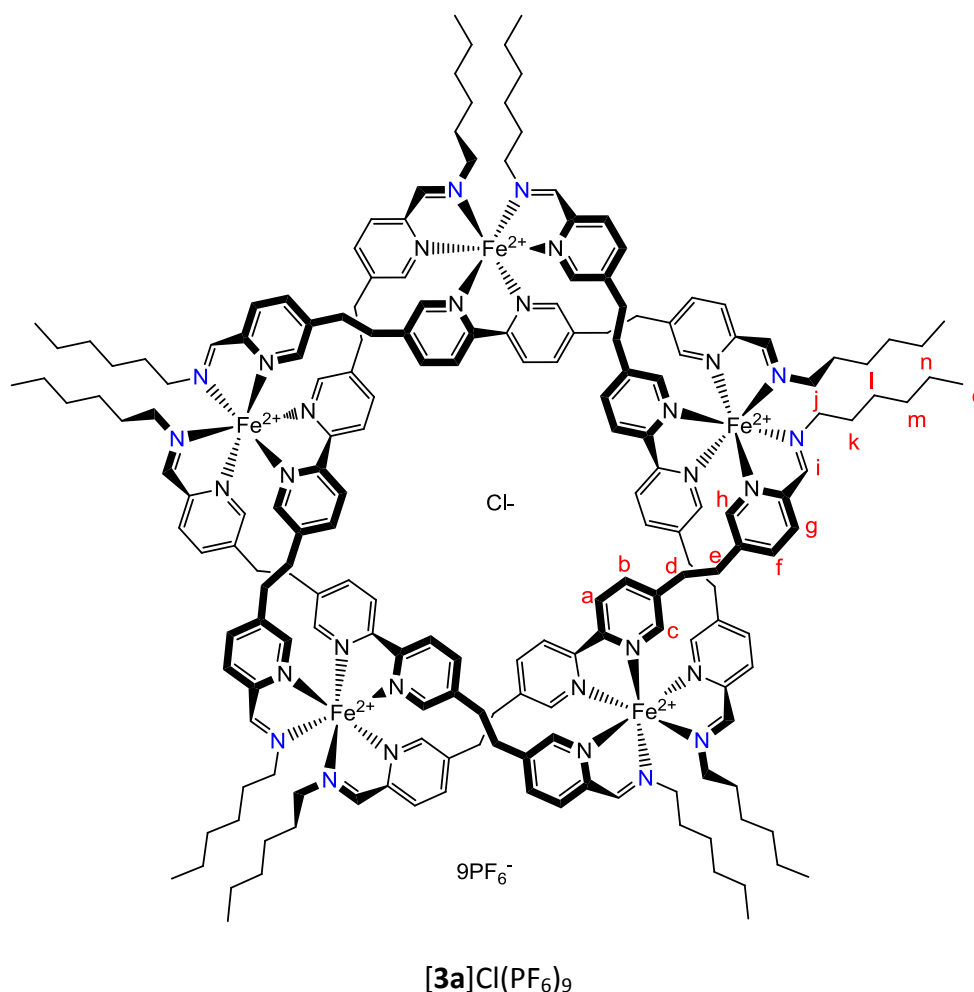
Dialdehyde **1** (10 mg, 24 μmol) was dissolved in hot MeOH (50 mL) and two drops of glacial acetic acid were added. 1-Hexylamine (10 μL , 75 μmol , 3 eq) was added and the mixture was refluxed for 3h. The solution was cooled to room temperature and the volume reduced to precipitate **S9** as a fine colorless powder which was collected and washed with chilled MeOH (~5mL) (17mg, 29 μmol , 55%). ^1H NMR (500 MHz, CDCl_3) δ 8.47–8.41 (m, 4H, $\text{H}^{\text{c}}/\text{H}^{\text{h}}$), 8.34 (t, $J = 1.5$ Hz, 2H, H^{i}), 8.26 (dd, $J = 8.2, 0.5$ Hz, 2H, H^{a}), 7.89 (dd, $J = 8.1, 0.6$ Hz, 2H, H^{g}), 7.56 (dd, $J = 8.2, 2.3$ Hz, 2H, H^{b}), 7.50 (dd, $J = 8.1, 2.1$ Hz, 2H, H^{f}), 3.65 (td, $J = 7.0, 1.1$ Hz, 4H, H^{j}), 3.01 (s, 8H, $\text{H}^{\text{d}}+\text{H}^{\text{e}}$), 1.71 (p, $J = 7.1$ Hz, 4H, H^{k}), 1.45 – 1.24 (m, 12H, $\text{H}^{\text{l}} + \text{H}^{\text{m}} + \text{H}^{\text{n}}$), 0.89 (t, $J = 7.0$ Hz, 6H, CH_3). ^{13}C NMR (126 MHz, CDCl_3) δ 161.6 (C^{i}), 154.5 (N– C^{a}), 153.1 (N– C^{g}), 149.7 (C^{c}), 149.4 (C^{h}), 137.4 ($\text{C}^{\text{f}}-\text{C}^{\text{h}}$), 137.1 (C^{e}), 136.8 (C^{f}), 136.0 ($\text{C}^{\text{c}}-\text{C}^{\text{b}}$), 121.1 (C^{g}), 120.8 (C^{a}), 61.8 (C^{j}), 34.6 ($\text{C}^{\text{d}}/\text{C}^{\text{e}}$), 34.4 ($\text{C}^{\text{d}}/\text{C}^{\text{e}}$), 31.8 (C^{m}), 30.9 (C^{k}), 27.2 (C^{l}), 22.8 (C^{n}), 14.2 (CH_3). HRESI-MS: $m/z = 589.3997$ [$\text{M}+\text{H}$] $^+$ (calcd. for $\text{C}_{38}\text{H}_{49}\text{N}_6$, 589.4013). m.p. 256–258 $^\circ\text{C}$.

2.5.1.3. Synthesis of cyclic helicates

The general synthetic procedure for forming circular helicates is shown in Scheme 2.



Scheme 2. Preparation of helicates **[3a-g]Cl(PF₆)₉** and knot **[6]Cl(PF₆)₉**. Reagents and conditions: (i) a) DMSO, 60 °C, 24 h (48 h for **[3g]Cl(PF₆)₉**), b) Excess saturated aqueous KPF₆.

2.5.1.3.1. Preparation of helicate $[3a]Cl(PF_6)_9$ 

A DMSO- d_6 solution of anhydrous $FeCl_2$ (250 μ L of 210 mM, 52 μ mol, 1.1 eq.) was added to dialdehyde **1** (20 mg, 47 μ mol, 1 eq) in DMSO- d_6 (10 mL) The resulting purple solution was treated in an ultrasonic bath for 10 min and heated at 60°C for 30 min to ensure complete dissolution of the dialdehyde. A DMSO- d_6 solution of hexylamine (1.00 mL of a 100 mM DMSO- d_6 solution, 100 μ mol, 2.2 equivalents) was added to the mixture. The resulting dark purple mixture was heated at 60 °C for one day. After cooling to room temperature, excess saturated aqueous KPF_6 was added (~5 mL). A fine suspension of a purple material formed which was collected on Celite, thoroughly washed with water, EtOH, DCM and

diethylether. The purple solid was dissolved in acetonitrile and concentrated under reduced pressure to give **[3a]**Cl(PF₆)₉ as a purple powder (27 mg, 5.9 μmol, 63%). ¹H NMR: (500 MHz, CD₃CN) δ 9.93 (d, *J* = 8.3 Hz, 10H, H^a), 9.06 (s, 10H, Hⁱ), 7.98 (d, *J* = 8.1 Hz, 10H, H^g), 7.82 (d, *J* = 8.0 Hz, 10H, H^f), 7.54 (d, *J* = 8.3 Hz, 10H, H^b), 7.17 (s, 10H, H^c), 6.42 (s, 10H, H^h), 3.55–3.34 (m, 10H, C^jH_A), 3.20–3.10 (m, 10H, C^dH_B), 3.10–3.01 (m, 20H, C^eH_A + C^jH_B), 3.01–2.92 (m, 10H, C^eH_B), 2.92–2.78 (m, 10H, C^dH_A), 1.62–1.39 (m, 20H, H^e), 1.19 (dq, *J* = 13.9, 7.1 Hz, 20H, Hⁿ), 1.15–1.03 (m, 40H, H^l + H^m), 0.84 (t, *J* = 7.3 Hz, 30H, CH₃). ¹³C NMR: (126 MHz, CD₃CN) δ 171.4 (Cⁱ), 157.5 (N–C–C^a/N–C–C^g), 156.8 (N–C–C^a/N–C–C^g), 153.8 (C^h) 153.4 (C^c), 140.7 (C^c–C^b)/C^f–C–C^h), 140.3 (C^e), 140.1 (C^c–C–C^b)/C^f–C–C^h), 138.9 (C^f), 129.2 (C^g) 125.5 (C^a), 60.8 (C^j), 31.8 (C^l/C^m), 31.0 (C^e), 30.3 (C^d), 29.9 (C^k), 27.0 (C^l/C^m), 23.1 (Cⁿ), 14.3 (CH₃). ESI-MS: *m/z* 1377.4 [M–3PF₆]³⁺ requires 1376.8 ; 996.1 [M–4PF₆]⁴⁺ requires 996.6; 767.8 [M–5PF₆]⁵⁺ requires 768.5; 615.8 [M–6PF₆]⁶⁺ requires 616.4, 507.1 [M–6PF₆]⁷⁺ requires 507.8 *m/z*.

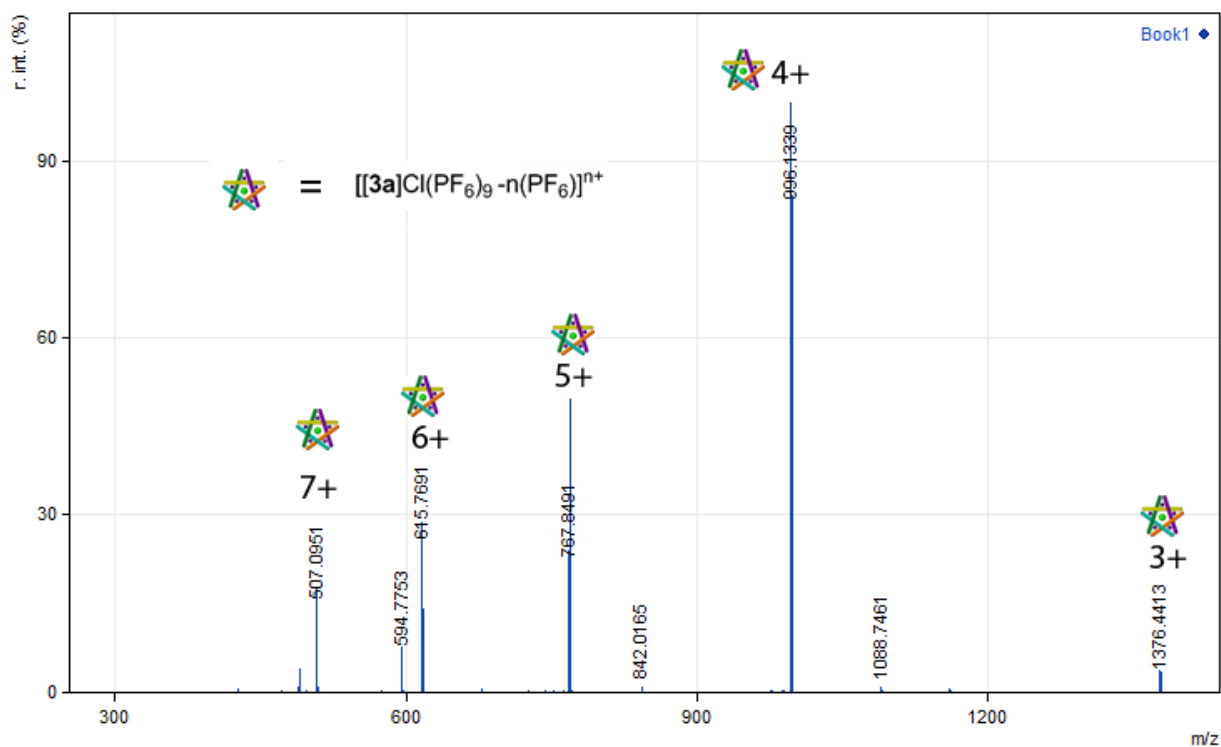
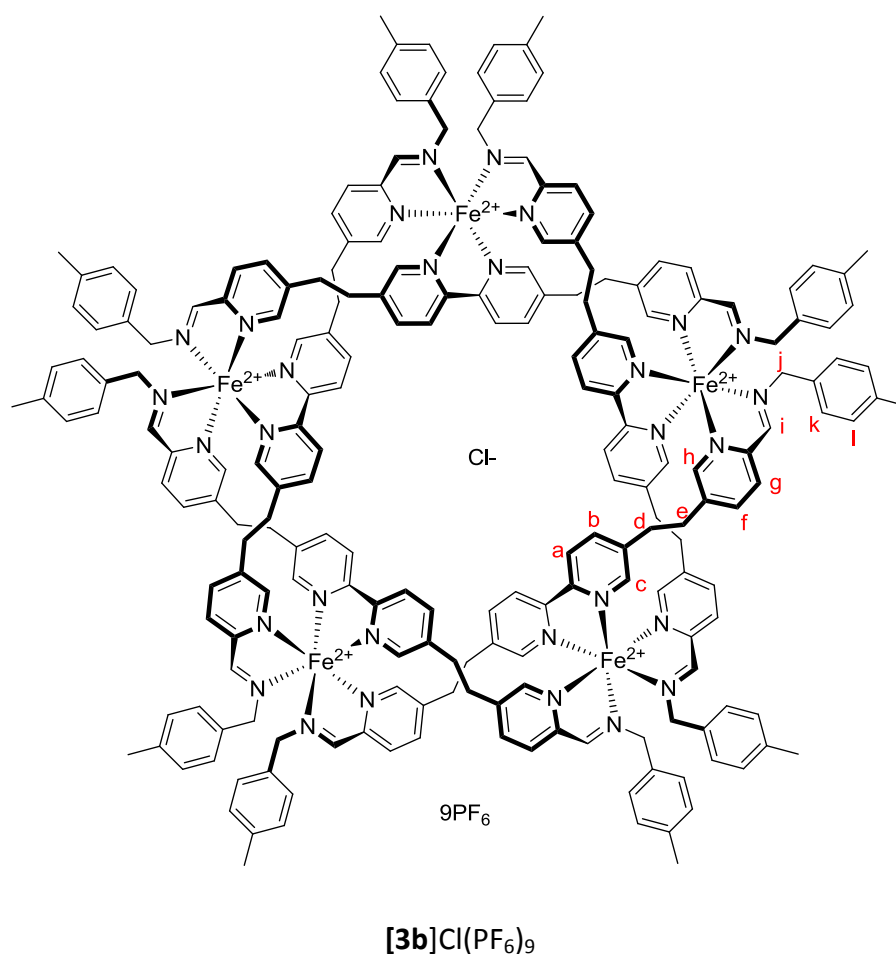


Figure 5. Low-resolution ESI-MS of helicate **[3a]**Cl(PF₆)₉. Calculated peaks (*m/z*): 1376.8 [M–3PF₆]³⁺; 996.6 [M–4PF₆]⁴⁺; 768.5 [M–5PF₆]⁵⁺; 616.4 [M–6PF₆]⁶⁺, 507.8 [M–6PF₆]⁷⁺.

2.5.1.3.2. *Preparation of helicate [3b]Cl(PF₆)₉*

A DMSO-d₆ solution of anhydrous FeCl₂ (250 μL of 210 mM, 52 μmol, 1.1 eq.) was added to dialdehyde **1** (20 mg, 47 μmol, 1 eq) in DMSO-d₆ (10 mL). The resulting purple solution was treated in an ultrasonic bath for 10 min and heated at 60°C for 30 min to ensure complete dissolution of the dialdehyde. A DMSO-d₆ solution of 4-methylbenzylamine (1.00 mL of a 100 mM DMSO-d₆ solution, 100 μmol, 2.2 equivalents) was added to the mixture. The resulting dark purple mixture was heated at 60 °C for one day. After cooling to room temperature, excess saturated aqueous KPF₆ was added (~5 mL). A fine suspension of a purple material formed which was collected on Celite, thoroughly washed with water, EtOH, DCM and diethylether. The purple solid was dissolved in acetonitrile and concentrated

under reduced pressure to give **[3b]**Cl(PF₆)₉ as a purple powder (25 mg, 5.3 μmol, 56%). ¹H NMR: (500 MHz, CD₃CN) δ 9.85 (d, *J* = 8.3 Hz, 10H, H^a), 8.57 (s, 10H, Hⁱ), 7.74 (d, *J* = 8.1 Hz, 10H, H^g), 7.59 (d, *J* = 8.1 Hz, 10H, H^f), 7.48 (d, *J* = 8.2 Hz, 10H, H^b), 7.16 (d, *J* = 7.8 Hz, 20H, H^{c3}), 7.14 (d, *J* = 8.0 Hz, 10H, H^c), 6.71 (d, *J* = 7.9 Hz, 20H, H^{c2}), 6.30 (s, 10H, H^h), 4.60 (d, *J* = 15.2 Hz, 10H, H^j), 4.24 (d, *J* = 15.4 Hz, 10H, C^jH_B), 3.16–3.09 (m, 10H, C^dH_B), 3.01 (dd, *J* = 10.4, 6.6 Hz, 20H, H^e), 2.88–2.80 (m, 10H, H^a), 2.37 (s, 30H, CH₃). ¹³C NMR: (126 MHz, CD₃CN) δ 171.8 (C^j), 157.5 (N–C–C^g), 156.8 (N–C–C^a), 153.8 (C^h), 153.2 (C^c), 140.6 (C^c–C–C^b)/C^f–C–C^h), 140.3 (C^e), 140.1 x 2 (C^c–C–C^b)/C^f–C–C^h + C^l–C–C^l/C_k–C–C_k), 138.8 (C^f), 131.0 (C^l–C–C^l/C_k–C–C_k), 130.8 (C^l), 130.2 (C^k), 129.6 (C^g), 125.4 (C^a), 64.9 (C^j), 31.2 (C^e), 30.2 (C^d), 21.3 (CH₃). HRESI-MS: *m/z* = 807.6309 [M-4(PF₆)]⁵⁺ (calcd. for C₂₁₀H₂₀₀ClF₂₄Fe₅N₃₀P₄, 807.6323).

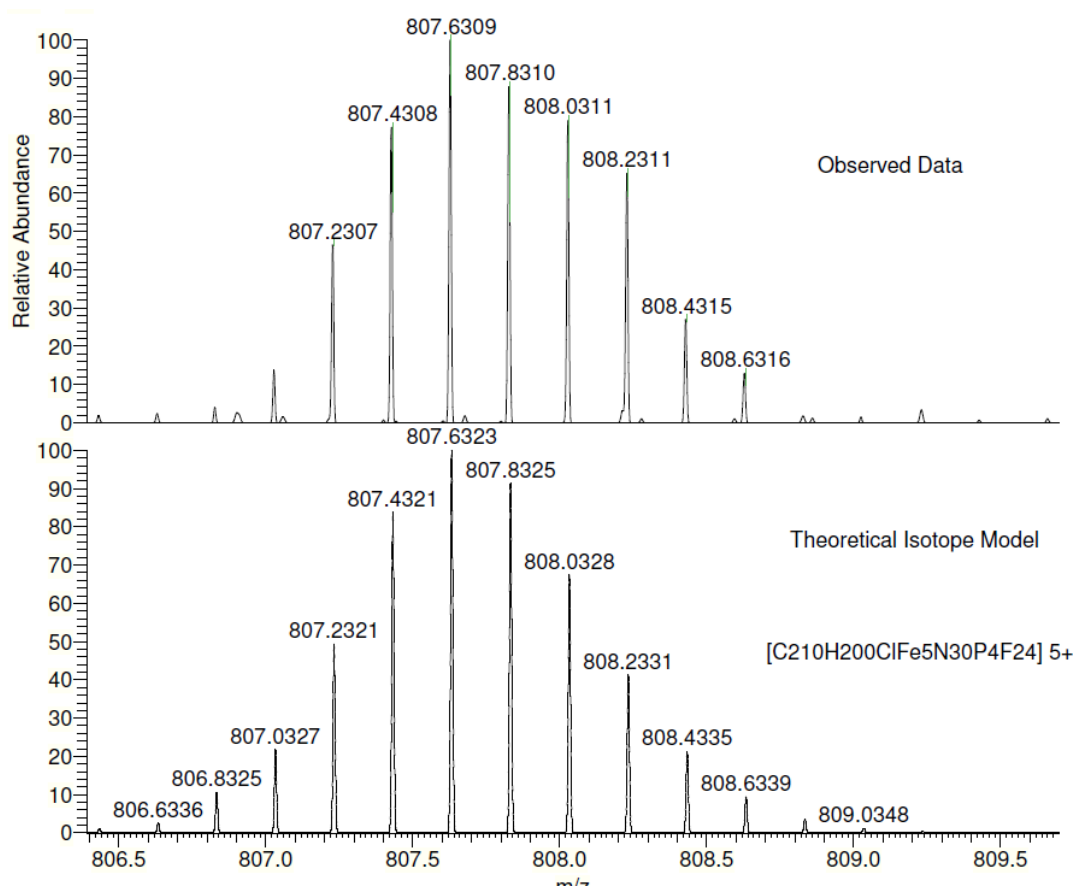


Figure 6. High-resolution ESI-MS of [M-4PF₆]⁵⁺ peak of **[3b]**Cl(PF₆)₉. Experimental spectrum (top) and calculated (bottom).

2.5.1.3.3. *Preparation of helicates [3c-f]Cl(PF₆)₉*

Helicates **3c-f** were prepared using the follow procedure.

Dialdehyde **1** (2mg, 4.7 μ mmol) was dissolved in 1.7 mL of DMSO-d₆ and FeCl₂ (20 μ L of 260 μ M DMSO-d₆ solution, 5.2 μ mol) was added. The mixture was treated in an ultrasonic bath for 10 mins. The appropriate amine was added (2.2 eq in 20 μ L DMSO-d₆) and the sample was heated at 60 °C for 24 h. Excess KPF_{6(aq)} was added and the resulting precipitate was collected on Celite and washed well with water, EtOH and diethylether; and redissolved in MeCN. Removal of the solvent gave helicates **3c-f** as purple powders which were dissolved in CD₃CN and the ¹H NMR spectra collected (Figure 3).

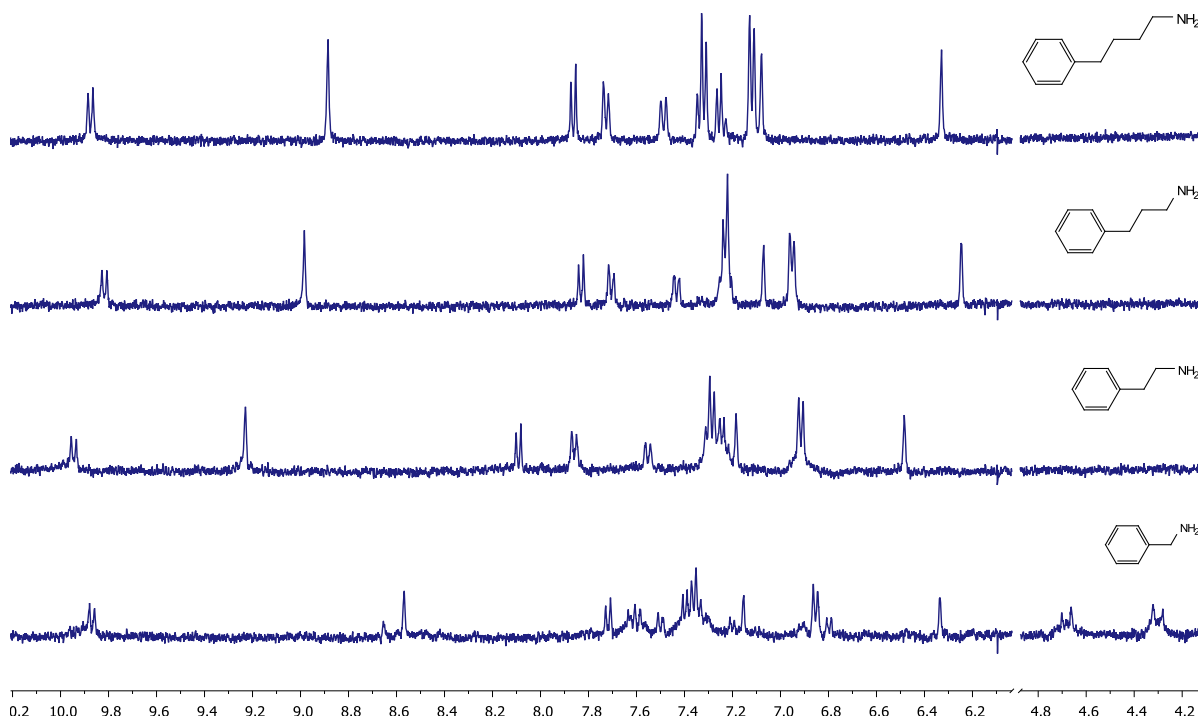
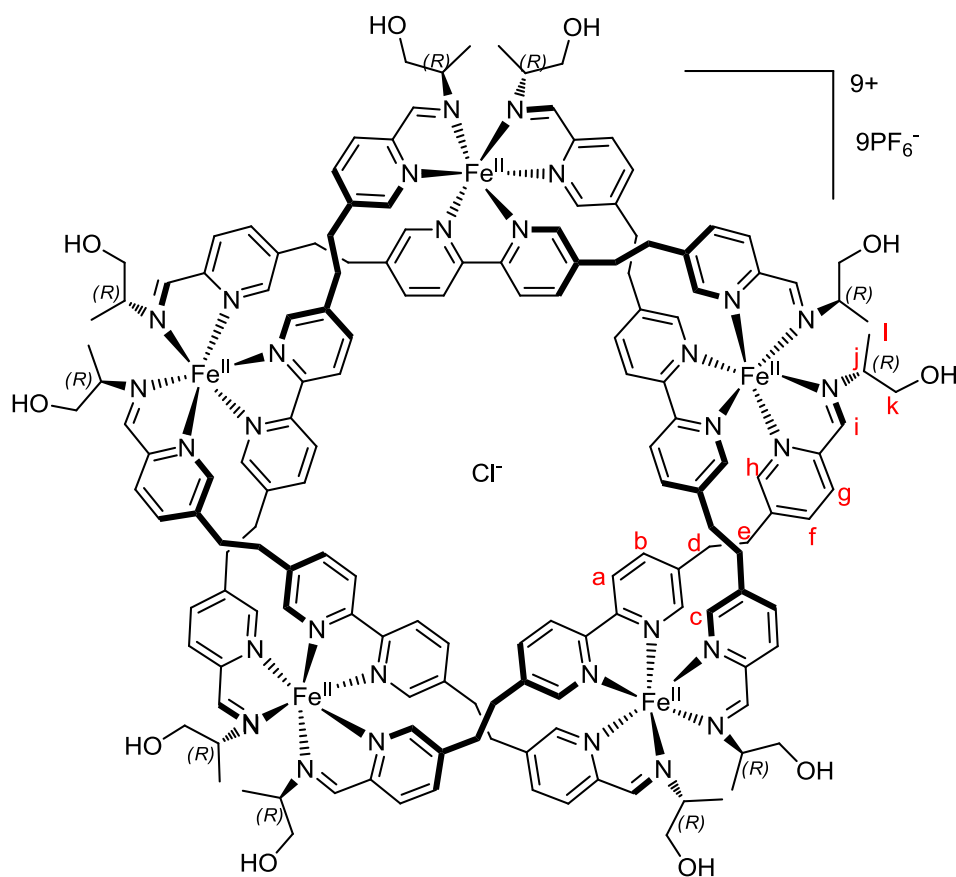


Figure 7. ¹H NMR (CD₃CN, 500 MHz) of helicates **3c-f**.

2.5.1.3.4. *Preparation of diastereoselective helicate [3g]Cl(PF₆)₉****M*-($\Delta\Delta\Delta\Delta\Delta$)-[3g]Cl(PF₆)₉**

(*R*)-2-Amino-1-propanol (430 μ L of a 240 μ M DMSO solution, 100 μ mol, 2.2 equivalents) was added to a solution of dialdehyde **1** (20 mg, 47 μ mol) in 20 mL of DMSO-*d*₆ with anhydrous FeCl₂ (220 μ L of 240 μ M DMSO-*d*₆ solution, 52 μ mol, 1.1 eq). The mixture was heated at 60 °C for 48 h. After cooling to room temperature the mixture was added to excess aqueous KPF₆ (~100 mL). A fine suspension of a purple material formed which was collected on Celite, thoroughly washed with water, little EtOH (complex is soluble) and diethyl ether. The purple solid was dissolved in acetonitrile and concentrated under reduced pressure to give *M*-($\Delta\Delta\Delta\Delta\Delta$)-[3g]Cl(PF₆)₉ as a purple powder (14 mg, 3.2 μ mol, 34%). ¹H NMR (500 MHz,

CD₃CN) δ 9.88 (d, *J* = 8.3 Hz, 10H, H^a), 9.04 (s, 10H, Hⁱ), 8.04 (d, *J* = 8.0 Hz, 10H, H^g), 7.80 (s, 10H, H^c), 7.69 (d, *J* = 8.0 Hz, 10H, H^f), 7.52 (d, *J* = 8.3 Hz, 10H, H^b), 6.52 (s, 10H, H^h), 3.80–3.52 (m, 30H, C^kH_A + OH), 3.38–3.29 (m, 10H, C^kH_B), 3.22 (ddd, *J* = 14.8, 8.2, 5.4 Hz, 10H, H^d+H^e), 3.19–3.02 (m, 20H, H^j + H^d+H^e), 2.96 – 2.81 (m, 20H, H^d+H^e), 1.08 (d, *J* = 6.7 Hz, 30H, Me). ¹³C NMR (126 MHz, CD₃CN) δ 171.9 (Cⁱ), 158.0 (N–C–C^g), 156.9 (N–C–C^a), 154.7 (Cⁱ), 153.8 (C^h), 140.7 (C^c–C–C^b)/C^f–C–C^h), 140.6 (C^c–C–C^b)/C^f–C–C^h), 140.0 (C^e), 138.9 (C^f), 129.9 (C^g), 125.2 (C^a), 64.7 (C^j), 62.3 (C^k), 30.4 (C^d/C^e), 30.3 (C^d/C^e), 18.4 (Me). ESI-MS: *m/z* 1288.8, [M-3PF₆]³⁺ requires 1288.6; 930.4 [M-4PF₆]⁴⁺ requires 930.2; 715.4, [M-5PF₆]⁵⁺ requires 715.2; 571.8, [M-6PF₆]⁶⁺ requires 571.8 *m/z*.

An identical procedure using (*S*)-2-amino-1-propanol gave *P*-(ΛΛΛΛ)-[**3g**]Cl(PF₆)₉ with identical ¹H and ¹³C NMR.

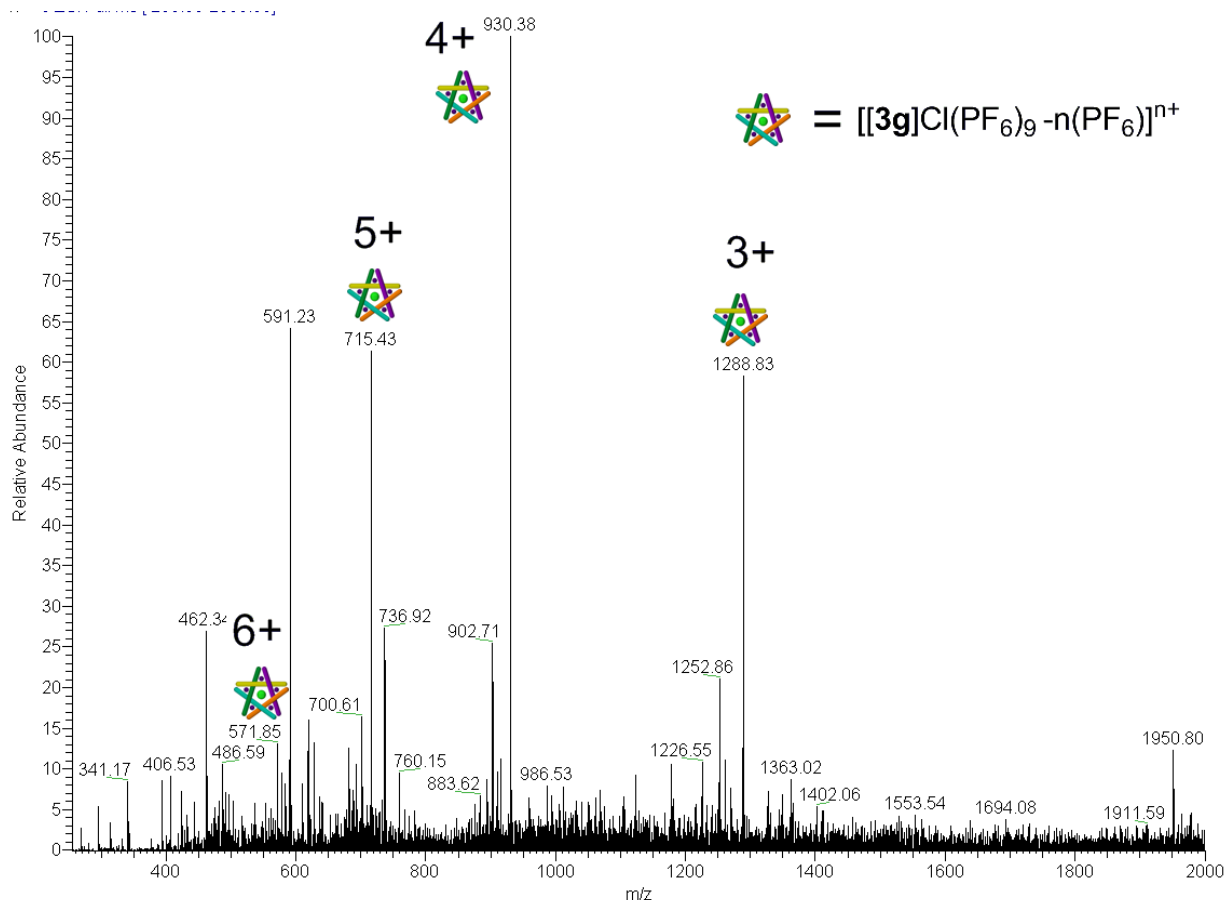
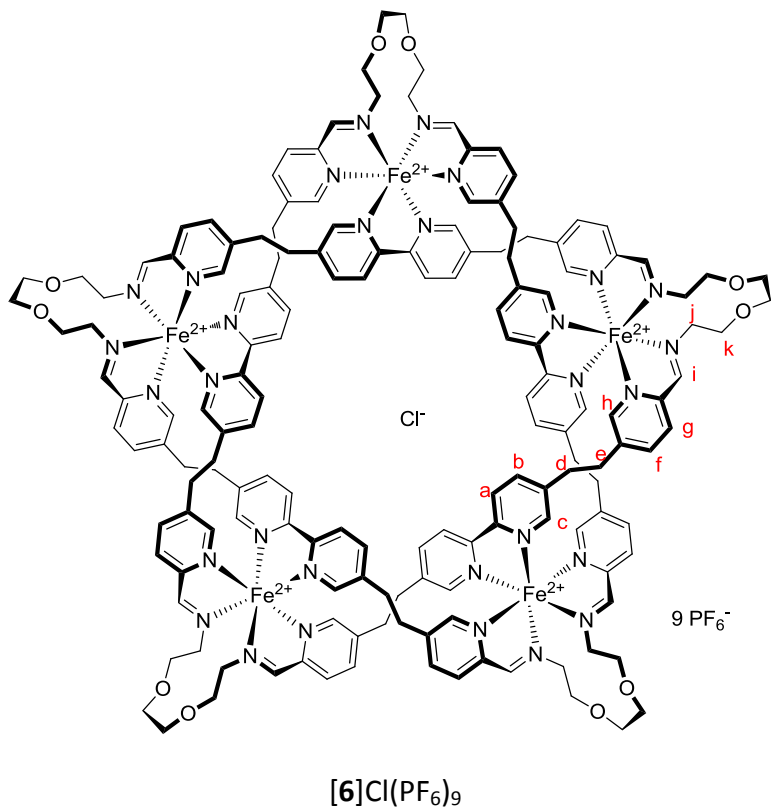


Figure 8. Low-resolution ESI-MS spectrum of enantiopure helicate $[3\mathbf{g}]\text{Cl}(\text{PF}_6)_9$. Calculated peaks (m/z): 1288.6 $[\text{M}-3\text{PF}_6]^{3+}$; 930.2 $[\text{M}-4\text{PF}_6]^{4+}$; 715.2 $[\text{M}-5\text{PF}_6]^{5+}$; 571.8 $[\text{M}-6\text{PF}_6]^{6+}$.

2.5.1.3.5. Preparation of pentafoil knot $[6]\text{Cl}(\text{PF}_6)_9$



A DMSO- d_6 solution of anhydrous FeCl_2 (250 μL of 210 mM, 52 μmol , 1.1 eq.) was added to dialdehyde **1** (20 mg, 47 μmol , 1 eq) 10 mL of DMSO- d_6 . The resulting purple solution was treated in an ultrasonic bath for 10 min and heated at 60°C for 30 min to ensure complete dissolution of the dialdehyde. A DMSO- d_6 solution of 2,2'-(ethylenedioxy)bis(ethylamine) (1.00 mL of a 52 mM DMSO- d_6 solution, 52 μmol , 1.1 equivalents) was added to the mixture. The resulting dark purple mixture was heated at 60 °C for 2 days. After cooling to room temperature, excess saturated aqueous KPF_6 was added (~5 mL). A fine suspension of a purple material formed which was collected on Celite, thoroughly washed with water, EtOH, DCM and diethylether. The purple solid was dissolved in acetonitrile and

concentrated under reduced pressure to give [6]Cl(PF₆)₉ as a purple powder (18 mg, 4.2 μmol, 44%). ¹H NMR (500 MHz, CD₃CN) δ 9.90 (d, *J* = 8.2 Hz, 10H, H^a), 9.04 (s, 10H, Hⁱ), 8.03 (d, *J* = 7.9 Hz, 10H, H^g), 7.86 (d, *J* = 7.7 Hz, 10H, H^f), 7.50 (d, *J* = 7.9 Hz, 10H, H^b), 7.20 (s, 10H, H^c), 6.43 (s, 10H, H^h), 4.15–4.06 (m, 10H, C^jH_A), 3.66 (d, *J* = 9.6 Hz, 20H, C^kH_A + C^lH_A), 3.32 (d, *J* = 9.3 Hz, 10H, C^lH_B), 3.23 (d, *J* = 13.9 Hz, C^jH_B), 3.19–3.15 (m, 10H, C^dH_B), 3.15–3.07 (m, 10H, C^eH_A), 3.03 – 2.89 (m, 20H, C^kH_B + C^eH_B), 2.88–2.80 (m, 10H, C^dH_A). ¹³C NMR (126 MHz, CD₃CN) δ 174.0 (Cⁱ), 157.2 (N-C-C^a), 156.8 (N-C-C^g), 154.1 (C^h), 153.4 (C^c), 140.9 (C^c-C-C^b)/C^f-C-C^h), 140.7 (C^c-C-C^b)/C^f-C-C^h), 140.3 (C^e), 138.9 (C^f), 129.5 (C^g), 125.5 (C^a), 71.4 (C^l), 68.9 (C^k), 61.4 (C^j), 31.0 (C^e), 30.2 (C^d). HRESI-MS: *m/z* = 713.5736 [M-4(PF₆)]⁵⁺ (calcd. for C₁₆₀H₁₇₀ClF₂₄Fe₅N₃₀O₁₀P₄, 713.5750).

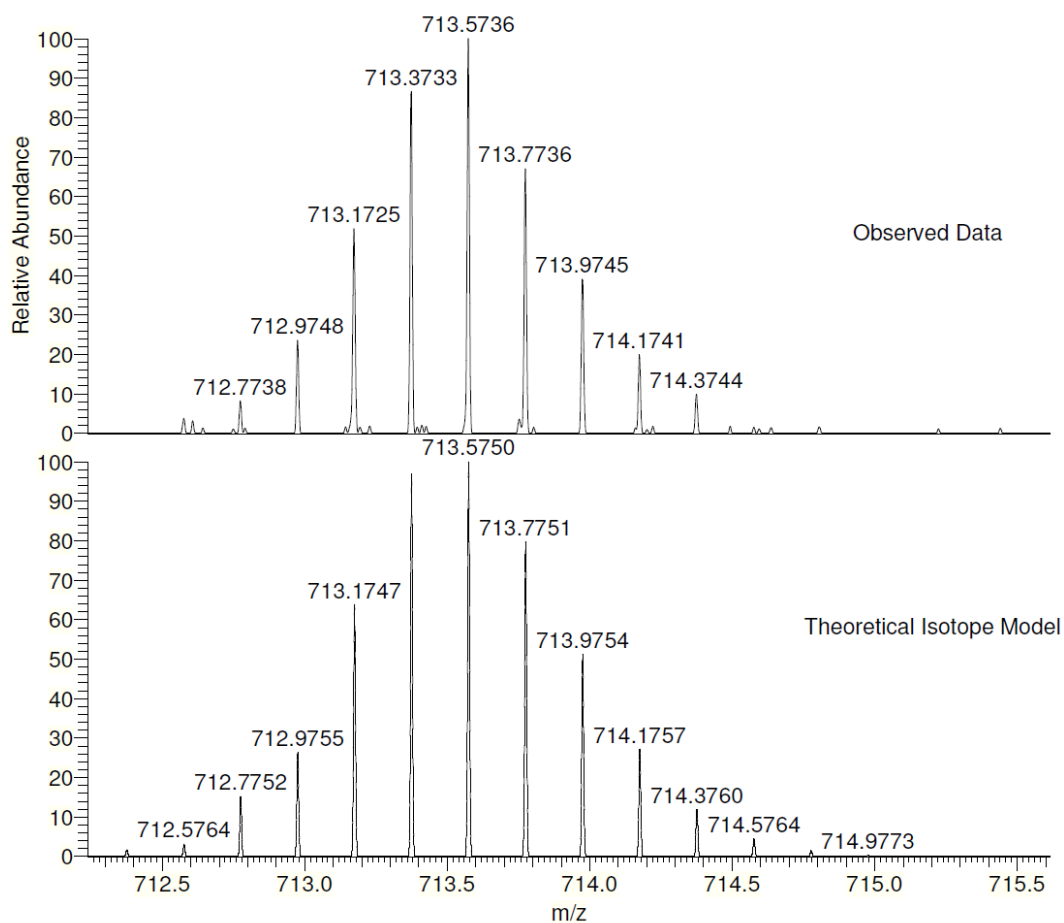
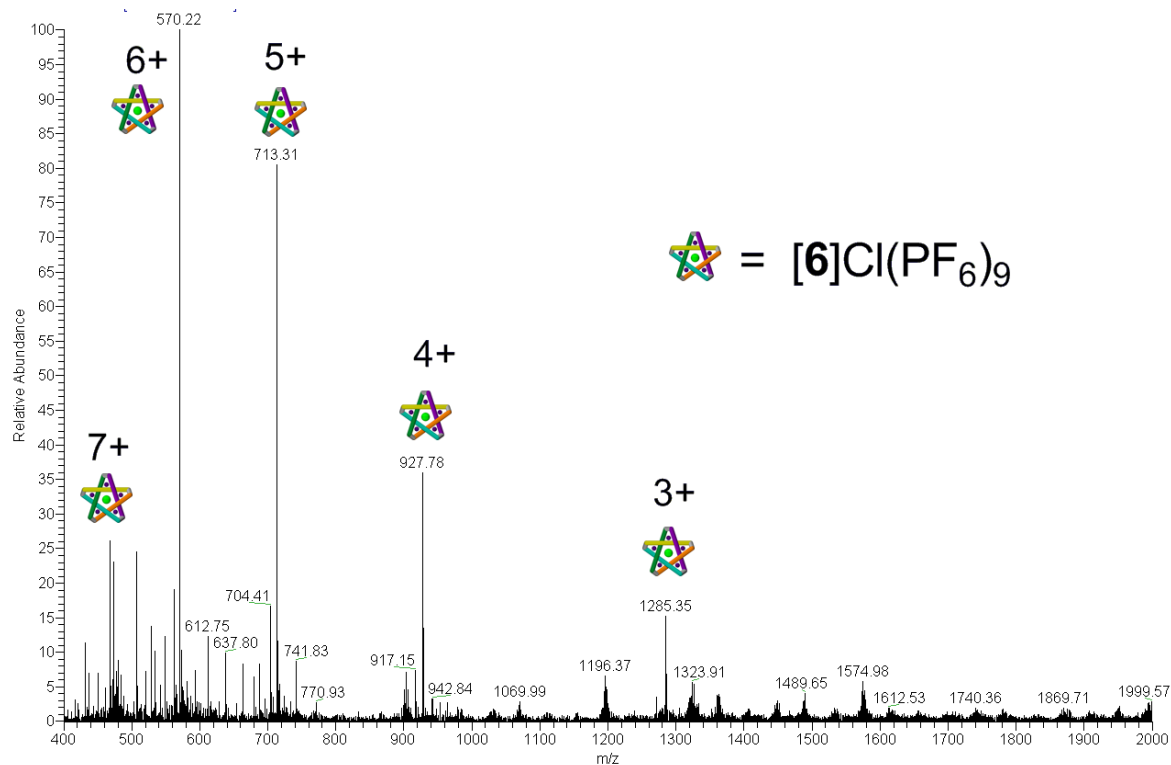
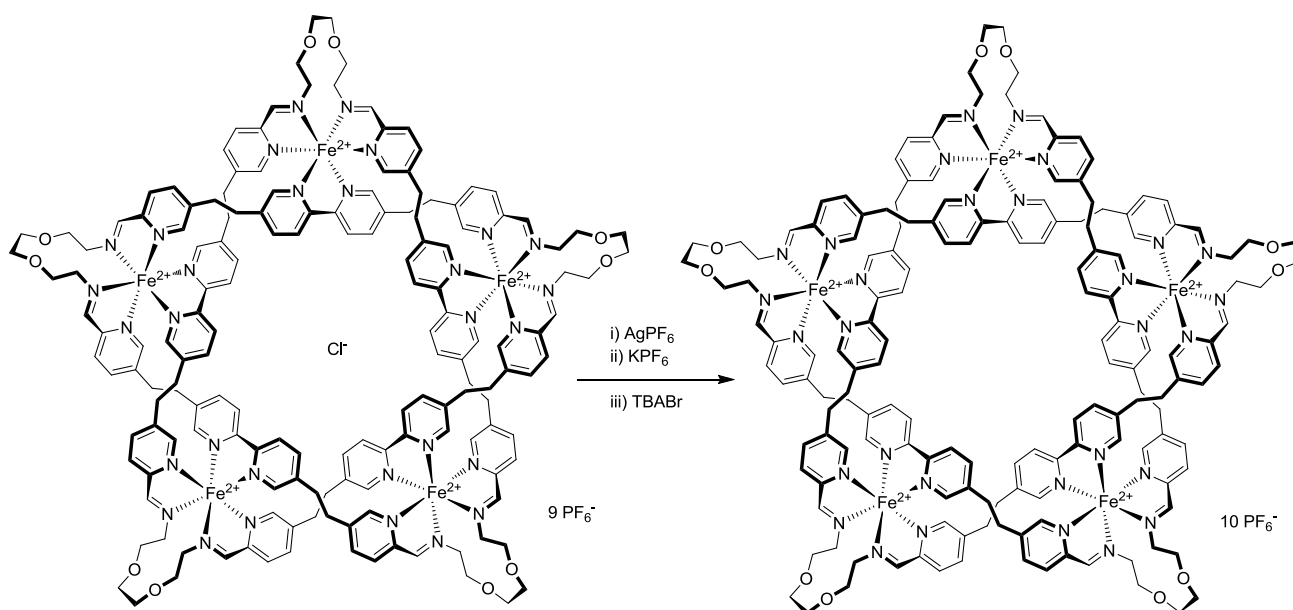


Figure 9. Low-resolution ESI-MS of pentafoil knot $[6]Cl(PF_6)_9$ (top), and high-resolution isotope pattern (bottom) of $[M-4PF_6]^{5+}$ peak.

2.5.1.3.6. Removal of Cl⁻ from central cavity of [6]¹⁰⁺

Scheme 3 Removal of central chloride ion from [6]Cl(PF₆)₉ with AgPF₆

Pentafoil knot [6]Cl(PF₆)₉ was dissolved in CD₃ CN and 10 eq of AgPF₆ in CD₃CN was added and the mixture treated in an ultrasonic bath for 30 min. Although no precipitate was apparent - unsurprising considering the amount of AgCl_(s) expected to be formed - ¹H NMR indicated complete removal of the Cl⁻ anion. Excess KPF_{6(aq)} was added, followed by Bu₄NBr (which did not change the ¹H NMR spectrum) in MeCN. The resulting fine suspension (AgBr) was removed by filtration through celite and the solvent reduced to precipitate [6](PF₆)₁₀ as a purple powder which was collected on Celite and washed with water, EtOH and diethyl ether before being re-dissolved in MeCN. Removal of the solvent gave [6](PF₆)₁₀. ¹H NMR (500 MHz, CD₃CN) δ 9.11 (s, 2H, Hⁱ), 8.95 (d, *J* = 8.0 Hz, 2H, H^a), 8.08 (d, *J* = 8.0 Hz, 2H, H^b), 7.91 (d, *J* = 7.7 Hz, 2H, H^f), 7.50 (d, *J* = 7.9 Hz, 2H, H^b), 7.31 (s, 2H, H^c), 6.58 (s, 2H, H^h), 4.12 (t, *J* = 10.2 Hz, 2H, C^jH_A/H_B), 3.79–3.60 (m, 4H, C^kH_A/H_B+ C^lH_A/H_B), 3.34 (d, *J* = 9.7 Hz, 2H, C^lH_A/H_B), 3.29–3.16 (m, 4H, C^eH_A/H_B+C^jH_A/H_B), 3.08 (m, 2H, C^dH_A/H_B), 3.00 (t, *J* = 8.9 Hz, 4H,

$C^kH_A/H_B + C^dH_A/H_B$, 2.91–2.77 (m, 2H, C^eH_A/H_B). ESI-MS (m/z): $[[6]Cl(OH)(H_2O)(PF_6)_6]^{3+}$ requires 1285.96, found 1285.93; $[[6](OH)(H_2O)(PF_6)_5]^{4+}$ requires 928.23, found 928.21.

2.5.1.4. Discussion of stereochemistry assignment of helicate $[3g]Cl(PF_6)_9$

2.5.1.4.1. Background

The interpretation of CD-spectra of octahedral coordination complexes has been shown to be a reliable means of assigning absolute stereochemistry of $M(N^{\wedge}N)_2X_2$ and $M(N^{\wedge}N)_3$ ($N^{\wedge}N = 2,2'$ -bipyridine, 9,10-phenanthroline) type complexes using exciton theory.⁵⁰⁻⁵² This theory is based on the coupling of two or more electric dipole transition moments via a dipole-dipole interactions.⁵² In 2,2'-bipyridine type ligands there are two strong $\pi-\pi^*$ transitions which are long- and short-axis polarized, as shown below.⁵²

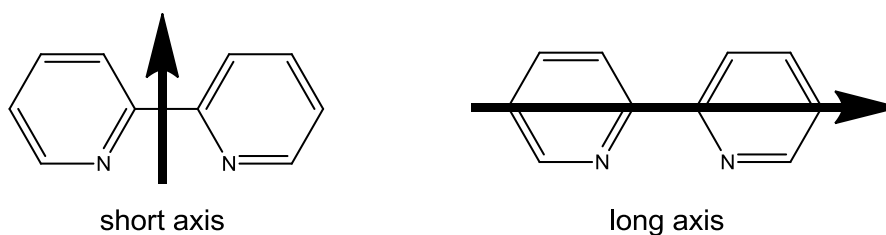


Figure 10. Long- and short-axis polarized electric dipole transition moments.⁹

A general rule⁵⁰ is that in regions of long-axis-polarised transitions of the ligands (such as these strong $\pi-\pi^*$ transition typically around 260-350 nm for bpy, phen and related diimines) the CD will appear *strongly positive* at lower energy and *strongly negative* at higher energies for complexes with the Λ - $M(N^{\wedge}N)_3$ configuration (by relation to (-)- $[Fe(phen)_3]^{2+}$, which was shown to be Λ by X-ray crystallography). Experimentally this has been established as a reliable treatment with, for example, the CD-spectra of (-)- $[Fe(bpy)_3]^{2+}$ and (-)- $[Fe(phen)_3]^{2+}$ (both shown to be Λ - $[Fe(N^{\wedge}N)_3]$)¹⁰ being reported decades ago^{53,54} and both exhibit CD bands for the $\pi-\pi^*$ exciton pair (centered around 270 and 300 nm

respectively) as predicted. More closely related to the current cyclic helicates are examples of enantiopure dinuclear triple helicates formed with Fe(II) ions and bis(2,2'-bipyridine) ligands which have been reported^{55,56} where Δ^{12} and Λ^{13} assignments were made on the basis of similar CD data. Optically pure $[\text{Fe}(\text{A-B})_3]^{2+}$ complexes based on pyridyl-imines have recently been reported,⁵⁷ and characterized by X-ray crystallography and CD spectra. These complexes have (qualitatively) similar CD spectra to $[\mathbf{3g}]\text{Cl}(\text{PF}_6)_2$ and confirm that previous assignments for bipy-based systems can be readily applied to pyridyl-imines. They found a strong negative CD-band around 300 nm for Δ -Fe(II), in agreement with earlier predictions.⁵⁰

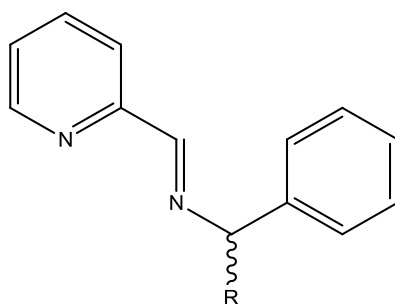


Figure 11. Pyridyl-imine ligands reported to form optically pure *fac*- $[\text{Fe}(\text{L})_3]^{2+}$ complexes,⁵⁷ showing similar CD spectra to $[\mathbf{3g}]\text{Cl}(\text{PF}_6)_9$.

2.5.1.4.2. *Experimental results*

The CD spectra of (R)- $[\mathbf{3g}]\text{Cl}(\text{PF}_6)_2$ and (S)- $[\mathbf{3g}]\text{Cl}(\text{PF}_6)_2$ are shown in Figure 12. Using the method discussed above, based on the π - π^* transitions around 300 nm, (R)- $[\mathbf{3g}]^{10+}$ corresponds to $\Delta\Delta\Delta\Delta$ - $[\mathbf{3g}]^{10+}$ and (S)- $[\mathbf{3g}]^{10+}$ corresponds to $\Lambda\Lambda\Lambda\Lambda$ - $[\mathbf{3g}]^{10+}$. This is in agreement with both previous simple pyridyl-imine complexes⁵⁷ and a triple-stranded dinuclear Fe(II)-containing helicate.⁵⁵ Additionally, the CD band for the MLCT transition of (S)- $\mathbf{3g}$ also corresponds to sign of that of Λ - $[\text{Fe}(\text{bpy})_3]^{52,58}$ and Λ - $[\text{Ru}(\text{phen})_3]^{50}$.

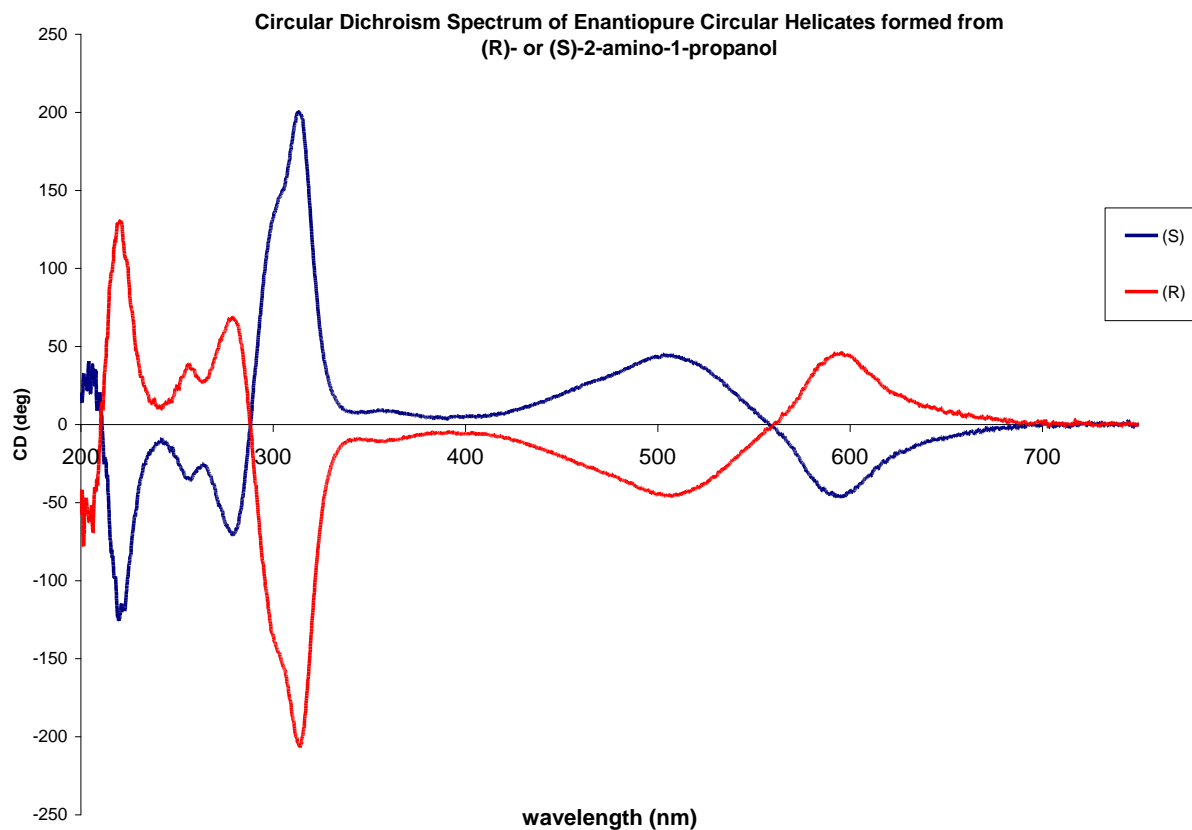


Figure 12. Circular dichroism spectra of (R)-[**3g**]Cl(PF₆)₉ and (S)-[**3g**]Cl(PF₆)₉ in MeCN.

Finally, by comparison with the X-ray crystal structure of [**6**]Cl(PF₆)₉, (R)-[**3g**]¹⁰⁺ and (S)-[**3g**]¹⁰⁺ correspond to *M*-($\Delta\Delta\Delta\Delta$)-[**3g**]Cl(PF₆)₉ and *P*-($\Lambda\Lambda\Lambda\Lambda$)-[**3g**]Cl(PF₆)₉. All these assignments are also supported by 2D-ROESY NMR data.

2.5.2. Knot assembly process: additional data

2.5.2.1. Monitoring of crude reaction mixture of [6](Cl)¹⁰⁺

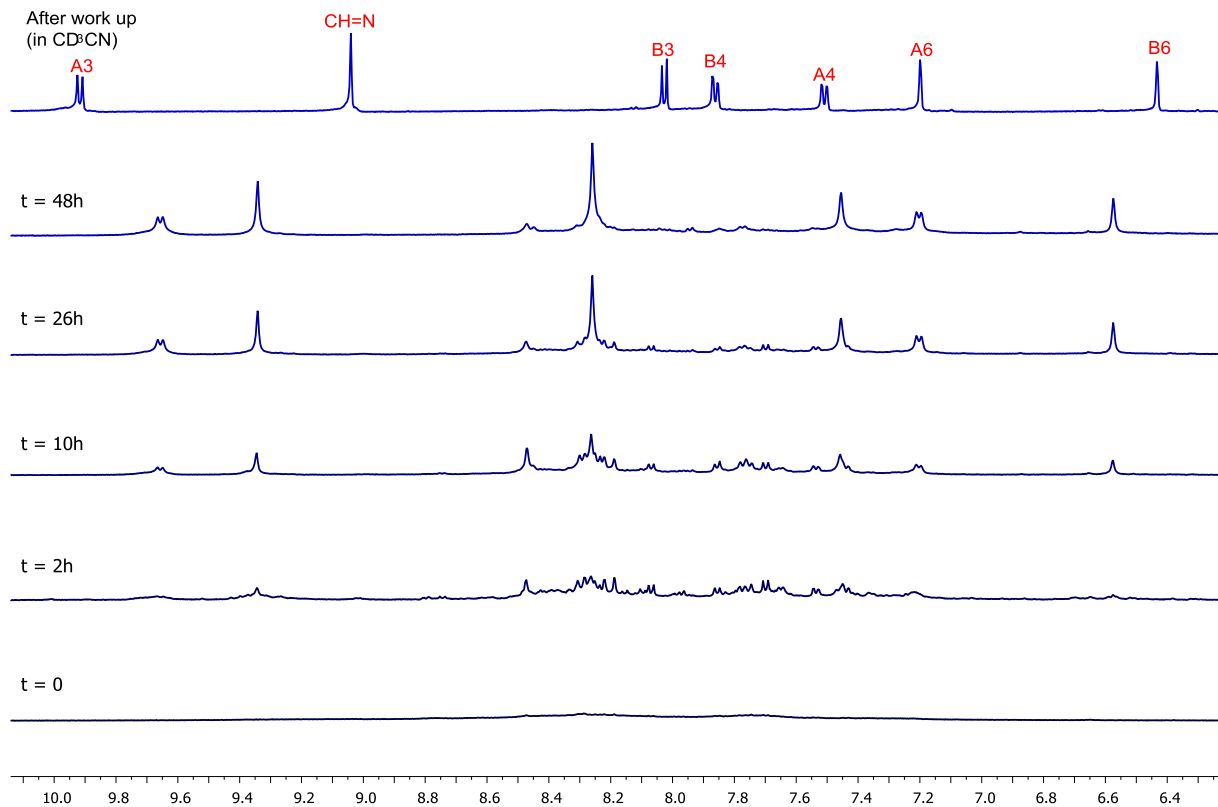


Figure 13. Formation of pentafoil knot [6]¹⁰⁺ monitored by ¹H NMR (DMSO-d₆, 500 MHz), aromatic region of spectrum shown. Spectra were collected of the crude reaction mixture after t = 0 (bottom), 2h, 10h, 26h and 48h. The top spectra is of the same sample after work-up (¹H NMR in CD₃CN) with ¹H NMR assignments indicated.

2.5.2.2. Effect of reaction stoichiometry on knot yield

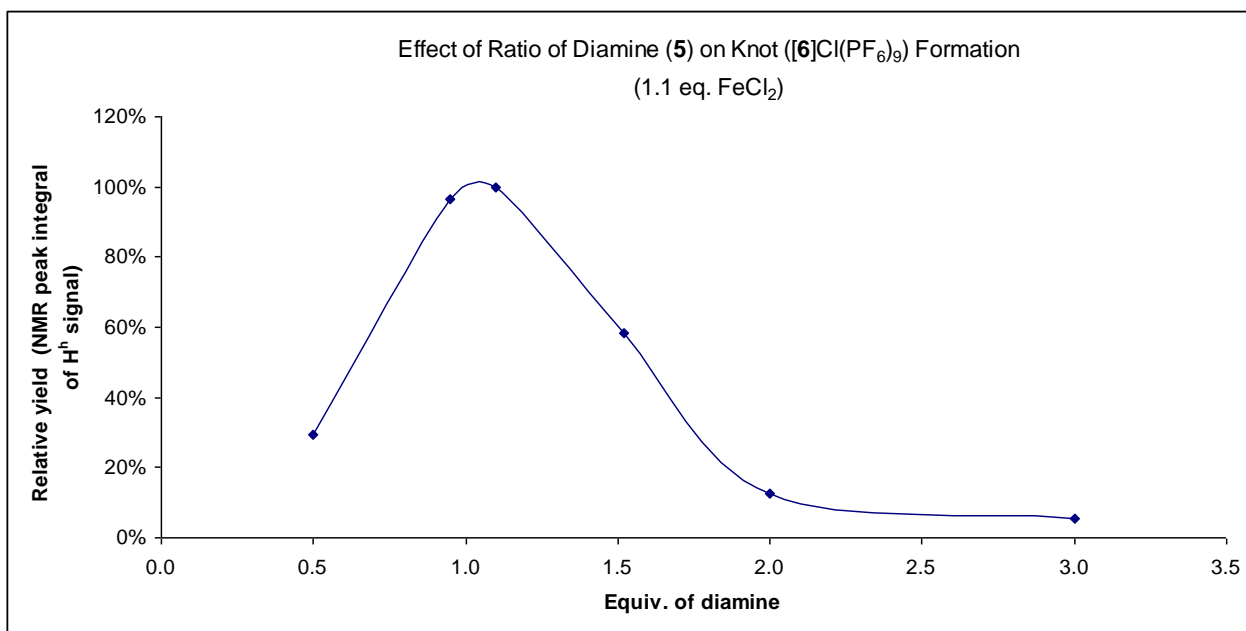


Figure 14. Effect on relative isolated yield of increasing the ratio of diamine (5) to dialdehyde 1, with 1.1 equiv. of FeCl₂ in all cases. Relative yields measured from ¹H NMR peak integrals (CD₃CN, 500 MHz). As the equivalents of amine is increased above 1.1 equivalents, the yield drops rapidly.

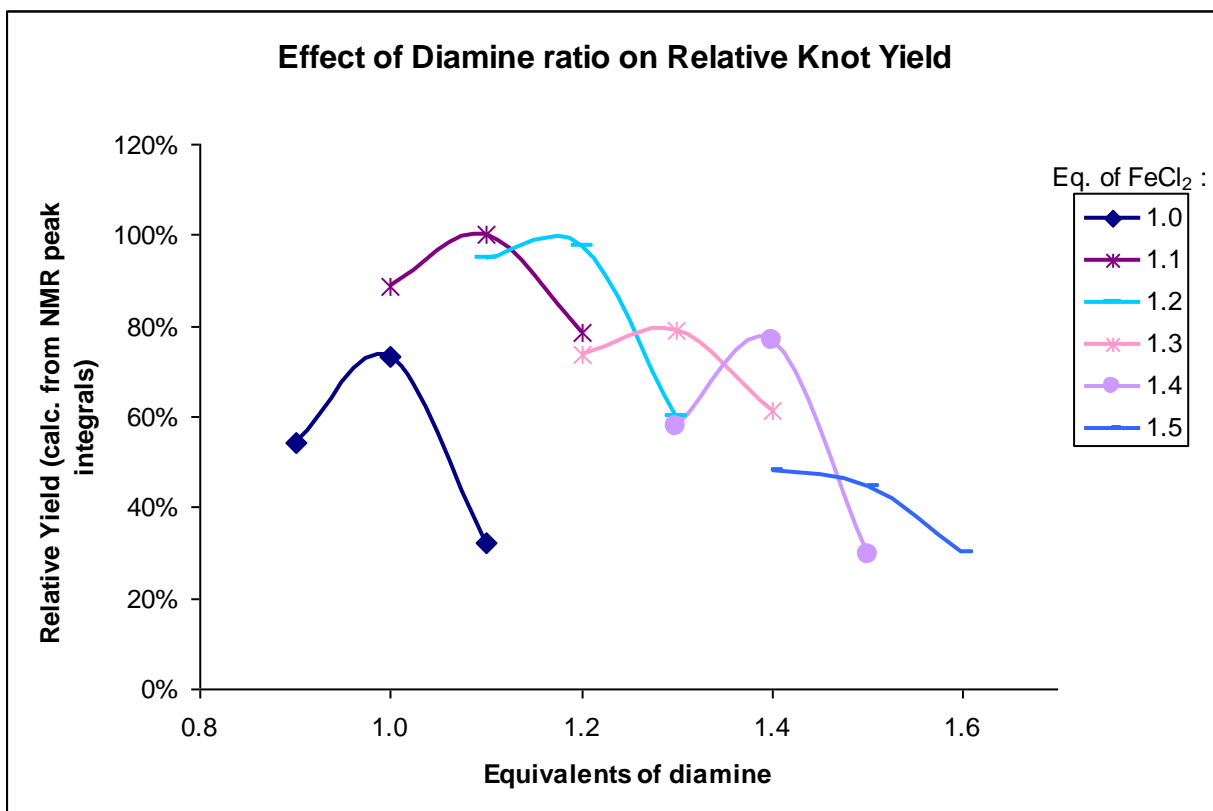


Figure 15. Effect on relative isolated yield of increasing the ratio of FeCl₂ and diamine (**5**) to dialdehyde **1**. ¹H NMR peak integrals (CD₃CN, 500 MHz). For any given ratio of FeCl₂, an equimolar amount of diamine gave the highest yield, with yields steadily decreasing as the ratio of FeCl₂ and diamine to dialdehyde increase. Estimated errors ±4%.

2.5.3. X-Ray crystal structure of [6]Cl(PF₆)₉·xSolvent

2.5.3.1. Experimental details

Purple crystals pentafoil knot [6]Cl(PF₆)₉·xSolvent were obtained by slow vapor diffusion of diethyl ether into a MeCN:Toluene (3:2) solution of [6]Cl(PF₆)₉ over 1 month. The structural analysis was performed using single crystal synchrotron X-ray diffraction data collected on beamline I19 at Diamond Light Source (UK) ($\lambda = 0.6889\text{\AA}$) at 100K. The CrystalClear-SM Expert 2.0 r5 suite of programs⁵⁹ was used for the data measurement and reduction. The structure were solved by charge flipping method using SUPERFLIP⁶⁰ and refined by full-matrix least-squares methods using the WinGX-software,⁶¹ which utilizes the SHELXL-97 module.⁶² Multi-scan absorption correction was applied.⁵⁹ All C-H hydrogen positions were calculated using a riding atom model with $U_H = 1.2 \times U_C$. The crystal lattice contains a lot of disordered solvents and anions. Only eight of the nine PF₆ anions could be located, one of them severely disordered, also some of the ethylene glycol loops showed very large thermal motion (maybe due positional disorder, which however could not be modeled) and thus a few bond distance restraints between the loop atoms (C-O and C-C) had to be applied in order to avoid chemically unreasonable bond distances. All atoms, except some of the disordered O- and C-atoms with occupancy 1/3 and H-atoms, were refined anisotropically, with only a few thermal parameter restraints (EADP). The helicate [6]Cl(PF₆)₉ is solvated by a large number of badly disordered solvent molecules, only two acetonitrile molecules could

be modeled (one with full occupancy, the second divided into three positions with occupancy 0.33) resulting in a moderate quality structure solution. One of the PF_6 anion that could not be located and all unresolved solvate molecules were modeled as isolated carbon or oxygen atoms with partial occupancies until plateau of ca. $1 \text{ e}/\text{\AA}^3$ was reached. The crystal lattice contains very large voids filled with a lot of scattered electron density, the SQUEEZE protocol inside PLATON⁶³ was used to remove the void electron density. Crystal data for $[\mathbf{6}]\text{Cl}(\text{PF}_6)_9$: $M = 4432.87$ [$\text{C}_{168}\text{H}_{176}\text{ClF}_{49}\text{Fe}_5\text{N}_{32}\text{O}_{18.5}\text{P}_8$], purple needles, $3 \times 40 \times 50 \mu\text{m}^3$ [$0.003 \times 0.040 \times 0.050 \text{ mm}^3$], monoclinic, space group $P2_1/c$, $a = 23.444(5) \text{ \AA}$, $b = 36.333(7) \text{ \AA}$, $c = 29.094(7) \text{ \AA}$, $\beta = 105.335(5)^\circ$, $V = 23900(9) \text{ \AA}^3$, $Z = 4$, $D_c = 1.232 \text{ g/cm}^3$, $F000 = 9056$, $\mu = 0.455 \text{ mm}^{-1}$, $T = 100.0(1) \text{ K}$, $2\theta_{\text{max}} = 48.42^\circ$, 40213 reflections, 13300 with $I_o > 2\sigma(I_o)$, $R_{\text{int}} = 0.1218$, 2431 parameters, 7 restraints, $\text{GoF} = 1.022$, $R = 0.138$ [$I_o > 2\sigma(I_o)$], $wR = 0.422$ (all reflections), $1.207 < \Delta\rho < -0.609 \text{ e}/\text{\AA}^3$. CCDC-XXXXXX contains the supplementary crystallographic data for this paper. These data can be obtained free of charge from The Cambridge Crystallographic Data Centre via www.ccdc.cam.ac.uk/data_request/cif;

2.5.3.2. Additional X-ray structure pictures

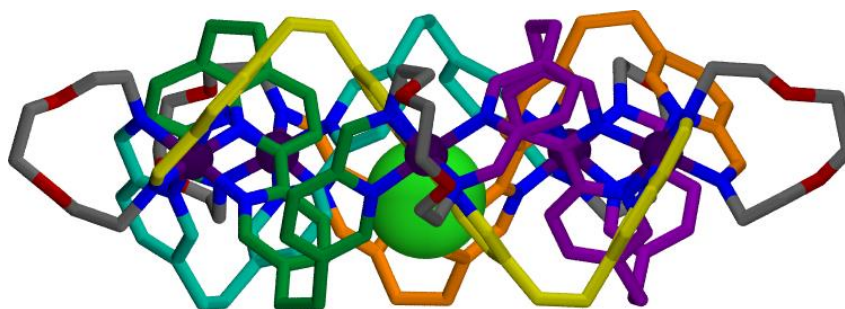


Figure 16. Side-view of $[\mathbf{6}]\text{Cl}$ showing the displacement of the chloride ion from the centre of the helicate and the woven nature of the ligand strands

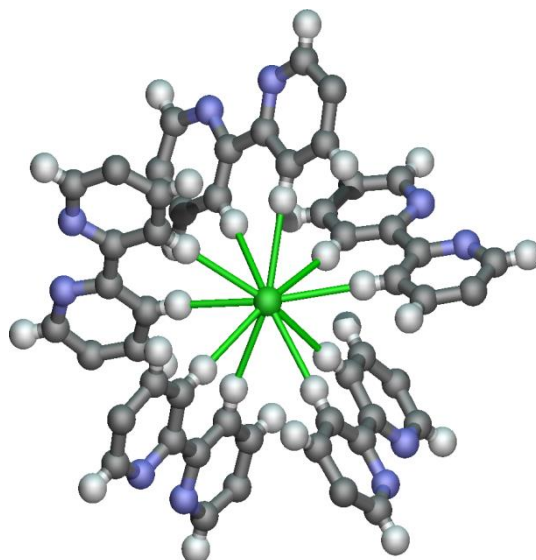


Figure 17. Chloride ion binding in the center of the helicate. The 10 CH...Cl contacts are shown.

2.5.3.3. Crystal packing diagrams

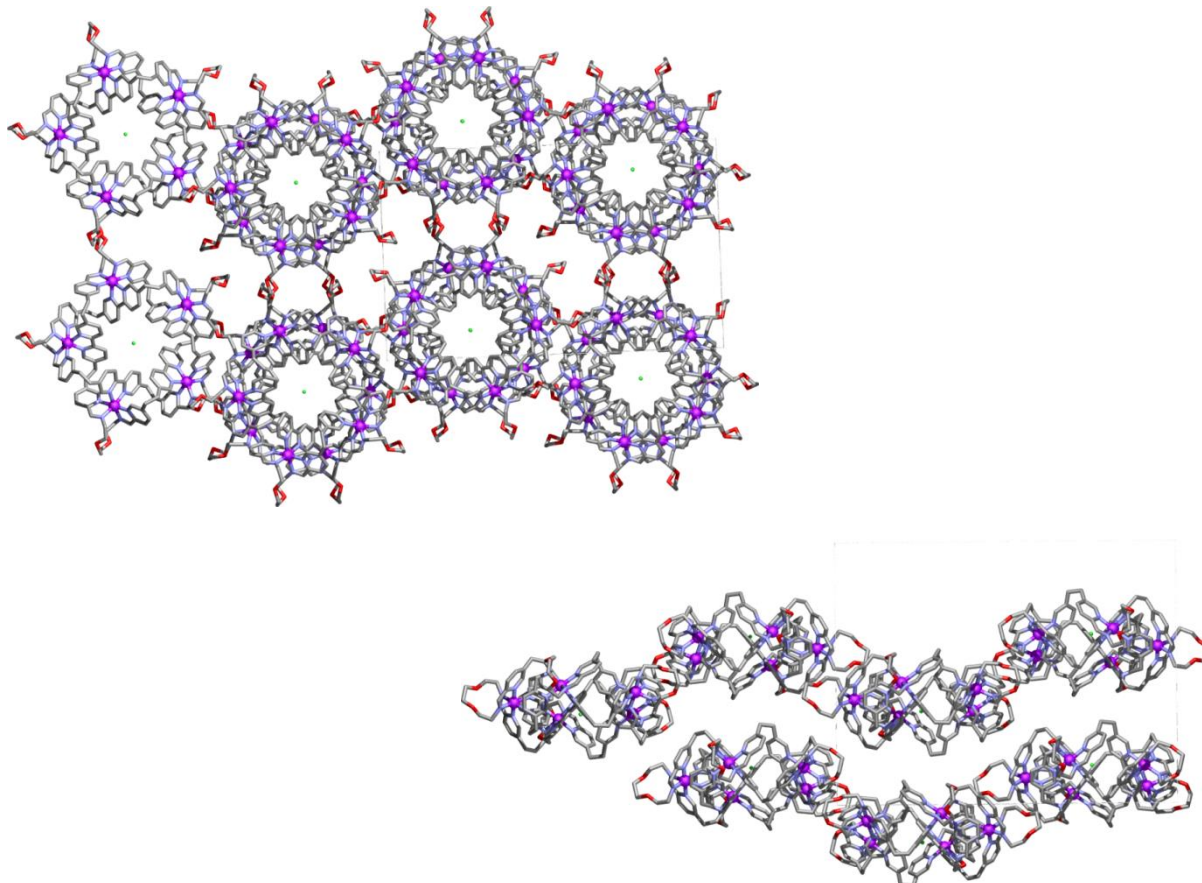


Figure 18. Partial crystal packing diagram of $[6]Cl(PF_6) \cdot x(\text{solvent})$. Views shown down c -axis (top) and a -axis (bottom) shown.

2.5.4. Comparison with Lehn's cyclic helicate

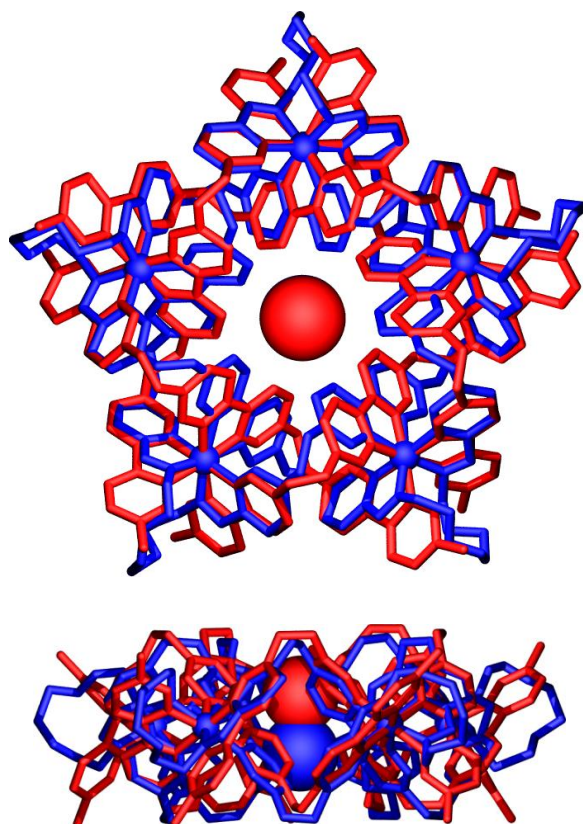


Figure 19. Superimposition of the X-ray crystal structure of $[6]\text{Cl}(\text{PF}_6)_9$ (blue) with that of Lehn's original circular helicate (red) (CSD code: TWITEY).³¹

Displacement of Cl from least-squares-plane of Fe atoms in Lehn's helicate is 1.41Å, 1.1Å (two molecules in asymmetric unit); in X-ray structure of $[6]\text{Cl}(\text{PF}_6)_9$: 1.30Å.

2.6. Notes and References

1. Wasserman, S. A. & Cozzarelli, N. R. *Science*, **1986**, 232, 951–960.
2. Taylor, W. R. *Nature*, **2000**, 406, 916–919.
3. Taylor, W. R. & Lin, K. *Nature*, **2003**, 421, 25.
4. Wagner, J. R., Brunzelle, J. S., Forest, K. T. & Vierstra, R. D. *Nature*, **2005**, 438, 325–331.
5. Taylor, W. R. *Comput. Biol. Chem.*, **2007**, 31, 151–162.
6. Saitta, A. M., Soper, P. D., Wasserman, E. & Klein, M. L. *Nature*, **1999**, 399, 46–48.
7. Arai, Y. *et al.* *Nature*, **1999**, 399, 446–448 (1999).
8. Menasco and M. Thistlethwaite (eds), *Handbook of Knot Theory*, (Elsevier, **2005**).
9. Fenlon, E. E. *Eur. J. Org. Chem.*, **2008**, 5023–5035.
10. Beves, J. E., Blight, B. A., Campbell, C. J., Leigh, D. A. & McBurney, R. T. *Angew. Chem. Int. Ed.*, **2011**, 50, 9260–9327.
11. Alexander, J. W. & Briggs, G. B. *Ann. Math.*, **1926–1927**, 28, 562–586.
12. Adams, C.C. *The Knot Book* (American Mathematical Society, **2004**).
13. Dietrich-Buchecker, C. O. & Sauvage, J-P. *Angew. Chem. Int. Ed. Engl.*, **1989**, 28, 189–192.
14. Piguet, C., Bernardinelli, G. & Hopfgartner, G. *Chem. Rev.*, **1997**, 97, 2005–2062.
15. Ashton, P. R. *et al.* *Liebigs Ann. Recueil*, **1997**, 2485–2494.
16. Rapenne, G., Dietrich-Buchecker, C. & Sauvage, J-P. *J. Am. Chem. Soc.*, **1999**, 121, 994–1001.
17. Safarowsky, O., Nieger, M., Fröhlich, R. & Vögtle, F. *Angew. Chem. Int. Ed.*, **2000**, 39, 1616–1618.
18. Lukin, O. & Vögtle, F. *Angew. Chem. Int. Ed.*, **2005**, 44, 1456–1477.
19. Feigel, M., Ladberg, R., Engels, S., Herbst-Irmer, R. & Fröhlich, R. *Angew. Chem. Int. Ed.*, **2006**, 45, 5698–5702.
20. Fenlon, E. E. & Ito, B. R. *Eur. J. Org. Chem.*, **2008**, 3065–3068.
21. Guo, J., Mayers, P. C., Breault, G. A. & Hunter, C. A. *Nature Chem.*, **2010**, 2, 218–222.
22. Barran, P. E. *et al.* *Angew. Chem. Int. Ed.*, **2011**, 50, 12280–12284.
23. Carina, R.F., Dietrich-Buchecker, C. & Sauvage, J.-P., *J. Am. Chem. Soc.*, **1996**, 118, 9110–9116.

24. Fujita, M., Ibukuro, F., Hagihara, H. & Ogura, K. *Nature*, **1994**, *367*, 720–723.
25. Wang, L., Vysotsky, M. O., Bogdan, A., Bolte, M. & Böhmer, V. *Science*, **2004**, *304*, 1312–1314.
26. Lam, R. T. S. *et al.* *Science*, **2005**, *308*, 667–669.
27. Ronson, T. K. *et al.* *Nature Chem.*, **2009**, *1*, 212–216.
28. Hasell, T. *et al.* *Nature Chem.*, **2010**, *2*, 750–755.
29. Chichak, K. S. *et al.* *Science*, **2004**, *304*, 1308–1312.
30. Dietrich-Buchecker, C., Colasson, B., Jouvenot, D. & Sauvage, J-P. *Chem. Eur. J.*, **2005**, *11*, 4374–4386.
31. Hasenknopf, B., Lehn, J-M., Kneisel, B. O., Baum, G. & Fenske, D. *Angew. Chem. Int. Ed. Engl.*, **1996**, *35*, 1838–1840.
32. Hasenknopf, B. *et al.* *J. Am. Chem. Soc.*, **1997**, *119*, 10956–10962.
33. Hasenknopf, B., Lehn, J-M., Boumediene, N., Leize, E. & Van Dorsselaer, A. *Angew. Chem. Int. Ed.*, **1998**, *37*, 3265–3268.
34. Leigh, D. A., Lusby, P. J., Teat, S. J., Wilson, A. J. & Wong, J. K. Y. *Angew. Chem. Int. Ed.*, **2001**, *40*, 1538–1543.
35. Hogg, L. *et al.* *Angew. Chem. Int. Ed.*, **2004**, *43*, 1218–1221.
36. Hutin, M., Schalley, C. A., Bernardinelli, G. & Nitschke, J. R. *Chem. Eur. J.*, **2006**, *12*, 4069–4076.
37. Price, J. R. *et al.* *Aust. J. Chem.*, **2009**, *62*, 1014–1019.
38. Murcko, M. A. & DiPaola, R. A. *J. Am. Chem. Soc.*, **1992**, *114*, 10010–10018.
39. Ohsawa, Y., DeArmond, M. K., Hanck, K. W. & Moreland, C. G. *J. Am. Chem. Soc.*, **1985**, *107*, 5383–5386.
40. Mamula, O., von Zelewsky, A. & Bernardinelli, G. *Angew. Chem. Int. Ed.*, **1998**, *37*, 290–293.
41. Krämer, R., Lehn, J-M. & Marquis-Rigault, A. *Proc. Natl Acad. Sci. USA*, **1993**, *90*, 5394–5398.
42. Albrecht, M. *Chem. Rev.*, **2001**, *101*, 3457–3497.
43. Nitschke, J. R. *Acc. Chem. Res.*, **2007**, *40*, 103–112.
44. Bai, X.-L., Liu, X.-D., Wang, M., Kang, C.-Q. & Gao, L.-X. *Synthesis*, **2005**, 458–464.
45. Case, F. H. *J. Am. Chem. Soc.*, **1946**, *68*, 2574–2577.

46. Khan, M. S. et al. *J. Chem. Soc., Dalton Trans.*, **2002**, 1358-1368.
47. Grosshenny, V., Romero, F. M. & Ziesel, R. *J. Org. Chem.*, **1997**, 62, 1491-1500.
48. Song, J. J. et al. *Org. Lett.*, **2004**, 6, 4905-4907.
49. Landa, A., Minkkila, A., Blay, G. & Joergensen, K. A. Bis(oxazoline) *Chem.- Eur. J.*, **2006**, 12, 3472-3483.
50. Bosnich, B. *Acc. Chem. Res.*, **1969**, 2, 266-273.
51. Mason, S. F. *Pure Appl. Chem.*, **1970**, 24, 335-359.
52. Ziegler, M. & von Zelewsky, A. *Coord. Chem. Rev.*, **1998**, 177, 257-300.
53. Mason, S. F. & Peart, B. J. *J. Chem. Soc., Dalton Trans.*, **1973**, 949-955.
54. Hidaka, J. & Douglas, B. E. *Inorg. Chem.*, **1964**, 3, 1180-1184.
55. Mürner, H., von Zelewsky, A. & Hopfgartner, G. *Inorg. Chim. Acta.*, **1998**, 271, 36-39.
56. Kiehne, U. & Luetzen, A. *Org. Lett.*, **2007**, 9, 5333-5336.
57. Howson, S. E. et al. *Chem. Commun.*, **2009**, 1727-1729.
58. Mason, S. F. & Peart, B. J. *J. Chem. Soc., Dalton Trans.*, **1973**, 949-955.
59. CrystalClear-SM Expert v. 2.0 r5 program suite (Rigaku Corporation, Japan, **2010**).
60. Palatinus, L. & Chapuis, G. *J. Appl. Crystallogr.*, **2007**, 40, 786-790.
61. Farrugia, L. J. *J. Appl. Crystallogr.*, **1999**, 32, 837-838.
62. Sheldrick, G. M. *Acta Crystallogr., Sect. A* A64, **2008**, 112-122.
63. PLATON, A Multipurpose Crystallographic Tool (Utrecht University, Utrecht, The Netherlands, **2008**).

Chapter III: "Pentameric Circular Iron(II) Double Helicates and a Molecular Pentafoil Knot"

Published as "Pentameric Circular Iron(II) Double Helicates and a Molecular Pentafoil Knot", J.-F. Ayme, J. E. Beves, D. A. Leigh, R. T. McBurney, K. Rissanen and D. Schultz, *J. Am. Chem. Soc.*, **2012**, *134*, 9488-9497.

Acknowledgements

Dr. D.Schultz and Dr. R. T. McBurney are gratefully acknowledged for their contribution to this chapter: D.S. and R.T.McB. had performed the synthesis of the knot $[7Cl](PF_6)_9$ prior to the other authors arrival in Edinburgh. In a joint effort J.F.A. and J.E.B. scaled up the synthesis of $[7Cl](PF_6)_9$ and obtained its full characterisation prior to studying the assembly process of the knot $[7Cl](PF_6)_9$ and its corresponding circular double helicates. K. Rissanen is acknowledged for solving the crystal structure of the knot $[7Cl](PF_6)_9$ and the helicate $[3bCl](PF_6)_9$.

3.1. Synopsis

This chapter reports the synthesis of eleven pentameric cyclic double helicates formed by imine condensation of alkyl monoamines with a common bis(formylpyridine)bipyridyl-derived building block, iron(II) and chloride ions. The cyclic double-stranded helicates were characterised by NMR spectroscopy, mass spectrometry, and in the case of a 2,4-dimethoxybenzylamine-derived pentameric cyclic helicate, X-ray crystallography. The importance of the sterical and electronic properties of the amine used in the self-assembly process is assessed along with the factors influencing the assembly process (reactant stoichiometry, concentration, solvent, nature and amount of anion, preformation of the imines). Surprisingly, the role of chloride in the assembly process appears not to be limited to that of a simple template, and larger circular helicates observed with related tris(bipyridine) ligands with different iron salts are not produced with the imine ligands. Using certain chiral amines, pentameric cyclic helices of single handedness could be isolated and the stereochemistry of the helix determined by circular dichroism. By employing a particular diamine, a closed-loop molecular pentafoil knot was prepared. The pentafoil knot was characterised by NMR spectroscopy, mass spectrometry, and X-ray crystallography, confirming the topology and providing insights into the reasons for its formation.

3.2. Introduction

The interweaving of molecular strands in DNA,¹ proteins,² and natural³ and synthetic polymers⁴ significantly affects their mechanical, physical, and chemical properties. The presence of knots in proteins can increase stability and improve function⁵ and has provided insights into the mechanisms of protein folding.^{2a, 3} Knots have been tied in biopolymers with optical tweezers⁶ and can also be formed from surfactant nanotubes⁷ and chiral nematic colloids.⁸ For synthetic chemists the key challenge in the synthesis of entwined and interlocked molecular structures is the generation and linking (with the correct connectivity) of crossing points.⁹ Template and self-assembly methods⁹⁻¹⁴—including the use of metal ions,^{9, 10} π - π interactions,¹¹ hydrogen bonding,¹² hydrophobic interactions,¹³ and anions¹⁴—have proven powerful tools for this task. Sauvage pioneered the use of linear metal helicates¹⁵ to access mechanically interlocked molecules, entwining ligands about one, two, or three tetrahedral copper(I) centers to generate the required crossing points for [2]catenanes,¹⁶ trefoil knots¹⁷ and a Solomon link,¹⁸ respectively. Despite these and other metal template syntheses of trefoil knots¹⁹ and strategies based on hydrogen bonding²⁰ and π - π stacking,²¹ higher-order non-DNA molecular knots remained elusive until the recently described²² synthesis of a molecular pentafoil knot, a closed-loop pentameric cyclic Fe(II) double helicate. Here we report on the chemistry behind that synthesis, including the assembly of 11 ‘open’ pentameric cyclic iron(II) double helicates prepared from monoamines, and the use of this framework to form the molecular pentafoil knot. The cyclic helicates are characterized in solution and the solid state, and the factors affecting the assembly

“Pentameric Circular Iron(II) Double Helicates and a Molecular Pentafoil Knot” process investigated. Both similarities and differences are found between the synthesis of these circular helicates featuring imine bonds and analogous circular helicates derived from tris(bipyridine) ligands.

3.3. Cyclic Helicates and Their Potential for Molecular Knot

Synthesis

Despite the success in using metal helicates to form interlocked molecules with up to four crossing points,¹⁶⁻¹⁸ attempts to generate interlocked structures from longer linear helicates have, to date, proved unsuccessful.²³ This is probably due to the large separation between the end groups of each of the ligand strands disfavoring their reaction to form structures with the required connectivity. Cyclic systems might offer a way of overcoming this problem, since the reactive end-groups can be brought close together in such architectures. The first circular helicates²⁴ were discovered by Lehn and co-workers,^{24a, 24b, 24d} who noted their potential for forming complex topologies.^{24a} However, multiple coupling reactions would be required to form entwined closed loops, which are inherently more demanding than single ring-closing reactions. The coupling reactions would need to be functional group specific, high yielding, and ideally, reversible to allow the potential for error correction of wrongly connected strands during the reaction. The conditions (ethylene glycol, 170 °C^{24a, 24b, 24d}) used to form circular helicates with Lehn’s original tris(bipyridine) ligands are not compatible with most types of reactive functional groups.

In recent years, great strides have been made in dynamic covalent chemistry.²⁵ Reversible imine-bond formation has proven highly effective for linking

“Pentameric Circular Iron(II) Double Helicates and a Molecular Pentafoil Knot” multiple building blocks in the construction of catenanes,²⁶ rotaxanes,²⁷ cages,²⁸ Solomon links,²⁹ and Borromean rings.³⁰ We decided to investigate this method for the formation of cyclic helicates using a ligand inspired by Lehn’s original three-bipyridine-strand design,^{24a} replacing the two terminal bipyridine units with 2-formylpyridine groups. Reaction of dialdehyde **1** with amines (to form imine groups) would generate a tris(bidentate) ligand strand, which we hoped could be assembled into cyclic double helicate structures with iron(II) ions.

3.4. Results and Discussion

Dialdehyde **1** was synthesized from commercially available 5-bromo-2-iodopyridine and 5-bromo-2-formylpyridine via a series of Sonogashira coupling reactions and deprotection steps in 19% overall yield, with six steps in the longest linear sequence (for details, see the Experimental Section).

Reaction of **1** with 2.2 equiv of 4-methoxybenzylamine (**2a**) in DMSO-*d*₆ and 1.1 equiv of anhydrous iron(II) chloride (Scheme 1) immediately gave an intensely colored purple solution, typical of low-spin iron(II) tris(diimine) complexes.³¹ The ¹H NMR spectrum (DMSO-*d*₆) of the initial reaction mixture contained only broad signals, indicative of the formation of poorly defined oligomeric and polymeric species. However, on heating at 60 °C, the spectrum gradually simplified until after 15 h a single major species was present in solution. Anion exchange was performed using excess aqueous potassium hexafluorophosphate (KPF₆) to give a fine purple suspension, which was collected, washed, and dissolved in acetonitrile, to give [**3aCl**](PF₆)₉ in 54% isolated yield. Electrospray mass spectrometry (ESI-MS, Figure 1)

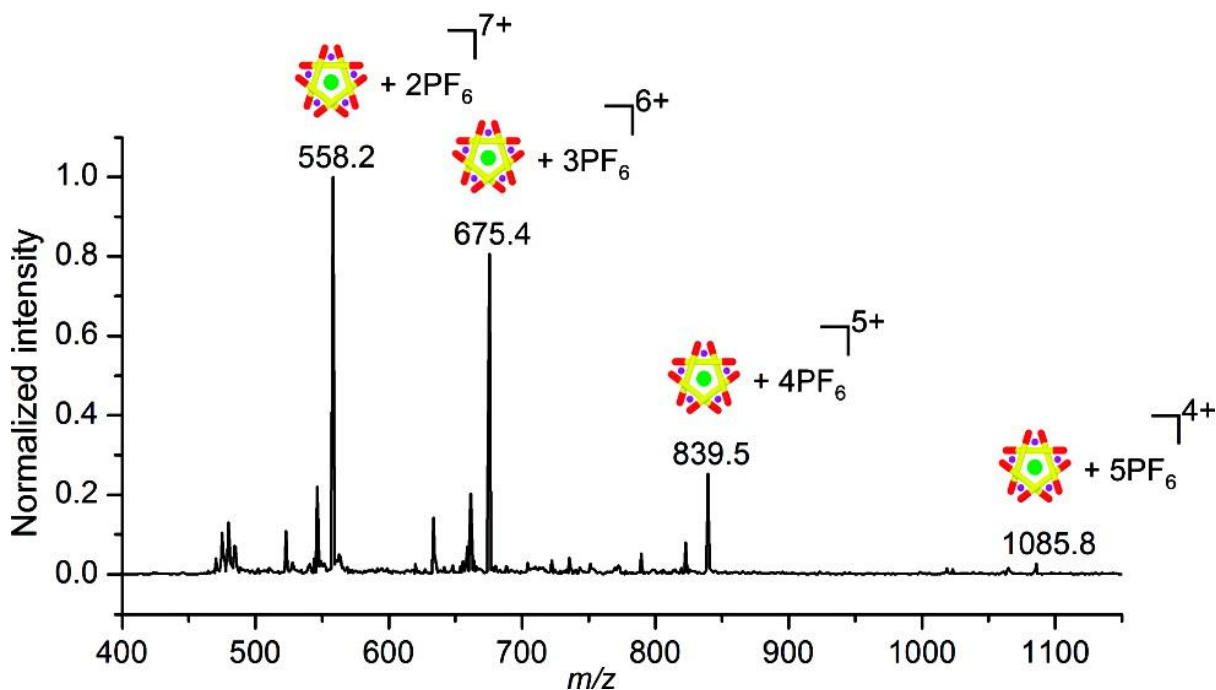


Figure 1. ESI-MS of cyclic helicate $[3aCl](PF_6)_9$ showing signals corresponding to sequential loss of PF_6 anions. Calculated peaks (m/z): 558.2 $[M-7PF_6]^{7+}$, 675.4 $[M-6PF_6]^{6+}$, 839.5 $[M-5PF_6]^{5+}$, 1085.8 $[M-4PF_6]^{4+}$.

showed 3+, 4+, 5+, 6+, and 7+ signals with isotope patterns corresponding to sequential loss of PF_6 anions from a pentameric species containing five ligands, five iron(II) cations, and one chloride anion. No chloride-free species were observed, confirming the binding of a single chloride ion that could not be removed by repeated anion exchange with KPF_6 .

The 1H NMR spectrum of the isolated product contained only one set of signals for each type of building block (no end-groups, Figure 2e), consistent with a symmetrical cyclic structure. Signals for the $py-CH_2$ and $N-CH_2$ methylene groups appear as diastereotopic pairs which, in combination with the ESI-MS data, confirmed the product to be a chiral (racemic) cyclic helicate $[3aCl]^{9+}$ (Scheme 1). The H^{A3} signal (see Scheme 1 for numbering scheme) is shifted to very low field (9.87 ppm), consistent

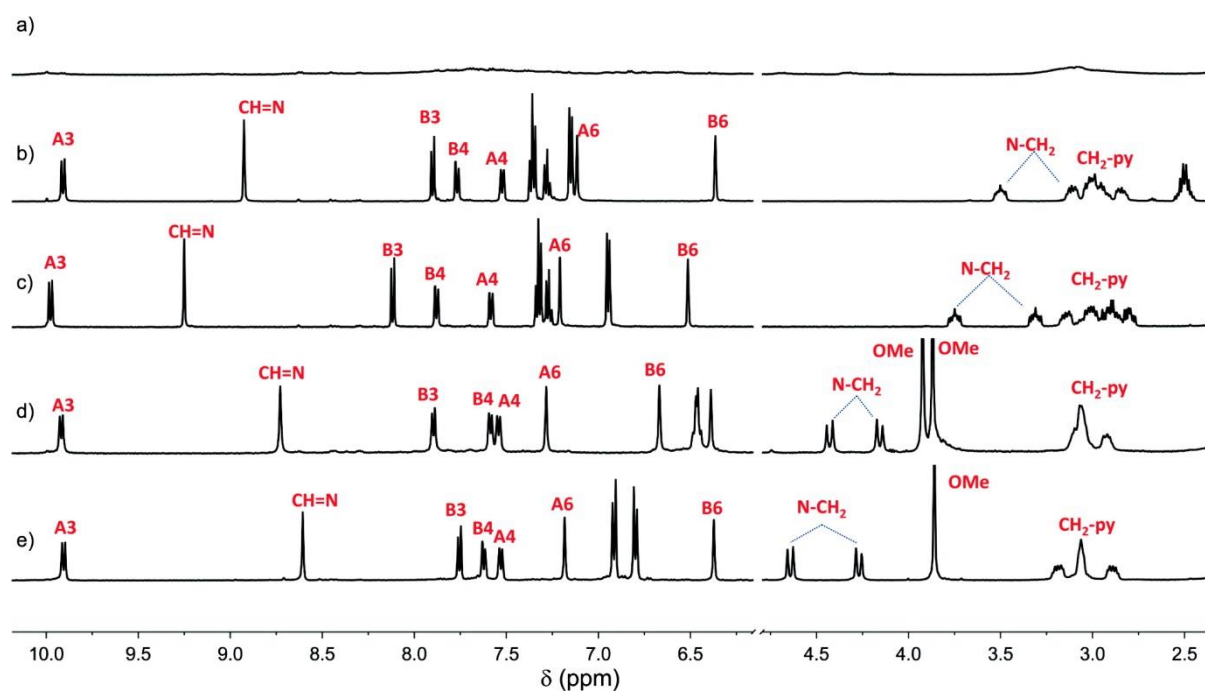
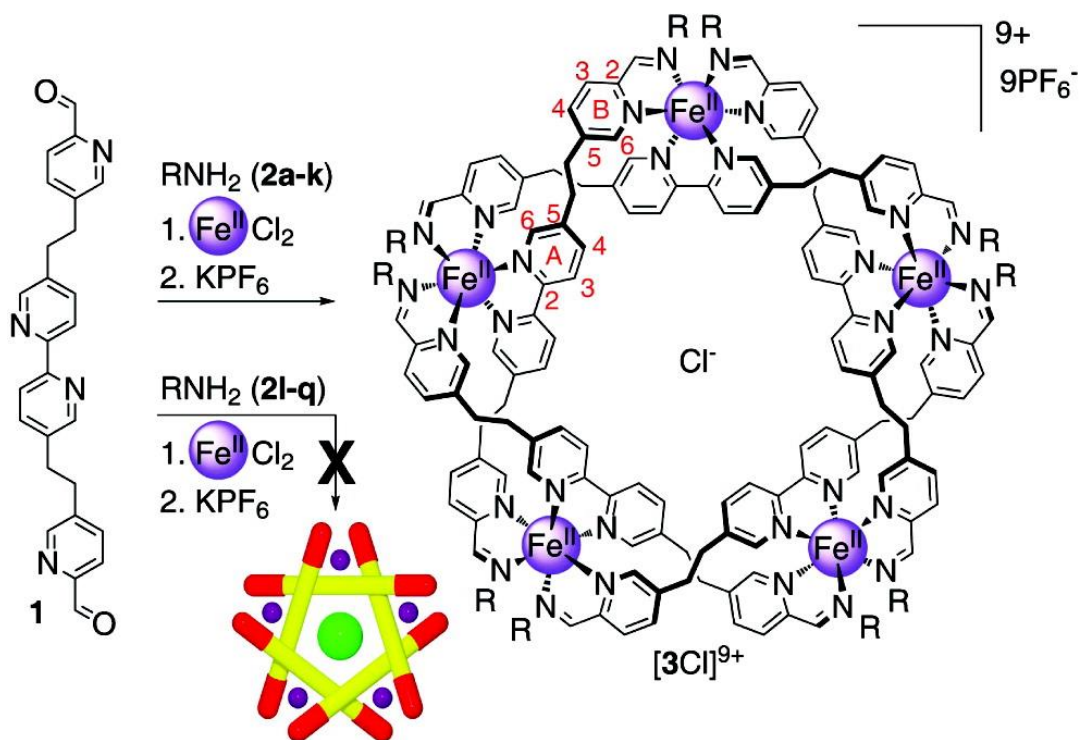


Figure 2. ^1H NMR (CD_3CN , 500 MHz, 298 K) of the products isolated from the reaction of dialdehyde **1** and various amines (**2i**, **2f**, **2e**, **2b**, and **2a**) in the presence of FeCl_2 (Scheme 1). (a) Amine used 4-bromobenzylamine (**2i**; Table1, entry 12). The broad ^1H NMR spectrum is characteristic of polymers. (b) $[\mathbf{3fCl}](\text{PF}_6)_9$. (c) $[\mathbf{3eCl}](\text{PF}_6)_9$. (d) $[\mathbf{3bCl}](\text{PF}_6)_9$. (e) $[\mathbf{3aCl}](\text{PF}_6)_9$. All samples were colored purple of similar intensities. The assignments correspond to the labeling shown in Scheme 1.

with strong hydrogen bonding of these protons to the central chloride ion. Having established that the reaction of these building blocks afforded pentameric cyclic helicates, we sought to probe the structural tolerance of the reaction and investigate factors that control the assembly process.



Scheme 1. Synthesis of Pentameric Cyclic Helicates [3a–k]Cl(PF₆)₉^a

^aReaction conditions: 1. Dialdehyde **1**/FeCl₂/amine **2a–q** (1:1.1:2.2), DMSO-*d*₆, 60 °C, 1–2 days. 2. Aqueous KPF₆.

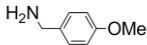
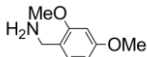
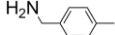
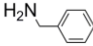
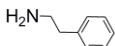
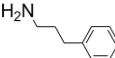

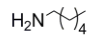
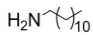
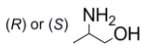
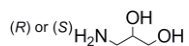
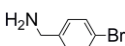
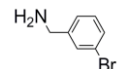
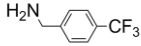
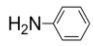
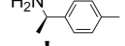
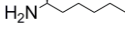
3.5. Structural Requirements for Pentameric Cyclic Helicate

Assembly

The pentameric cyclic helicate assembly process shown in Scheme 1 proved to be very sensitive to the nature of the monoamine building block (Table 1). The effect of having different substituents on benzylamine was profound: electron-withdrawing groups [4-bromo-**2l** (Table 1, entry 12); 3-bromo-**2m** (Table 1, entry 13); 4-trifluoromethyl-**2n**; (Table 1, entry 14)] gave exclusively polymeric or oligomeric products (e.g., Figure 2a). In contrast, the use of electron-rich benzylamine derivatives [4-methoxy-**2a** (Table 1, entry 1); 2,4-dimethoxy-**2b** (Table 1, entry 2)] formed the cyclic helicates in high yields with few byproducts (d and e of Figure 2).

Benzylamine itself gave a modest yield (30%) of cyclic helicate (Table 1, entry 4) accompanied by significant amounts of oligomeric byproducts in the crude reaction mixture.

Table 1. Yields of Pentameric Cyclic Helicates from the Reaction Shown in Scheme 1 with Monoamines 2a–q^a

Entry	Amine	Helicate [FeL ₅ Cl](PF ₆) ₉	Isolated yield (%)
1	2a 	[3aCl](PF₆)₉	54
2	2b 	[3bCl](PF₆)₉	48
3	2c 	[3cCl](PF₆)₉	52
4	2d 	[3dCl](PF₆)₉	30
5	2e 	[3eCl](PF₆)₉	43
6	2f 	[3fCl](PF₆)₉	55
7	2g 	[3gCl](PF₆)₉	52
8	2h 	[3hCl](PF₆)₉	63
9	2i 	[3iCl](PF₆)₉	53 ^b
10	2j 	[3jCl](PF₆)₉	34
11	2k 	[3kCl](PF₆)₉	46 ^c
12	2l 	-	- ^d
13	2m 	-	- ^d
14	2n 	-	- ^e
15	2o 	-	- ^e
16	2p 	-	- ^f
17	2q 	-	- ^f

^a Reaction conditions: 1.1:1.1:2.2 of 1:FeCl₂:amine, DMSO-d₆, 60 °C, 1 d (except Entry 10, 2 d). 2. Aqueous KPF₆. ^b Reaction performed in 1:1 CDCl₃:CD₃CN due to the poor solubility of 2i in DMSO. ^c Yield of major diastereoisomer. ^d Intensely colored purple solutions with only broad ¹H NMR signals, likely polymeric materials. ^e Initially gave an intensely colored purple solution, which became pale yellow upon heating overnight. ^f

“Pentameric Circular Iron(II) Double Helicates and a Molecular Pentafoil Knot”

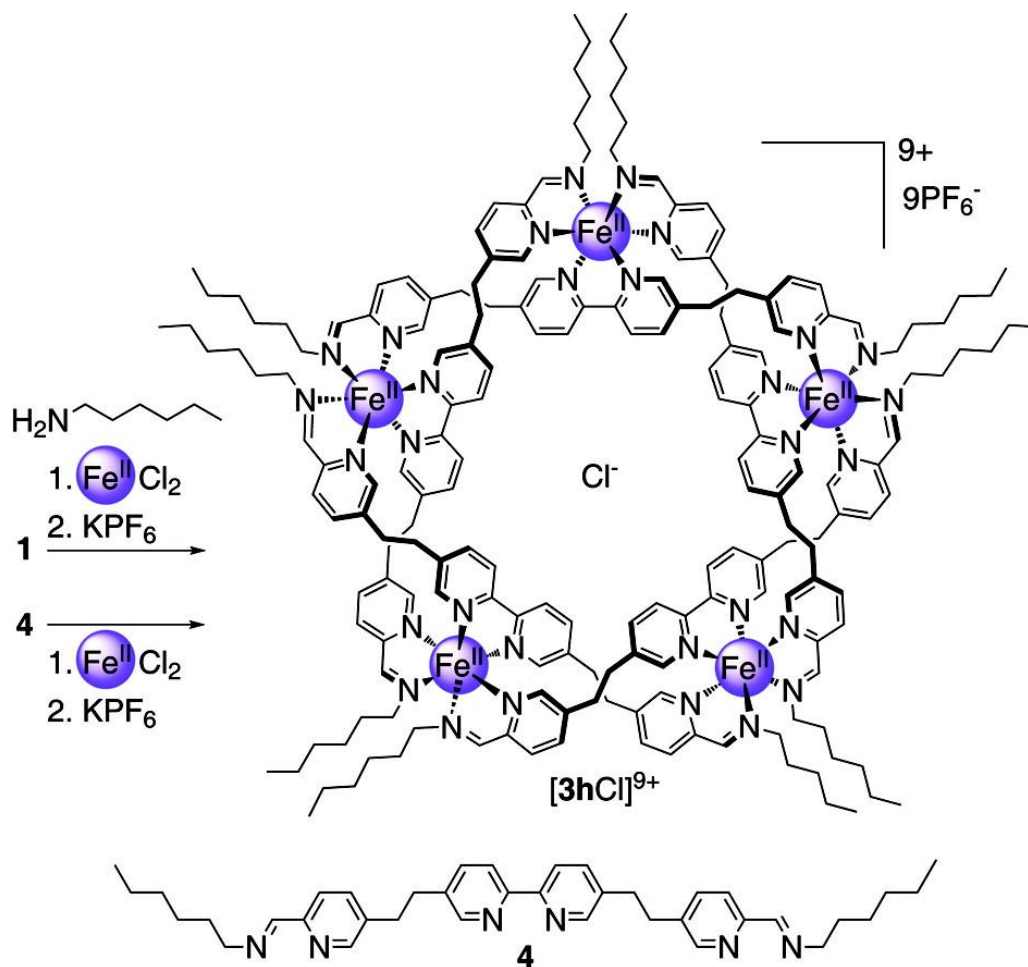
Pale yellow/orange solutions, assumed to be high-spin iron(II) complexes, with no ESI-MS evidence for cyclic helicate formation.

The steric bulk about the amine functional group also significantly influences the outcome of the reaction (Table 1). 3-Phenylpropylamine (**2f**, Table 1, entry 6, 55%) and 4-phenylbutylamine (**2g**, Table 1, entry 7, 52%) resulted in higher cyclic helicate yields than the more hindered 2-phenylethylamine (**2e**, Table 1, entry 5, 43%). The use of anilines (**2o**, Table 1, entry 15) or sterically hindered amines (**2p** and **2q**, Table 1, entries 16 and 17) initially gave intensely purple-colored solutions apparently consisting of polymeric species (broad ^1H NMR spectra). However, upon being heated, pale-orange high-spin iron(II) complexes were formed, with no ESI-MS evidence for the formation of short linear or cyclic helicates. Sterically unhindered aliphatic primary amines (e.g., hexylamine **2h** and dodecylamine **2i**, Table 1, entries 8 and 9) gave the highest yields of cyclic helicates (63% for $[\mathbf{3hCl}](\text{PF}_6)_3$) and the fewest byproducts.

3.6. Probing the Reaction Conditions of Pentameric Cyclic

Helicate Assembly

Various factors (reagent stoichiometry, influence of various anions, the role of chloride, the effect of solvent, concentration, and preforming the diimine ligand) influencing the outcome of the pentameric cyclic helicate-forming reaction shown in Scheme 1 were investigated, mainly through a series of studies using hexylamine (**2h**) as the amine (Scheme 2).



Scheme 2. Synthesis of Pentameric Cyclic Helicate $[\text{3h}]\text{Cl}(\text{PF}_6)_9$ from Dialdehyde **1** and Hexylamine (**2h**) or Preformed Diimine Ligand **4**^a

^aReaction conditions: 1. Dialdehyde **1**/ FeCl_2 /**2h** (1:1.1:2.2) or **4**/ FeCl_2 (1:1.1), $\text{DMSO}-d_6$, 60 °C, 1 day. 2. Aqueous KPF_6 .

3.6.1. Reactant Stoichiometry

Reactant stoichiometry proved to be extremely important, with a ratio of 1:1.1:2.2 dialdehyde**1**/ FeCl_2 /**2h** giving 63% of cyclic helicate $[\text{3h}]\text{Cl}(\text{PF}_6)_9$ (Table 1, entry 8). The use of less than 2 equiv of amine **2h** (with respect to **1**) gave mixtures of products, including $[\text{Fe}(\text{1})_3]^{6+}$ and related species (see Experimental Section, Figure 20). Substoichiometric amounts of FeCl_2 (with respect to **1**) gave low yields of circular helicate and complex mixtures of products (SI, Figure 19). Although employing an

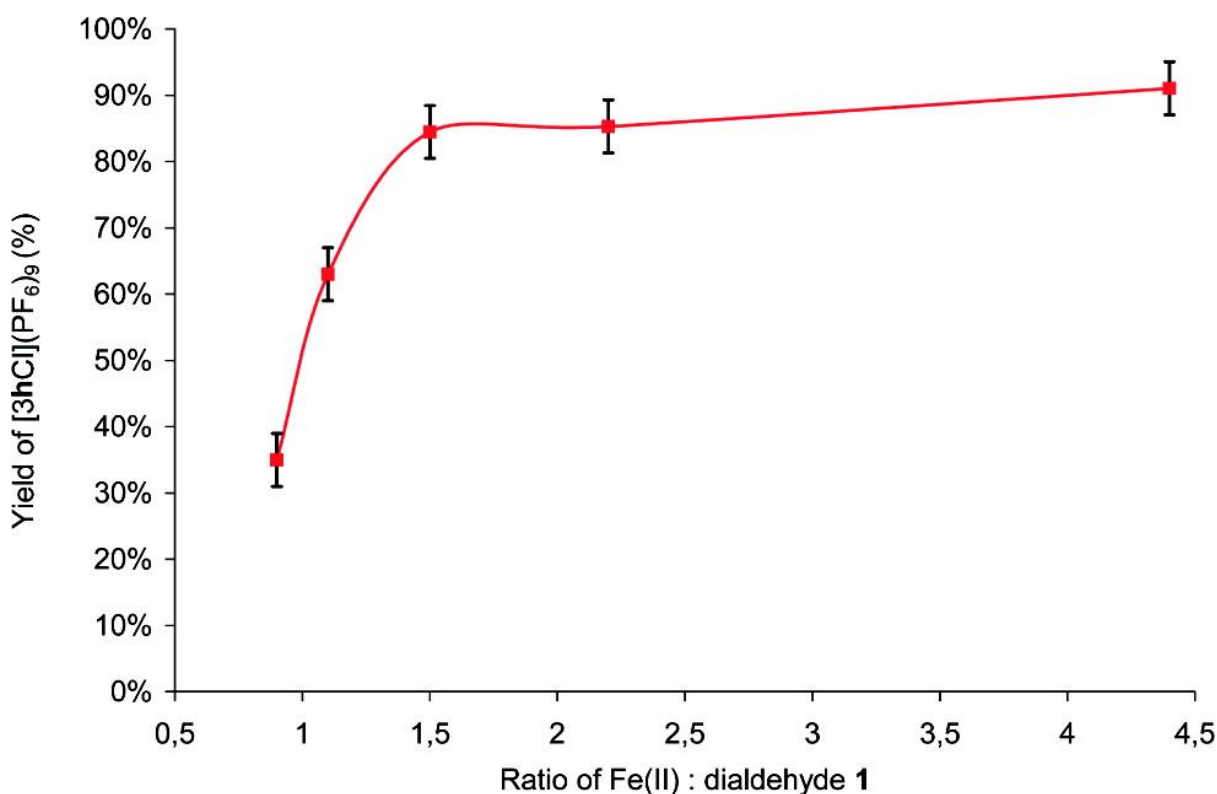


Figure 3. Influence of FeCl₂/dialdehyde **1** ratio [2.2 equiv of hexylamine (**2h**)] on the yield of [3hCl](PF₆)₉. Error bars ±5%.

excess of amine also resulted in a substantial decrease in yield (SI, Figure 20), the lack of other high-molecular weight byproducts meant that the cyclic helicate products were most easily isolated using these conditions. Somewhat surprisingly, the use of excess FeCl₂ gave the highest yields of cyclic helicate with 1.5, 2.2, and 4.4 equiv of FeCl₂ (with respect to **1**) giving 84, 85, and 91% yields of [3hCl](PF₆)₉, respectively (Figure 3).

3.6.2. Influence of Anions

The substitution of FeCl₂ for other iron(II) salts [Fe(SO₄)₂·7H₂O, Fe(CH₃CO₂)₂, Fe(BF₄)₂·6H₂O, Fe(ClO₄)₂·6H₂O, Fe(ClO₄)₂·xH₂O] in the reactions shown in Scheme 1 invariably gave complex mixtures with no ESI-MS evidence for the formation of

“Pentameric Circular Iron(II) Double Helicates and a Molecular Pentafoil Knot” circular helicates of any size, in contrast to the cyclic hexameric helicate reported by Lehn using his related tris(bipyridine) ligand with $\text{Fe}(\text{BF}_4)_2 \cdot 6\text{H}_2\text{O}$ or FeBr_2 .^{24b} However, when 4-methylbenzylamine (**2c**) was employed with iron(II) tetrafluoroborate [$\text{Fe}(\text{BF}_4)_2 \cdot 6\text{H}_2\text{O}$] or iron(II) perchlorate [$\text{Fe}(\text{ClO}_4)_2 \cdot 6\text{H}_2\text{O}$] a discrete low-molecular weight product was formed in under 10% yield; no related products were observed with hexylamine (**2h**) or other aliphatic amines. ESI-MS evidence supported the assignment of this minor product as the linear trinuclear triple-stranded helicate^{24a} [Fe_3L_3]⁶⁺ (see Experimental Section, page S22).

3.6.3. Role of Chloride Ions

The role of chloride in the pentameric cyclic helicate forming reaction shown in Scheme 2 was investigated using varying amounts of $\text{Fe}(\text{BF}_4)_2 \cdot 6\text{H}_2\text{O}$ and FeCl_2 in order to vary the amount of chloride present in the reaction while maintaining a constant iron(II) concentration (Figure 4, blue data points). The yield of the isolated cyclic pentameric helicate [**3hCl**]⁹⁺ increased steeply with the amount of chloride, up to 0.4 chloride ions per iron(II) (i.e., approximately two chloride ions per cyclic helicate, 44% yield), and then increased less sharply as the amount of chloride increased further up to 63% with 2.0 Cl^- per Fe(II).

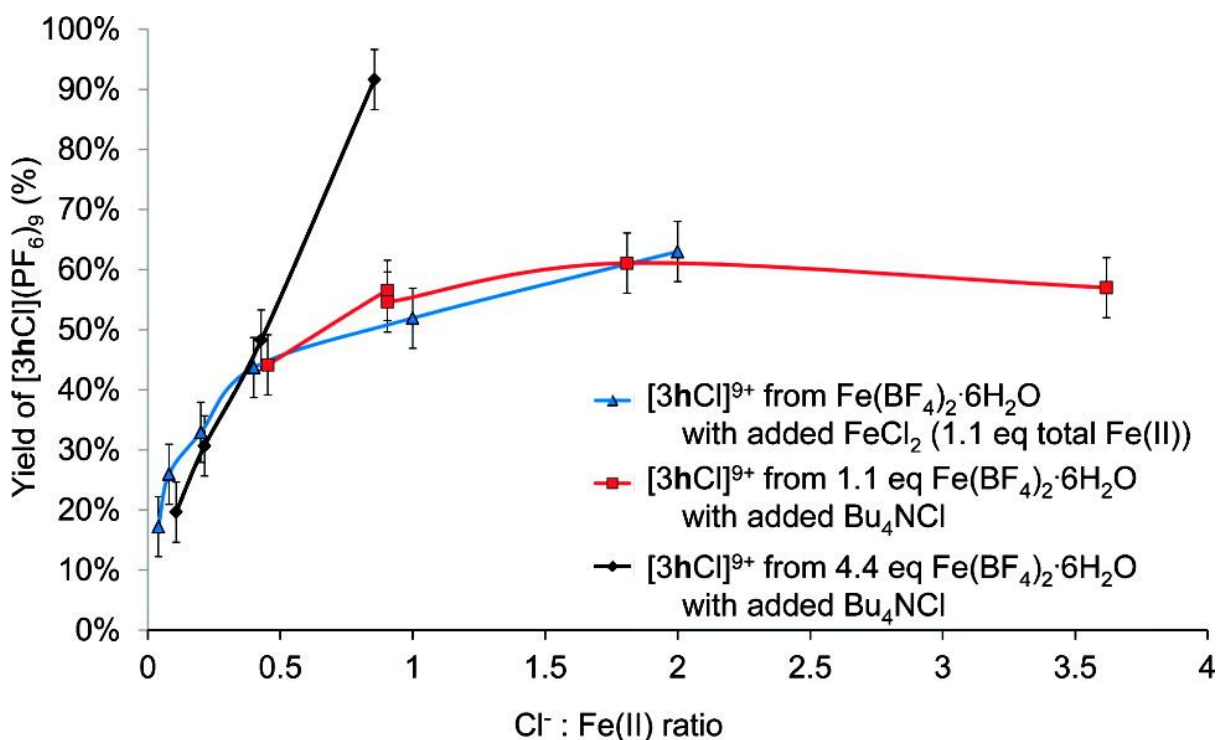


Figure 4. Effect of chloride ions on the yield of helicate $[3hCl]^{9+}$. The reactions were carried out using mixtures of either $Fe(BF_4)_2 \cdot 6H_2O$ and $FeCl_2$ (blue data points), or $Fe(BF_4)_2 \cdot 6H_2O$ and tetrabutylammonium chloride (red data points = 1.1 equiv of Fe(II); black data points = 4.4 total equiv of Fe(II)), with Bu_4NBF_4 added to maintain a constant Bu_4N^+ concentration. In all cases the ratio of dialdehyde (**1**)/hexylamine (**2h**) was 1:1.1. The highest yield, 90%, was obtained using 4.4 equiv of $Fe(BF_4)_2 \cdot 6H_2O$ (with respect to dialdehyde **1**) with 4 equiv of Bu_4NCl (i.e., 0.9 equiv of Cl^- per Fe(II); black line). Error bars $\pm 5\%$. See Experimental Section, Figure 24.

Similar results were obtained using $Fe(BF_4)_2 \cdot 6H_2O$ as the sole iron(II) source and adding tetrabutylammonium chloride³² (Figure 4, red data points, and SI, Figure 25). Under these conditions chloride/iron(II) ratios greater than 2:1 could be obtained, which resulted in slight decreases in yield (e.g., 4:1 Cl/Fe gave 60% yield of $[3hCl]^{9+}$). Interestingly, the use of higher ratios with respect to **1** of both Fe(II) and Cl^- resulted in significant increases in yield. For example, where 4.4 equiv of $Fe(BF_4)_2 \cdot 6H_2O$ was used (with respect to **1**) the yield of $[3hCl]^{9+}$ increased linearly with chloride concentration, with 90% yield being obtained where 4 equiv of chloride (with

“Pentameric Circular Iron(II) Double Helicates and a Molecular Pentafoil Knot” respect to dialdehyde **1**) was added (Figure 4, black data points). A similar yield was obtained where 4.4 equiv of FeCl₂ was used (see section 5.1, Reactant Stoichiometry). The pentameric cyclic helicates bind Cl⁻ ions extremely strongly ($K_a > 10^{10} \text{ M}^{-1}$) in a 1:1 complex.^{22a} The finding that one equivalent of chloride is not generally sufficient to effectively template the formation of the circular pentameric helicates at millimolar concentrations appears to rule out a simple thermodynamic template effect^{33,9} and indicates that the chloride ions play a more complicated role in the assembly process. It seems likely that they aid the rearrangement of oligomers in the reaction mixture until the stable chloride-binding pentameric cyclic helicate is formed.³⁴

3.6.4. Solvent and Concentration

DMSO proved to be the solvent of choice for the pentameric cyclic helicate-forming reactions for most amines, with methanol, ethanol, nitromethane, acetonitrile, diglyme (MeOCH₂CH₂OMe), and mixtures of these solvents with halogenated solvents either giving precipitates or pale-yellow solutions indicative of high-spin iron(II) complexes. Dodecylamine (**2i**) proved an exception,³⁵ with helicate [**3iCl**]⁹⁺ being formed in good yield in acetonitrile–chloroform (1:1) solution (Table 1, entry 9), presumably due to the solubilizing effect of the long alkyl chains. Generally, heating the reaction mixtures at higher temperatures (e.g., 100 °C in DMSO) resulted in discoloration over several hours, indicating decomposition of the putative Fe(II)–diimine complexes.³⁶ Reaction concentration is also important,^{24b} with relatively high initial concentrations of reactants (~5 mM) delivering the highest yields of pentameric cyclic helicate products. Very dilute reaction conditions (<0.01 mM) gave low yields of circular helicates.

3.6.5. Rate of Pentameric Circular Helicate Formation

The rate of formation of pentameric cyclic helicate $[3hCl]^{9+}$ (Scheme 2) was followed by 1H NMR spectroscopy (Figure 5, red data points). Under the standard reaction conditions (**1**/ $FeCl_2$ /**2h**(1:1.1:2.2), $DMSO-d_6$, 60 °C) the reaction was essentially complete after 24 h (after which time there was little change in the 1H NMR spectrum). In order to simplify the study of the assembly process, ligand **4** was prepared to both eliminate initial imine formation from the reaction kinetics and to allow a strict 1:1 ratio of amine/aldehyde to be employed (see Experimental Section, Figure 17).

When employing **4** instead of **1** and **2h** in the reaction shown in Scheme 2, the rate of pentameric cyclic helicate ($[3hCl]^{9+}$) formation was more rapid (Figure 5, pink data points), although some imine hydrolysis was also observed. A comparison of the rate of formation of $[3hCl]^{9+}$ when starting from **4** or **1/2h** confirms that metal–ligand exchange is likely the rate-limiting factor in the rearrangement of rapidly formed simple complexes (e.g., $Fe_3(4)_3$ and related species), oligomers, and polymers into the pentameric cyclic helicate.

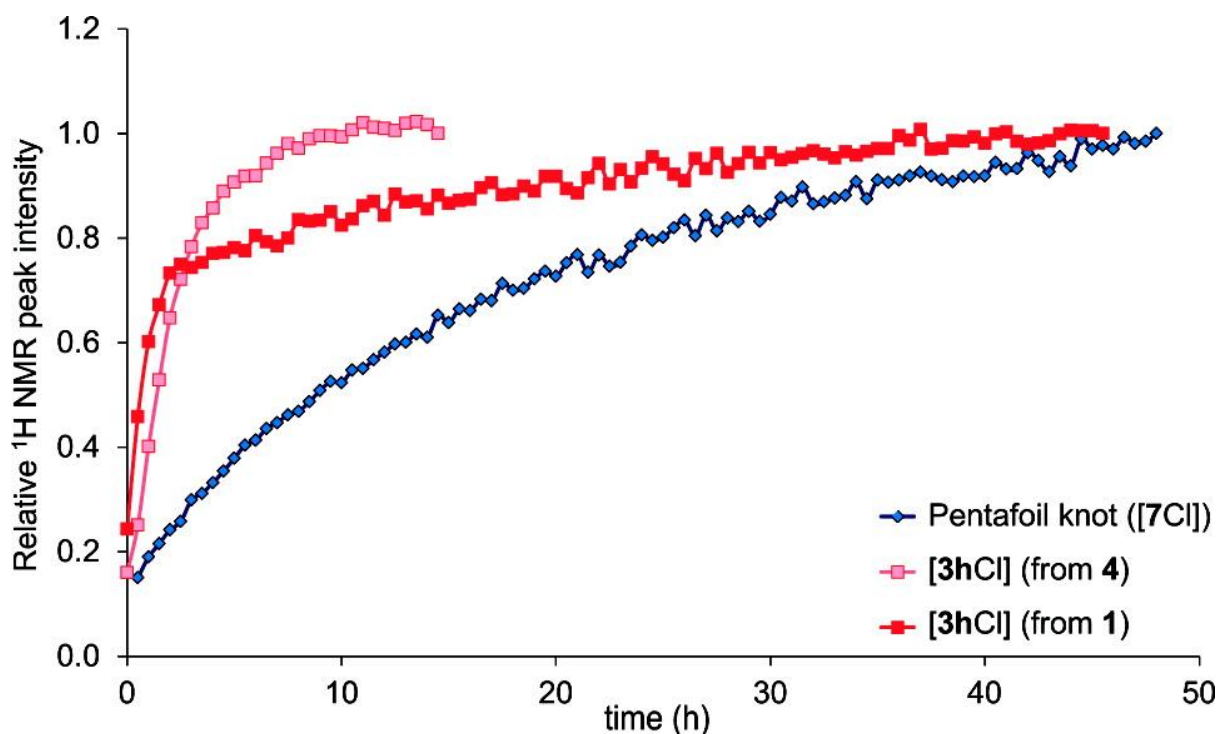


Figure 5. Rate of formation of pentameric cyclic helicate $[3hCl]^{9+}$ (Scheme 2) from dialdehyde **1** and hexylamine (**2h**) (pink squares) or from preformed ligand **4** (red squares). The rate of formation of pentafoil knot $[7Cl]^{9+}$ from dialdehyde **1** and diamine **6** (Scheme 3) is also shown (blue diamonds). The reactions were maintained at 60 °C and 1H NMR spectra collected (600 MHz, $DMSO-d_6$) every 30 min. Relative peak integral of imine peak shown, normalized to the integral of the final time-point in each case. See Experimental Section, Figure 17 and 18.

3.6.6. X-ray Crystal Structure of Pentameric Cyclic Helicate

$[3bCl](PF_6)_9$

Purple crystals of pentameric circular helicate $[3bCl](PF_6)_9$ suitable for single-crystal X-ray diffraction were grown by slow diffusion of diethyl ether vapor into a solution of the complex in nitromethane–acetonitrile. The structure crystallized in the $P2_1/c$ space group with the asymmetric unit containing a single pentameric cyclic helicate (Figure 6).³⁷ The five iron(II) centers lie in a near-perfect plane (maximum displacement of a Fe(II) from the least-squares plane is 0.091(1) Å). The coordination

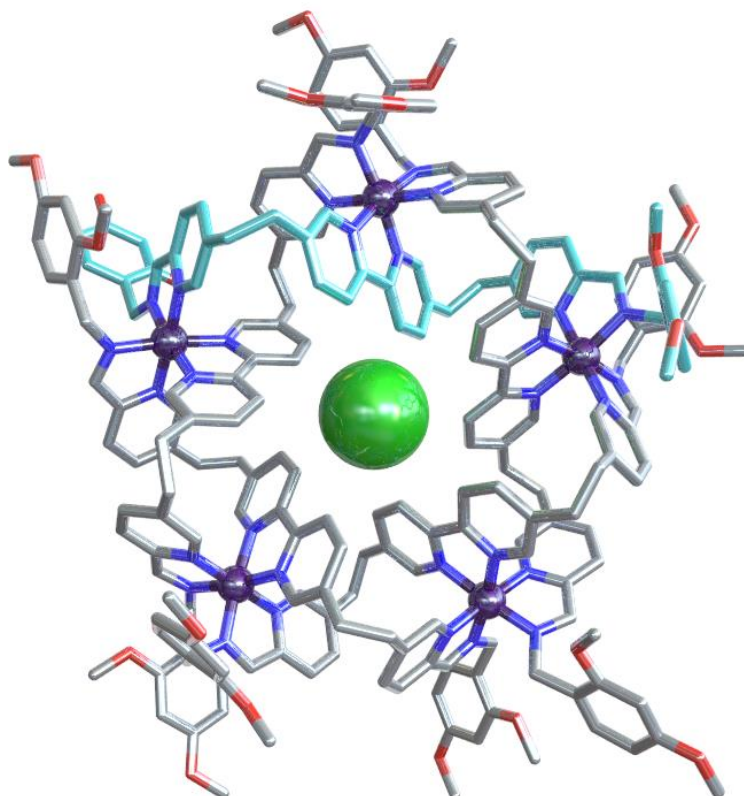


Figure 6. X-ray crystal structure of $[\mathbf{3bCl}](\text{PF}_6)_9 \cdot x\text{solvent}$, from a single crystal obtained by vapor diffusion of diethyl ether into a acetonitrile–nitromethane solution.³⁷ Anions, solvent molecules, and hydrogen atoms are omitted for clarity. Nitrogen atoms are shown in dark blue, oxygen atoms red, chlorine atom green, and carbon atoms gray; the carbon framework of a single ligand is colored light blue. Fe(II) centers shown at 50% van der Waals radius, Cl^- shown at 100%. $\text{Cl}^- \cdots \text{HC}$ distances (clockwise from top-left blue bipyridine unit): 2.75, 2.68, 2.69, 2.81, 2.78, 2.68, 2.71, 2.71, 2.73, 2.78 Å. C–H–Cl angles (deg) 176.3, 177.5, 175.5, 176.7, 178.4, 175.8, 178.1, 179.4, 174.0, 176.8. For packing diagrams, see Experimental Section, Figures S24 and S25.

geometry of the iron(II) ions shows Fe–N and N–Fe–N bond lengths and angles at the limits of normal ranges and, as for Lehn’s pentameric cyclic helicate,^{24a} the overall geometries of the metal centers are among the most distorted for $[\text{Fe}(\text{pyridine})_6]$ structures in the Cambridge Structural Database (CSD) (see Experimental Section). The chloride ion is in close contact with the 10 H^{A3} protons ($\text{Cl}^- \cdots \text{H}^{\text{A3}}\text{C}$ distances 2.679(1)–2.814(1) Å) and displaced from the least-squares plane defined by the five

“Pentameric Circular Iron(II) Double Helicates and a Molecular Pentafoil Knot”
Fe(II) centers by 1.475(1) Å, indicating that the symmetry of the solution ¹H NMR spectrum must result from oscillation of the anion between the two sides of the circular helicate that is fast on the NMR time scale. The phenyl rings adopt a range of orientations, engaging in weak π–π stacking interactions to form zigzag 2D sheets of helicates in the *ab*-plane (see Experimental Section), with weaker interactions between these sheets.

3.7. Controlling the Helix Stereochemistry of Pentameric

Cyclic Helicates

We next focused on attempting to form pentameric cyclic helicates of single handedness. Many examples of stereochemical control of linear helicate formation have been reported,³⁸ and one example of a single-stranded circular helicate,^{38d} usually by employing chiral auxiliaries covalently attached to the ends of the ligands or by incorporating chiral structures such as BINOL (1,1'-bi-2-naphthol) or *trans*-1,2-diaminocyclohexane into the center regions of the ligands. The aldehyde groups at either end of building block **1** enables the straightforward preparation of enantiopure ligands by condensation reactions with appropriate chiral amines.^{38m}

Initially, we investigated chiral derivatives closely related to those of monoamines found to form pentameric cyclic helicates in reasonable yields, i.e. amines **2p** and **2q** (Table 1, entries 16 and 17). Disappointingly, however, both amines generated only pale yellow reaction mixtures (indicative of high-spin iron(II) complexes) and no discrete complexes could be isolated following anion exchange. This also proved to be the case for a range of other chiral α-substituted amines (see

“Pentameric Circular Iron(II) Double Helicates and a Molecular Pentafoil Knot” Experimental Section, Figure 15). We speculated that the methyl group adjacent to the amine might be too sterically demanding to allow helicate formation (see section 4, Structural Requirements for Pentameric Cyclic Helicate Assembly) and tried a primary amine with a chiral hydroxyl group two atoms away from the amine center ((*R*)-**2k**). This formed both diastereoisomers of pentameric cyclic helicate [**3kCl**]⁹⁺ with ~1:2 diastereoselectivity (Table 1, entry 11, and Figure 7c). The major diastereomer was isolated in 46% yield by recrystallization from acetonitrile–water (the minor diastereoisomer has significantly higher solubility).

Finally, in contrast to the unsuccessful reactions with other α -substituted primary amines (Table 1, entries 16 and 17, and SI, Figure 15), enantiopure (*R*)- or (*S*)-2-amino-1-propanol (**2j**) generated pentameric cyclic helicate [**3jCl**]⁹⁺ with complete diastereoselectivity (the enantiomers of the amine-producing pentameric cyclic helicates of opposite helix stereochemistry), in isolated yields of 32%. The ¹H NMR spectra showed a large and unexpected peak shift for the H^{A6} signal, shifted downfield by 0.63 ppm relative to the equivalent signal of helicate [**3hCl**](PF₆)₉. A ROESY NMR spectrum was consistent with the presence of a CH...O hydrogen bond between the OH group and H^{A6} of the bipyridine unit (SI, Figure 28) which likely plays a significant stabilizing role in formation of the pentameric cyclic helicate from this hindered amine.

The helix stereochemistry of the pentameric cyclic helicates formed from the chiral amines was investigated by circular dichroism (CD). The UV–visible absorption spectrum of helicate [**3jCl**](PF₆)₉ is shown in Figure 8 and is representative of helicates [**3a–kCl**](PF₆)₉. An intense and broad MLCT transition is centered at 566 nm,

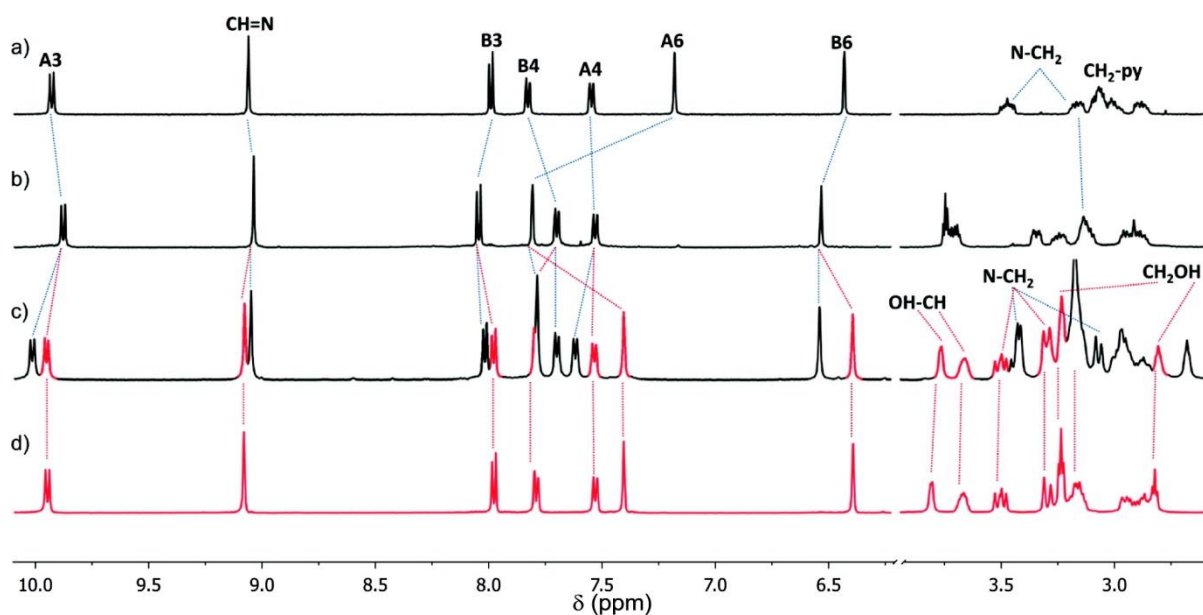


Figure 7. ^1H NMR (500 MHz, CD_3CN , 298 K) of pentameric cyclic helicates derived from (a) hexylamine ($[\mathbf{3hCl}](\text{PF}_6)_9$), (b) diastereoselective helicate $[\mathbf{3jCl}](\text{PF}_6)_9$, (c) mixture of diastereomers formed with (*R*)-amino-2,3-propanediol ($\mathbf{2k}$) (This spectrum is after partial workup and has been enriched in the minor diastereomer. The crude reaction mixture shows a $\sim 1:2$ ratio of diastereomers.), and (d) isolated major diastereoisomer ($[\mathbf{3kCl}](\text{PF}_6)_9$) from (*R*)-amino-2,3-propanediol ($\mathbf{2k}$). The assignments correspond to the labeling shown in Scheme 1.

with a shoulder at higher energy (centered at 520 nm)³⁹ and a strong $\pi\text{-}\pi^*$ transition at 310 nm, typical of low-spin $[\text{Fe}(\text{diimine})_3]^{2+}$ complexes. The CD spectra of (*R*)- $[\mathbf{3jCl}](\text{PF}_6)_9$ and (*S*)- $[\mathbf{3jCl}](\text{PF}_6)_9$ are shown in Figure 8 and are qualitatively similar to those of related systems.⁴⁰ The interpretation of CD spectra of octahedral coordination complexes has been shown to be a reliable means of assigning absolute stereochemistry of $\text{M}(\text{N}^{\wedge}\text{N})_3$ ($\text{N}^{\wedge}\text{N}$ = 2,2'-bipyridine, 1,10-phenanthroline)-type complexes using exciton theory.⁴¹ Using this method, the CD spectra of [(*R*)- $\mathbf{3jCl}$]⁹⁺ and [(*S*)- $\mathbf{3jCl}$]⁹⁺ were assigned as $\Delta\Delta\Delta\Delta$ - $[\mathbf{3jCl}]^{9+}$ and $\Lambda\Lambda\Lambda\Lambda$ - $[\mathbf{3jCl}]^{9+}$, respectively, in agreement with related assignments (SI, pages S38–S40).⁴² The isolated major diastereomer [(*R*)- $\mathbf{3kCl}$]⁹⁺ has a CD spectrum similar to that of [(*S*)-

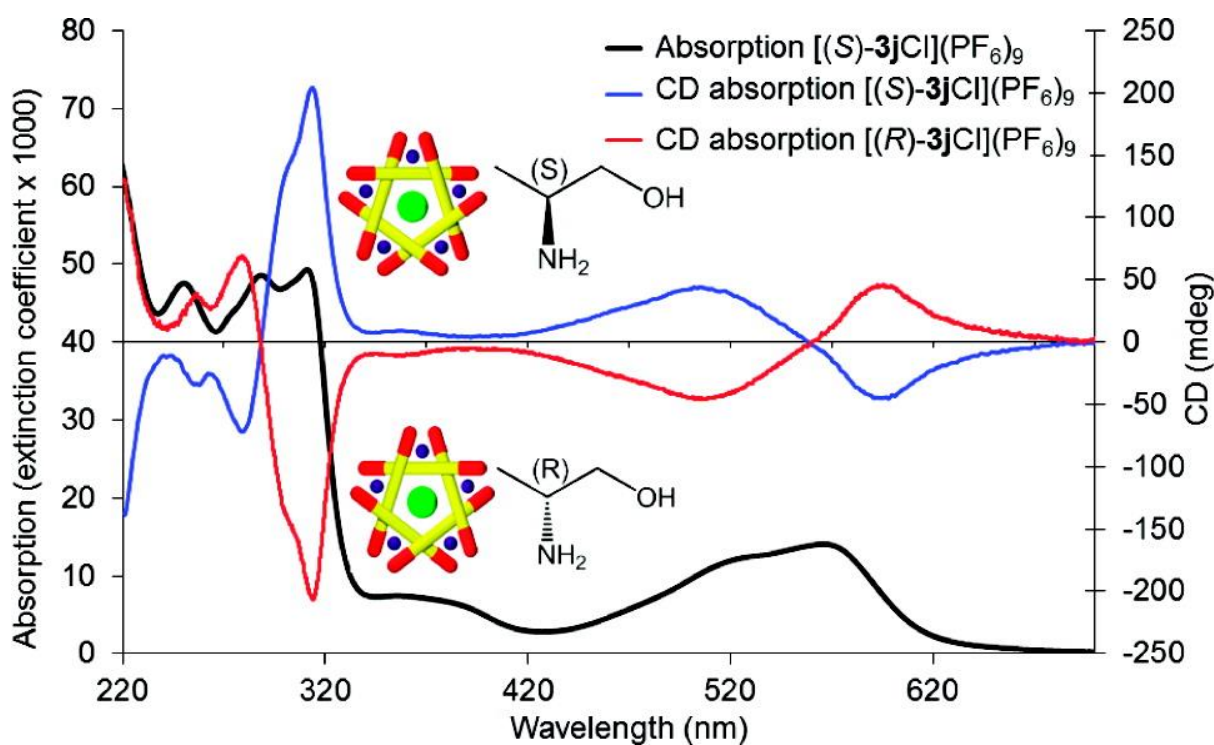
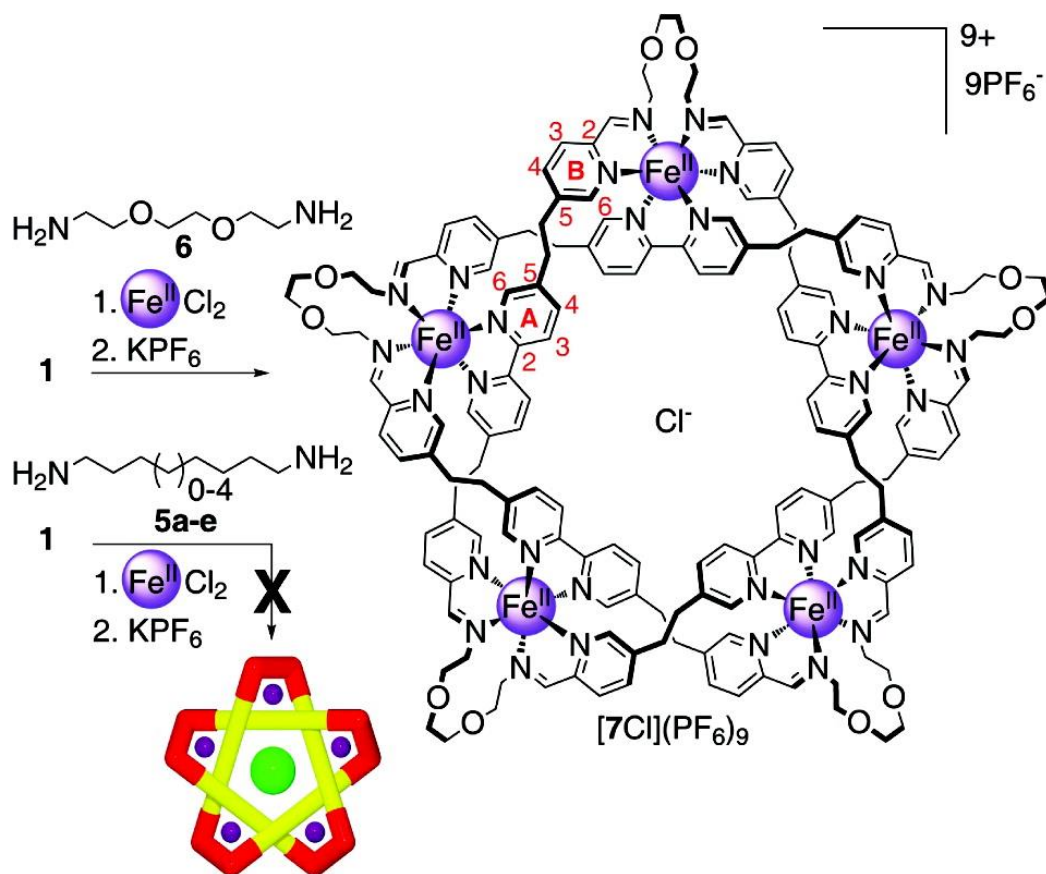


Figure 8. UV-vis absorption (black, left axis) and circular dichroism of pentameric cyclic helicates $[(R)\text{-}3\text{jCl}](\text{PF}_6)_9$ and $[(S)\text{-}3\text{jCl}](\text{PF}_6)_9$ in CH_3CN (0.12 mM).

$3\text{jCl}]^{9+}$, corresponding to $\Lambda\Lambda\Lambda\Lambda\text{-}[3\text{kCl}]^{9+}$, and in agreement with NMR ROESY data (SI, Figure 28).

3.8. Assembly of a Molecular Pentafoil Knot

Having established that nonhindered, aliphatic monoamines formed pentameric circular helicates in the highest yields with the fewest byproducts, we reasoned that the use of alkyl diamines could allow the formation of a molecular pentafoil knot (Scheme 3).²² Somewhat unexpectedly, the use of $\text{C}_6\text{-C}_{12}$ diaminoalkanes (**5a-e**) gave only intractable material, with no evidence for the formation of the desired knots. Similarly, diamines based on bridged 4-(alkoxy)benzylamines gave only oligomeric/polymeric products (see Experimental Section, Figure 15). When



Scheme 3. Synthesis of Molecular Pentafoil Knot $[7Cl](PF_6)_9$.^a

^aReaction conditions: 1. Dialdehyde 1/ $FeCl_2$ /diamine 6 (1:1.1:2.2), $DMSO-d_6$, 60 °C, 2 days. 2. Aqueous KPF_6 . 44% yield $[7Cl](PF_6)_9$. The use of diamines 5a–e instead of 6 did not generate the corresponding pentafoil knots.

employing a glycol linker, 2,2'-(ethylenedioxy)bis(ethylamine) (6), the reaction mixture also initially gave a featureless 1H NMR spectrum (Figure 9e). However, on heating at 60 °C, the mixture slowly rearranged over two days to form a single major species (Figure 9a). Aspects of the 1H NMR spectrum are very similar to that of the hexylamine derivative $[3hCl](PF_6)_9$, suggesting that these two compounds have closely related structures. After workup, the molecular pentafoil knot $[7Cl](PF_6)_9$ was isolated in 44% yield and its structure confirmed by ESI-MS (see Experimental Section, page S21).²²

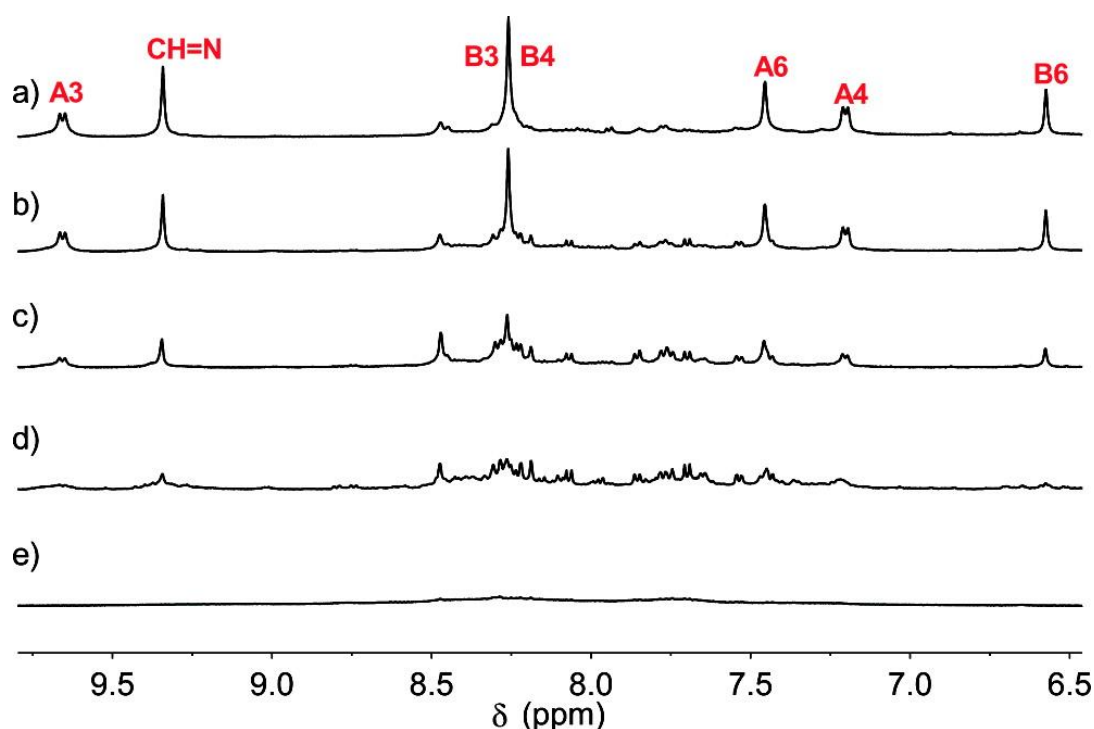


Figure 9. ^1H NMR spectra (DMSO- d_6 , 500 MHz, 298 K) of the formation of pentafoil knot $[\mathbf{7Cl}]^{9+}$ (Scheme 3). Reaction mixture after (e) 5 min, (d) 2 h, (c) 10 h, (b) 26 h, and (a) 48 h at 60 °C. The assignments correspond to the labeling shown in Scheme 3.

Some aspects of the assembly of the open cyclic helicates $[\mathbf{3a-kCl}]^{9+}$ translate poorly to the pentafoil knot $[\mathbf{7Cl}]^{9+}$ assembly process. First, the rate of formation of the knot is significantly slower than that of the open cyclic helicates (Figure 5), indicating that interconversions and rearrangements of the intermediates are slower with the diamine. Second, the stoichiometry of reagents proved to be more critical for the pentafoil knot than for the open circular helicate systems. The use of increasing amounts of FeCl_2 relative to dialdehyde **1** resulted in lower yields (e.g., the use of 2 equiv of FeCl_2 with respect to dialdehyde **1** resulted in a 40% drop in yield relative to when 1.1 equiv of FeCl_2 was used; SI, Figure 22). This is in contrast with the findings for the open systems where increased ratios of FeCl_2 substantially increased yields (see section 5.1. Reactant Stoichiometry). The use of excess diamine in the knot-

forming reaction resulted in even more severe reductions in yield (e.g., 2.0 equiv of diamine **6** resulted in a 90% fall in relative yield, SI, Figure 21). Finally, the reaction also proved very sensitive to the ratio of FeCl₂/amine employed, with a 1:1 ratio giving the highest yields (SI, Figure 23). As with the open systems, the formation of pentafoil knot [7Cl]⁹⁺ was sensitive to the amount of chloride present, with the yield increasing to a maximum with a ratio of 2:1 chloride/iron(II) (SI, Figure 25). The requirement for more than one Cl⁻ ion per molecular pentafoil knot despite very strong knot/chloride 1:1 binding²² suggests that the role of Cl⁻ in the assembly process is more complicated than just as a simple template. Higher amounts of chloride ion in the reaction did not increase the yield of pentafoil knot further (SI, Figure 25 and S16).

Purple crystals of pentafoil knot [7Cl](PF₆)₉·x(solvent) were grown by slow diffusion of diethyl ether vapor into an acetonitrile–toluene (3:2) solution of the complex and the X-ray structure determined using diffraction data collected on beamline I19 at the Diamond Light Source (U.K.).²² The solid state structure (Figure 10) confirmed the topology of the pentafoil knot. As for the open cyclic helicate [3bCl](PF₆)₉ (Figure 6), the structure contains a single helicate in the asymmetric unit and crystallizes in the *P*2₁/*c* space group. The planar geometry of the iron centers and the displacement of the chloride ion from this plane are similar to that in [3bCl]⁹⁺. Eight of the nine PF₆ anions are located in the difference map, and the structure also contains disordered solvent molecules. The structure is generally well-ordered (see Experimental Section, Chapter II section 2.5.3., for ORTEP plot), with the exception of the glycol linkers which show large thermal displacement parameters. The glycol

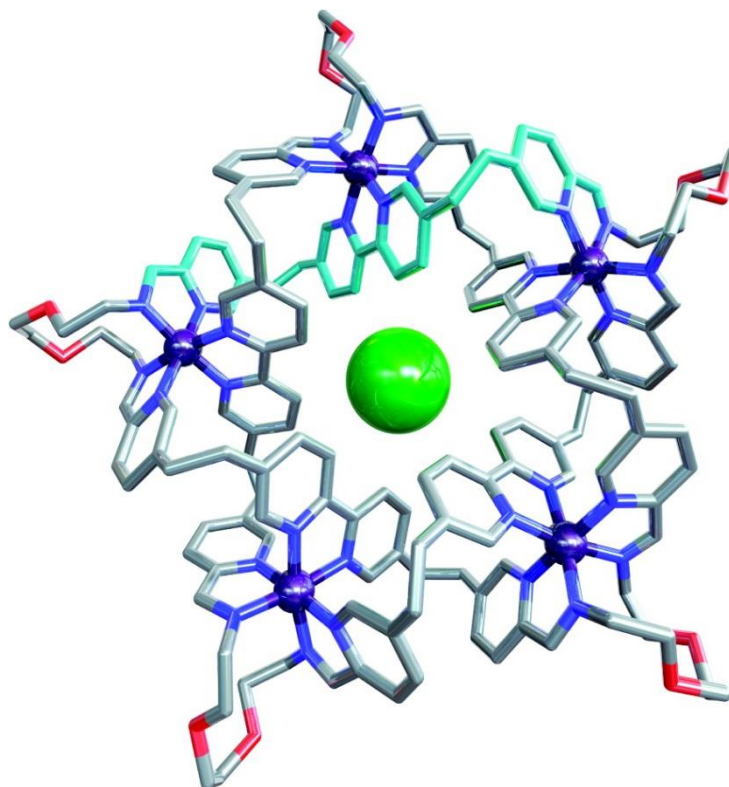


Figure 10. X-ray crystal structure of pentafoil knot $[7\text{Cl}](\text{PF}_6)_9$, from a single crystal obtained by vapor diffusion of diethyl ether into a acetonitrile–toluene solution.²² Hexafluorophosphate anions, solvent molecules, and hydrogen atoms are omitted for clarity. Nitrogen atoms are shown in dark blue, oxygen atoms red, chlorine atom green, and carbon atoms gray (the carbon framework originating from a single building block of **1** is colored light blue). Fe(II) centers shown at 50% van der Waals radius, Cl^- shown at 100%. $\text{Cl}\cdots\text{HC}$ distances (clockwise from top left blue bipyridine unit): 2.71, 2.75, 2.76, 2.70, 2.76, 2.70, 2.69, 2.71, 2.71, 2.69. C-H-Cl angles (deg): 172, 179, 170, 176, 172, 177, 176, 176, 170, 178. For an ORTEP plot, see the SI, Figure Chapter II section 2.5.3.

chains have O-C-C-O torsion angles ranging from $57(3)^\circ$ to $77(2)^\circ$. It seems likely that the gauche effect⁴³ (the preference for O-C-C-O chains to adopt torsion angles of 60° rather than the 180° angle of all-carbon chains) stabilizes this low-energy turn which is likely responsible for diamine **6** forming the closed-loop pentafoil knot, whereas other diaminoalkanes of similar length (**5a–e**) do not (Scheme 3).⁴⁴ The

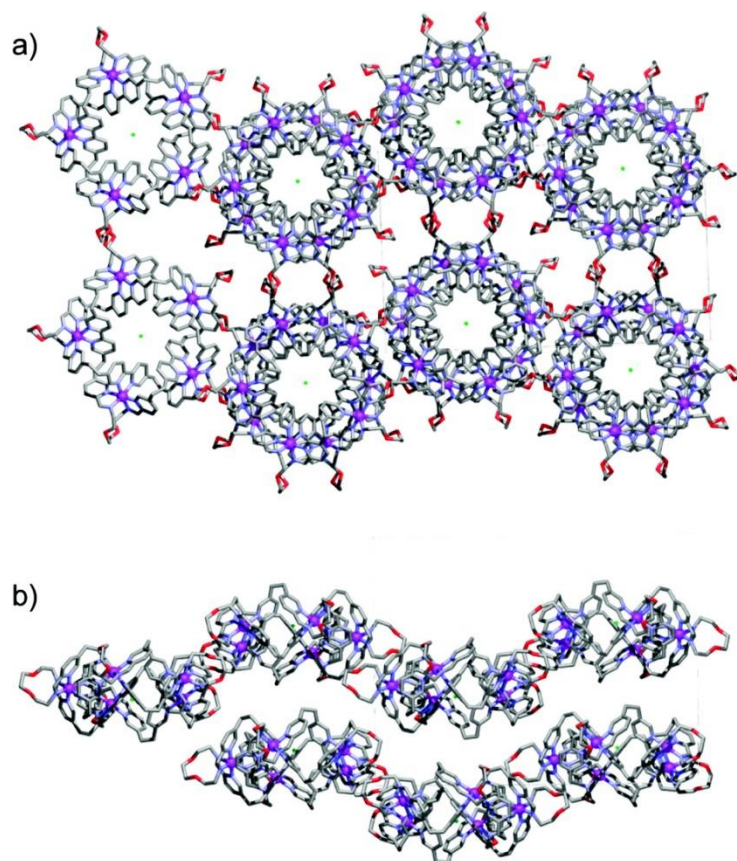


Figure 11. Crystal packing diagrams for the X-ray structure of $[7\text{Cl}](\text{PF}_6)_9 \cdot x\text{solvent}$ viewed down (a) the crystallographic c -axis and (b) the crystallographic a -axis. Close contacts between glycol chains dominate the intermolecular contacts, forming 2D sheets of the molecular knots that are separated by disordered solvent and anions (omitted for clarity).

molecules are packed in 2D zigzag arrays, with close contacts between the glycol linkers ($\text{CH}\cdots\text{HC}$ contacts as short as 2.22 Å, Figure 11).

3.9. Conclusion

Pentameric cyclic double helicates can be efficiently assembled in a one-pot reaction from iron(II) cations, dialdehyde **1**, and a range of monoamines (**2a–k**) in the presence of chloride anions. The assembly process is very sensitive to the structure of the amine, reactant stoichiometry (dialdehyde/Fe(II)/amine:Cl⁻) and reaction

“Pentameric Circular Iron(II) Double Helicates and a Molecular Pentafoil Knot” conditions (solvent, concentration). Some of the ways that these factors influence the assembly process are somewhat unexpected:

The reagent stoichiometry that corresponds to the composition of the pentameric circular helicate products [5:5:10:1 dialdehyde/Fe(II)/amine/Cl⁻] does not give the highest yield. Rather the use of significant excesses of iron(II) and chloride ions give the highest (virtually quantitative) yields of open circular helicates, indicating that these ions likely play more important roles in the assembly process than that of a simple thermodynamic template.

Due to the symmetry of the cyclic helicate structure, the effect of individually rather weak interactions on the assembly process is magnified, and can significantly alter the product distribution in the reaction mixture. In some cases this can be beneficial (for example, to form cyclic helicates of specific handedness with particular chiral amines) and in others detrimental (for example, sterically hindered amines favoring polymer formation over circular helicates).

The subtle effects of structure on the assembly reaction is also illustrated by the fact that circular helices other than the pentamer are not observed in the reaction of **1** with amines and different iron(II) salts. This contrasts with the formation of hexameric circular helicates with Lehn’s tris(bipyridine) ligands and Fe(BF₄)₂·6H₂O or FeBr₂.^{24b}

By using a diamine that can form a low-energy turn due to the gauche effect on its glycol linkers the assembly system was successfully used to form a molecular pentafoil knot.²² The reagent stoichiometry effects observed for open circular helicate formation do not all translate to the pentafoil knot. For example, the use of

an increased amount of iron(II) with respect to **1** lowered the yield of the knot, the opposite of that found for the open circular helicates.

The use of cyclic helicates as scaffolds for the assembly of interlocked molecules builds upon, and complements, the linear helicate strategy introduced by Sauvage in the 1980s.¹⁰ We anticipate that the information gleaned from the investigation of the assembly processes presented here will be useful for the rational synthesis of higher-order topologically complex molecular architectures.

3.10. Experimental section

3.10.1. Synthesis

3.10.1.1. Synthesis of dialdehyde **1**

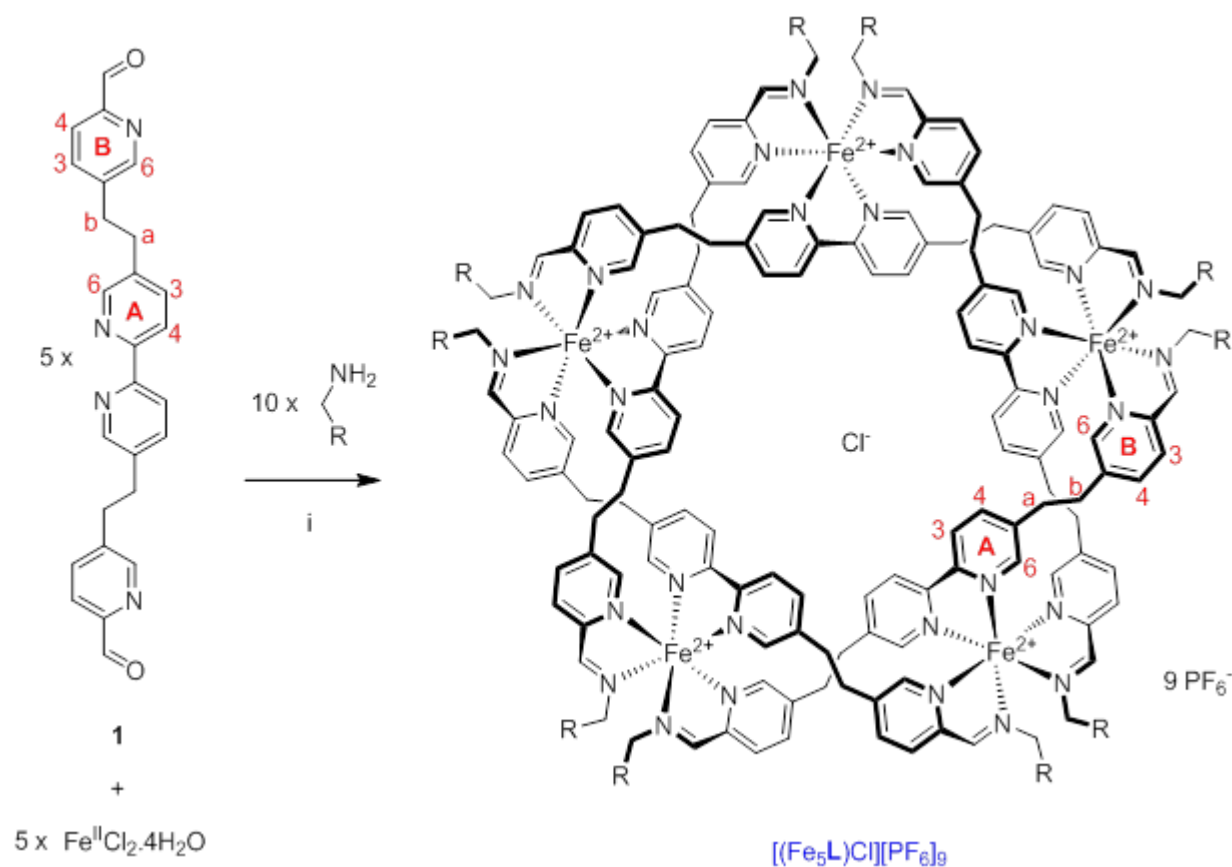
The synthesis of ligand **1** has been previously reported in Chapter II section 2.5.1.1.

3.10.1.2. Synthesis of bis(imino) ligands **S8** and **4**

The synthesis of bis(imino) ligands **S8** and **4** have been previously reported in Chapter II section 2.5.1.2.

3.10.1.3. General synthesis of pentameric circular helicates

The general synthetic procedure for forming circular helicates is shown in Scheme 4.



Scheme 4. Preparation of circular helicates $[\mathbf{3a-gCl}](\text{PF}_6)_9$. Reagents and conditions: (i) a) DMSO, 60 °C, 24 h (48 h for $[\mathbf{3gCl}](\text{PF}_6)_9$), b) Excess saturated aqueous KPF_6 .

3.10.1.4. Synthesis of circular helicates

3.10.1.4.1. Representative large-scale synthetic procedure (circular helicate $[\mathbf{3hCl}](\text{PF}_6)_9$)

A DMSO- d_6 solution of anhydrous FeCl_2 (250 μL of 210 mM, 52 μmol , 1.1 eq.) was added to dialdehyde **1** (20 mg, 47 μmol , 1 eq) in DMSO- d_6 (10 mL) The resulting purple solution was treated in an ultrasonic bath for 10 min and heated at 60°C for 30 min to ensure complete dissolution of the dialdehyde. A DMSO- d_6 solution of hexylamine (1.00 mL of a 100 mM DMSO- d_6 solution, 100 μmol , 2.2 equivalents) was

“Pentameric Circular Iron(II) Double Helicates and a Molecular Pentafoil Knot”
added to the mixture. The resulting dark purple mixture was heated at 60 °C for one day. After cooling to room temperature, excess saturated aqueous KPF_6 was added (~5 mL). A fine suspension of a purple material formed which was collected on Celite, thoroughly washed with water, EtOH, DCM and diethylether. The purple solid was dissolved in acetonitrile and concentrated under reduced pressure to give $[\mathbf{3hCl}](\text{PF}_6)_9$ as a purple powder (27 mg, 5.9 μmol , 63%).

3.10.1.4.2. Representative small-scale synthetic procedure (circular helicate $[\mathbf{3hCl}](\text{PF}_6)_9$)

Anhydrous FeCl_2 (45mg) was dissolved in DMSO-d_6 (1.7 mL) and mixed and sonicated for 5 min to ensure the sample was completely dissolved. Dialdehyde **1** (2 mg, 4.7 μmol , 1 eq) was suspended in DMSO-d_6 (1 mL) and sonicated to generate a homogenous solution. FeCl_2 solution (25 μL , 1.1 eq) was added to the dialdehyde solution using a microsyringe and the resulting purple solution was treated in an ultrasonic bath for 10 min to ensure complete dissolution of the dialdehyde. Hexylamine (**2h**) (36 mg, 350 μmol) was dissolved in DMSO-d_6 (1.7 mL) and mixed and sonicated for 20 min to ensure complete dissolution of the amine (often found to be a problem with other amines). An aliquot (50 μL , 10 μmol , 2.2 eq) of this solution was added to the reaction mixture with a microsyringe, resulting in an immediate color change (initially becoming paler, followed by a slower darkening of the solution over 30 min). The resulting mixture was heated at 60 °C for one day. After cooling to room temperature, excess saturated aqueous KPF_6 was slowly added (~0.1 mL). A fine suspension of a purple material formed which was collected on Celite, thoroughly washed with water, EtOH, DCM and diethylether. The purple solid

was dissolved in acetonitrile and concentrated under reduced pressure to give $[3hCl](PF_6)_9$ as a purple powder (~2.5 mg, ~0.6 μmol , ~60%). The yields were found to be highly reproducible.

¹H NMR (CD₃CN, 500 MHz) of circular helicates

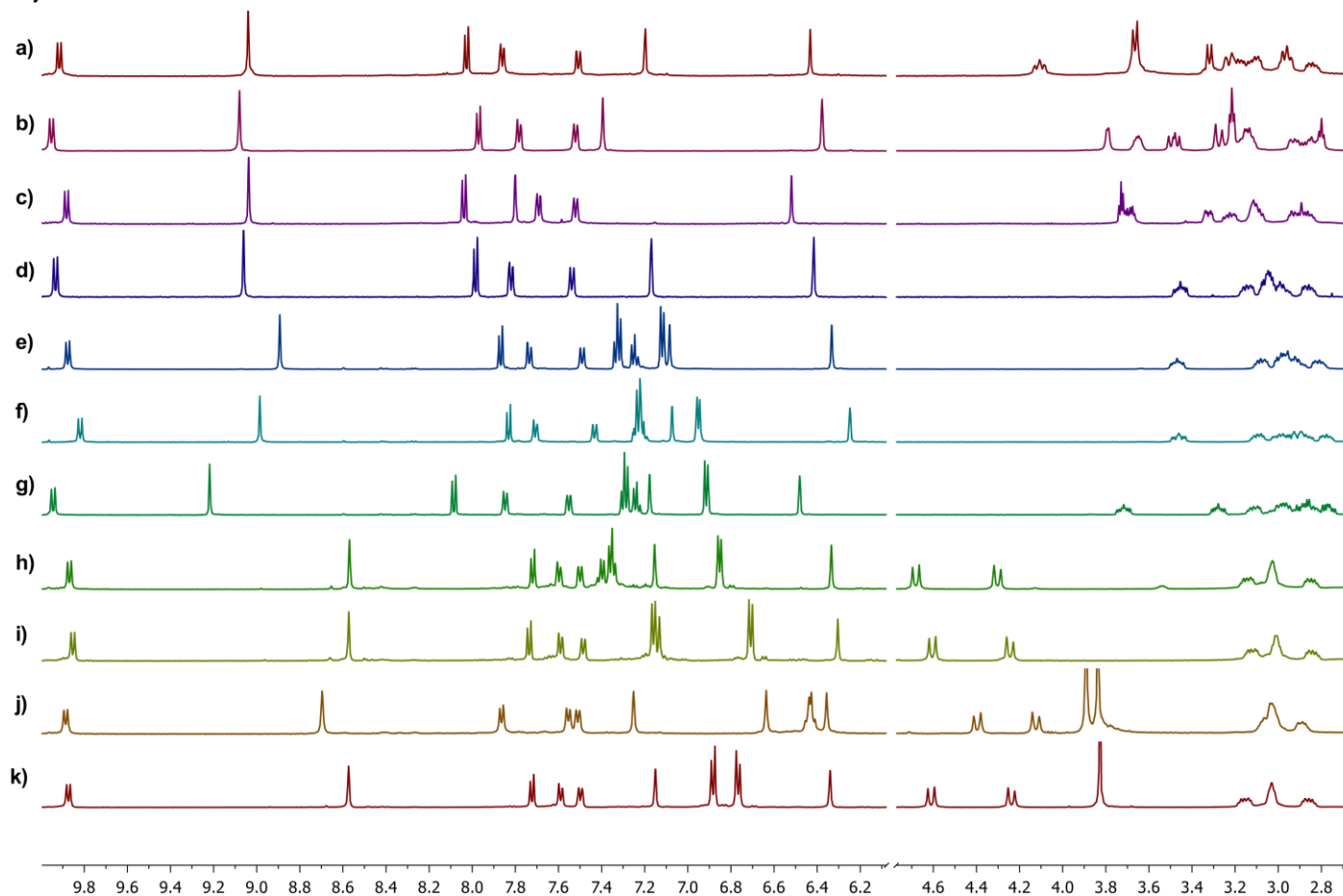
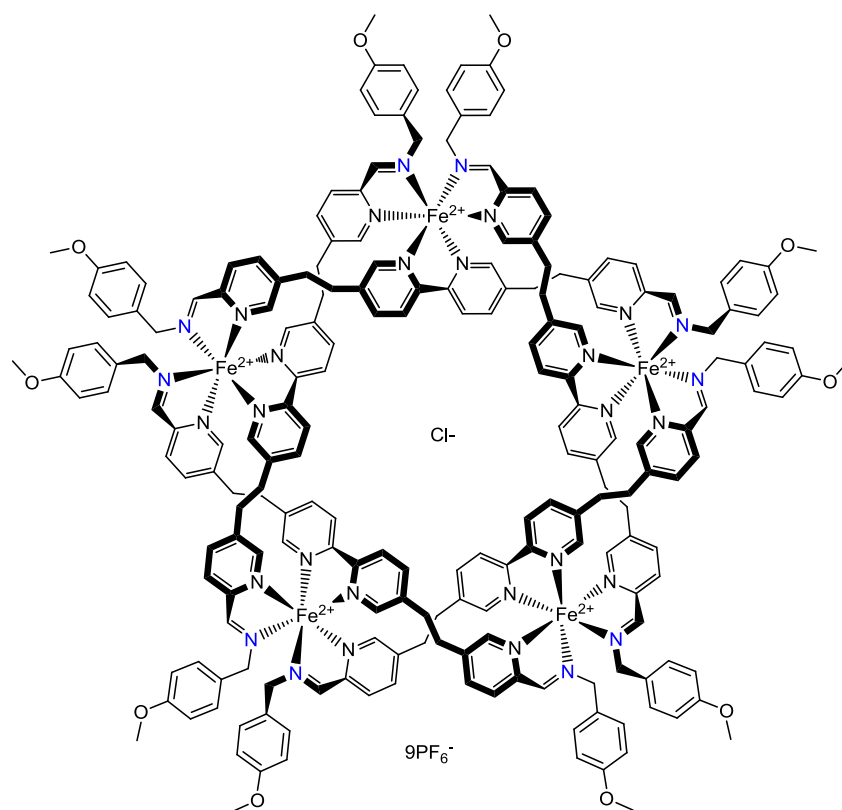
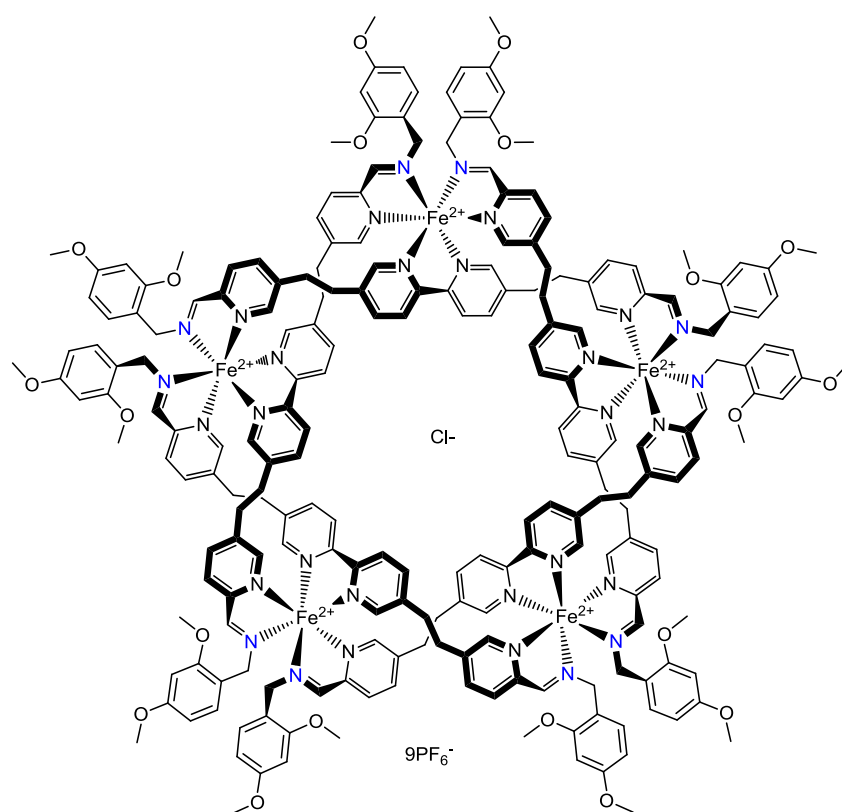


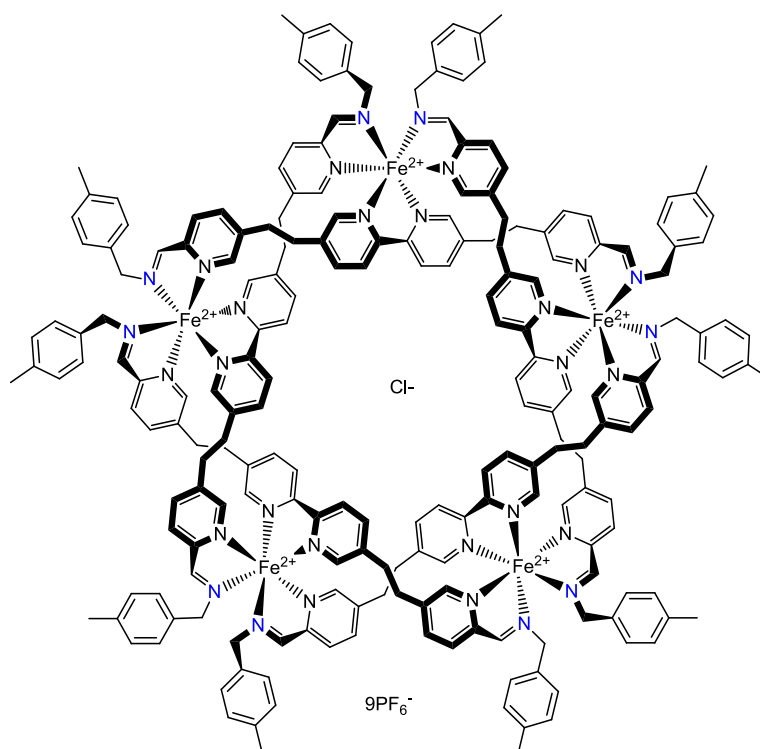
Figure 12. ¹H NMR (CD₃CN, 500MHz) of a) pentafoil knot [7Cl]⁹⁺; b) major diastereomer of [R-3kCl]⁹⁺; c) [R-3jCl]⁹⁺; d) [3hCl]⁹⁺; e) [3gCl]⁹⁺; f) [3fCl]⁹⁺; g) [3eCl]⁹⁺; h) [3dCl]⁹⁺; i) [3cCl]⁹⁺, j) [3bCl]⁹⁺, k) [3aCl]⁹⁺.

3.10.1.4.3. Synthesis of circular helicate $[3aCl](PF_6)_9$ 

^1H NMR (500 MHz, CD_3CN) δ 9.87 (d, $J = 8.3$, 10H, $\text{H}^{\text{A}3}$), 8.57 (s, 10H, $\text{H}^{\text{CH}=\text{N}}$), 7.72 (d, $J = 8.1$, 10H, $\text{H}^{\text{B}3}$), 7.59 (d, $J = 7.0$, 10H, $\text{H}^{\text{B}4}$), 7.50 (d, $J = 7.4$, 10H, $\text{H}^{\text{A}4}$), 7.15 (s, 10H, $\text{H}^{\text{A}6}$), 6.88 (d, $J = 8.6$, 20H, $\text{H}^{\text{C}3}$), 6.77 (d, $J = 8.6$, 20H, $\text{H}^{\text{C}2}$), 6.34 (s, 10H, $\text{H}^{\text{B}6}$), 4.61 (d, $J = 15.5$, 10H, $\text{H}^{\text{CH}_2-\text{N}}$), 4.24 (d, $J = 15.6$, 10H, $\text{H}^{\text{CH}_2-\text{N}}$), 3.83 (s, 30H, H^{OMe}), 3.16 (m, 6.1, 10H, H^{a}), 3.03 (s, 20H, H^{b}), 2.86 (m, 10H, H^{a}). ^{13}C NMR (126 MHz, CD_3CN) δ 171.53 ($\text{C}^{\text{CH}=\text{N}}$), 161.07 ($\text{C}^{\text{C}4}$), 157.44 ($\text{C}^{\text{B}2}$), 156.78 ($\text{C}^{\text{A}2}$), 153.77 ($\text{C}^{\text{B}6}$), 153.13 ($\text{C}^{\text{A}6}$), 140.63 ($\text{C}^{\text{A}5}$), 140.33 ($\text{C}^{\text{A}4}$), 140.01 ($\text{C}^{\text{B}5}$), 138.84 ($\text{C}^{\text{B}4}$), 131.57 ($\text{C}^{\text{C}2}$), 129.51 ($\text{C}^{\text{B}3}$), 125.92 ($\text{C}^{\text{C}1}$), 125.48 ($\text{C}^{\text{A}3}$), 115.52 ($\text{C}^{\text{C}3}$), 64.58 ($\text{C}^{\text{CH}_2-\text{N}}$), 56.17 (C^{OMe}), 31.27 (C^{b}), 30.23 (C^{a}). ESI-MS: m/z 1085.63 $[\text{M}-4\text{PF}_6]^{4+}$ requires 1085.8; 840.0 $[\text{M}-5\text{PF}_6]^{5+}$ requires 839.6; 675.4 $[\text{M}-6\text{PF}_6]^{6+}$ requires 675.5; 558.2 $[\text{M}-7\text{PF}_6]^{7+}$ requires 558.3 m/z . HRESI-MS: m/z 839.6221 $[\text{M}-4(\text{PF}_6)]^{5+}$ (calcd. for $\text{C}_{210}\text{H}_{200}\text{ClF}_{24}\text{Fe}_5\text{N}_{30}\text{P}_4$, 839.6221).

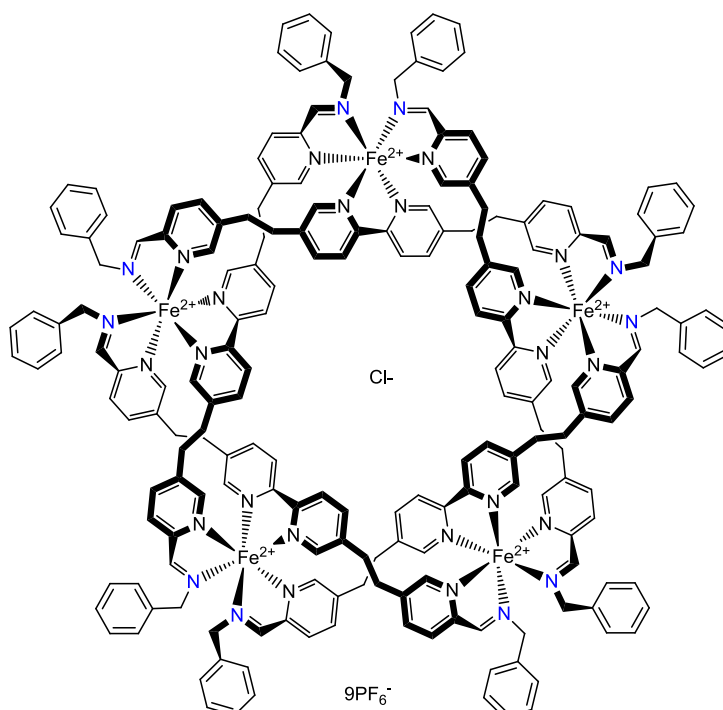
3.10.1.4.4. Synthesis of circular helicate [3bCl](PF₆)₉

¹H NMR: (500 MHz, CD₃CN) δ 9.89 (d, *J* = 8.3, 10H, H^{A3}), 8.70 (s, 10H, H^{CH=N}), 7.86 (d, *J* = 8.0, 10H, H^{B3}), 7.55 (d, *J* = 7.7, 10H, H^{B4}), 7.51 (d, *J* = 7.8, 10H, H^{A4}), 7.25 (s, 10H, H^{A6}), 6.64 (s, 10H, H^{C3}), 6.44 (d, *J* = 8.4, 10H, H^{C5}), 6.42 (d, *J* = 8.3, 10H, H^{C6}), 6.36 (s, 10H, H^{B6}), 4.40 (d, *J* = 15.9, 10H, H^{CH2-N}), 4.12 (d, *J* = 15.9, 10H, H^{CH2-N}), 3.89 (s, 30H, H^{OMe2}), 3.84 (s, 30H, H^{OMe4}), 3.17 – 2.94 (m, 30H, H^{a+b}), 2.89 (dd, *J* = 13.0, 3.3, 10H, H^a). ¹³C NMR (126 MHz, CD₃CN) δ 171.07 (C^{CH=N}), 163.11 (C^{C4}), 160.50 (C^{C2}), 157.61 (C^{B2}), 156.83 (C^{A2}), 153.84 (C^{B6}), 153.29 (C^{A6}), 140.48 (C^{A5}), 140.15 (C^{A4}), 139.72 (C^{B5}), 138.59 (C^{B4}), 133.22 (C^{C6}), 129.60 (C^{B3}), 125.41 (C^{A3}), 114.20 (C^{C1}), 106.43 (C^{C5}), 100.16 (C^{C3}), 59.69 (C^{CH2-N}), 57.12 (C^{OMe}), 56.33 (C^{OMe}), 31.01 (C^b), 30.38 (C^a). ESI-MS: *m/z* 1160.5 [M-4PF₆]⁴⁺ requires 1060.8; 899.6 [M-5PF₆]⁵⁺ requires 899.6; 725.5 [M-6PF₆]⁶⁺ requires 725.5, 601.2 [M-7PF₆]⁷⁺ requires, 508.0 [M-8PF₆]⁸⁺ requires 507.9 *m/z*. HRESI-MS: *m/z* 899.6422 [M-4(PF₆)]⁵⁺ (calcd. for C₂₂₀H₂₂₀ClF₂₄Fe₅N₃₀P₄, 899.6433).

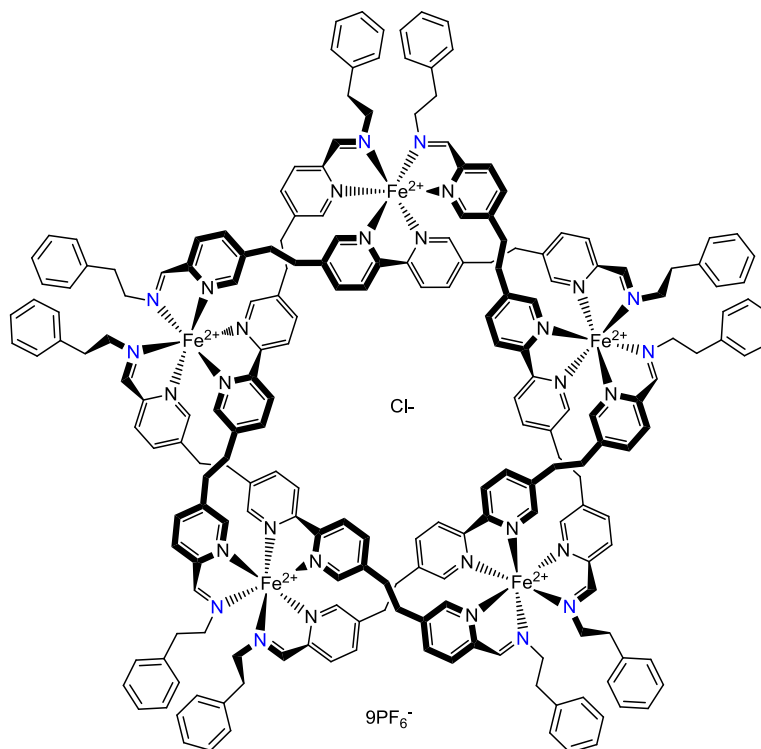
3.10.1.4.5. Synthesis of circular helicate [3cCl](PF₆)₉

¹H-NMR: (500 MHz, CD₃CN) δ 9.85 (d, *J* = 8.3 Hz, 10H, H^{A3}), 8.57 (s, 10H, H^{CH=N}), 7.74 (d, *J* = 8.1 Hz, 10H, H^{B3}), 7.59 (d, *J* = 8.1 Hz, 10H, H^{B4}), 7.48 (d, *J* = 8.2 Hz, 10H, H^{A4}), 7.16 (d, *J* = 7.8 Hz, 20H, H^{C3}), 7.14 (d, *J* = 8.0 Hz, 10H, H^{A6}), 6.71 (d, *J* = 7.9 Hz, 20H, H^{C2}), 6.30 (s, 10H, H^{B6}), 4.60 (d, *J* = 15.2 Hz, 10H, H^{CH2-N}), 4.24 (d, *J* = 15.4 Hz, 10H, H^{CH2-N}), 3.16 – 3.09 (m, 10H, H^a), 3.01 (dd, *J* = 10.4, 6.6 Hz, 20H, H^b), 2.88 – 2.80 (m, 10H, H^a), 2.37 (s, 30H, Me). ¹³C-NMR: (126 MHz, CD₃CN) δ 171.8 (C^{CH=N}), 157.5 (C^{B2}), 156.8 (C^{A2}), 153.8 (C^{B6}), 153.2 (C^{A6}), 140.6 (C^{A5}), 140.3 (C^{A4}), 140.1 x2 (C^{B5+C1}), 138.8 (C^{B4}), 131.0 (C^{C4}), 130.8 (C^{C3}), 130.2 (C^{C2}), 129.6 (C^{B3}), 125.4 (C^{A3}), 64.9 (C^{CH2-N}), 31.2 (C^b), 30.2 (C^a), 21.3 (Me). ESI-MS: *m/z* 1045.5 [M-4PF₆]⁴⁺ requires 1045.8; 807.3 [M-5PF₆]⁵⁺ requires 807.6; 648.7 [M-6PF₆]⁶⁺ requires 648.9, 535.3 [M-7PF₆]⁷⁺ requires 535.5 *m/z*. HRESI-MS: *m/z* = 807.6309 [M-4(PF₆)]⁵⁺ (calcd. for C₂₁₀H₂₀₀ClF₂₄Fe₅N₃₀P₄, 807.6323).

3.10.1.4.6. *Synthesis of circular helicate [3dCl](PF₆)₉*

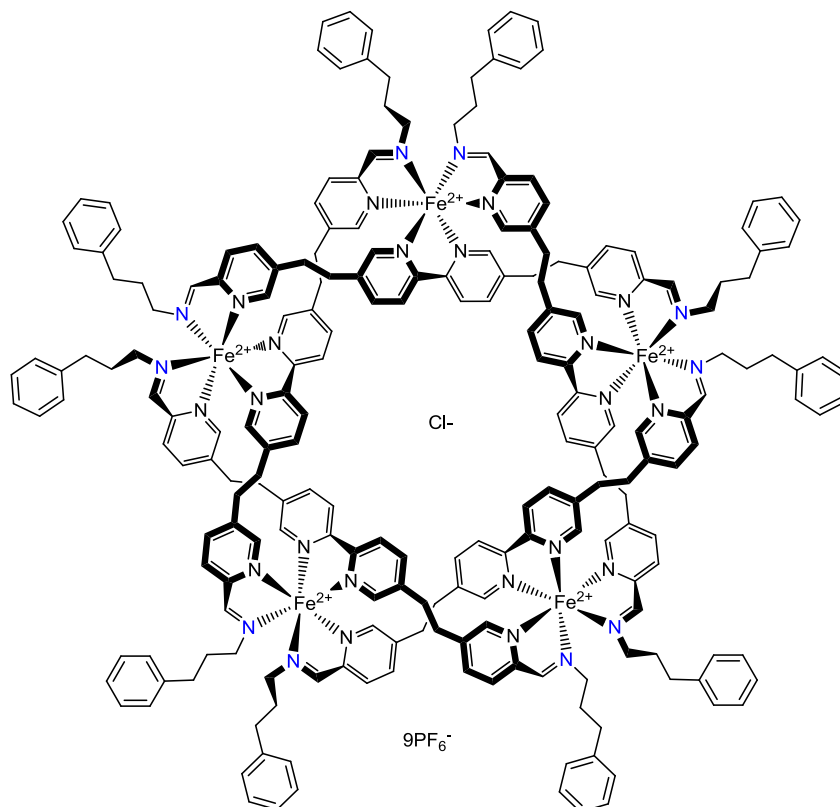


¹H NMR (500 MHz, CD₃CN) δ 9.87 (d, *J* = 8.3 Hz, 10H, H^{A3}), 8.57 (s, 10H, CH=N), 7.72 (d, *J* = 8.1 Hz, 10H, H^{B3}), 7.60 (d, *J* = 7.7 Hz, 10H, H^{B4}), 7.50 (d, *J* = 8.1 Hz, 10H, H^{A4}), 7.40 (t, *J* = 7.4 Hz, 10H, H^{C4}), 7.35 (t, *J* = 7.3 Hz, 20H, H^{C3}), 7.15 (s, 10H, H^{A6}), 6.85 (d, *J* = 7.2 Hz, 20H, H^{C2}), 6.33 (s, 10H, H^{B6}), 4.68 (d, *J* = 15.3 Hz, 10H, CH₂-N), 4.30 (d, *J* = 15.4 Hz, 10H, CH₂-N), 3.21 – 3.10 (m, 10H, CH₂-py_B), 3.10 – 2.94 (m, 20H, CH₂-py_A), 2.92 – 2.77 (m, 10H, CH₂-py_B) ¹³C NMR (126 MHz, CD₃CN) δ 172.0 (CH=N), 157.4 (C^{B2}), 156.7 (C^{A2}), 153.8 (C^{B6}), 153.1 (C^{A6}), 140.6 (C^{A5}), 140.4 (C^{A4}), 140.2 (C^{B5}), 138.9 (C^{B4}), 134.0 (C^{C1}), 130.3 (C^{C2/C3}), 130.2 (C^{C2/C3}), 130.0 (C^{C4}), 129.6 (C^{B3}), 125.5 (C^{A3}), 65.2 (CH₂-N), 31.2 (py_B-CH₂), 30.2 (py_A-CH₂). ESI-MS: *m/z* 1010.5 [M-4PF₆]⁴⁺ requires 1010.7; 779.4 [M-5PF₆]⁵⁺ requires 779.6; 625.5 [M-6PF₆]⁶⁺ requires 625.5, 515.3 [M-7PF₆]⁷⁺ requires 515.4 *m/z*. HRESI-MS: *m/z* 1010.7231 [M-4(PF₆)]⁵⁺ (calcd. for C₂₀₀H₁₈₀ClF₃₀Fe₅N₃₀P₅, 1010.7423).

3.10.1.4.7. Synthesis of circular helicate $[3eCl](PF_6)_9$ 

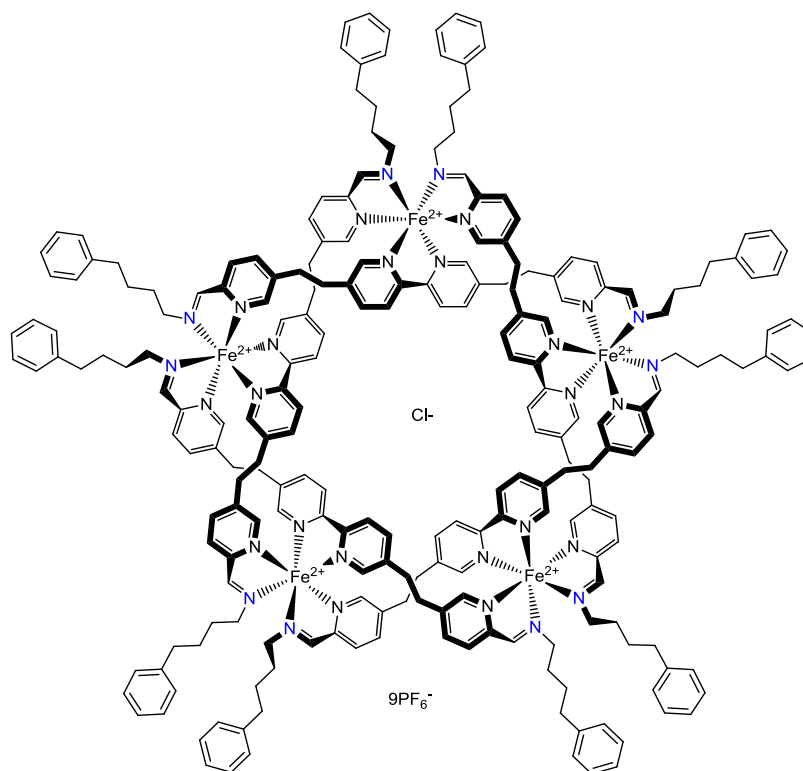
^1H NMR (500 MHz, CD_3CN) δ 9.94 (d, $J = 8.3$ Hz, 10H, $\text{H}^{\text{A}3}$), 9.22 (s, 10H, $\text{H}^{\text{CH}=\text{N}}$), 8.08 (d, $J = 8.0$ Hz, 10H, $\text{H}^{\text{B}3}$), 7.85 (dd, $J = 8.1, 1.4$ Hz, 10H, $\text{H}^{\text{B}4}$), 7.55 (dd, $J = 8.3, 1.4$ Hz, 10H, $\text{H}^{\text{A}4}$), 7.33 – 7.26 (m, 20H, $\text{H}^{\text{C}2+\text{C}3}$), 7.26 – 7.21 (m, 10H, $\text{H}^{\text{C}4}$), 7.18 (d, $J = 1.1$ Hz, 10H, $\text{H}^{\text{A}6}$), 6.91 (d, $J = 7.1$ Hz, 20H, $\text{H}^{\text{C}2+3+5+6}$), 6.48 (s, 10H, $\text{H}^{\text{B}6}$), 3.75 – 3.68 (m, 10H, $\text{H}^{\text{CH}2-\text{N}}$), 3.34 – 3.22 (m, 10H, $\text{H}^{\text{CH}2-\text{N}}$), 3.19 – 2.73 (m, 60H, $\text{H}^{\text{a}+\text{b}+\text{CH}2-\text{Ph}}$). ^{13}C NMR (126 MHz, CD_3CN) δ 172.43 ($\text{C}^{\text{CH}=\text{N}}$), 157.41 ($\text{C}^{\text{A}2}$), 156.81 ($\text{C}^{\text{B}2}$), 154.05 ($\text{C}^{\text{B}6}$), 153.47 ($\text{C}^{\text{A}6}$), 140.84 ($\text{C}^{\text{A}5/\text{B}5}$), 140.48 ($\text{C}^{\text{A}5/\text{B}5}$), 140.38 ($\text{C}^{\text{A}4}$), 139.17 ($\text{C}^{\text{B}4}$), 138.21 ($\text{C}^{\text{CH}2-\text{CH}2-\text{N}}$), 129.88 ($\text{C}^{\text{B}3/\text{C}2/\text{C}3}$), 129.56 ($\text{C}^{\text{B}3/\text{C}2/\text{C}3}$), 129.49 ($\text{C}^{\text{B}3/\text{C}2/\text{C}3}$), 128.05 ($\text{C}^{\text{C}4}$), 125.56 ($\text{C}^{\text{A}3}$), 61.77 ($\text{C}^{\text{CH}2-\text{N}}$), 36.13 ($\text{C}^{\text{CH}2-\text{Ph}}$), 30.98 (C^{b}), 30.20 (C^{a}). ESI-MS: m/z 1045.5 $[\text{M}-4\text{PF}_6]^{4+}$ requires 1045.8; 807.3 $[\text{M}-5\text{PF}_6]^{5+}$ requires 807.6; 648.7 $[\text{M}-6\text{PF}_6]^{6+}$ requires 648.9; 535.3 $[\text{M}-7\text{PF}_6]^{7+}$ requires 535.5 m/z . HRESI-MS: m/z 807.8184 $[\text{M}-4(\text{PF}_6)]^{5+}$ (calcd. for $\text{C}_{210}\text{H}_{200}\text{ClF}_{24}\text{Fe}_5\text{N}_{30}\text{P}_4$, 807.8330).

3.10.1.4.8. Synthesis of circular helicate [3fCl](PF₆)₉



¹H NMR (500 MHz, CD₃CN) δ 9.82 (d, *J* = 8.3 Hz, 10H, H^{A3}), 8.99 (s, 10H, H^{CH=N}), 7.83 (d, *J* = 8.0 Hz, 10H, H^{B3}), 7.71 (dd, *J* = 8.1, 1.5 Hz, 10H, H^{B4}), 7.43 (dd, *J* = 8.3, 1.4 Hz, 10H, H^{A4}), 7.28 – 7.15 (m, 30H, H^{C3+C4}), 7.07 (d, *J* = 1.2 Hz, 10H, H^{A6}), 6.95 (dd, *J* = 7.7, 1.5 Hz, 20H, H^{C2}), 6.25 (s, 10H, H^{B6}), 3.49 – 3.43 (m, 10H, H^{CH2-N}), 3.20 – 3.04 (m, 10H, H^{CH2-N}), 3.05 – 2.72 (m, 40H, H^{a+b}), 2.54 – 2.35 (m, 20H, H^{-CH2-}), 1.98 – 1.85 (m, 10H, H^{-CH2-}), 1.76 – 1.67 (m, 10H, H^{-CH2-}). ¹³C NMR (126 MHz, CD₃CN) δ 171.62 (C^{CH=N}), 157.06 (C^{B2}), 156.66 (C^{A2}), 153.49 (C^{B6}), 153.25 (C^{A6}), 141.56 (C^{C1}), 140.62 (C^{A5}), 140.16 (C^{A4}), 139.93 (C^{B5}), 138.97 (C^{B4}), 129.51 (C^{C2/C3/B3}), 129.19 (C^{C2/C3/B3}), 127.21 (C^{C4}), 125.39 (C^{A3}), 59.90 (C^{CH2-N}), 33.25 (C^{CH2-Ph}), 31.97 (C^{-CH2-}), 30.86 (C^b), 30.15 (C^a). ESI-MS: *m/z* 1080.4 [M-4PF₆]⁴⁺ requires 1080.8; 835.7 [M-5PF₆]⁵⁺ requires 835.7; 672.2 [M-6PF₆]⁶⁺ requires 672.2, 555.5 [M-7PF₆]⁷⁺ requires 555.5 *m/z*. HRESI-MS: *m/z* 835.6487 [M-5(PF₆)]⁵⁺ (calcd. for C₂₂₀H₂₂₀ClF₂₄Fe₅N₃₀P₄, 835.6636).

3.10.1.4.9. Synthesis of circular helicate [3gCl](PF₆)₉

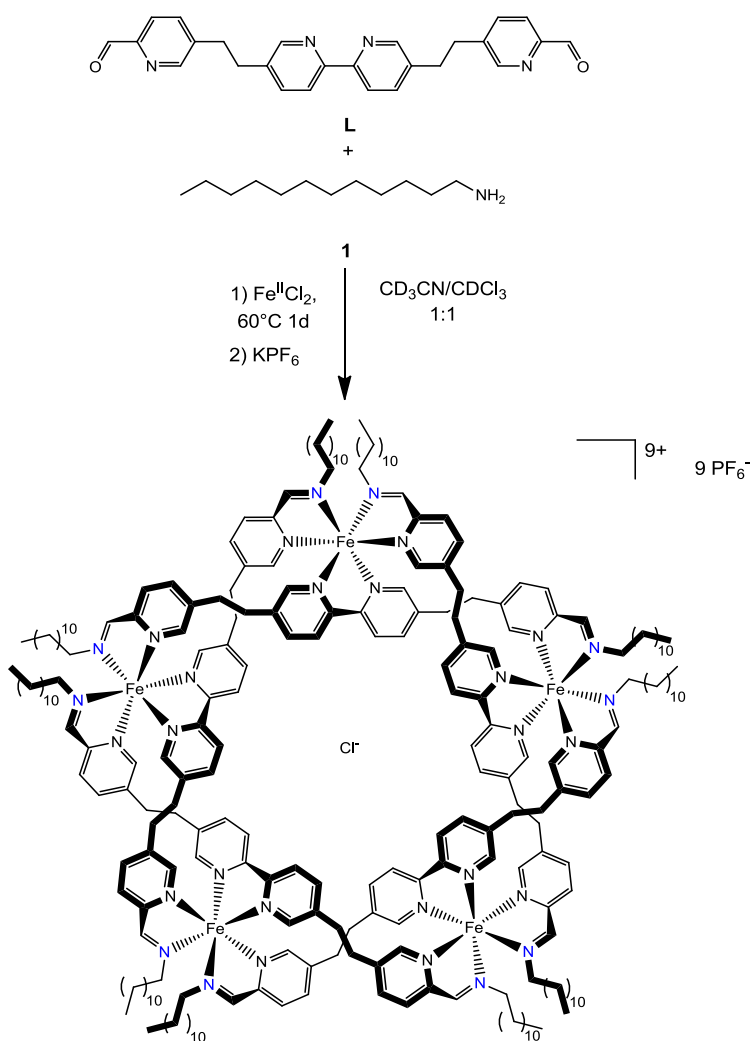


¹H NMR (500 MHz, CD₃CN) δ 9.88 (d, *J* = 8.3 Hz, 10H, H^{A3}), 8.89 (s, 10H, H^{CH=N}), 7.87 (d, *J* = 8.1 Hz, 10H, H^{B3}), 7.74 (dd, *J* = 8.1, 1.5 Hz, 10H, H^{B4}), 7.49 (dd, *J* = 8.3, 1.3 Hz, 10H, H^{A4}), 7.33 (t, *J* = 7.4, 20H, H^{C3}), 7.25 (t, *J* = 7.4, 10H, H^{C4}), 7.12 (d, *J* = 7.0, 20H, H^{C2}), 7.08 (d, *J* = 1.1, 10H, H^{A6}), 6.33 (s, 10H, H^{B6}), 3.49 – 3.43 (m, 10H, H^{CH2-N}), 3.15 – 3.03 (m, 10H, H^a), 3.03 – 2.86 (m, 30H, H^{b/CH2-N}), 2.86 – 2.70 (m, 10H, H^a), 2.53 – 2.38 (m, 20H, H^{CH2-Ph}), 1.57 – 1.24 (m, 40H, C^{-CH2-}). ¹³C NMR (126 MHz, CD₃CN) δ 171.30 (C^{CH=N}), 157.24 (C^{B2}), 156.78 (C^{A2}), 153.70 (C^{B6}), 153.27 (C^{A6}), 142.80 (C^{C1}), 140.65 (C^{A5}), 140.25 (C^{A4}), 140.04 (C^{B5}), 138.82 (C^{B4}), 129.52 (C^{C3}), 129.35 (C^{C2}), 129.16 (C^{B3}), 127.08 (C^{C4}), 125.47 (C^{A3}), 60.74 (C^{CH2-N}), 35.63 (C^{CH2-Ph}), 30.93 (C^b), 30.21 (C^a), 29.47 (C^{-CH2-}), 29.13 (C^{-CH2-}). ESI-MS: *m/z* 1115.7 [M-4PF₆]⁴⁺ requires 1115.9; 863.7 [M-5PF₆]⁵⁺ requires 863.7; 695.5 [M-6PF₆]⁶⁺ requires 695.6, 575.5 [M-7PF₆]⁷⁺ requires 575.5 *m/z*. HRESI-MS: *m/z* 1115.877 [M-4(PF₆)]⁴⁺ (calcd. for C₂₃₀H₂₄₀ClF₃₀Fe₅N₃₀P₅, 1115.8699).

3.10.1.4.10. Synthesis of circular helicate [3hCl](PF₆)₉

The synthesis of circular helicate [3hCl](PF₆)₉ has been previously reported in Chapter II section 2.5.1.3.1.

3.10.1.4.11. Synthesis of circular helicate [3iCl](PF₆)₉



Scheme 5. Synthesis of [3iCl](PF₆)₉ in CDCl₃:CD₃CN (1:1)

Anhydrous FeCl₂ (0,7 mg, 5,3 μmol, 1,1 eq) and dialdehyde **1** (2 mg, 4,7 μmol, 1 eq) were suspended in 1 mL of a 1:1 mixture of CDCl₃ and CD₃CN. Dodecylamine (**2i**) (38 mg, 207 μmol) was dissolved in CDCl₃ (1 mL) and mixed/sonicated for 20 min to ensure complete dissolution of the amine. An aliquot (50ul, 10 μmol, 2,2 eq) of this solution was added to the

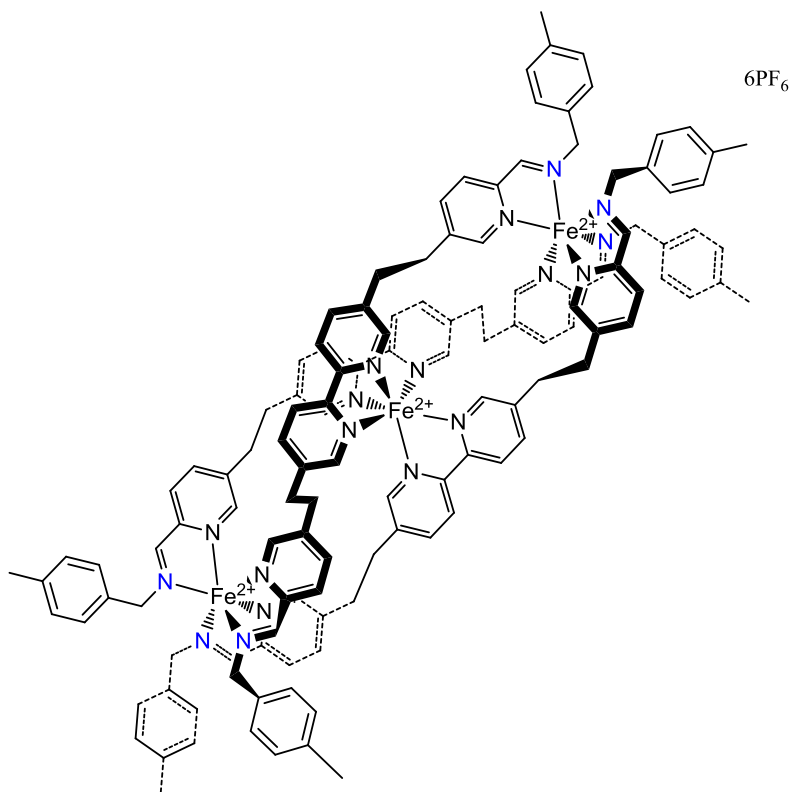
reaction mixture with a microsyringe. The resulting suspension slowly became a purple solution when heated at 60 °C. After a day of heating, the reaction mixture was allowed to cool down to room temperature, excess saturated aqueous KPF_6 was slowly added (~0.1 mL). A fine suspension of a purple material formed which was collected on Celite, thoroughly washed with water, EtOH and diethylether. The purple solid was dissolved in acetonitrile and concentrated under reduced pressure to give $[\mathbf{3iCl}](\text{PF}_6)_9$ as a purple powder (~2.1 mg, ~0.5 μmol , ~53%).

^1H NMR (500 MHz, CD_3CN) δ 9.93 (d, $J = 8.3$ Hz, 10H, H^{A3}), 9.06 (s, 10H, CH=N), 7.98 (d, $J = 8.0$ Hz, 10H, H^{B3}), 7.82 (d, $J = 7.6$ Hz, 10H, H^{B4}), 7.54 (d, $J = 8.0$ Hz, 10H, H^{A4}), 7.17 (s, 10H, H^{A6}), 6.41 (s, 10H, H^{B6}), 3.52 – 3.41 (m, 10H, $\text{CH}_2\text{-N}$), 3.21 – 3.10 (m, 10H, $\text{CH}_2\text{-Py}$), 3.10-2.93 (m, 30H, $\text{CH}_2\text{-N} + \text{CH}_2\text{-py}$), 2.96 – 2.82 (m, 10H, $\text{CH}_2\text{-py}$), 1.62-1.47 (m, 40H, $\text{CH}_2\text{-CH}_2\text{N}$), 1.37-1.07 (m, 100H, 5 x CH_2), 0.92 (t, $J = 6.8$ Hz, 30H, CH_3). ^{13}C NMR (126 MHz, CD_3CN) δ 171.3 (CH=N), 157.5 (C^{B2}), 156.8 (C^{A2}), 153.8 (C^{B6}), 153.4 (C^{A6}), 140.7 (C^{A5}), 140.3 (C^{A4}), 140.0 (C^{B5}), 138.9 (C^{B4}), 129.1 (C^{B3}), 125.5 (C^{B3}), 60.8 ($\text{CH}_2\text{-N}$), 32.7 ($\text{CH}_2\text{-CH}_2\text{N}$), 30.4 x 2 (CH_2 x 2), 30.3 (CH_2), 30.2 (CH_2), 30.1 (CH_2), 29.9 (CH_2), 29.8 (CH_2), 27.4 ($\text{CH}_2\text{-CH}_2\text{-CH}_2\text{N}$), 23.4 ($\text{CH}_2\text{-CH}_3$), 14.4 (CH_3). ESI-MS: m/z 1205.8 $[\text{M-4PF}_6]^{4+}$ requires 1206.1; 935.8 $[\text{M-5PF}_6]^{5+}$ requires 935.9; 755.7 $[\text{M-6PF}_6]^{6+}$ requires 755.7, 627.1 $[\text{M-7PF}_6]^{7+}$ requires 627.1 m/z . HRESI-MS: m/z 935.8811 $[\text{M-4}(\text{PF}_6)]^{5+}$ (calcd. for $\text{C}_{250}\text{H}_{360}\text{ClF}_{24}\text{Fe}_5\text{N}_{30}\text{P}_4$, 935.8829).

3.10.1.4.12. Synthesis of pentafoil knot $[7Cl](PF_6)_9$

The synthesis of pentafoil knot $[7Cl](PF_6)_9$ has been previously reported in Chapter II section 2.5.1.3.5.

3.10.2. Formation of linear triple helicate $[Fe_3(S8)](PF_6)_6$



$Fe(BF_4)_2 \cdot 6H_2O$ (35 mg) was dissolved in $DMSO-d_6$ (1 mL) and mixed and sonicated for 5 min to ensure the sample was completely dissolved. Dialdehyde **1** (2 mg, 4.7 μmol , 1 eq) was suspended in $DMSO-d_6$ (1 mL) and sonicated to generate a homogenous solution. $Fe(BF_4)_2 \cdot 6H_2O$ solution (50 μL , 1.1 eq) was added to the dialdehyde solution using a microsyringe and the resulting purple solution was treated in an ultrasonic bath for 10 min to ensure complete dissolution of the dialdehyde. 4-Methylbenzylamine (**2c**) (25 mg, 207 μmol) was dissolved in $DMSO-d_6$ (1 mL) and mixed/sonicated for 20 min to ensure complete dissolution of the amine (often found to be a problem). An aquilot (50 μL , 10 μmol , 2.2 eq) of

this solution was added to the reaction mixture with a microsyringe, to give an immediate color change (initially becoming paler, followed by a slower darkening of the solution over 30 min). The resulting mixture was heated at 60 °C for one day. After cooling to room temperature, excess saturated aqueous KPF_6 was slowly added (~0.1 mL). A fine suspension of a purple material formed which was collected on Celite, thoroughly washed with water, EtOH, DCM and diethylether. The purple solid was dissolved in acetonitrile and concentrated under reduced pressure to give $[Fe_3(\mathbf{S8})_3](PF_6)_6$ as the major product of a complex mixture of oligomers and polymers. 1H NMR (500 MHz, CD_3CN) δ = 8.39 (d, $J=8.3$, 6H, H^{A3}), 8.35 (s, 6H, $H^{CH=N}$), 8.00 (d, $J=8.3$, 6H H^{A4}), 7.82 (d, $J=7.9$, 6H, H^{B4}), 7.50 (d, $J=8.0$, 6H, H^{B3}), 6.86 (d, $J=7.8$, 12H, H^{C3}), 6.81 (s, 6H, H^{A6}), 6.66 (d, $J=7.8$, 12H, H^{C2}), 6.39 (s, 6H, H^{B6}), 5.39 (d, $J=14.0$, 6H, H^{CH_2-N}), 5.00 (d, $J=13.9$, 6H, H^{CH_2-N}), 3.53 – 2.76 (m, 42H). ^{13}C NMR (126 MHz, CD_3CN) δ = 174.4 ($C^{CH=N}$), 158.9 ($C^{A2/B2}$), 157.42 ($C^{A2/B2}$), 153.1 (C^{A6}), 152.6 (C^{B6}), 143.5 ($C^{A5/B5}$), 142.4 ($C^{A5/B5}$), 139.3 (C^{C1}), 138.8 (C^{A4}), 137.9 (C^{B4}), 131.9 (C^{C4}), 130.5 (C^{C3}), 130.1 (C^{B3}), 128.0 (C^{C2}), 125.0 (C^{A3}), 66.1 (CH_2-N), 34.7($C^{a/b}$), 33.9 ($C^{a/b}$), 21.03 (Me). ESI-MS: m/z 1316.1 $[M-2PF_6]^{2+}$ requires 1316.3; 829.1 $[M-3PF_6]^{3+}$ requires 829.2; 585.7 $[M-4PF_6]^{4+}$ requires 585.7.

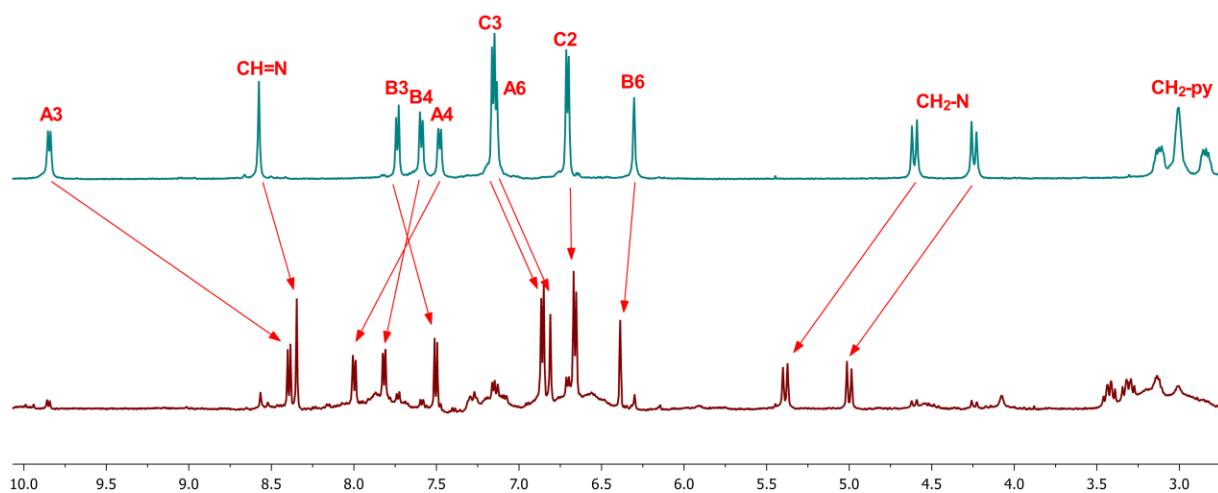


Figure 13. Comparison of ^1H NMR (500 MHz, CD_3CN) of circular pentameric helicate $[\mathbf{3cCl}](\text{PF}_6)_9$ and linear triple helicate $[\text{Fe}_3(\mathbf{S8})_3](\text{PF}_6)_6$. Peak shifts are indicated; a contaminate of $[\mathbf{3cCl}](\text{PF}_6)_9$ is observed in the spectrum of $[\text{Fe}_3(\mathbf{S8})_3](\text{PF}_6)_6$, due to the high affinity of the pentamer for trace amounts of chloride in the reaction mixture.

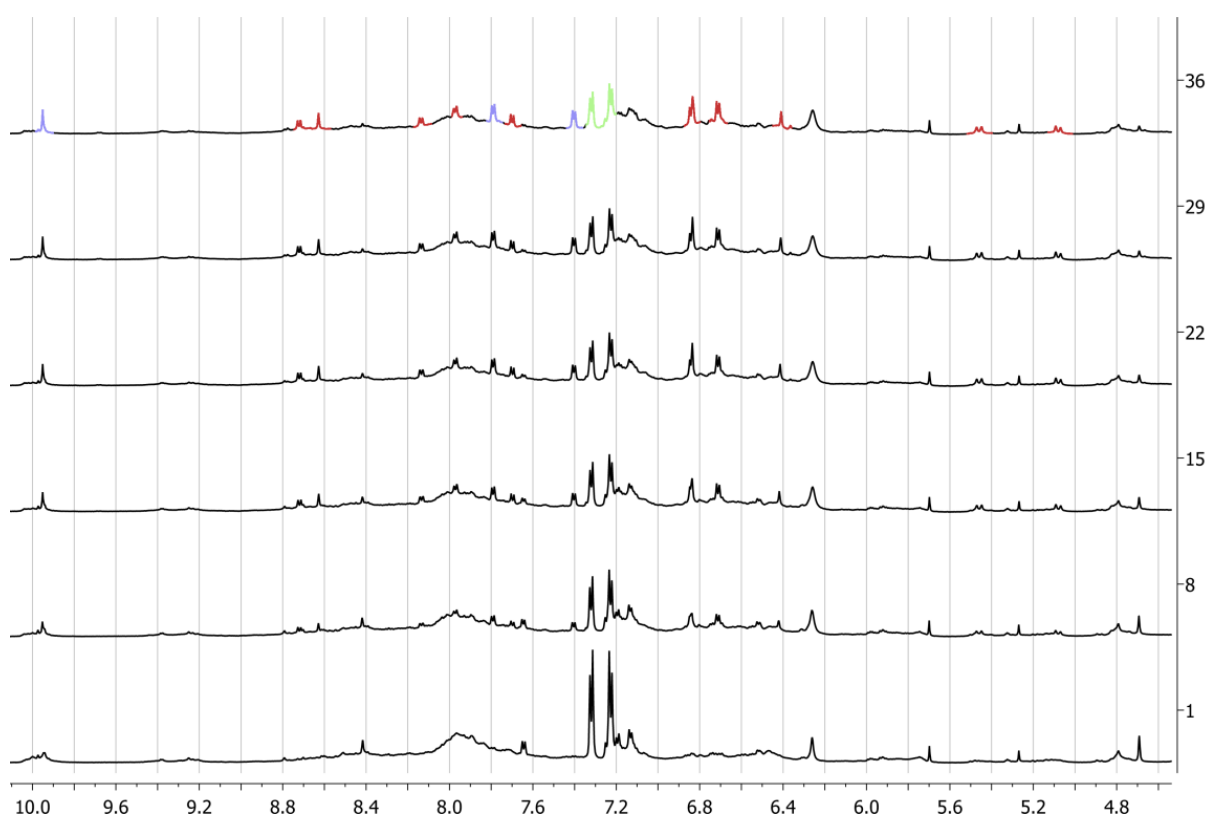


Figure 14. Formation of linear triple helicate $[\text{Fe}_3(\mathbf{S8})_3](\text{PF}_6)_6$, monitored by ^1H NMR (500 MHz, CD_3CN) Spectra are shown after 30 min, 1h, 2h, 3h..... 18h.

3.10.3. Failed synthesis of circular helicates with various amines

Attempts to form helicates using amino acids (Thr, Ala, Gly) as the monoamine gave only pale orange solutions, with no evidence for the formation of well-defined species. Other simple chiral amines (Figure 15a) and diamines such as *ortho*-diaminoxylylene and a catechol derivative (Figure 15b), and BINAP derivatives (Figure 15d) and bridged 4-alkoxybenzylamines (Figure 15e), gave intractable mixtures of oligomers.

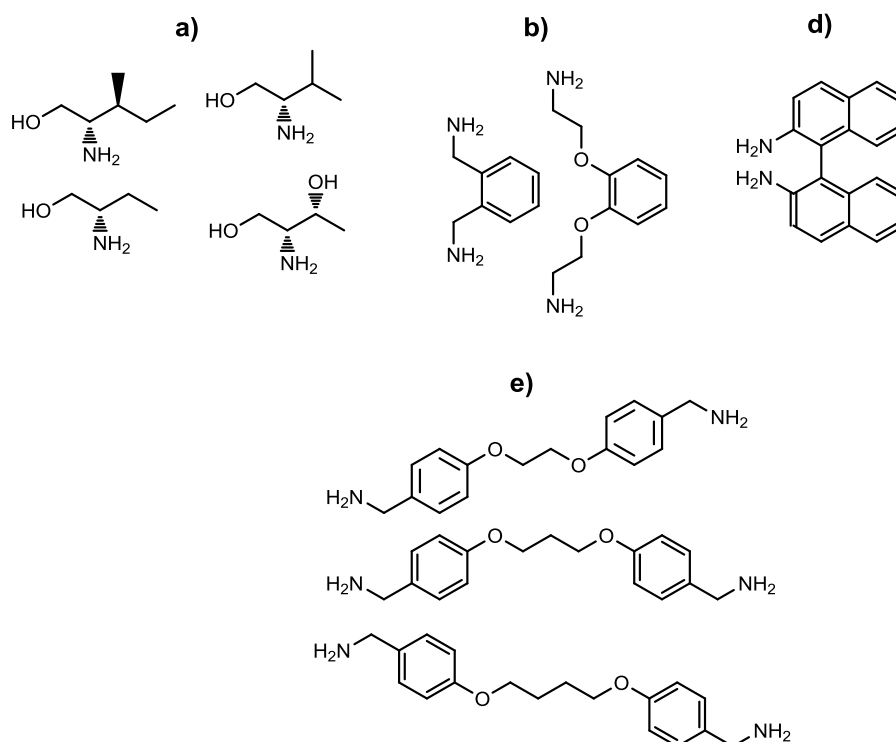


Figure 15. Amines used in unsuccessful circular helicate syntheses.

3.10.4. Monitoring reaction kinetics

3.10.4.1. Formation of circular helicate ([3hCl]Cl₉) from dialdehyde **1** and hexylamine (**2h**)

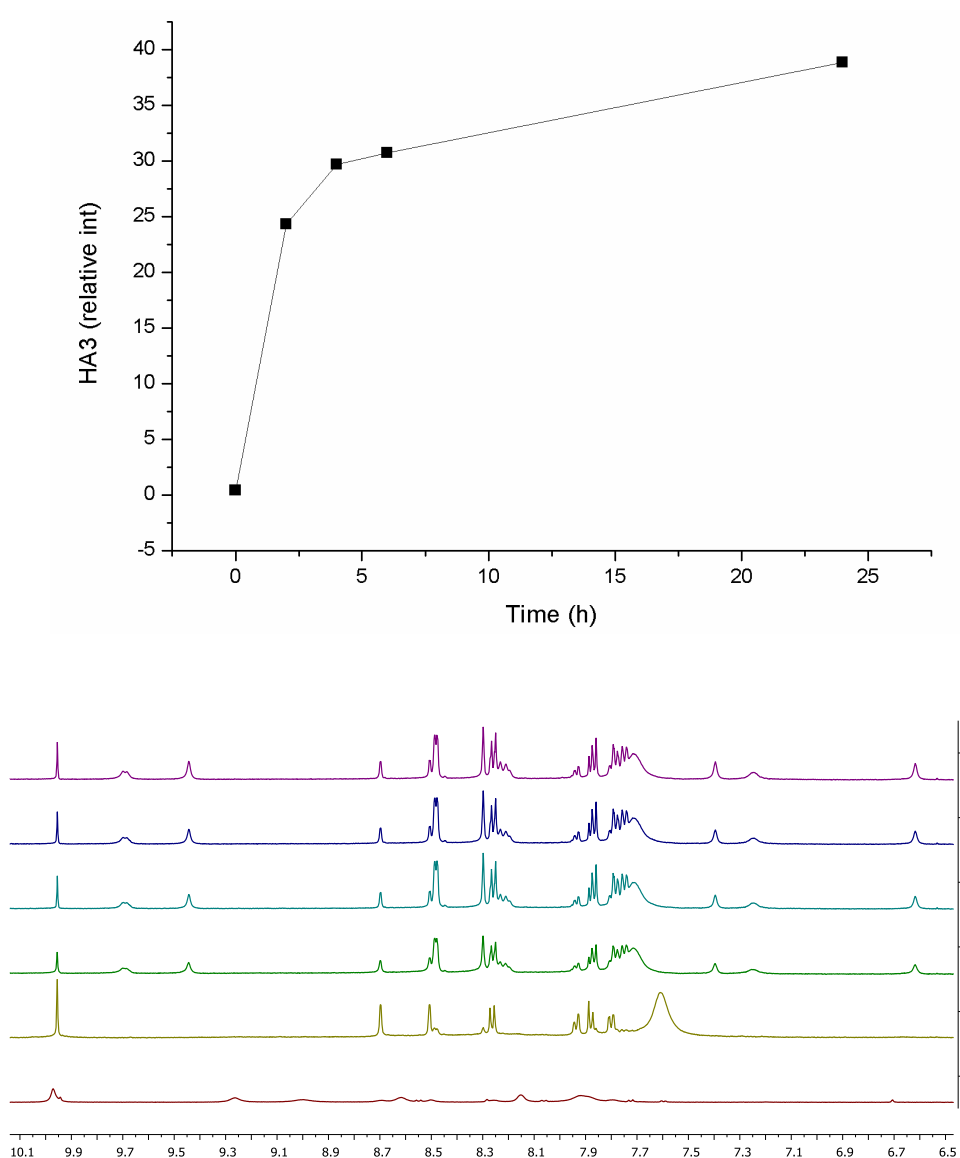


Figure 16. Monitoring the formation of hexylamine-derived helicate [3hCl]Cl₉ by ¹H NMR (crude reaction mixture, DMSO-d₆, 500 MHz), data plotted using the imine signal integral. Bottom to top: f) before hexylamine (**2h**) addition, e) immediately after amine addition, d) heating at 60 °C for 2h, c) 4h, b) 6h and a) 24h (top). Reaction conditions: 1:1:2.2 of dialdehyde **1**:FeCl₂:hexylamine, 4.7 mM in DMSO-d₆, 60 °C.

3.10.4.2. Formation of circular helicate ($[3hCl]Cl_9$) from pre-formed ligand **4**

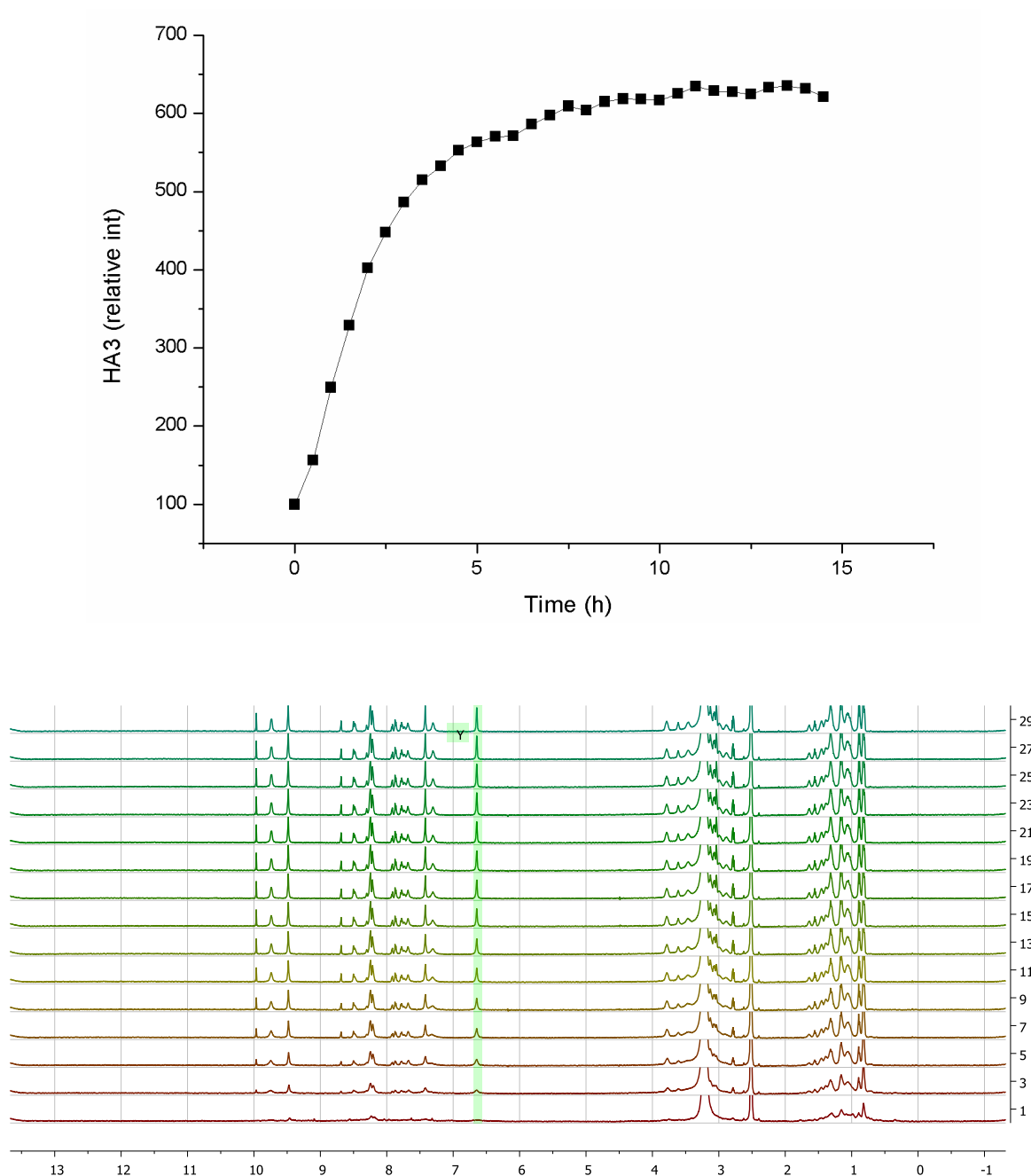


Figure 17. Monitoring the formation of pentameric circular helicate ($[3hCl]Cl_9$) from pre-formed bis(diimine) ligand **4** and 1.1 eq of $FeCl_2$ in $DMSO-d_6$. Sample was maintained at 60 °C and spectra of crude reaction mixture were recorded every 30 min; graph plotting using H^{B6} signal. Reaction conditions: 1: 1.1 of ligand **4** : $FeCl_2$, 4.7 mM in $DMSO-d_6$, 60 °C.

3.10.4.3. Formation of pentafoil knot ($[7Cl]Cl_9$) from dialdehyde **1** and diamine

6

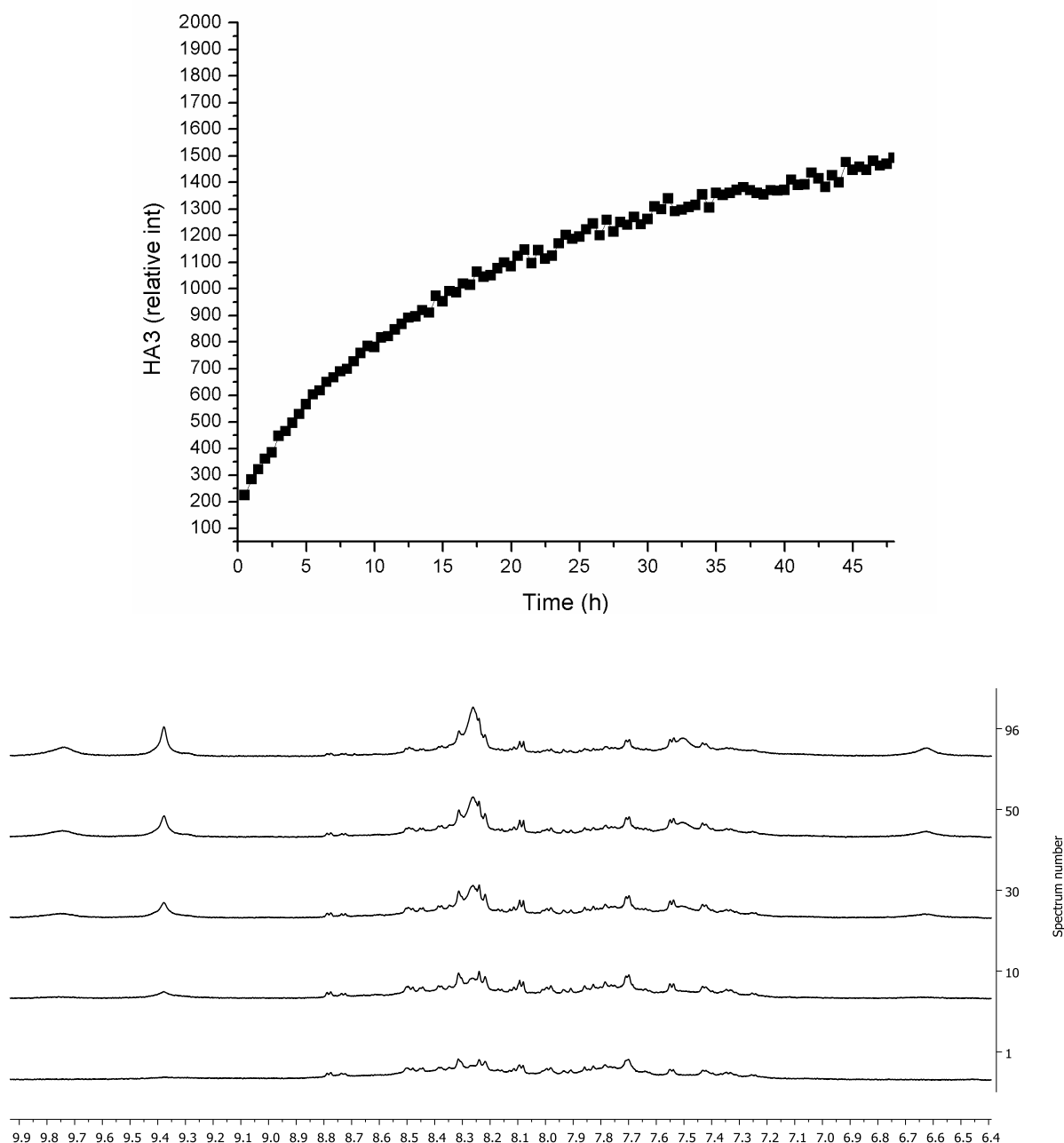


Figure 18. Formation of pentafoil knot $[7Cl]Cl_9$ monitored by 1H NMR (crude reaction mixture, DMSO- d_6 , 500 MHz), aromatic region of spectrum shown. Spectra were collected of the crude reaction mixture after $t = 0$ (bottom), 5h, 15h, 25h and 48h. Graph is of imine peak intensity (as shown). Reaction conditions: 1:1:1.1 of dialdehyde **1**: $FeCl_2$:diamine **10**, 4.7 mM in DMSO- d_6 , 60 °C.

3.10.5. Reaction stoichiometry

3.10.5.1. Effect of Fe(II):dialdehyde/amine ratio on hexylamine pentameric circular helicate (**3h**) yield

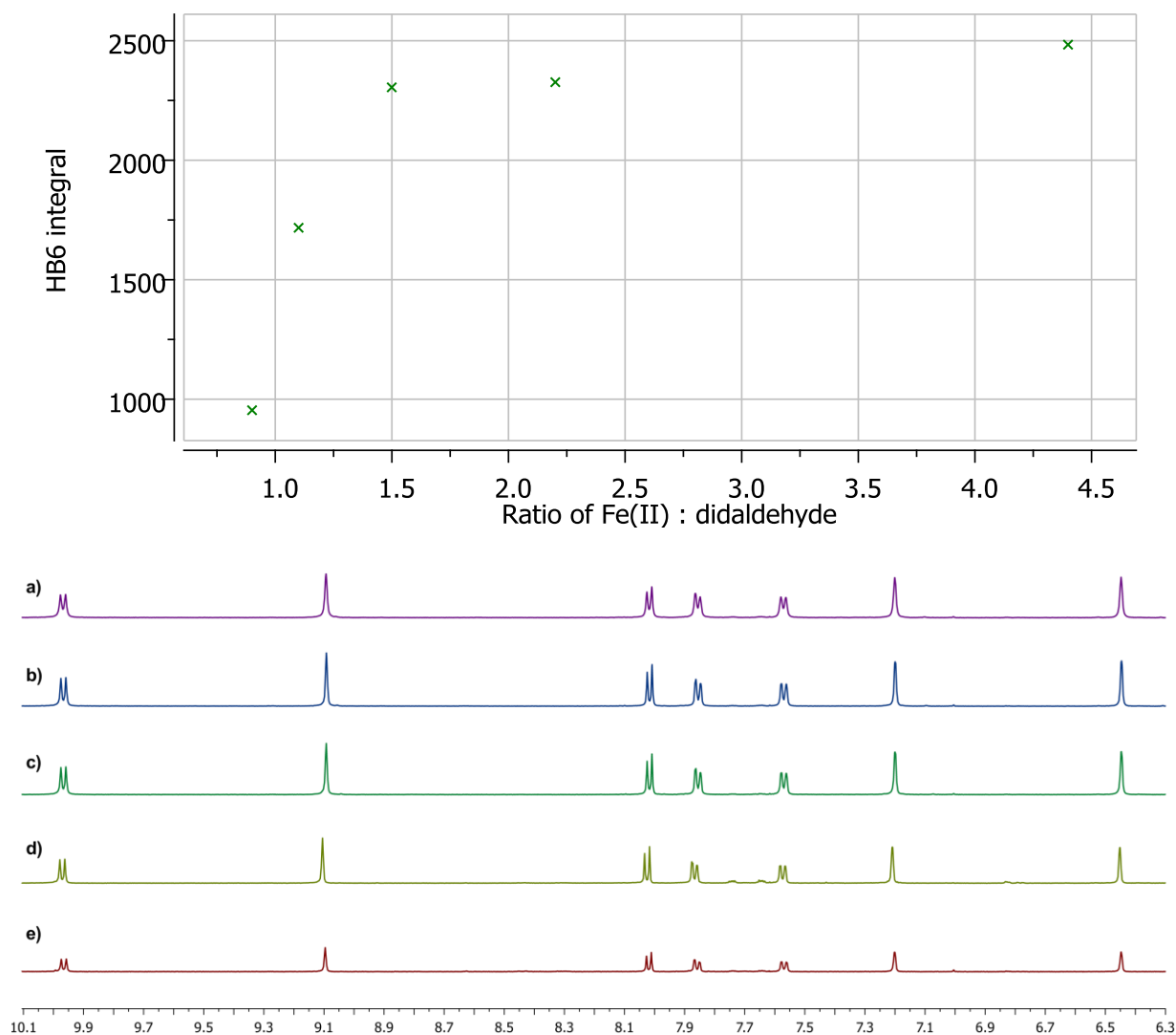


Figure 19. ^1H NMR (CD_3CN , 500 MHz) of isolated samples of helicate $[\mathbf{3hCl}](\text{PF}_6)_9$ formed from reaction of dialdehyde **1**:hexylamine (**2h**) of 1:2.2 with different ratios of FeCl_2 (top bottom): a) 4.4; b) 2.2; c) 1.5; d) 1.1; e) 0.9. Reaction conditions, 1:1.1: 2.2 of dialdehyde **1**: FeCl_2 :hexylamine (**2h**), 4.7 mM in DMSO-d_6 , 60 °C for 2d. Excess $\text{KPF}_6(\text{aq})$ added, product collected on Celite, washed and re-dissolved MeCN, the solvent removed and redissolved in 0.6mL CD_3CN and the ^1H NMR spectrum collected.

3.10.5.2. Effect of amine:dialdehyde/Fe(II) ratio on hexylamine circular pentameric helicate (**3h**) yield

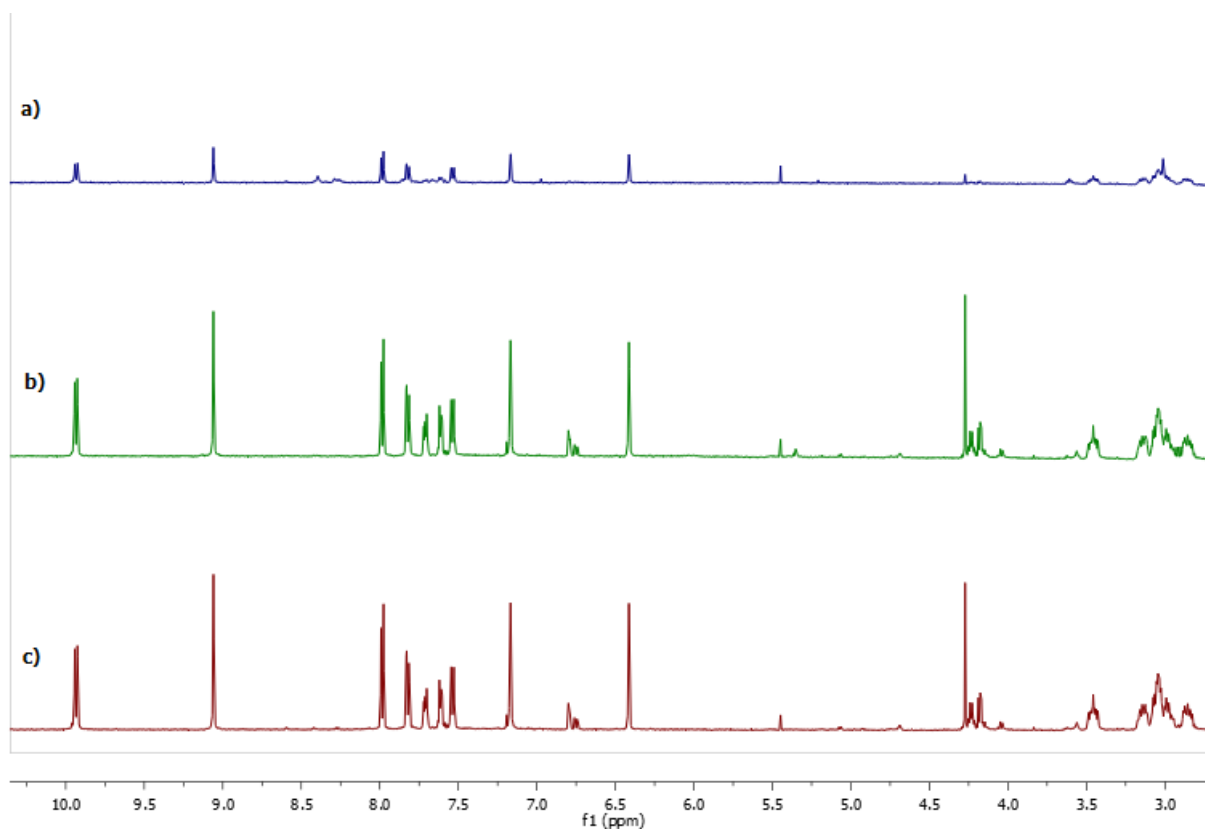
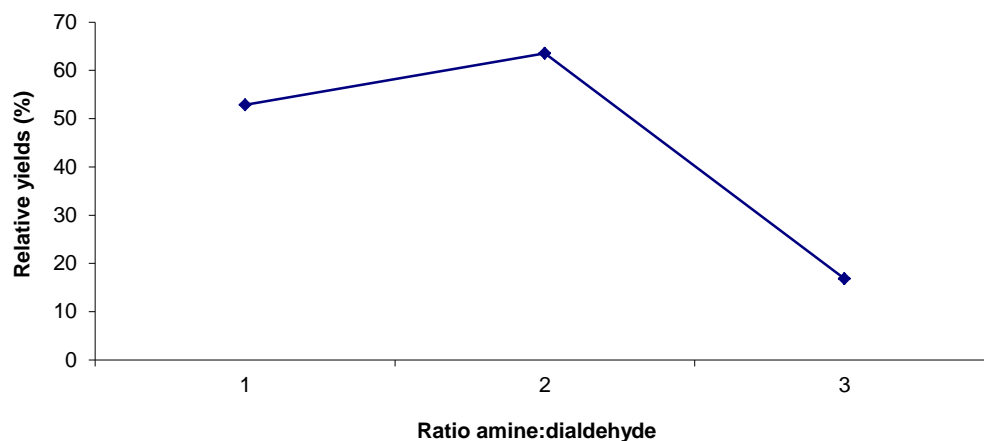


Figure 20. Effect on yield of increasing the ratio of amine (**3h**) to dialdehyde **1**, with 1.1 equiv. of FeCl_2 in all cases. Relative yields measured from ^1H NMR peak integrals (CD_3CN , 500 MHz). As the equivalents of amine is increased above 2.2 equivalents, the yield drops rapidly. Reaction conditions, 1: 1.1 dialdehyde **1**: FeCl_2 with different ratio of hexylamine **3h** (top bottom): a) 3.3; b) 2.2; c) 1.5; 4.7 mM in DMSO-d_6 , 60 °C for 24 h. Excess $\text{KPF}_6(\text{aq})$ added, product collected on Celite, washed and re-dissolved MeCN, the solvent removed and redissolved in 0.5mL CD_3CN and the ^1H NMR spectrum collected.

3.10.5.3. Effect of diamine:dialdehyde/Fe(II) ratio on pentafoil knot [7Cl](PF₆)₉ yield

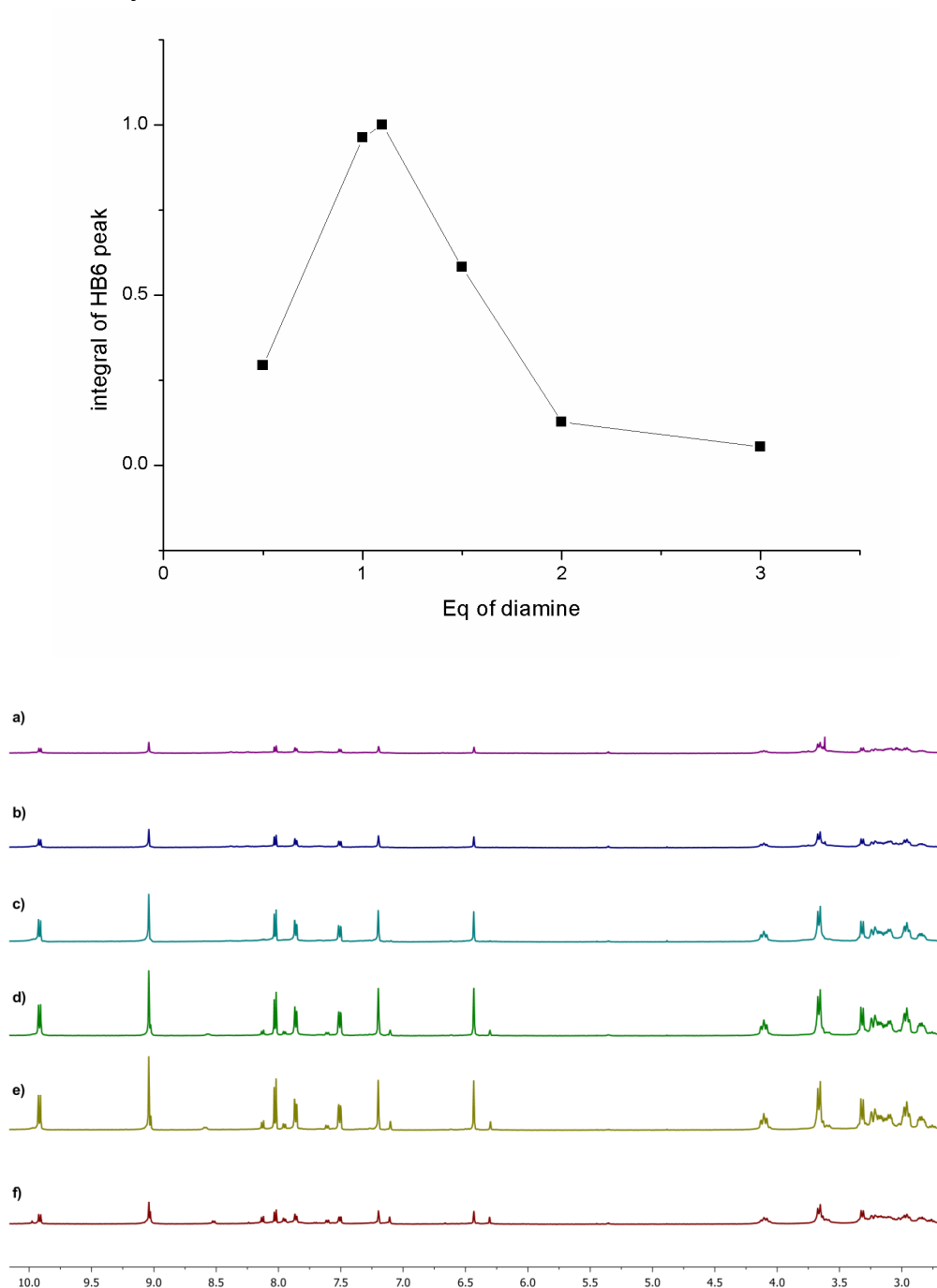


Figure 21. Effect on yield of increasing the ratio of diamine (**6**) to dialdehyde **1**, with 1.1 equiv. of FeCl₂ in all cases. Relative yields measured from ¹H NMR peak integrals (CD₃CN, 500 MHz). As the equivalents of amine is increased above 1.1 equivalents, the yield drops rapidly. Reaction conditions, 1:1.1 of dialdehyde **1**:FeCl₂ with different ratio of diamine **6** (top bottom): a) 3; b) 2; c) 1.5; d) 1.1; e) 0.95; f) 0.5; 4.7 mM in DMSO-d₆, 60 °C for 2d. Excess KPF_{6(aq)} added, product collected on Celite, washed and re-dissolved MeCN, the solvent removed and redissolved in 0.6mL CD₃CN and the ¹H NMR spectrum collected.

3.10.5.4. Effect of Fe(II):diamine/dialdehyde ratio on pentafoil knot [7Cl](PF₆)₉ yield

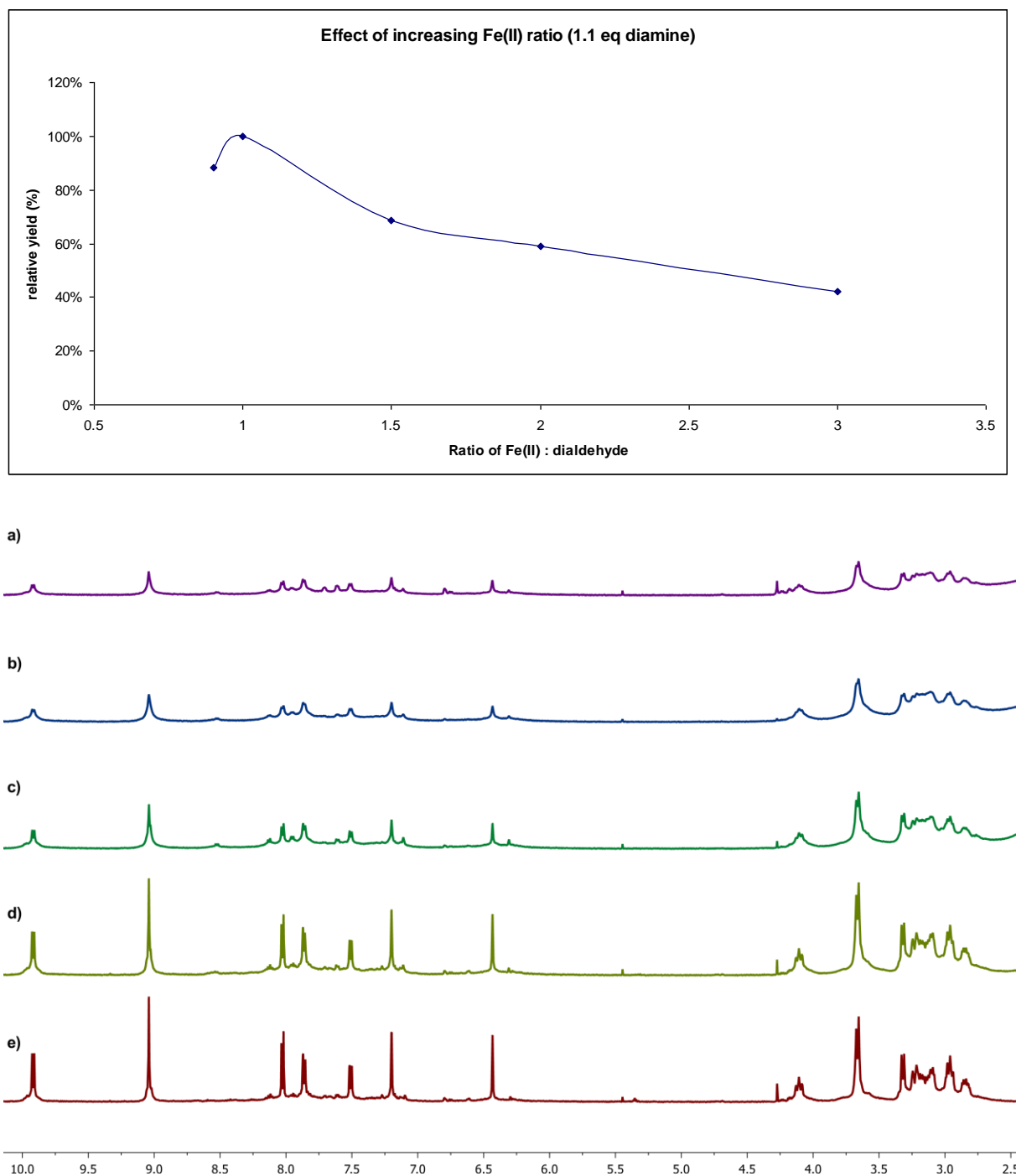


Figure 22. Effect on yield of increasing ratio of FeCl₂ to dialdehyde (**1**), with 1.1 equiv. of diamine (**6**) in all cases. Relative yields measured from ¹H NMR peak integrals (CD₃CN, 500 MHz). Reaction conditions, 1:1.1 of dialdehyde **1**:diamine (**6**) with different ratio of FeCl₂; 4.7 mM in DMSO-d₆, 60 °C for 2d. Excess KPF_{6(aq)} added, product collected on Celite, washed and re-dissolved MeCN, the solvent removed and redissolved in 0.6mL CD₃CN and the ¹H NMR spectrum collected. Ratio of Fe(II) a) 3.0 b) 2.0 ; c) 1.5; d) 1.0; e) 0.9.

3.10.5.5. Effect of diamine (6):FeCl₂ ratio on pentafoil knot [7Cl](PF₆)₉ yield

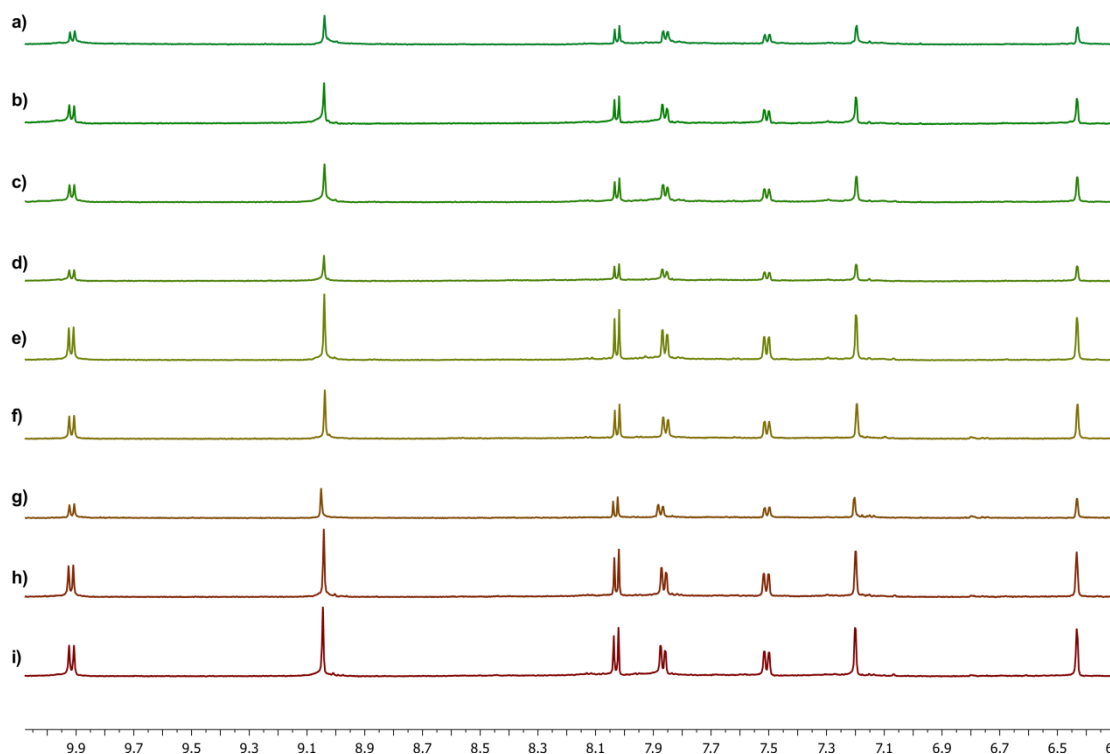
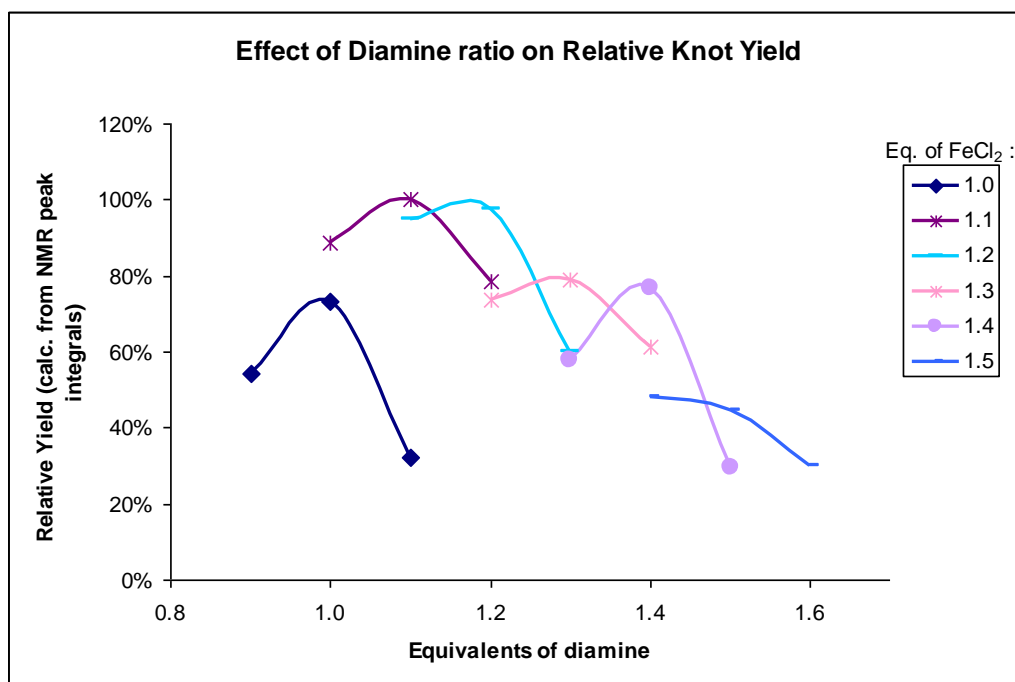


Figure 23. Effect on yield of pentafoil knot [7Cl](PF₆)₉ of increasing the ratio of FeCl₂ and diamine (6) to dialdehyde 1. ¹H NMR peak integrals (CD₃CN, 500 MHz). For any given ratio of FeCl₂, an equimolar amount of diamine gave the highest yield, with yields steadily decreasing as the ratio of FeCl₂ and diamine to dialdehyde increase. Estimated error ±4%. Reaction conditions, 1 eq. of dialdehyde 1 with different ratio of FeCl₂ and diamine 6 respectively from

top to bottom: a) 1.5:1.6 ; b) 1.5:1.5; c) 1.5:1.4; d) 1:1.1; e) 1:1; f) 1:0.9; g) 0.9:1.1; h) 0.9:1 ; i) 0.9:0.9. Reaction details: 4.7 mM in DMSO-d₆, 60 °C for 2d. Excess KPF_{6(aq)} added, product collected on Celite, washed and re-dissolved MeCN, the solvent removed and redissolved in 0.6mL CD₃CN and the ¹H NMR spectrum collected.

3.10.5.6. Effect of chloride on the yield of pentameric cyclic helicate [3hCl](PF₆)₉ and pentafoil knot [7Cl](PF₆)₉

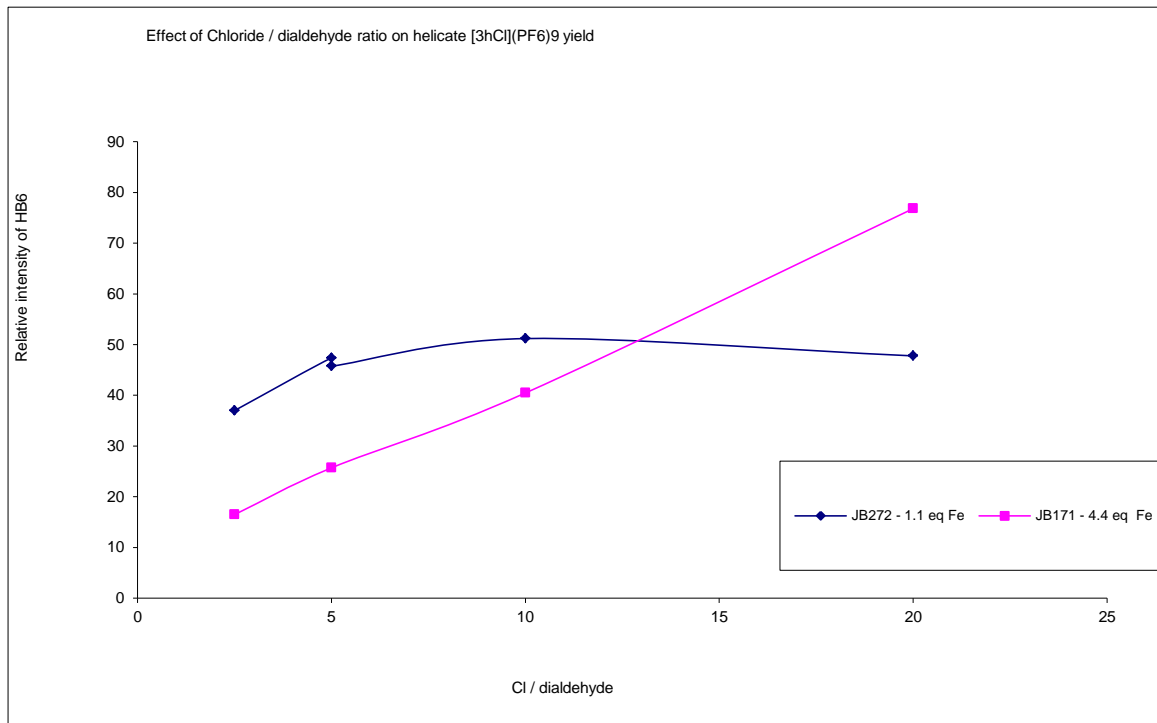
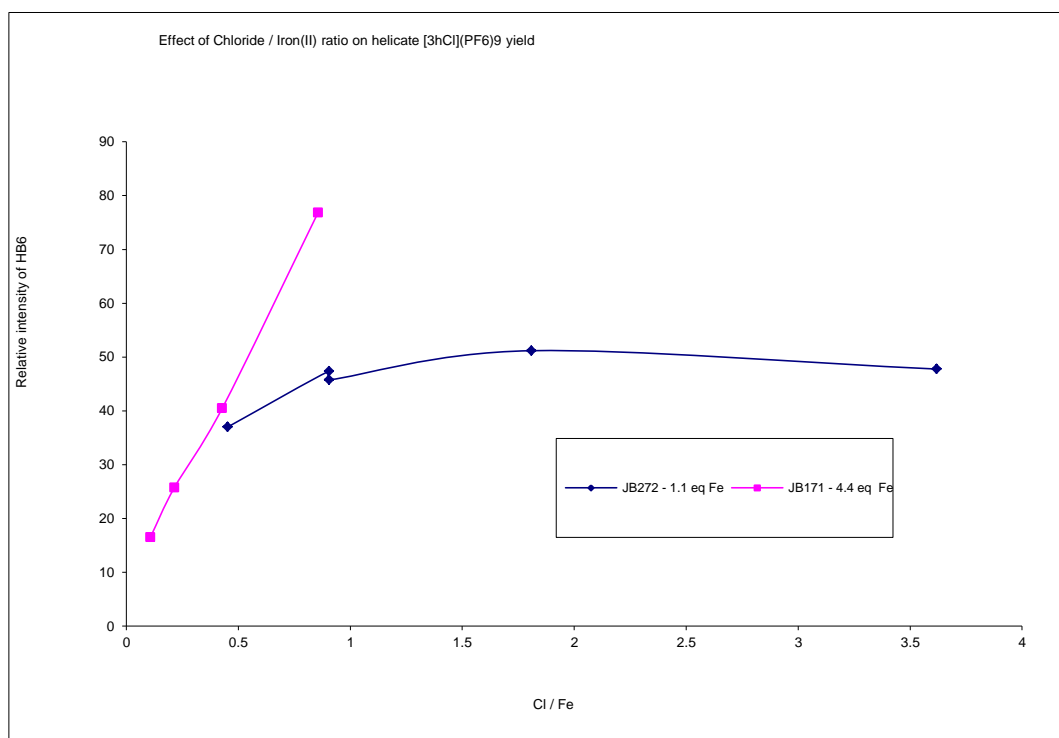


Figure 24. Effect of chloride on the template assembly of helicate [3hCl](PF₆)₉, plotted to show the ratio of chloride to iron(II) (left) and dialdehyde **1** (right). With respect to dialdehyde **1**, 2.2 equivalents of hexylamine and 1.1 or 4.4 eq of Fe(BF₄)₂·6H₂O were used, with added TBACl,

(and TBABF₄ to maintain constant TBA⁺ concentration). Reaction conditions: i) 4.7 mM, DMSO-d₆, 60 °C, 1d, ii) KPF_{6(aq)}, iii) collect, wash, dissolve in 0.6 mL CD₃CN). ¹H NMR peak intensity of H^{B6} signal plotted.

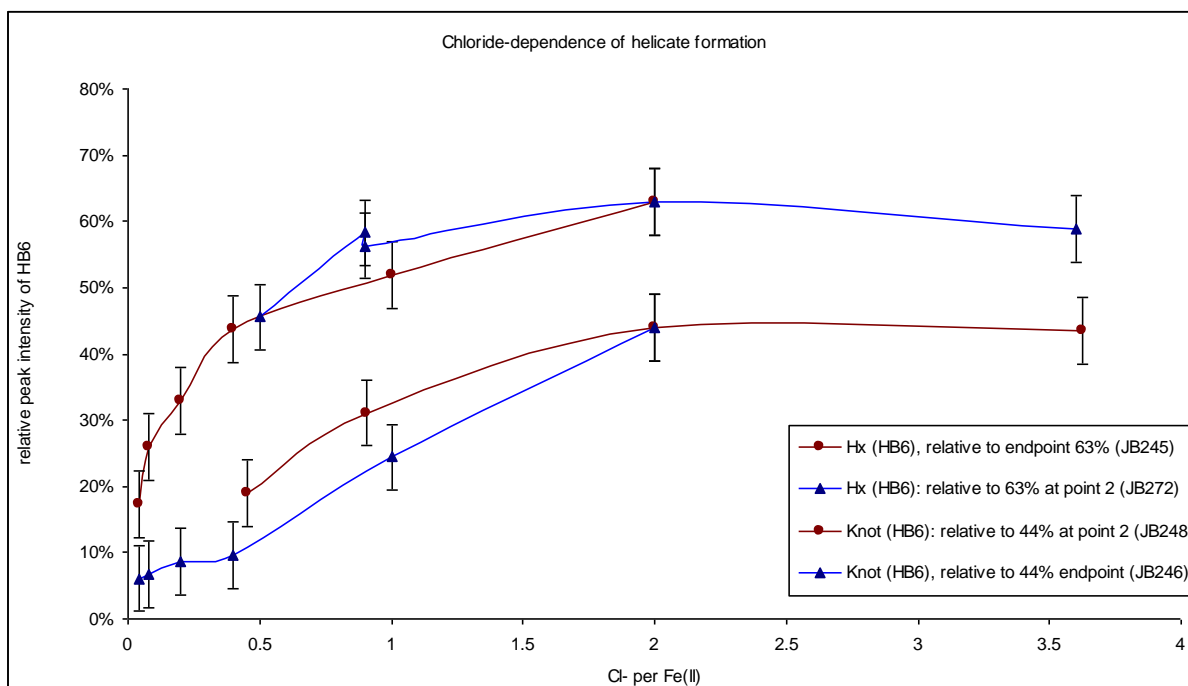


Figure 25. Effect on yield of pentameric circular helicates [3hCl](PF₆)₉ and [7Cl](PF₆)₉ and on increasing the ratio of FeCl₂ to Fe(BF₄)₂·6H₂O, maintaining a dialdehyde (**1**) : Fe(II) : amine ratio of 1 : 1.1 : 2.2 in all cases (amine = **2h** or **6**) (brown). Separate experiments using Fe(BF₄)₂·6H₂O as the Fe(II) source, with added TBACl (and TBABF₄ to maintain constant TBA⁺ concentration) are also plotted (blue), showing the TBABF₄ has no effect on the assembly process, and that the use of more than two equivalents of chloride per Fe(II) does not further increase the isolated yield. ¹H NMR peak integrals (CD₃CN, 500 MHz) for H^{B6} signal used for graph. Reaction conditions: 4.7 mM in DMSO-d₆, 60 °C for 2d. Excess KPF_{6(aq)} added, product collected on Celite, washed and re-dissolved MeCN, the solvent removed and redissolved in 0.6mL CD₃CN and the ¹H NMR spectrum collected.

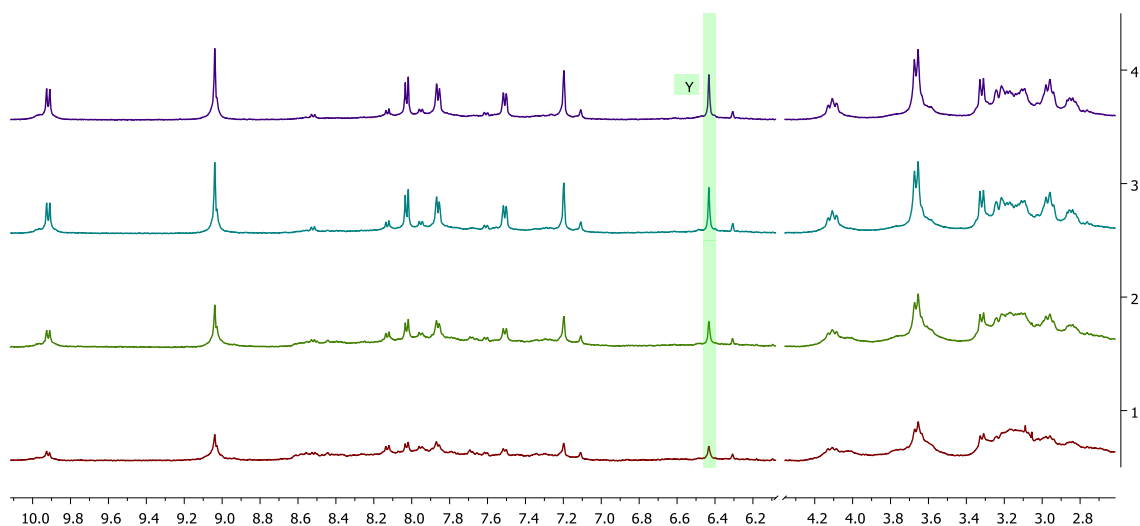


Figure 26. Effect on yield of pentafoil knot $[7Cl](PF_6)_9$ on increasing the ratio of TBACl : TBABF₄, with constant TBA concentration and dialdehyde (**1**) : Fe(II) : diamine (**6**) ratio of 1 : 1.1 : 1.1 in all case. Relative chloride: Fe(II) ratios (bottom to top): 3.6, 2.0, 0.9, 0.45. ¹H NMR peak integrals (CD₃CN, 500 MHz) for H^{B6} signal. Similar results were obtained for $[3hCl](PF_6)_9$.

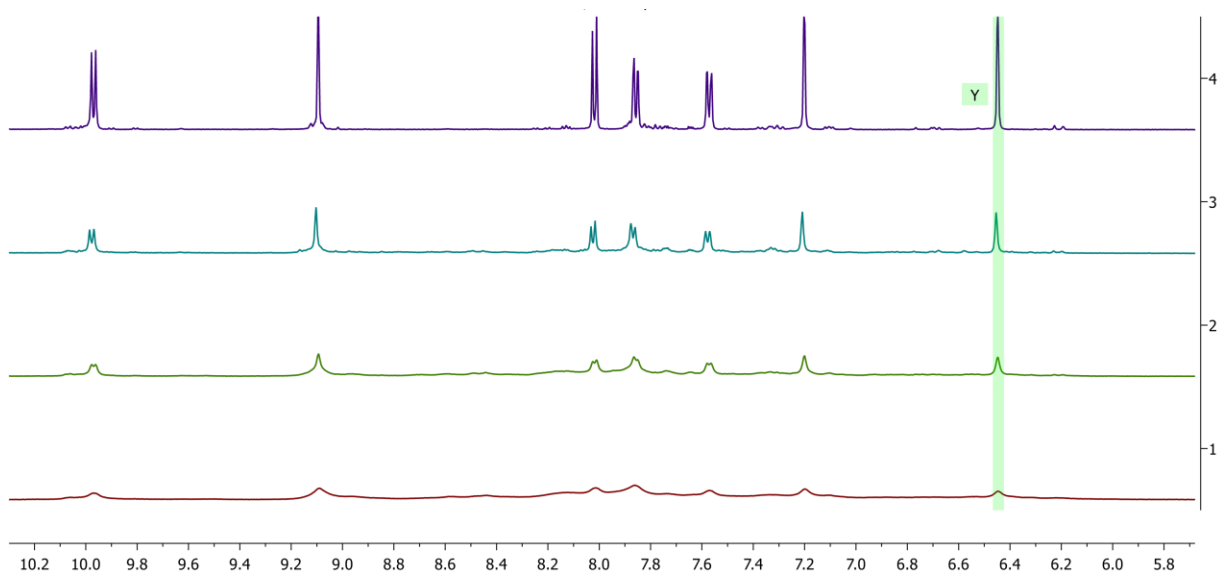
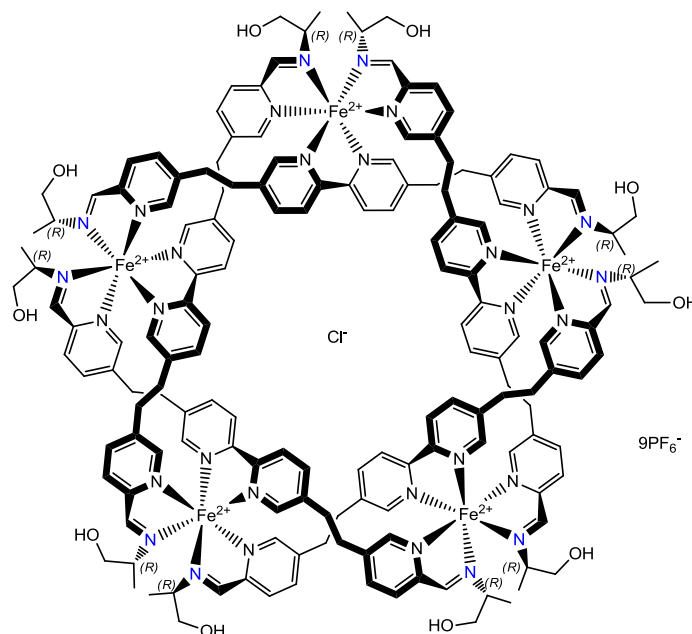


Figure 27. Effect on yield of pentameric circular helicate $[3hCl](PF_6)_9$ on increasing the ratio of TBACl : TBABF₄, with constant TBA concentration and a dialdehyde: Fe(II) : hexylamine (**2h**) ratio of 1 : 4.4 : 1.1 in all case. Relative chloride: Fe(II) (bottom to top): 3.6, 1.8, 0.9, 0.45. ¹H NMR peak integrals (CD₃CN, 500 MHz) for H^{B6} signal.

3.10.6. Diastereoselective pentameric circular helicates

3.10.6.1. Synthesis of diastereoselective pentameric circular helicate [R/S-3]Cl](PF₆)₉



¹H NMR (500 MHz, CD₃CN) δ 9.88 (d, *J* = 8.3 Hz, 10H, H^{A3}), 9.04 (s, 10H, H^{CH=N}), 8.04 (d, *J* = 8.0 Hz, 10H, H^{B3}), 7.80 (s, 10H, H^{A6}), 7.69 (d, *J* = 8.0 Hz, 10H, H^{B4}), 7.52 (d, *J* = 8.3 Hz, 10H, H^{A4}), 6.52 (s, 10H, H^{A6}), 3.80 – 3.52 (m, 30H, H^e+OH), 3.38 – 3.29 (m, 10H, H^{e'}), 3.22 (ddd, *J* = 14.8, 8.2, 5.4 Hz, 10H, H^{CH₂-py}), 3.19 – 3.02 (m, 20H, H^{CH₂-N+CH₂-py}), 2.96 – 2.81 (m, 20H, H^{CH₂-py}), 1.08 (d, *J* = 6.7 Hz, 30H, Me). ¹³C NMR (126 MHz, CD₃CN) δ 171.9 (C^{CH=N}), 158.0 (C^{B2}), 156.9 (C^{A2}), 154.7 (C^{A6}), 153.8 (C^{B6}), 140.7 (C^{A5/B5}), 140.6 (C^{A5/B5}), 140.0 (C^{A4}), 138.9 (C^{B4}), 129.9 (C^{B3}), 125.2 (C^{A3}), 64.7 (C^{CH₂-N}), 62.3 (C^e), 30.4 (C^{CH₂-py}), 30.3 (C^{CH₂-py}), 18.4 (C^{Me}). ESI-MS: *m/z* 1289.4 [M-3PF₆]³⁺ requires 1289.0; 930.3 [M-4PF₆]⁴⁺ requires 930.5; 715.4 [M-5PF₆]⁵⁺ requires 715.4 *m/z*.

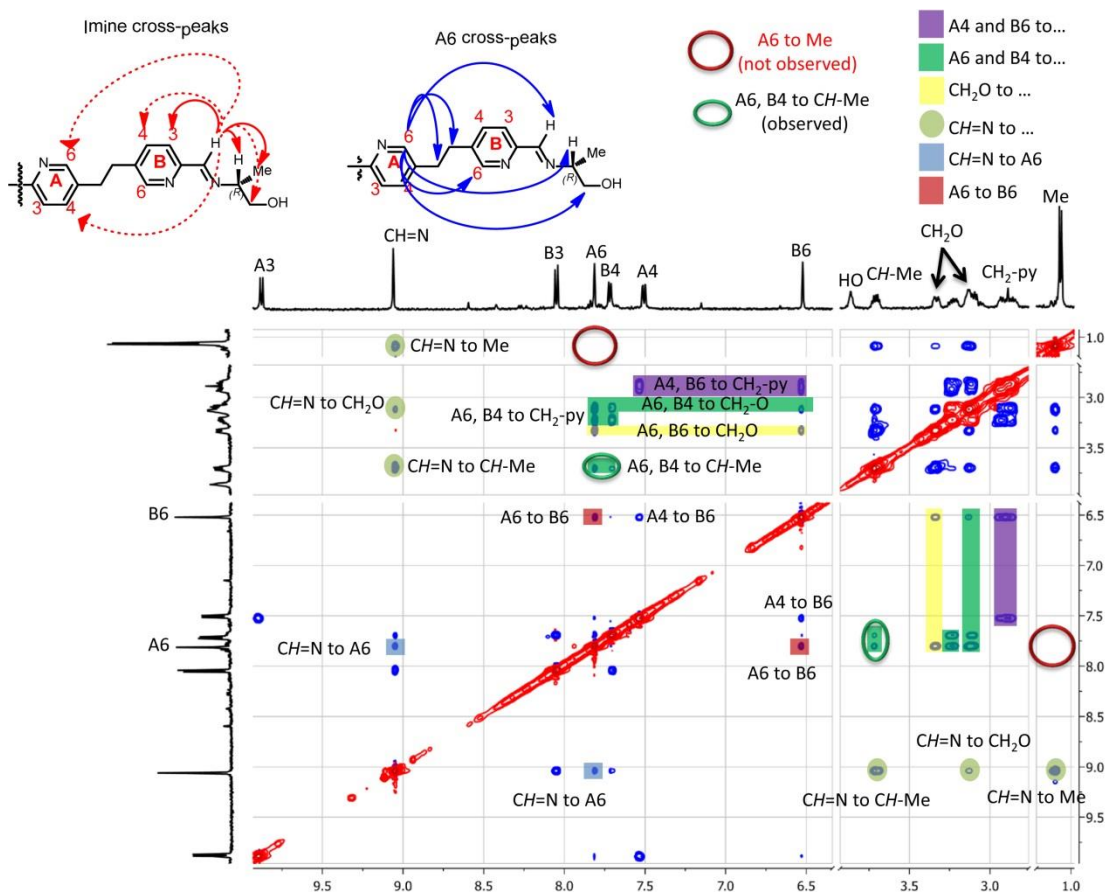
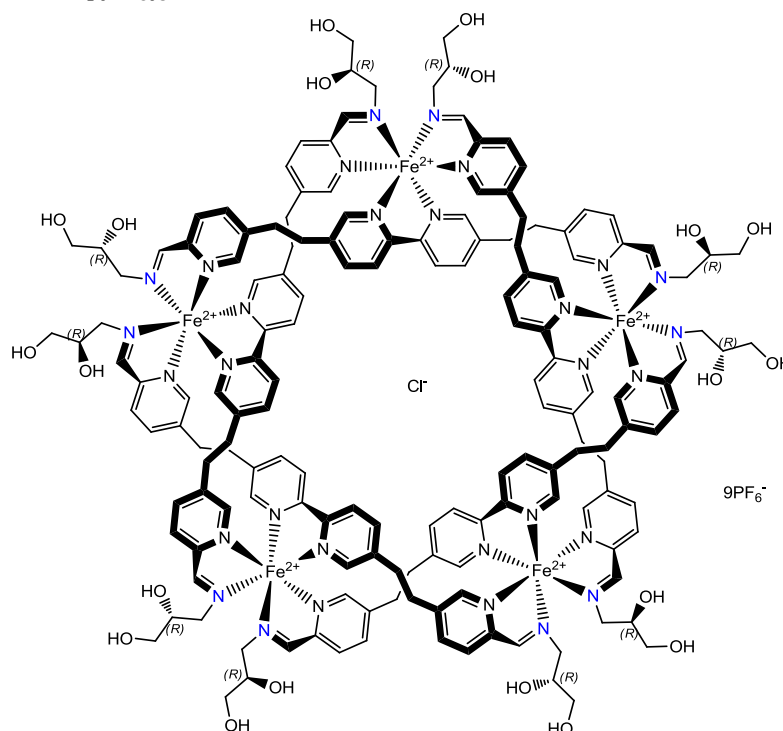


Figure 28. ROESY (CD_3CN , 500 MHz) NMR spectrum of pentameric circular helicate



3.10.6.2. Synthesis of diastereoisomers of pentameric circular helicate [(R)-3kCl](PF₆)₉



Reaction conducted following the standard procedure. Upon KPF₆ addition (minimum volume of water used, ~0.05 mL) a fine precipitate was formed, which was collected on Celite and washed well with ethanol, chloroform and ether. A significant amount of purple material passed through the Celite. The residue was dissolved in acetonitrile (10 mL) and aqueous KPF₆ (~3mL) was added. The volume was reduced under vacuum to precipitate the product, which was washed again with the same solvent procedure to give the major diastereoisomer. The filtrate from the first anion exchange was concentrated to precipitate an approximate 1:1 mixture of the two diastereoisomers (¹H NMR shown in Figure 29). Major diastereoisomer: ¹H NMR (500 MHz, CD₃CN) δ 9.95 (d, *J* = 8.6 Hz, 10H, H^{A3}), 9.08 (s, 10H, CH=N), 7.97 (d, *J* = 8.0 Hz, 10H, H^{B3}), 7.78 (d, *J* = 6.8 Hz, 10H, H^{B4}), 7.52 (d, *J* = 7.5 Hz, 10H, H^{A4}), 7.40 (s, 10H, H^{A6}), 6.38 (s, 10H, H^{B6}), 3.78 (d, *J* = 4.8 Hz, 10H, HO-CH), 3.73 – 3.59 (m, 10H, CH-OH), 3.48 (dd, *J* = 14.7, 10.3 Hz, 10H, CH₂-N), 3.28 (d, *J* = 14.6 Hz, 10H, CH₂-N), 3.22 (t, *J* = 5.5 Hz, 20H, CH₂-OH), 3.19 – 2.82 (series of m, 40H, CH₂-py), 2.80 (t, *J* = 5.5 Hz,

10H, HO-CH₂). ¹³C NMR (126 MHz, CD₃CN) δ 172.7 (CH=N), 157.2 (C^{B2}), 156.9 (C^{A2}), 154.0 (C^{B6}), 153.8 (C^{A6}), 140.8 (C^{A5}), 140.4 (C^{B5}), 140.2 (C^{A4}), 138.8 (C^{B4}), 129.2 (C^{B3}), 125.5 (C^{A3}), 69.3 (CH-OH), 64.6 (CH₂-OH), 63.4 (CH₂-N), 30.9 (CH₂-py), 30.3 (CH₂-py). ESI-MS: *m/z* 1342.5 [M-3PF₆]³⁺ requires 1342.3; 970.8 [M-4PF₆]⁴⁺ requires 970.5; 747.5 [M-5PF₆]⁵⁺ requires 747.4; 598.9 [M-6PF₆]⁶⁺ requires 598.7 *m/z*. HRESI-MS: *m/z* = 970.7211 [M-4(PF₆)]⁴⁺ (calcd. for C₁₆₀H₁₈₀ClF₃₆Fe₅N₃₀O₂₀P₆ requires 970.7072).

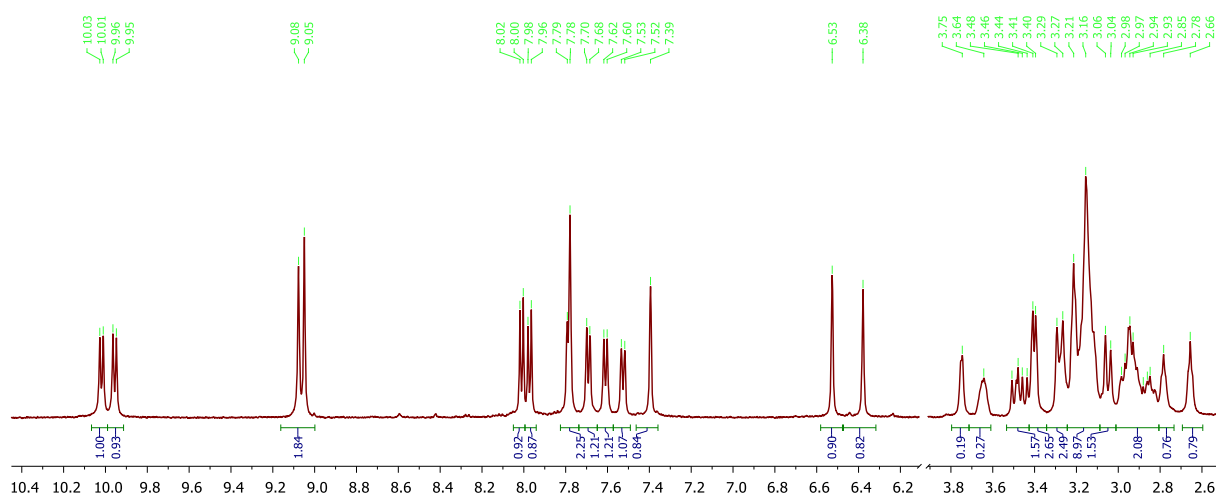


Figure 29. ¹H NMR spectrum of the sample isolated from the filtrate of the workup of [3kCl](PF₆)₉, showing a 1:1 mixture of the two diastereoisomers formed using diol **2k**.

3.10.6.3. Discussion of stereochemistry assignment of pentameric circular helicate R -[**3j**]Cl(PF₆)₉, S -[**3j**]Cl(PF₆)₉ and the major diastereoisomer of R -[**3k**]Cl(PF₆)₉

3.10.6.3.1. Background

See Chapter II section 2.5.1.4.

3.10.6.3.2. Experimental results

The CD spectra of (R) -[**3j**]Cl(PF₆)₉ and (S) -[**3j**]Cl(PF₆)₉ are shown in Figure 16. Using the method discussed above, based on the π - π^* transitions around 300 nm, (R) -[**3j**]¹⁰⁺ corresponds to $\Delta\Delta\Delta\Delta$ -[**3j**]¹⁰⁺ and (S) -[**3j**]¹⁰⁺ corresponds to $\Lambda\Lambda\Lambda\Lambda$ -[**3j**]¹⁰⁺. This is in agreement with both previous simple pyridyl-imine complexes⁴⁷ and a triple-stranded dinuclear Fe(II)-containing helicate.^{5a} Additionally, the CD band for the MLCT transition of (S) -[**3j**]Cl(PF₆)₉ also corresponds to sign of that of Λ -[Fe(bpy)₃]^{48,45c} and Λ -[Ru(phen)₃].^{45a}

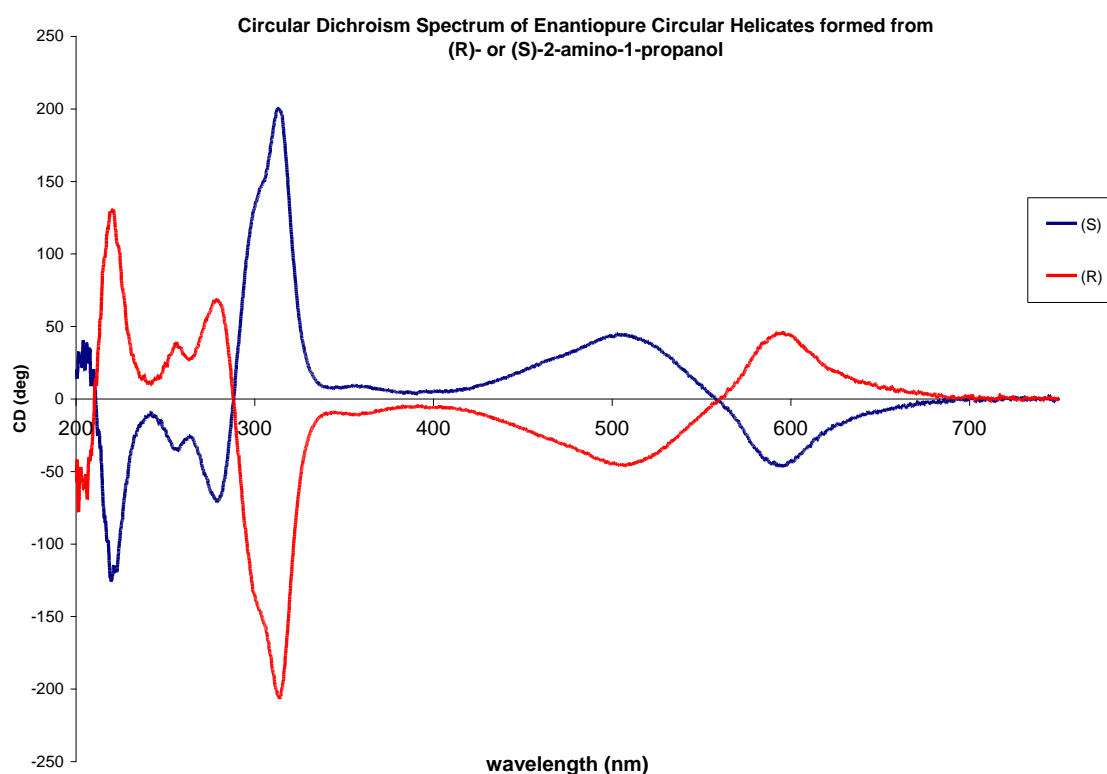


Figure 30. Circular dichroism spectra of (R) -[**3g**]Cl(PF₆)₉ and (S) -[**3g**]Cl(PF₆)₉ in MeCN.

Finally, by comparison with the X-ray crystal structure of $[7]Cl(PF_6)_9$, $(R)-[3j]^{10+}$ and $(S)-[3j]^{10+}$ correspond to $M-(\Delta\Delta\Delta\Delta)-[3jCl](PF_6)_9$ and $P-(\Lambda\Lambda\Lambda\Lambda)-[3jCl](PF_6)_9$. All these assignments are also supported by 2D-ROESY NMR data. The absorption and CD spectra of major diastereoisomer of $[3kCl](PF_6)_2$ is shown in Figure X, and is essentially identical to that of $(S)-[3j]^{10+}$, and is subsequently assigned as corresponding to $P-(\Lambda\Lambda\Lambda\Lambda)-[3kCl](PF_6)_9$.

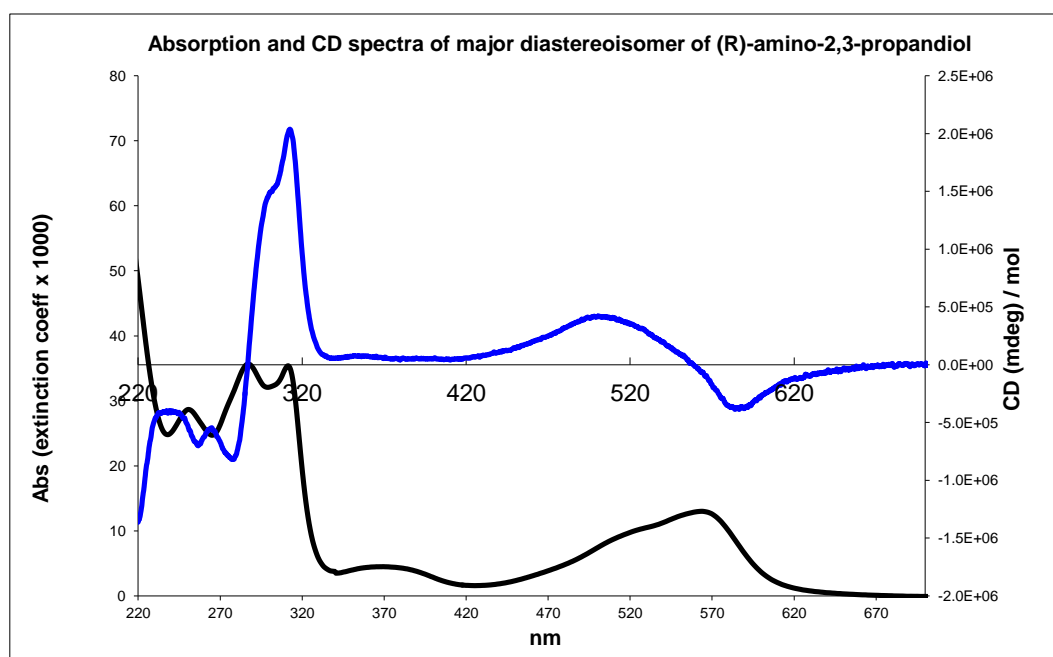


Figure 31. Circular dichroism and absorption spectra of $(R)-[3kCl](PF_6)_9$ (CH_3CN)

3.10.7. X-ray crystal structure experimental

3.10.7.1. X-Ray crystal structure of $[3bCl](PF_6)_9 \cdot xSolvent$

3.10.7.1.1. Experimental details

Purple crystals $[3bCl](PF_6)_9 \cdot xSolvent$ were obtained by vapor diffusion of a diethyl ether into a nitromethane-acetonitrile (1:1) solution of $[3bCl](PF_6)_9$. The structural analysis was performed using a Rigaku Saturn944+ rotating Cu-anode generator ($\lambda = 1.54178 \text{ \AA}$) at 100 K.

The CrystalClear-SM Expert 2.0 r7 suite of programs⁴⁹ was used for the data collection and reduction. The structure were solved by charge flipping method using SUPERFLIP⁵⁰ and refined by full-matrix least-squares methods using the WinGX-software,⁵¹ which utilizes the SHELXL-97 module.⁵² Multi-scan absorption correction⁴⁹. All C-H hydrogen positions were calculated using a riding atom model with UH = 1.2 x UC. The crystal lattice contains a lot of badly resolved and disordered solvents and anions. Only 7.5 of the nine PF₆ anions could be located, one of them with 0.5 occupancy. Due to the moderate quality of the crystal some parts of the molecule, especially some of the methoxy groups showed very large very large thermal motion (maybe due positional disorder, which however could not be modeled). Two of the methoxy carbons from a same benzene ring could not be located at all. In order to avoid a large number of restrains only a minimal number (151) to bond distances and thermal parameters (DFIX, EADP, ISOR) were applied. The [3bCl](PF₆)₉ is solvated by a large number of badly disordered solvent molecules, could not be modeled resulting in a moderate quality structure solution. As the 1.5 PF₆ anions and possible lattice solvents could not be located and thus all unresolved anions and solvate molecules were modeled as isolated carbon atoms with partial occupancies until plateau of ca. 1.2 e/Å³ was reached. The crystal lattice contains very large voids filled with a lot of scattered electron density, the SQUEEZE protocol inside PLATON⁵³ was used to remove the void electron density. Crystal data for [3bCl](PF₆)₉•xSolvent: *M* = 5358.62 [C₂₄₀H₂₃₄ClF₄₅N₃₇O₂₀P_{7.5}Fe₅], purple blocks, 0.11 × 0.15 × 0.32 mm monoclinic, space group *P*2₁/*c*, *a* = 34.023(2) Å, *b* = 23.714(2) Å, *c* = 36.537(2) Å, *β* = 94.386(2)°, *V* = 29393(4) Å³, *Z* = 4, *D*_c = 1.211 g/cm³, *F*000 = 11030, *μ* = 3.157 mm⁻¹, *T* = 100(2) K, 2θ_{max} = 60°, 43584 independent reflections, 30867 with *I*_o > 2σ(*I*_o), *R*_{int} = 0.0875, 3206 parameters, 151 restraints, GoF = 1.409, *R* = 0.1392 [*I*_o > 2σ(*I*_o)], *wR* = 0.3835 (all reflections). 1.277 < Δρ < -0.800 e/Å³. CCDC-XXXXXX contains the supplementary

crystallographic data for this paper. These data can be obtained free of charge from The Cambridge Crystallographic Data Centre via www.ccdc.cam.ac.uk/data_request/cif;

3.10.7.1.2. Crystal packing diagrams for $[3bCl](PF_6)_9 \cdot xSolvent$

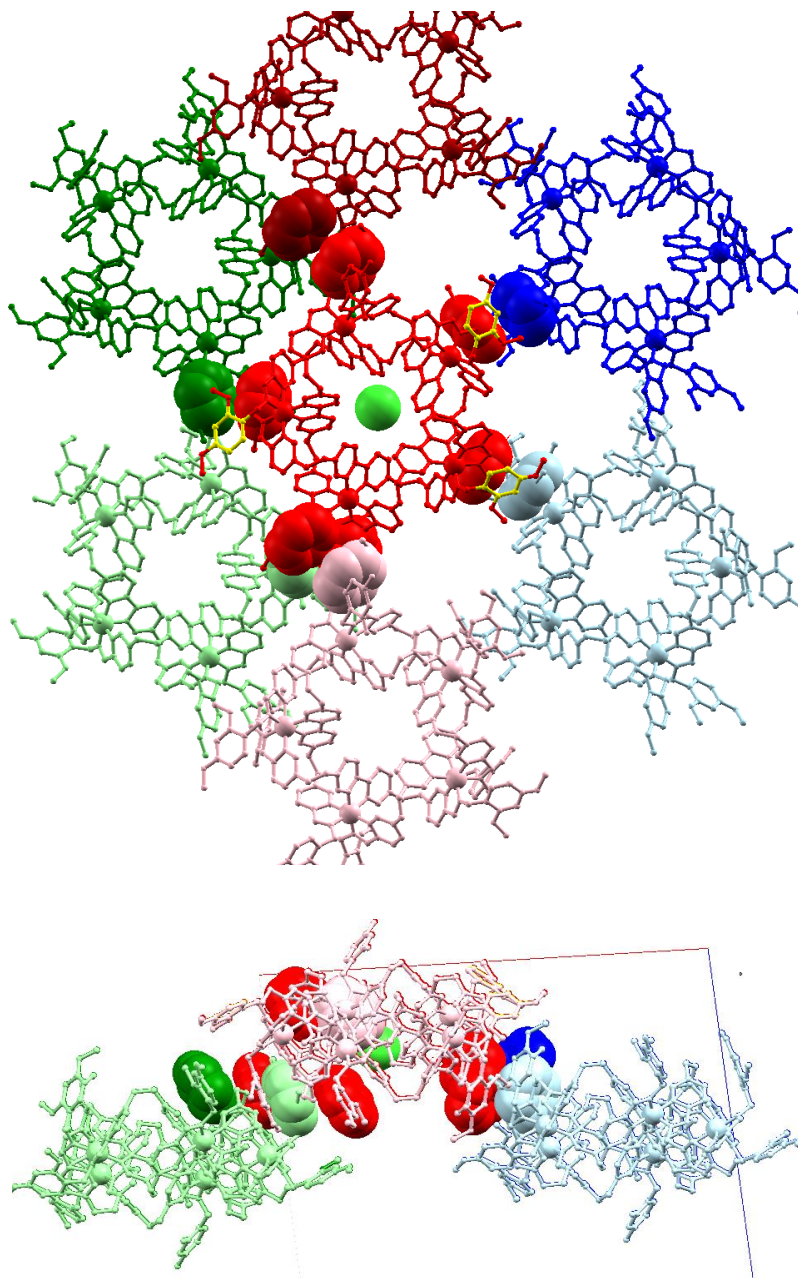


Figure 32. Packing showing viewed down b -axis, (c -axis (blue) and a -axis (red)]. Weak p-p interactions are shown between the phenyl rings represented in CPK representation. Phenyl rings in yellow are involved in Ph-imine interactions. Packing between these 2D sheets is via less defined interactions, and accounts for the large thermal parameters (and missing methyl groups).

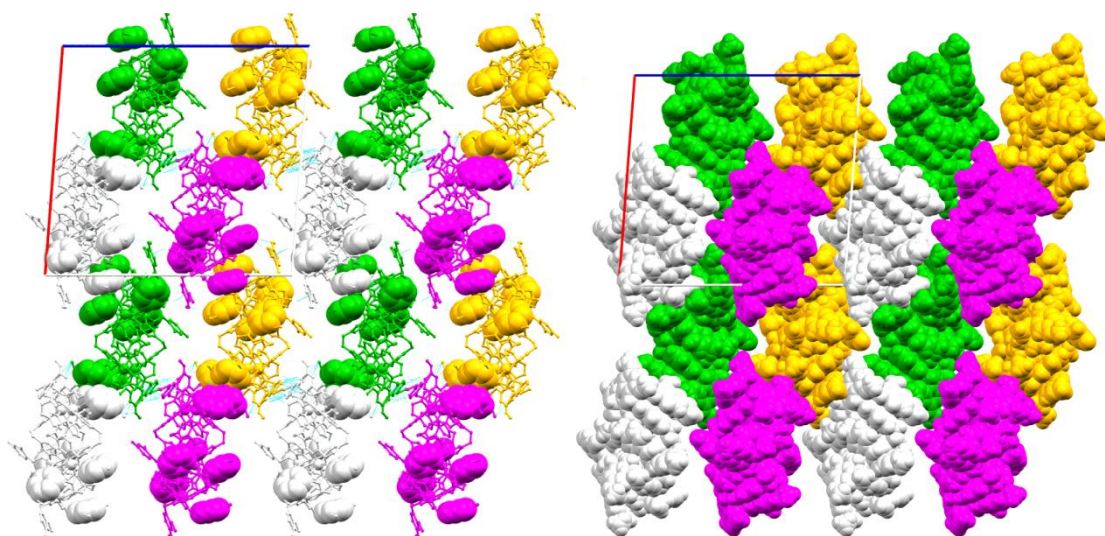


Figure 33. Crystal packing in the X-ray structure of $[3bCl](PF_6)_9$, looking down the b -axis; c -axis shown in blue, a -axis in red. Hydrogens, anions and solvent have been removed for clarity. Molecules are colored by symmetry equivalence. Within the chains along the a -axis (vertical as shown) the phenyl rings of the helicates are involved in weak π - π stacking; those phenyl rings involved (see previous figure) are shown in CPK representation; all others are in ball-and-stick representation. White-Green interactions are based on the strongest π - π stacking interactions. Green-purple contacts (shown with blue lines) are VdW contacts between Ph rings, and Ph - CH_2 -py contacts (via an inversion center). CPK representation of the same view (b), shows the overall close-packing arrangement.

3.10.7.1.3. Pertinent intra- and intermolecular contact distances

Intermolecular face-to-face π - π stacking interactions between pendant phenyl rings

Distance from centroid (C143, C144, C145, C146, C147, C148) to plane of (C103, C104, C105, C106, C107, C108) is 3.63 Å

Distance from centroid (C153, C154, C155, C156, C157, C158) to plane of (C4, C5, C6, C7, C8, C3) is 3.92 Å

Intramolecular face-to-face phenyl-to-imine contacts:

Distance from least-squares plane of Ph ring (C194, C195, C196, C197, C198) to N210 (3.259 Å), C211 (3.218), C212 (3.02 Å)

Ph ring (C43, C44, C45, C46, C47, C48) to N60 (3.350), C61 (3.29 Å), C62 (3.01 Å)

Ph ring (C243, C244, C245, C246, C247, C248) to C11 (3.23 Å), C12 (3.04 Å), N10 (3.24 Å)

Intermolecular phenyl to methylene contacts

Contact Ph(C244) - B-CH₂(H11B) = 2.67 Å; O-Ph (O544) to H11B 2.17 Å

3.10.7.2. X-Ray crystal structure of [7Cl](PF₆)₉·xSolvent

The X-Ray crystal structure of [7Cl](PF₆)₉·xSolvent was discussed in details in Chapter II section 2.5.3.

3.11. Notes and references

- (a) Wasserman, S. A.; Cozzarelli, N. R. *Science*, **1986**, *232*, 951–960; (b) Du, S. M.; Seeman, N. C. *J. Am. Chem. Soc.*, **1992**, *114*, 9652–9655; (c) Du, S. M.; Stollar, B. D.; Seeman, N. C. *J. Am. Chem. Soc.*, **1995**, *117*, 1194–1200.
- (a) Taylor, W. R. *Nature*, **2000**, *406*, 916–919; (b) King, N. P.; Jacobitz, A. W.; Sawaya, M. R.; Goldschmidt, L.; Yeates, T. O. *Proc. Natl. Acad. Sci. U.S.A.*, **2010**, *107*, 20732–20737.
- (a) Andersson, F. I.; Pina, D. G.; Mallam, A. L.; Blaser, G.; Jackson, S. E. *FEBS*, **2009**, *276*, 2625–2635; (b) Mallam, A. L.; Rogers, J. M.; Jackson, S. E. *Proc. Natl. Acad. Sci. U.S.A.* **2010**, *107*, 8189–8194; (c) Meluzzi, D.; Smith, D. E.; Arya, G. *Annu. Rev. Biophys.* **2010**, *39*, 349–366.
- (a) Saitta, A. M.; Soper, P. D.; Wasserman, E.; Klein, M. L. *Nature* **1999**, *399*, 46–48; (b) Virnau, P.; Kantor, Y.; Kardar, M. *J. Am. Chem. Soc.* **2005**, *127*, 15102–15106
- Belmonte, A. *Proc. Natl. Acad. Sci. U.S.A.* **2007**, *104*, 17243–17244.
- Arai, Y.; Yasuda, R.; Akashi, K.-I.; Harada, Y.; Miyata, H.; Kinoshita, K., Jr.; Itoh, H. *Nature* **1999**, *399*, 446–448.
- Lobovkina, T.; Dommersnes, P.; Joanny, J.-F.; Bassereau, P.; Karlsson, M.; Orwar, O. *Proc. Natl. Acad. Sci. U.S.A.* **2004**, *101*, 7949–7953.
- Tkalec, U.; Ravnik, M.; Čopar, S.; Žumer, S.; Muševič, I. *Science* **2011**, *333*, 62–65
- Beves, J. E.; Blight, B. A.; Campbell, C. J.; Leigh, D. A.; McBurney, R. T. *Angew. Chem., Int. Ed.* **2011**, *50*, 9260–9327.
- (a) Chambron, J.-C.; Dietrich-Buchecker, C.; Sauvage, J.-P. In *Comprehensive Supramolecular Chemistry*; Sauvage, J.-P.; Hosseini, M. W., Eds.; Elsevier: Oxford, **1996**; Vol. 9, pp 43–83; (b) Hubin, T. J.; Busch, D. H. *Coord. Chem. Rev.* **2000**, *200*, 5–52; (c) Collin, J.-P.; Dietrich-Buchecker, C.; Hamann, C.; Jouvenot, D.; Kern, J.-M.; Mobian, P.; Sauvage, J.-P. In *Comprehensive Coordination Chemistry II*; McCleverty, J. A.; Meyer, T. J., Eds.; Elsevier: Amsterdam, **2004**; Vol. 7, pp 303–326.
- (a) Loeb, S. J. *Chem. Soc. Rev.* **2007**, *36*, 226–235; (b) Griffiths, K. E.; Stoddart, J. F. *Pure Appl. Chem.* **2008**, *80*, 485–506.

12. (a) Cantrill, S. J.; Pease, A. R.; Stoddart, J. F. *J. Chem. Soc., Dalton Trans.* **2000**, 3715–3734; (b) Kay, E. R.; Leigh, D. A. *Top. Curr. Chem.* **2005**, 262,133–177.
13. (a) Fujita, M. *Acc. Chem. Res.*, **1999**, 32, 53–61; (b) Frampton, M. J.; Anderson, H. L. *Angew. Chem., Int. Ed.*, **2007**, 46, 1028–1064.
14. Mullen, K. M.; Beer, P. D. *Chem. Soc. Rev.*, **2009**, 38, 1701–1713.
15. Albrecht, M. *Top. Curr. Chem.*, **2004**, 248, 105–139.
16. Dietrich-Buchecker, C. O.; Sauvage, J.-P.; Kintzinger, J.-P. *Tetrahedron Lett.*, **1983**, 24,5095–5098.
17. (a) Dietrich-Buchecker, C. O.; Sauvage, J.-P. *Angew. Chem., Int. Ed. Engl.*, **1989**, 28, 189–192; (b) Rapenne, G.; Dietrich-Buchecker, C.; Sauvage, J.-P. *J. Am. Chem. Soc.*, **1996**, 118, 10932–10933; (c) Meyer, M.; Albrecht-Gary, A.-M.; Dietrich-Buchecker, C. O.; Sauvage, J.-P. *J. Am. Chem. Soc.*, **1997**, 119, 4599–4607
18. Nierengarten, J. F.; Dietrich-Buchecker, C. O.; Sauvage, J. P. *J. Am. Chem. Soc.*, **1994**, 116, 375–376.
19. (a) Rapenne, G.; Dietrich-Buchecker, C.; Sauvage, J.-P. *J. Am. Chem. Soc.*, **1999**, 121,994–1001; (b) Adams, H.; Ashworth, E.; Breault, G. A.; Guo, J.; Hunter, C. A.; Mayers, P. C. *Nature*, **2001**, 411, 763–763; (c) Guo, J.; Mayers, P. C.; Breault, G. A.; Hunter, C. A. *Nature Chem.*, **2010**, 2, 218–222; (d) Barran, P. E.; Cole, H. L.; Goldup, S. M.; Leigh, D. A.; McGonigal, P. R.; Symes, M. D.; Wu, J.; Zengerle, M. *Angew. Chem., Int. Ed.*, **2011**, 50, 12280–12284.
20. (a) Safarowsky, O.; Nieger, M.; Fröhlich, R.; Vögtle, F. *Angew. Chem., Int. Ed.*, **2000**, 39,1616–1618; (b) Vögtle, F.; Hunten, A.; Vogel, E.; Buschbeck, S.; Safarowsky, O.; Recker, J.; Parham, A.-H.; Knott, M.; Müller, W. M.; Müller, U.; Okamoto, Y.; Kubota, T.; Lindner, W.; Francotte, E.; Grimme, S. *Angew. Chem., Int. Ed.*, **2001**, 40, 2468–2471; (c) Lukin, O.; Kubota, T.; Okamoto, Y.; Kaufmann, A.; Vögtle, F. *Chem.—Eur. J.*, **2004**, 10, 2804–2810; (d) Lukin, O.; Vögtle, F. *Angew. Chem., Int. Ed.*, **2005**, 44, 1456–1477; (e) Feigel, M.; Ladberg, R.; Engels; Herbst-Irmer, R.; Fröhlich, R. *Angew. Chem., Int. Ed.*, **2006**, 45,5698–5702; (f) Passaniti, P.; Ceroni, P.; Balzani, V.; Lukin, O.; Yoneva, A.; Vögtle, F. *Chem.—Eur. J.*, **2006**, 12, 5685–5690; (g) Brüggemann, J.; Bitter, S.; Müller, S.; Müller, W. M.; Müller, U.; Maier, N. M.; Lindner, W.; Vögtle, F. *Angew. Chem., Int. Ed.*, **2007**, 46, 254–259.

21. Ashton, P. R.; Matthews, O. A.; Menzer, S.; Raymo, F. M.; Spencer, N.; Stoddart, J. F.; Williams, D. J. *Liebigs Ann./Recl.*, **1997**, 2485– 2494.
22. (a) Ayme, J.-A.; Beves, J. E.; Leigh, D. A.; McBurney, R. T.; Rissanen, K.; Schultz, D. *Nature Chem.*, **2012**, *4*, 15– 20; (b) Hardie, M. J. *Nature Chem.*, **2012**, *4*, 7– 8
23. Dietrich-Buchecker, C.; Colasson, B.; Jouvenot, D.; Sauvage, J.-P. *Chem.—Eur. J.*, **2005**, *11*, 4374– 4386.
24. (a) Hasenknopf, B.; Lehn, J.-M.; Kneisel, B. O.; Baum, G.; Fenske, D. *Angew. Chem., Int. Ed. Engl.*, **1996**, *35*, 1838– 1840; (b) Hasenknopf, B.; Lehn, J.-M.; Boumediene, N.; Dupont-Gervais, A.; Van Dorsselaer, A.; Kneisel, B.; Fenske, D. *J. Am. Chem. Soc.*, **1997**, *119*, 10956– 10962; (c) Provent, C.; Hewage, S.; Brand, G.; Bernardinelli, G.; Charbonnière, L. J.; Williams, A. F. *Angew. Chem., Int. Ed. Engl.*, **1997**, *36*, 1287– 1289; (d) Hasenknopf, B.; Lehn, J.-M.; Boumediene, N.; Leize, E.; Van Dorsselaer, A. *Angew. Chem., Int. Ed.*, **1998**, *37*, 3265– 3268; (e) Provent, C.; Rivara-Minten, E.; Hewage, S.; Brunner, G.; Williams, A. F. *Chem.—Eur. J.*, **1999**, *5*, 3487–3494; (f) Childs, L. J.; Alcock, N. W.; Hannon, M. J. *Angew. Chem., Int. Ed.*, **2002**, *41*, 4244– 4247; (g) Tuna, F.; Hamblin, J.; Jackson, A.; Clarkson, G.; Alcock, N. W.; Hannon, M. J. *Dalton Trans.*, **2003**, 2141– 2148; (h) Childs, L. J.; Pascu, M.; Clarke, A. J.; Alcock, N. W.; Hannon, M. J. *Chem.—Eur. J.*, **2004**, *10*, 4291– 4300; (i) Senegas, J.-M.; Koeller, S.; Bernardinelli, G.; Piguët, C. *Chem. Commun.*, **2005**, 2235– 2237; (j) Hamblin, J.; Tuna, F.; Bunce, S.; Childs, L. J.; Jackson, A.; Errington, W.; Alcock, N. W.; Nierengarten, H.; Van Dorsselaer, A.; Leize-Wagner, E.; Hannon, M. J. *Chem.—Eur. J.*, **2007**, *13*, 9286– 9296; (k) Pang, Y.; Cui, S.; Li, B.; Zhang, J.; Wang, Y.; Zhang, H. *Inorg. Chem.*, **2008**, *47*, 10317– 10324; (l) Allen, K. E.; Faulkner, R. A.; Harding, L. P.; Rice, C. R.; Riis-Johannessen, T.; Voss, M. L.; Whitehead, M. *Angew. Chem., Int. Ed.*, **2010**, *49*, 6655–6658; (m) Bain, L.; Bullock, S.; Harding, L.; Riis-Johannessen, T.; Midgley, G.; Rice, Craig, R.; Whitehead, M. *Chem. Commun.*, **2010**, *46*, 3496– 3498; (n) Tanh Jeazet, H. B.; Gloe, K.; Doert, T.; Kataeva, O. N.; Jäger, A.; Geipel, G.; Bernhard, G.; Büchner, B.; Gloe, K. *Chem. Commun.*, **2010**, *46*, 2373– 2375; (o) Giles, I. D.; Chifotides, H. T.; Shatruk, M.; Dunbar, K. R. *Chem. Commun.*, **2011**, *47*, 12604– 12606.

25. (a) Corbett, P. T.; Leclaire, J.; Vial, L.; West, K. R.; Wietor, J.-L.; Sanders, J. K. M.; Otto, S. *Chem. Rev.*, **2006**, *106*, 3652– 3711; (b) Lehn, J.-M. *Chem. Soc. Rev.*, **2007**, *36*, 151– 160.
26. (a) Leigh, D. A.; Lusby, P. J.; Teat, S. J.; Wilson, A. J.; Wong, J. K. Y. *Angew. Chem., Int. Ed.*, **2001**, *40*, 1538– 1543; (b) Price, J. R.; Clegg, J. K.; Fenton, R. R.; Lindoy, L. F.; McMurtrie, J. C.; Meehan, G. V.; Parkin, A.; Perkins, D.; Turner, P. *Aust. J. Chem.*, **2009**, *62*, 1014– 1019.
27. Hogg, L.; Leigh, D. A.; Lusby, P. J.; Morelli, A.; Parsons, S.; Wong, J. K. Y. *Angew. Chem., Int. Ed.*, **2004**, *43*, 1218– 1221.
28. Hutin, M.; Frantz, R.; Nitschke, J. R. *Chem.—Eur. J.*, **2006**, *12*, 4077– 4082.
29. Pentecost, C. D.; Chichak, K. S.; Peters, A. J.; Cave, G. W. V.; Cantrill, S. J.; Stoddart, J. F. *Angew. Chem., Int. Ed.*, **2007**, *46*, 218– 222.
30. Chichak, K. S.; Cantrill, S. J.; Pease, A. R.; Chiu, S.-H.; Cave, G. W. V.; Atwood, J. L.; Stoddart, J. F. *Science*, **2004**, *304*, 1308– 1312.
31. Twigg, M. V.; Burgess, J. In *Comprehensive Coordination Chemistry II*; McCleverty, J. A.; Meyer, T. J., Eds.; Elsevier: Amsterdam, **2004**; Vol. 5, pp 403– 553.
32. Bu_4NBF_4 was also added to maintain a constant Bu_4N^+ concentration.
33. Thompson, M. C.; Busch, D. H. *J. Am. Chem. Soc.*, **1964**, *86*, 213– 217.
34. Chloride ions have been previously shown to catalyze the rate of ligand exchange of $[\text{Fe}(\text{phen})_3]^{2+}$ complexes in DMSO, see Farrinton, D. J.; Jones, J. O.; Twigg, M. V. *Inorg. Chim. Acta*, **1977**, *25*, L75– L76.
35. This is likely primarily a solubility issue: in order for the kinetic distribution of oligomers which are initially formed to rearrange into the thermodynamically preferred product, these must all remain in solution at all times. Dodecylamine (which is not soluble in DMSO) affords the circular helicate increased solubility in chloroform (by comparison with circular helicates $[\mathbf{3a-3g}]^{10+}$) and allows the rearrangement process to proceed readily.
36. The isolated pentameric circular helicates were found to be stable in MeCN at 60 °C for several weeks, with no evidence for decomposition. However, the addition of a monoamine to isolated samples of the circular helicates resulted only in the decomposition of the helicate, with little evidence for amine exchange. Attempts were made to reduce the imine groups of the molecular pentafoil knot

[7Cl](PF₆)₉ using standard procedures (NaBH₄), but these resulted in decomplexation, and no organic knot could be isolated from the reaction mixture.

37. Crystal data for [3bCl](PF₆)₉·xsolvent: purple blocks, 0.11 mm × 0.15 mm × 0.32 mm, $M = 5358.62$, C₂₄₀H₂₃₄ClF₄₅N₃₇O₂₀P_{7.5}Fe₅, monoclinic, space group $P2_1/c$, $a = 34.023(2)$ Å, $b = 23.714(2)$ Å, $c = 36.537(2)$ Å, $\beta = 94.386(2)^\circ$, $V = 29393(4)$ Å³, $Z = 4$, $D_c = 1.211$ g/cm³, 3211 parameters, 151 restraints, $R = 0.1388$ [$I_o > 2\sigma(I_o)$], $wR = 0.3829$ (all reflections).
38. (a) Zarges, W.; Hall, J.; Lehn, J. M.; Bolm, C. *Helv. Chim. Acta*, **1991**, *74*, 1843–1852; (b) Constable, E. C.; Kulke, T.; Baum, G.; Fenske, D. *Chem. Commun.*, **1997**, 2043–2044; (c) Constable, E. C.; Kulke, T.; Baum, G.; Fenske, D. *Inorg. Chem. Commun.*, **1998**, *1*, 80–82; (d) Mamula, O.; von Zelewsky, A.; Bernardinelli, G. *Angew. Chem., Int. Ed.*, **1998**, *37*, 290–293; (e) Baum, G.; Constable, E. C.; Fenske, D.; Housecroft, C. E.; Kulke, T. *Chem.—Eur. J.*, **1999**, *5*, 1862–1873; (f) Lutzen, A.; Hapke, M.; Griep-Raming, J.; Haase, D.; Saak, W. *Angew. Chem., Int. Ed.*, **2002**, *41*, 2086–2089; (g) Orita, A.; Nakano, T.; An, D. L.; Tanikawa, K.; Wakamatsu, K.; Otera, J. *J. Am. Chem. Soc.*, **2004**, *126*, 10389–10396; (h) Wood, T. E.; Dalgleish, N. D.; Power, E. D.; Thompson, A.; Chen, X.; Okamoto, Y. *J. Am. Chem. Soc.*, **2005**, *127*, 5740–5741; (i) Kreckmann, T.; Diedrich, C.; Pape, T.; Huynh, H. V.; Grimme, S.; Hahn, F. E. *J. Am. Chem. Soc.*, **2006**, *128*, 11808–11819; (j) Bunzen, J.; Bruhn, T.; Bringmann, G.; Lützen, A. *J. Am. Chem. Soc.*, **2009**, *131*, 3621–3630; (k) Stomeo, F.; Lincheneau, C.; Leonard, J. P.; O’Brien, J. E.; Peacock, R. D.; McCoy, C. P.; Gunnlaugsson, T. *J. Am. Chem. Soc.*, **2009**, *131*, 9636–9637; (l) Amendola, V.; Boiocchi, M.; Brega, V.; Fabbrizzi, L.; Mosca, L. *Inorg. Chem.*, **2010**, *49*, 997–1007; (m) Howson, S. E.; Bolhuis, A.; Brabec, V.; Clarkson, G. J.; Malina, J.; Rodger, A.; Scott, P. *Nature Chem.*, **2012**, *4*, 31–36.
39. This is typical for Fe(diimine)₃ complexes. It is known that the isomeric forms of these complexes have practically identical absorption spectra [Krumholz, P. *Inorg. Chem.*, **1965**, 609], and that the energy of the MLCT is strongly influenced by the number of coordinated aromatic rings [(b) Busch, D. H.; Bailar, J. C., Jr. *J. Am. Chem. Soc.*, **1956**, *78*, 1137–1142]. For example, MLCT in water: Fe(Me-N=CH–CH=N–Me)₃ 568 nm, (39b) [Fe(py-CH=NH–CH₃)₃]₂ 551 nm, (39b) and [Fe(py-CH=NH–

$\text{CH}_3)_3](\text{ClO}_4)_2$ 551 nm.(39a) As the number of coordinated aromatic rings increases, the energy of the MLCT increases, with $[\text{Fe}(\text{bpy})_3]^{2+}$ and $[\text{Fe}(\text{phen})_3]^{2+}$ exhibiting λ_{max} at 490 and 510 nm, respectively. Combined, these data surprisingly suggest that the the ligands in the present helicates behave less like aromatic ligands such as bipyridine and more like nonaromatic diimines.

40. (a) Mürner, H.; von Zelewsky, A.; Hopfgartner, G. *Inorg. Chim. Acta*, **1998**, *271*, 36–39; (b) Kiehne, U.; Lützen, A. *Org. Lett.*, **2007**, *9*, 5333–5336; (c) Howson, S. E.; Allan, L. E. N.; Chmel, N. P.; Clarkson, G. J.; van Gorkum, R.; Scott, P. *Chem. Commun.*, **2009**, 1727–1729.
41. (a) Bosnich, B. *Acc. Chem. Res.*, **1969**, *2*, 266–273; (b) Mason, S. F. *Pure Appl. Chem.*, **1970**, *24*, 335–359; (c) Ziegler, M.; von Zelewsky, A. *Coord. Chem. Rev.*, **1998**, *177*, 257–300.
42. This is in agreement with both previous simple pyridyl–imine complexes(40c) and a triple-stranded dinuclear Fe(II)-containing helicate.
 (a) Mürner, H.; von Zelewsky, A.; Hopfgartner, G. *Inorg. Chim. Acta* **1998**, *271*, 36–39
 Additionally, the CD band for the MLCT transition of (S)-[3jCl](PF₆)₉ also corresponds to that of Λ -[Fe(bpy)₃]: (b) Mason, S. F.; Peart, B. J. *J. Chem. Soc., Dalton Trans.*, **1973**, 949–955 (ref 41c) and Λ -[Ru(phen)₃] (ref 41a)
43. Wolfe, S. *Acc. Chem. Res.*, **1972**, *5*, 102–111.
44. We reasoned that a more rigid and preorganized diamine based on the same glycol linker, but with an aromatic ring at the center in place of an ethyl spacer, may generate the corresponding pentafoil knot in higher yield. However, we found that diamine 2,2'-(1,2-bisoxypyphenylene)diethanamine gave exclusively polymeric material, with no evidence for pentamer formation.
45. (a) Bosnich, B. *Acc. Chem. Res.* 1969, *2*, 266–273; (b) Mason, S. F. *Pure Appl. Chem.* **1970**, *24*, 335–359; (c) Ziegler, M.; von Zelewsky, A. *Coord. Chem. Rev.* **1998**, *177*, 257–300.
46. (a) Mürner, H.; von Zelewsky, A.; Hopfgartner, G. *Inorg. Chim. Acta* **1998**, *271*, 36–39; (b) Kiehne, U.; Luetzen, A. *Org. Lett.* **2007**, *9*, 5333–5336.
47. Howson, S. E.; Allan, L. E. N.; Chmel, N. P.; Clarkson, G. J.; van Gorkum, R.; Scott, P. *Chem. Commun.* **2009**, 1727–1729.
48. Mason, S. F.; Peart, B. J. *J. Chem. Soc., Dalton Trans.* **1973**, 949–955.

49. 2.0 r5 program suite ed.; Rigaku Corporation: Japan, **2010**.
50. Palatinus, L.; Chapuis, G. J. *Appl. Crystallogr.* **2007**, *40*, 786-790.
51. Farrugia, L. J. *J. Appl. Crystallogr.* **1999**, *32*, 837-838.
52. Sheldrick, G. M. *Acta Crystallogr., Sect. A* **2008**, *A64*, 112-122.
53. PLATON, A Multipurpose Crystallographic Tool (Utrecht University, Utrecht, The Netherlands, **2008**).

Chapter IV: "The Self-Sorting Behavior of Circular Helicates and Molecular Knots and Links"

Published as "The self-sorting behavior of circular helicates and molecular knots and links", J.-F. Ayme, J. E. Beves, C. J. Campbell and D. A. Leigh, *Angew. Chem. Int. Ed.*, **2014**, *53*, 7823–7827.

Acknowledgements

Dr. J. E. Beves and Dr. C. J. Campbell are gratefully acknowledged for their contribution to this chapter: C.J.C. synthesised dialdehyde **1** and performed the self-sorting experiments with J.E.B., dialdehyde **2** was synthesized by J.F.A. and J.E.B. The results of the self-sorting experiments were analysed in a joint effort between the authors.

4.1. Synopsis

Self-sorting refers to the ability of a system to spontaneously segregate molecular building blocks within a mixture into discrete species. This chapter reports the study of the self-sorting behaviour of a molecular Solomon link and a molecular pentafoil knot and their related non-interlocked systems. Despite differing in length and structure by only two oxygen atoms, two dialdehyde ligand strands self-sort to form open circular helicates of different sizes when they were put in presence of a primary monoamine and iron(II) chloride ions. The corresponding closed circular helicates that are formed from a diamine—a molecular Solomon link and a pentafoil knot—also self-sort, but up to two of the Solomon-link-forming ligand strands can be accommodated within the pentafoil knot structure and are either incorporated or omitted depending on the stage that the components are mixed.

4.2. Introduction

The spontaneous segregation of molecular building blocks into discrete species within a mixture is known as self-sorting,¹ a phenomenon that helps to maintain structural control over complex dynamic systems in nature.² The use of orthogonal recognition elements is a convenient way to achieve sorting in artificial systems,^{1,3} but other methods,⁴ including subtle differences in ligand design,⁵⁻⁷ can also be remarkably effective. A beautiful example is the classic experiment by Lehn and co-workers⁵ in which a mixture of ligand strands containing two to five 2,2'-bipyridine groups spontaneously self-sort into linear double helicates, each containing two ligands with equal numbers of binding sites, in the presence of Cu^I ions.

We recently described the synthesis of a molecular Solomon link⁸ (a doubly entwined [2]catenane⁹) and a molecular pentafoil knot,¹⁰ each formed through a combination of metal–ligand coordination, an anion template, and geometric restrictions. These closely related structures are derived from tetra-⁸ and pentameric¹⁰ circular helicate scaffolds, respectively, and are assembled from up to 20 common, or similar, components. Here we investigate the self-sorting behavior of both the closed molecular topologies and the open circular helicate scaffolds on which they are based (Figure 1). The study provides insights into the self-assembly processes of the individual species and reveals a subtle interplay between the driving forces and kinetic traps involved in their assembly.

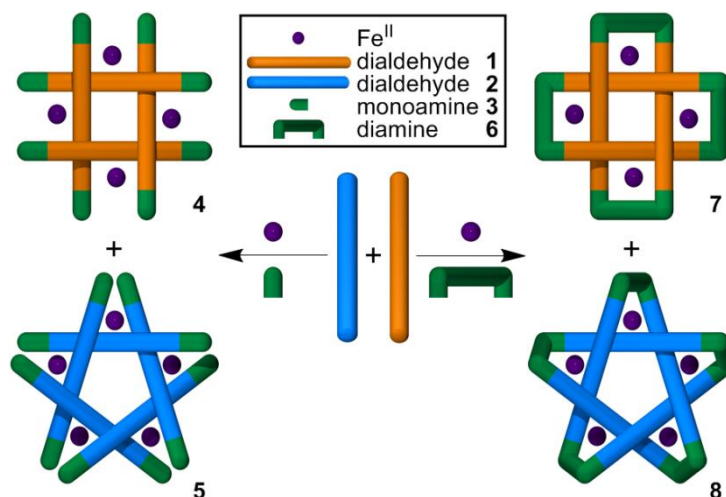
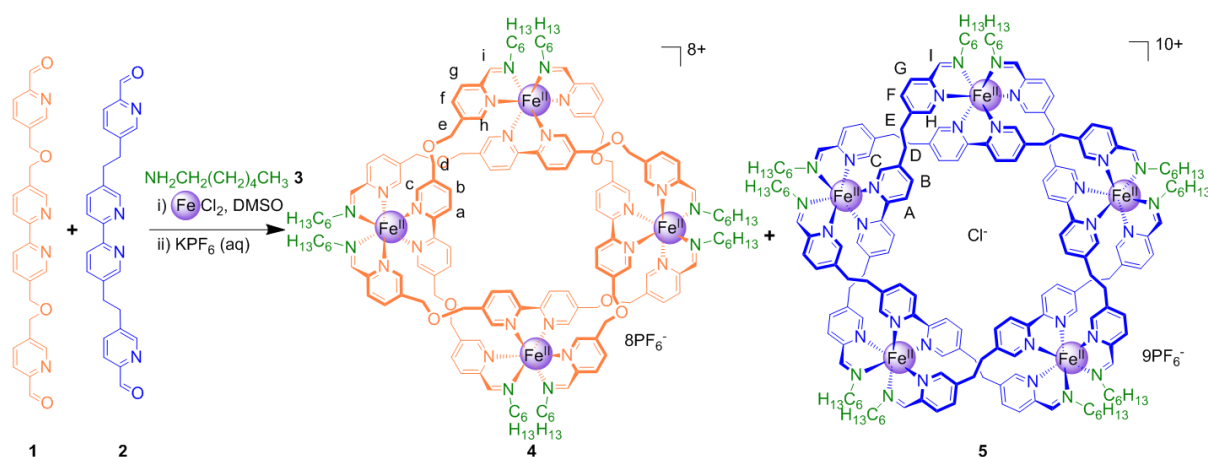


Figure 1. The assembly of circular helicates of different sizes and topologies from a primary amine (**3**) or diamine (**6**), Fe^{II} ions, and dialdehyde ligand strands (**1** and **2**).

4.3. Results and Discussion

Despite their structural similarities (a difference of just two oxygen atoms in length), dialdehydes **1** and **2** react individually with a suitable monoamine and FeCl_2 to generate different-sized circular helicates: tetrameric⁸ with **1** and pentameric¹⁰ with **2**. To investigate the self-sorting potential of the ligands, a 1:1 mixture of aldehydes **1** and **2** was allowed to react with FeCl_2 and *n*-hexylamine (**3**) in $[\text{D}_6]\text{DMSO}$ at 60°C for 18 h, followed by anion exchange through the addition of an aqueous solution of potassium hexafluorophosphate (Scheme 1). ^1H NMR spectroscopy (Figure 2 a, i) indicated the formation of both tetramer **4** and pentamer **5**, the spectrum of the reaction outcome being a superimposition of the spectra from the reaction of the individual aldehydes under similar experimental conditions (Figure 2 a, ii and iii). Electrospray mass spectrometry (ESIMS) confirmed perfect self-sorting, with no detectable formation of mixed-ligand species (Figure 2 b). Such fidelity is remarkable for such complex multicomponent systems made up from building blocks that vary only by a one-atom difference in the spacing of identical binding sites. The dynamics of

this self-sorting system were further probed through experiments in which dialdehydes **1** and **2** were mixed at different points during the course of the reaction and monitored for up to four days at different concentrations (see the Experimental Section), which established that under these conditions the open circular helicates self-assemble and self-sort under thermodynamic control (see Section 4.5.1.4. in the Experimental Section for details).



Scheme 1. Perfect self-sorting of remarkably similar ligand strands in the formation of circular helicates of different sizes. A 1:1 ratio of aldehydes **1** and **2** was treated with two equivalents of FeCl_2 and four equivalents of n -hexylamine (**3**) in $[\text{D}_6]\text{DMSO}$ at 60°C for 18 h, followed by anion exchange with aqueous KPF_6 , thereby generating a mixture of circular helicates **4** and **5**.

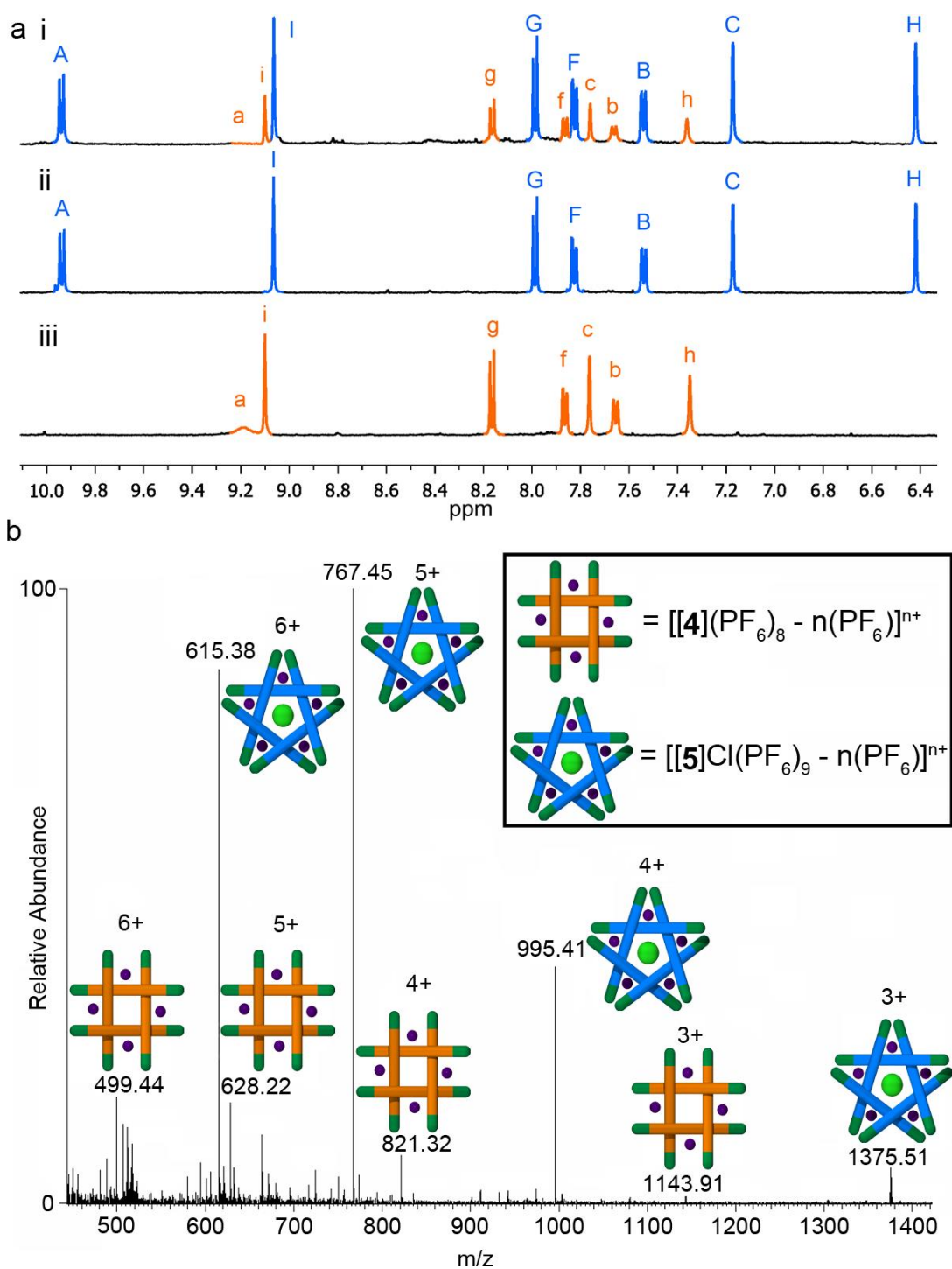


Figure 2. Spectroscopic analysis of the self-sorting reaction shown in Scheme 1. a) 1H NMR spectra (500 MHz, CD_3CN , 298 K). i) The self-sorted mixture of open cyclic helicates **4** (orange) and **5** (blue), ii) pentameric cyclic helicate **5**, and iii) tetrameric cyclic helicate **4**. The broadness of the H^a signal is a function of chloride ion concentration.⁸ b) ESI mass spectrum of the self-sorted species shown in Scheme 1. Signals corresponding to helicates **4** and **5** with sequential loss of PF_6 counterions are indicated.

The reaction of either aldehyde **1** or **2** with diamine **6** in the presence of Fe^{II} ions generates topological complex molecules:¹¹ a Solomon link (four crossings arising from the tetrameric circular helicate scaffold)⁸ and pentafoil knot (five crossings arising from the pentameric circular helicate scaffold),¹⁰ respectively. However, the behavior of these closed circular helicate systems upon mixing was found to differ from that of the open analogues. The self-sorting experiment was conducted as previously, but with *n*-hexylamine substituted for 0.5 equiv of 2,2'-(ethylenedioxy)bis(ethylamine) (**6**) and the reaction times increased to four days (Scheme 2). After work up, the ¹H NMR spectrum (Figure 3 a) showed two sets of signals corresponding to the formation of Solomon link **7** and pentafoil knot **8** accompanied by a series of low-intensity signals (shown in red in Figure 3 a). ESIMS analysis confirmed that the Solomon link is assembled almost exclusively from ligand **1**.¹² However, in addition to pentafoil knot **8** (formed from five strands of ligand **2**), significant amounts of two other pentafoil knots, **9** and **10**, were present which arise from the incorporation of one or two strands of **1** into the pentafoil knot structure (see Figure 13 in the Experimental Section). The mixed-ligand-strand species pentafoil knot **9**, in which one strand of ligand **2** had been replaced with **1**, could be fully characterized by COSY and ROESY correlation experiments (see Figure 16–18 in the Experimental Section) and is the main contributor to the low-intensity signals shown in red in Figure 3 a.¹³ Interestingly, the yield of Solomon link **7** in Scheme 2 remained unchanged relative to reactions in which only **2** was used (see Figure 19 in the Experimental Section), thus indicating that the mixed pentafoil knot species **9** and **10** arise principally at the expense of polymeric/oligomeric by-products rather than at the expense of the homoligand-strand pentafoil knot **8**. The product distribution was maintained over a range of concentrations (2–6 mM), with the relative yields of **7**, **8**, **9**, and **10** remaining constant throughout (see Figure 20–22 in the Experimental Section).

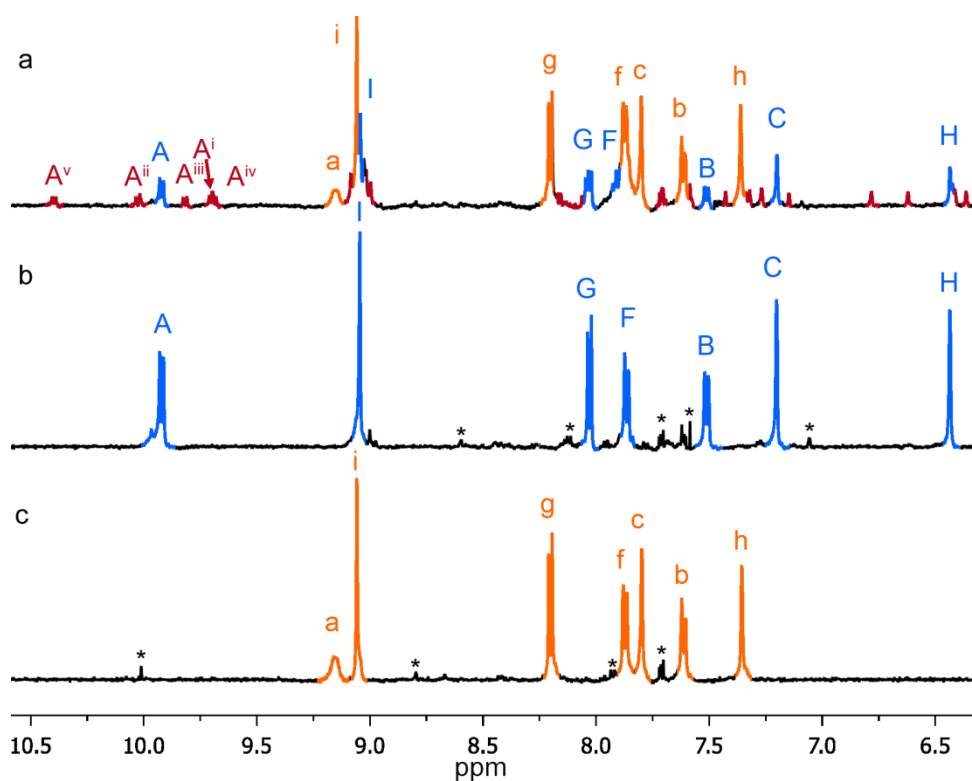
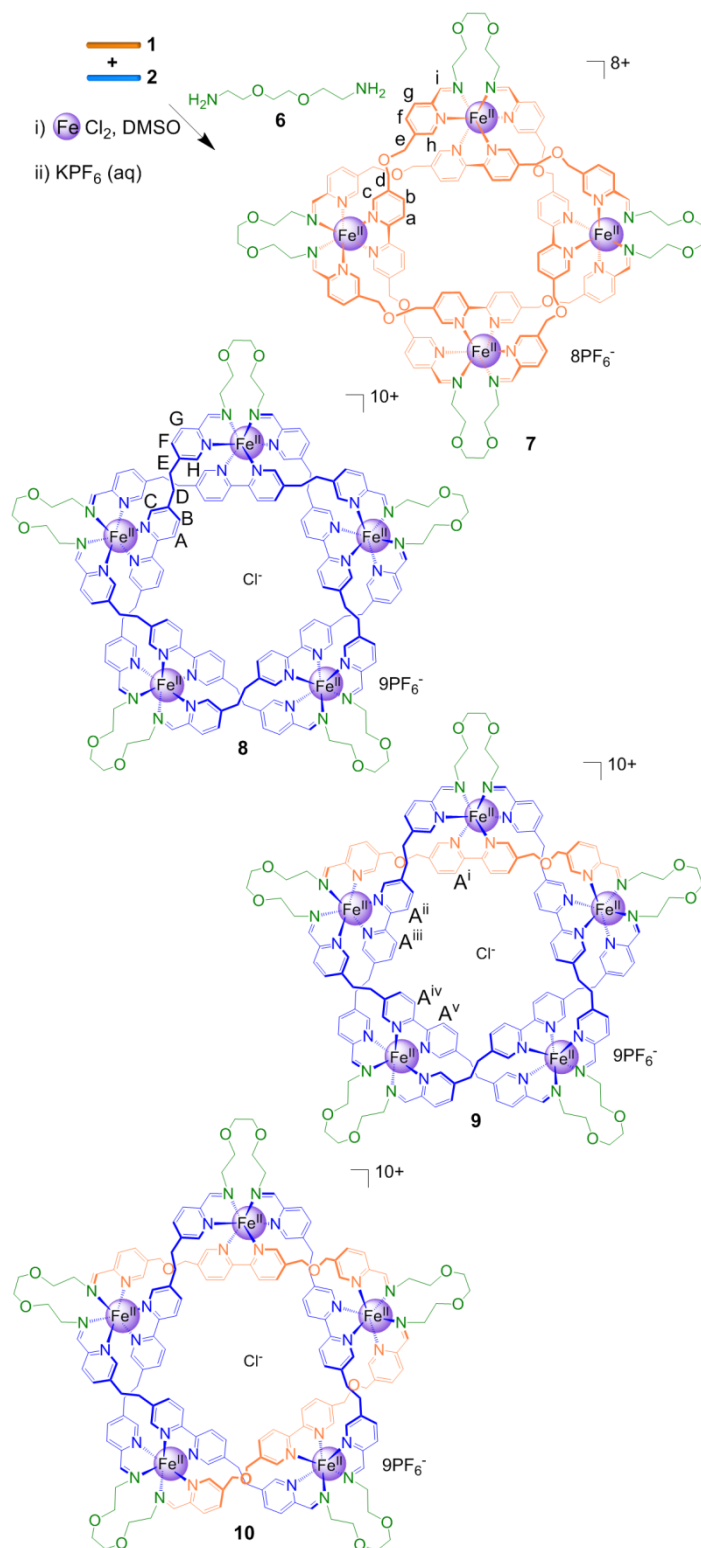


Figure 3. ¹H NMR spectra (500 MHz, CD₃CN, 298 K). a) The mixture of Solomon link **7** (orange), pentafoil knot **8** (blue), mixed pentafoil knots **9** (red), and **10** (too small an amount to be visible by ¹H NMR spectroscopy but observed using ESIMS; see Figure 14 in the Experimental Section) obtained by reaction of diamine **6** with dialdehydes **1** and **2**. Products formed using only one dialdehyde: b) pentafoil knot **8** (from **2**) and c) Solomon link **7** (from **1**) prior to purification. The * marks small signals corresponding to aldehyde-containing ligand strands (products of imine hydrolysis) in (b) and (c).



Scheme 2. The assembly of knots and links using diamine **6**. A 1:1 ratio of dialdehydes **1** and **2** was treated with two equivalents of FeCl_2 and two equivalents of diamine **6** in $[\text{D}_6]\text{DMSO}$ at 60°C for four days, followed by anion exchange with aqueous KPF_6 , to give Solomon link **7** and a mixture of pentafoil knots **8–10**. Only one of the two isomers of **10** is shown (see Figure 4).

To probe whether the distribution observed under the conditions employed in Scheme 2 is formed under thermodynamic control, two experiments were carried out that differed only in the time at which the dialdehydes were mixed (Figure 4). In the first experiment, dialdehydes **1** and **2** were mixed prior to the addition of amine **6** (Figure 4 a). In the second experiment, aldehydes **1** and **2** were allowed to react individually with diamine **6** (FeCl_2 , $[\text{D}_6]\text{DMSO}$, 60°C) for 24 h prior to combining both reactions (Figure 4 b). The resulting mixtures were heated at 60°C and the change in the product distribution monitored over seven days. If compounds **7–10** are under thermodynamic control, then both experimental procedures should equilibrate to the same distribution (as is observed with the monoamine-derived circular helicates (Scheme 1) and see Section 4.5.1.4. in the Experimental Section). However, the outcomes of the two experiments involving the diamine are very different (Figure 5). When the dialdehydes are combined from the start, the mixed-ligand-strand pentafoil knots **9** and **10** are formed (in addition to **7** and **8**) as expected (Figure 5 a). In contrast, when the aldehydes are allowed to react individually with diamine **6** and FeCl_2 for 24 h and then the reaction mixtures (which include not only some of the closed cyclic helicates, but also oligomers and polymeric by-products) are heated further, there is no evidence of mixed-ligand species even after seven days (Figure 5 b).

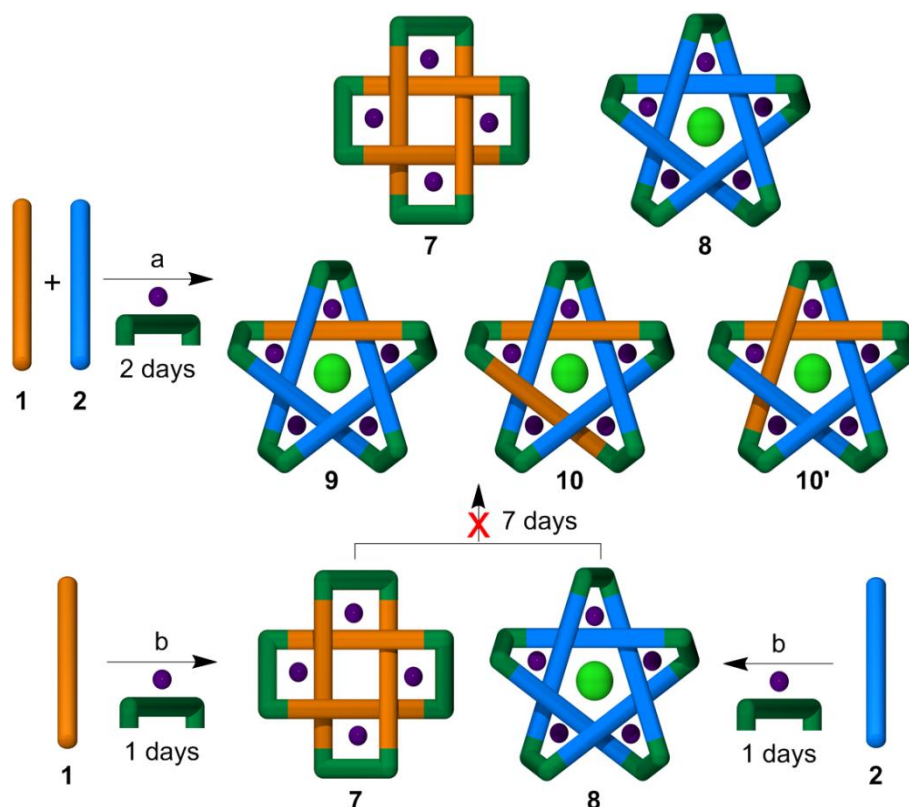


Figure 4. Assembly of molecular Solomon link **7** and pentafoil knots **8–10** using different experimental procedures. The product distribution of the closed topologies is dependent on when the reaction mixtures are combined.

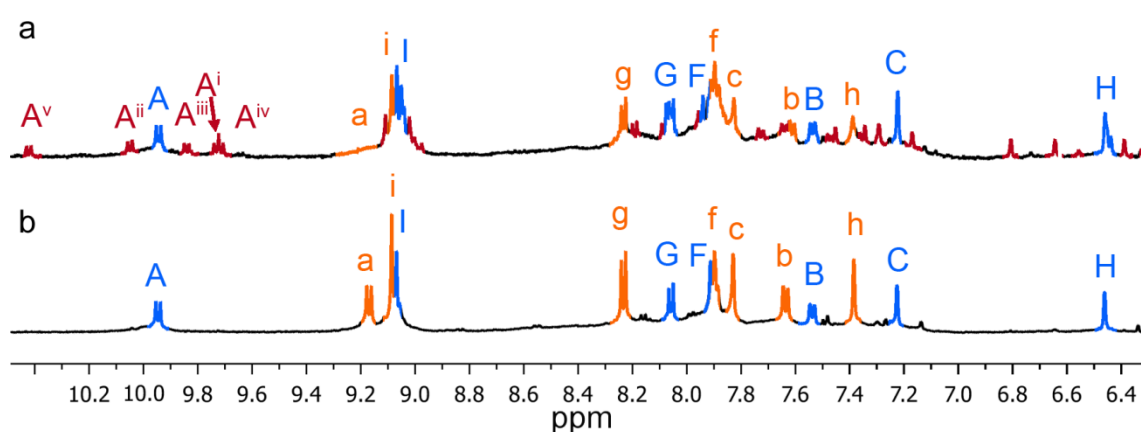


Figure 5. ^1H NMR spectra (500 MHz, CD_3CN , 298 K). a) Reaction mixture from Figure 4 a (after PF_6^- ion exchange), where aldehydes **1** and **2** are mixed prior to the addition of diamine **6**, showing significant amounts of mixed-ligand pentafoil knot **9** (red). b) Reaction mixture from Figure 4 b (after PF_6^- ion exchange), where preformed **7** (orange) and **8** (blue) were mixed, shows no indication of the presence of mixed-ligand pentafoil knots.

Clearly, under these conditions (60 °C, 7 days) this system is not under thermodynamic control. The mixed-ligand-strand pentafoil knots **9** and **10** are kinetic products, similar in accessibility to **8**. The rationale for the differing behavior of the open helicates and the closed molecular topologies is the relative ease of dissociation of the different types of ligands. In the open systems (**4** and **5**), the exchange of ligand units involves only metal–ligand dissociation of a single tris(bidentate) strand, which is sufficiently rapid for equilibrium to be reached under the reaction conditions. However, unless ligand exchange occurs by hydrolysis, then for a tris(bidentate) strand to be replaced in the closed systems the two neighboring strands also have to dissociate from iron centers for imine exchange of the diamine linker to occur. The energy cost of this additional process is evidently too high to allow efficient rearrangement of **9** and **10**, thereby preventing the closed systems from undergoing full “error-checking” under thermodynamic control.¹⁶

4.4. Conclusion

In conclusion, the reaction of **1** and **2** with *n*-hexylamine (**3**) leads to a perfectly self-sorted and dynamic mixture of open circular helicates of different sizes, **4** and **5**. Although this involves formation of imine bonds, it is effectively a cyclic version of the self-sorting experiment with linear helicates pioneered by Lehn and co-workers,⁵ but instead of using ligand strands that sort according to the number of bidentate binding sites and overall length, **1** and **2** have the same number of binding sites and differ only by a one atom spacing of those binding sites within the strand.^{14,15} Nonetheless, each ligand is able to effectively distinguish self from non-self in forming different-sized circular assemblies and the components are able to exchange in-and-out of the circular helicates in a facile manner. Dialdehydes **1** and **2** also largely self-sort according to the size of the circular helicate in their

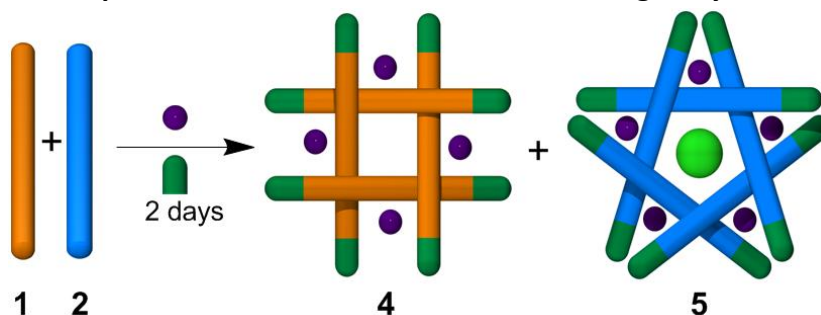
reaction with diamine **6**, thereby generating Solomon link **7** and pentafoil knot **8**, respectively. In this case, however, the self-sorting is imperfect and mixed-ligand-strand pentafoil knots **9** and **10** are also formed. The fully closed circular helicates do not readily exchange their ligand strands even over extended reaction times.

These systems illustrate not only the exquisite fidelity that is possible in the self-sorting of very similar building blocks within complex multicomponent assemblies, but also how the same modest differences in structure can tip the balance between thermodynamic control and kinetic trapping. Learning how to recognize, understand, and, ultimately, manipulate such processes will be an important step towards mimicking nature's mastery of molecular assembly with synthetic systems.

4.5. Experimental section

4.5.1. Open Systems

4.5.1.1. Experimental Procedure for the Self-Sorting of Cyclic Helicates **4** and **5**

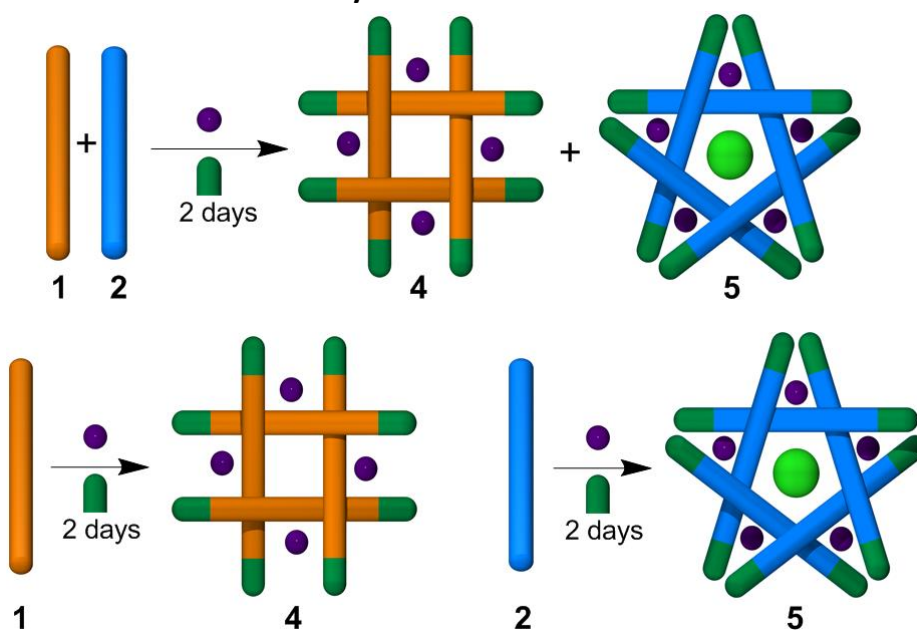


Scheme 3. Mixing experiments conducted with aldehyde **1** (orange) and aldehyde **2** (blue) with iron(II) (purple) and hexylamine (green) to form tetramer **4** and pentamer **5**.

To two separate DMSO- d_6 solutions of **1** (1.1 mg, 2.4 μmol , in 0.5 mL) and **2** (1.0 mg, 2.4 μmol in 0.5 mL) was added FeCl₂ (25 μL of a 0.10 M stock solution, 2.6 μmol). The two

purple solutions were mixed thoroughly to ensure complete dissolution of both aldehydes. The solutions were combined together in a clean NMR tube before addition of hexylamine (50 μL of a 0.21 M stock solution, 5.2 μmol). The resulting mixture was heated for 2d at 60 $^{\circ}\text{C}$ before being allowed to cool. The reaction mixture was precipitated using KPF_6 (saturated aqueous solution). The resulting purple powder was collected on celite and washed with water, a small amount of EtOH (**4** is soluble) and finally Et₂O. The product mixture was dissolved in CH₃CN and the solvent removed in vacuo to give a mixture of **4** and **5** as a purple powder. The mixture was fully soluble in CH₃CN and could be analyzed by ¹H NMR and LR-ESI (Figure 1). All results were consistent with previous reports for **4**⁸ and **5**¹⁰.

4.5.1.2. Experimental Procedure to Determine the Effects of Mixing on the Relative Yields of Cyclic Helicates **4** and **5**



Scheme 4. Self-sorting experiments conducted to determine the effect of mixing on the relative yields of **4** and **5**. Reactions were carried out using stock solutions of aldehydes **1** and **2** under identical conditions.

To two separate DMSO-*d*₆ solutions of **1** (2.1 mg, 4.7 μmol , in 1.0 mL) and **2** (2.0 mg, 4.7 μmol in 1.0 mL) was added FeCl₂ (50 μL of a 0.10 M stock solution, 5.2 μmol). The two

purple solutions were mixed thoroughly to ensure complete dissolution of both aldehydes. A 0.5 mL aliquot of **1**+FeCl₂ was mixed with a 0.5 mL aliquot of **2**+FeCl₂ in a clean NMR tube before addition of hexylamine (50 μL of a 0.208 M stock solution, 5.2 μmol). The remaining 0.5 mL aliquots of **1**+FeCl₂ and **2**+FeCl₂ were separately reacted with hexylamine (25 μL of a 0.21 M stock solution, 5.2 μmol, for each reaction). The three solutions were heated for 2d at 60 °C before being allowed to cool. The following purification procedure was applied to each sample individually: The reaction mixture was precipitated using KPF₆ (saturated aqueous solution). The resulting purple powder was collected on celite and washed with water, a small amount of EtOH (**4** is soluble) and finally Et₂O. The product mixture was dissolved in CH₃CN and the solvent removed in vacuo. The three samples were dissolved in 0.5 mL of CD₃CN and compared by ¹H NMR (Figure 6).

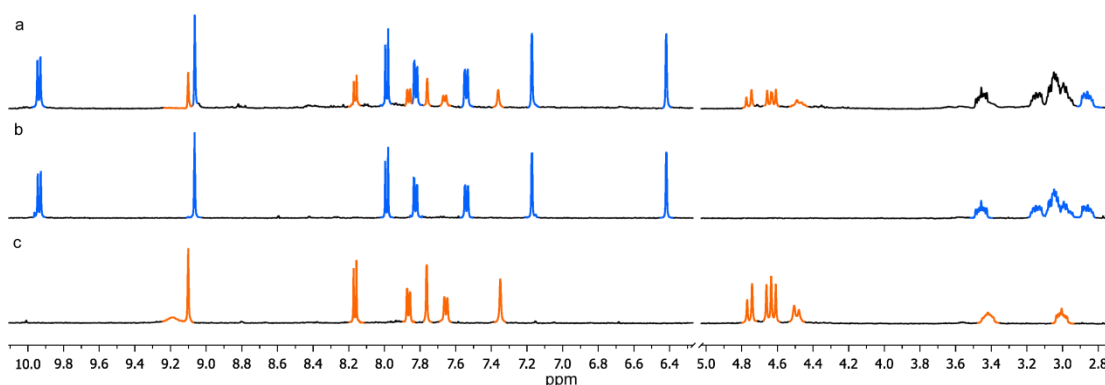


Figure 6. Effect of mixing on the yield of formation for helicates **4** and **5**. ¹H NMR (500 MHz, CD₃CN), (a) self-sorted mixture of **4** (orange) and **5** (blue), (b) **5** only, (c) **3** only. Reactions were run at the same concentration with aldehydes taken from a stock solution. As can be seen the yield of formation of pentamer **5** is unaffected by the presence of **4** whereas the yield of **4** is reduced by 50 % upon mixing.

4.5.1.3. Experimental Procedure to Determine the Effects of Concentration on the Self-Sorting of Helicates **1** and **2**

To two separate DMSO- d_6 solutions of **1** (6.4 mg, 14.2 μmol , in 2.4 mL) and **2** (6.0 mg, 14.2 μmol in 2.4 mL) was added FeCl_2 (150 μL of a 0.10 M stock solution, 15.6 μmol). The two purple solutions were mixed thoroughly to ensure complete dissolution of both aldehydes. Three mixed samples were analyzed differing in the concentration of the reaction mixture.

Sample 1, concentration 5.9 mM:

A 0.4 mL aliquot of **1**+ FeCl_2 was mixed with a 0.4 mL aliquot of **2**+ FeCl_2 in a clean NMR tube before addition of hexylamine (50 μL of a 0.208 M stock solution, 5.2 μmol). 0.4 mL aliquots of **1**+ FeCl_2 and **2**+ FeCl_2 were separately reacted with hexylamine (25 μL of a 0.21 M stock solution, 5.2 μmol , for each reaction).

Sample 2, concentration 4.7 mM:

A 0.4 mL aliquot of **1**+ FeCl_2 was mixed with a 0.4 mL aliquot of **2**+ FeCl_2 in a clean NMR tube before addition of DMSO- d_6 (0.6 mL) then hexylamine (50 μL of a 0.208 M stock solution, 5.2 μmol). 0.4 mL aliquots of **1**+ FeCl_2 and **2**+ FeCl_2 were separately diluted with DMSO- d_6 (0.1 mL) then reacted with hexylamine (25 μL of a 0.21 M stock solution, 5.2 μmol , for each reaction).

Sample 3, concentration 2.4 mM:

A 0.4 mL aliquot of **1**+ FeCl_2 was mixed with a 0.4 mL aliquot of **2**+ FeCl_2 in a clean NMR tube before addition of DMSO- d_6 (1.2 mL) then hexylamine (50 μL of a 0.208 M stock solution, 5.2 μmol). 0.4 mL aliquots of **1**+ FeCl_2 and **2**+ FeCl_2 were separately diluted with DMSO- d_6 (0.6 mL) then reacted with hexylamine (25 μL of a 0.21 M stock solution, 5.2 μmol , for each reaction).

All nine reactions were heated for 1d at 60 °C before being allowed to cool. The following purification procedure was applied to each sample individually: The reaction mixture was precipitated using KPF_6 (saturated aqueous solution). The resulting purple powder was collected on celite and washed with water, a small amount of EtOH (**4** is soluble) and finally Et_2O . The product mixture was dissolved in CH_3CN and the solvent removed in vacuo. The nine samples were dissolved in 0.5 mL of CD_3CN and compared by ^1H NMR (Sample 1, Figure 7. Sample 2, Figure 8. Sample 3, Figure 9).

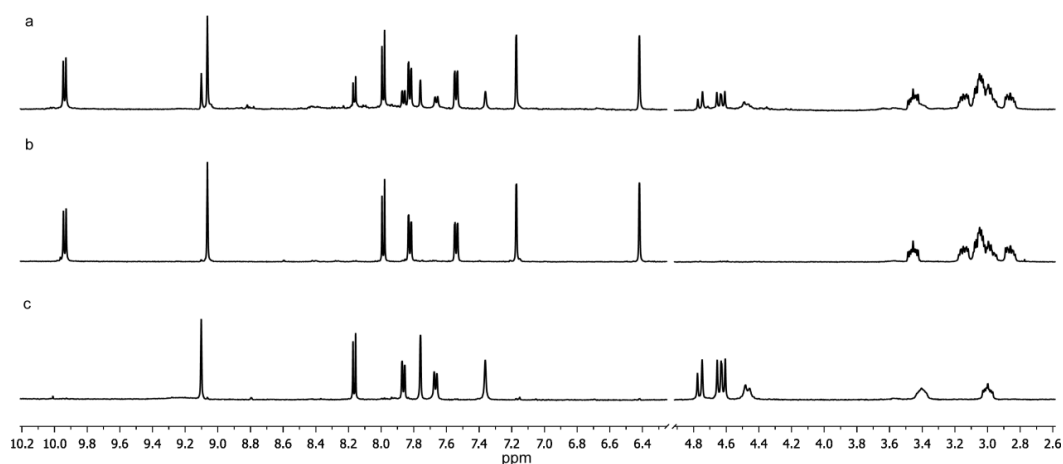


Figure 7. ^1H NMR (CD_3CN , 500 MHz) of sample 1 reaction concentration; 5.9 mM. (a) a mixture of **4** and **5**, (b) **5** and (c) **4**.

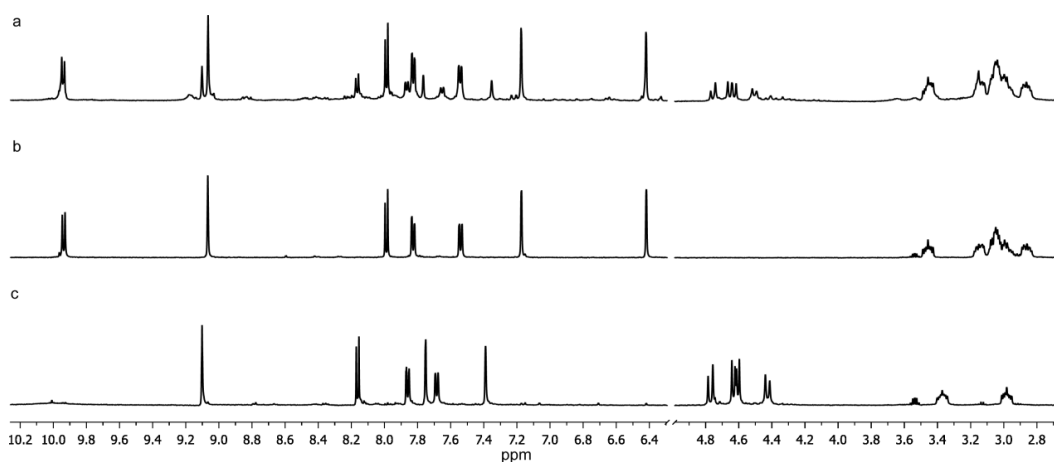


Figure 8. ^1H NMR (CD_3CN , 500 MHz) of sample 2 reaction concentration; 4.7 mM. (a) a mixture of **4** and **5**, (b) **5** and (c) **4**.

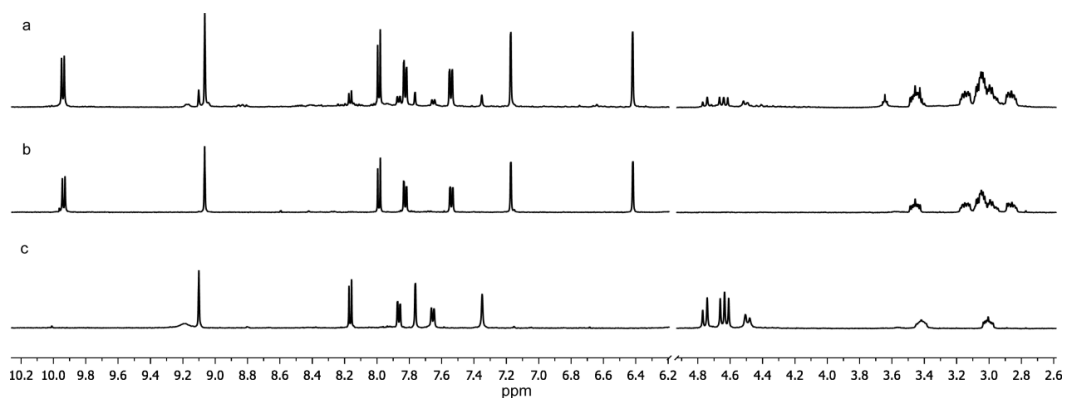
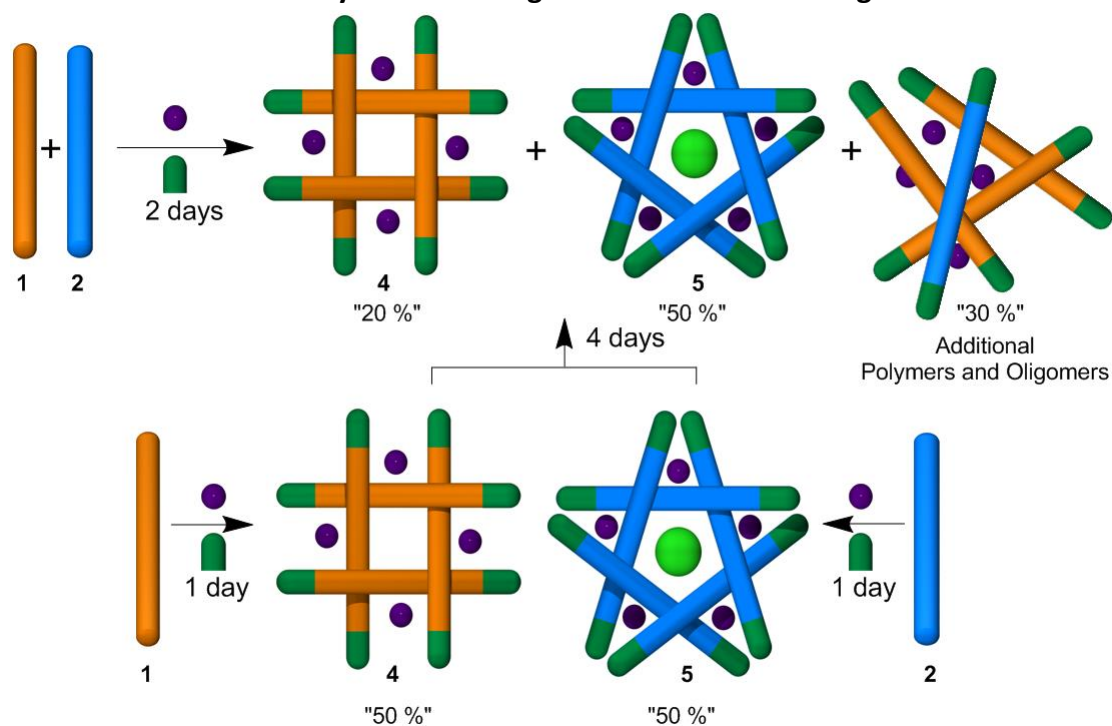


Figure 9. ^1H NMR (CD_3CN , 500 MHz) of sample 3 reaction concentration; 2.4 mM. (a) a mixture of **4** and **5**, (b) **5** and (c) **4**.

4.5.1.4. Thermodynamic Investigations of the Self-Sorting of Helicates **4** and **5**



Scheme 5. Thermodynamic investigations. The products of the mixing reaction are the same regardless of the time at which aldehydes **1** and **2** are mixed.

The thermodynamics of self-sorting was probed by monitoring reactions C and D mixed at different times during the self-assembly process (Scheme 5). Two samples were prepared (see below for details); In sample C aldehydes **1** and **2** (with FeCl_2) were mixed prior to the

addition of hexylamine **3** and sample D where each aldehyde (with FeCl_2) was reacted separately with hexylamine, then after 24h these reaction mixtures were combined. Both samples were heated at $60\text{ }^\circ\text{C}$ and monitored over the course of 4 days (Figure 10). As expected after the first day of heating sample C shows the required distribution of **4** and **5**, which remains constant over the course of 4d (see Figure 10d). Immediately after mixing sample D shows an approximately 1:1 distribution of helicates **4** and **5** (Figure 11a), which slowly rearranges to the $\sim 1:3$ ratio seen above (see Figure 11d). Upon work up both samples C and D appear to be identical (see Figures S7a and b) therefore both reactions reach the same end point irrespective of the times mixed. Indicating that the formation of **4** is dynamic (as its abundance was observed to decrease) and that it is possible to disassemble preformed tetrameric helicate **4** by addition of the reaction mixture for the formation of **5**.

4.5.1.5. Experimental Procedure for the Thermodynamic Investigations of the Self-Sorting of Helicates **4** and **5**

To two separate $\text{DMSO-}d_6$ solutions of **1** (2.1 mg, $4.7\text{ }\mu\text{mol}$, in 1.0 mL) and **2** (2.0 mg, $4.7\text{ }\mu\text{mol}$ in 1.0 mL) was added FeCl_2 ($50\text{ }\mu\text{L}$ of a 0.10 M stock solution, $5.2\text{ }\mu\text{mol}$). The two purple solutions were mixed thoroughly to ensure complete dissolution of both aldehydes. A 0.5 mL aliquot of **1**+ FeCl_2 was mixed with a 0.5 mL aliquot of **2**+ FeCl_2 in a clean NMR tube before addition of hexylamine ($50\text{ }\mu\text{L}$ of a 0.21 M stock solution, $5.2\text{ }\mu\text{mol}$) (sample C). The remaining 0.5 mL aliquots of **1**+ FeCl_2 and **2**+ FeCl_2 were separately reacted with hexylamine **3** ($25\text{ }\mu\text{L}$ of a 0.21 M stock solution, $5.2\text{ }\mu\text{mol}$, for each reaction). The three solutions were heated for 1d at $60\text{ }^\circ\text{C}$. The individual solutions of **1**+ FeCl_2 +**3** and **2**+ FeCl_2 +**3** were combined in a clean NMR tube and thoroughly mixed before being heated at $60\text{ }^\circ\text{C}$ for a further 4 days (sample D). Both samples C and D were monitored over this time (Figures S6 and S7). The two samples were allowed to cool and the following purification procedure was applied to

each sample individually: The reaction mixture was precipitated using KPF_6 (saturated aqueous solution). The resulting purple powder was collected on Celite and washed with water, a small amount of EtOH (**4** is soluble) and finally Et_2O . The product mixture was dissolved in CH_3CN and the solvent removed in vacuo. The two samples were dissolved in 0.5 mL of CD_3CN compared by ^1H NMR (Figure 12).

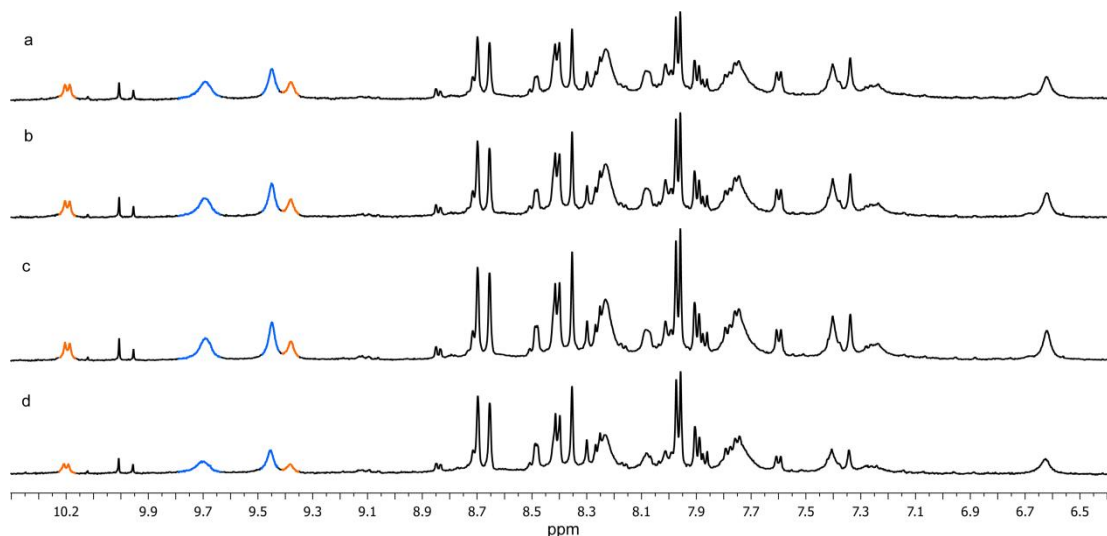


Figure 10. ^1H NMR ($\text{DMSO}-d_6$, 500 MHz) analysis over time of the crude reaction mixture of solution C for the formation of **4** (orange) and **5** (blue) where aldehydes **1** and **2** were mixed at the start of the reaction. Spectra correspond to the reaction mixture after (a) 1 day (b) 2 days, (c) 3 days, (d) 4 days. The ratio of **4:5** remains constant over the course of the experiment.

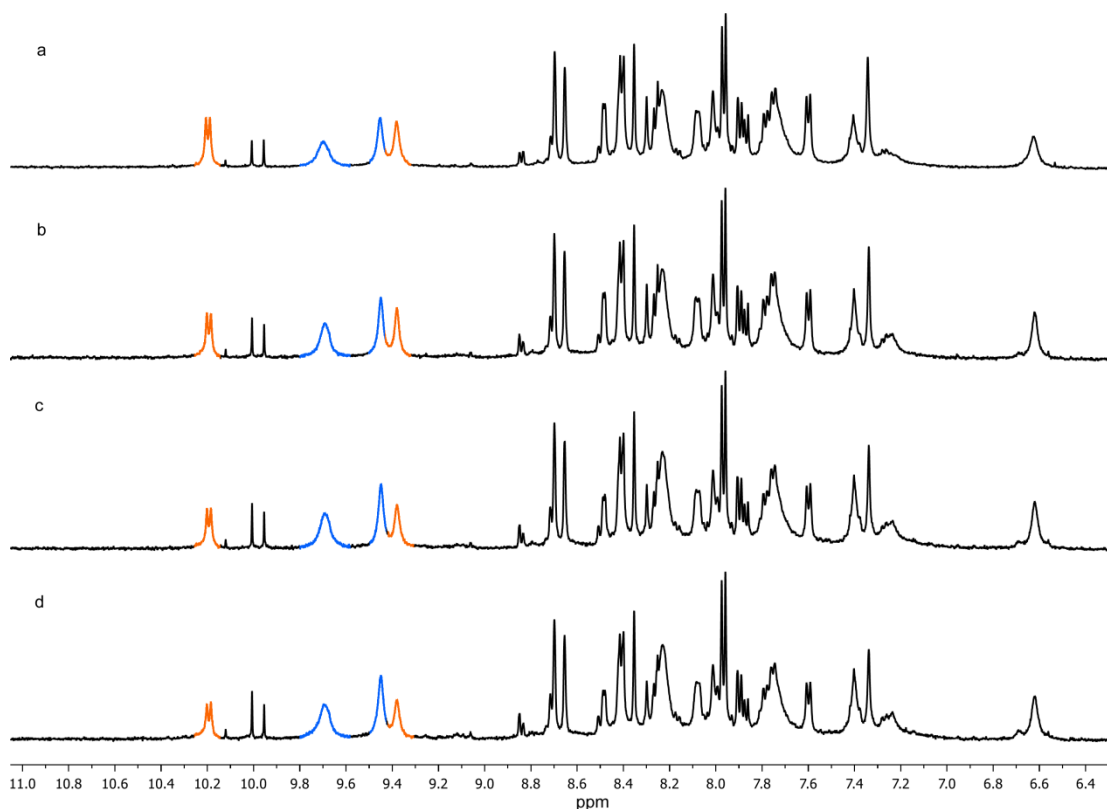


Figure 11. ^1H NMR ($\text{DMSO-}d_6$, 500 MHz) analysis over time of the crude reaction mixture of solution D the formation of **4** (orange) and **5** (blue) where aldehydes **1** and **2** were mixed after 1d. Spectra correspond to the reaction mixture (a) immediately after mixing (b) after 1 day, (c) 2 days, (d) 3 days. The ratio of **4**:**5** starts at 1:1 as expected for mixing equimolar solutions of **4** and **5**. Over time the yield of **5** is depleted until after 4 days of heating the ratio matches that in Figure 10.

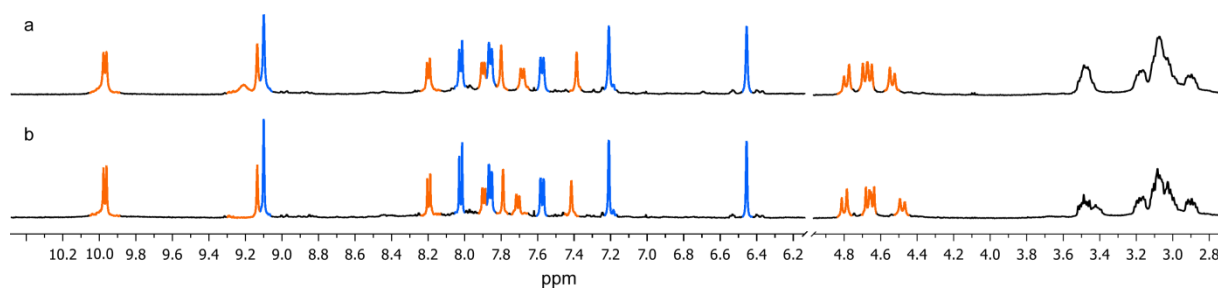
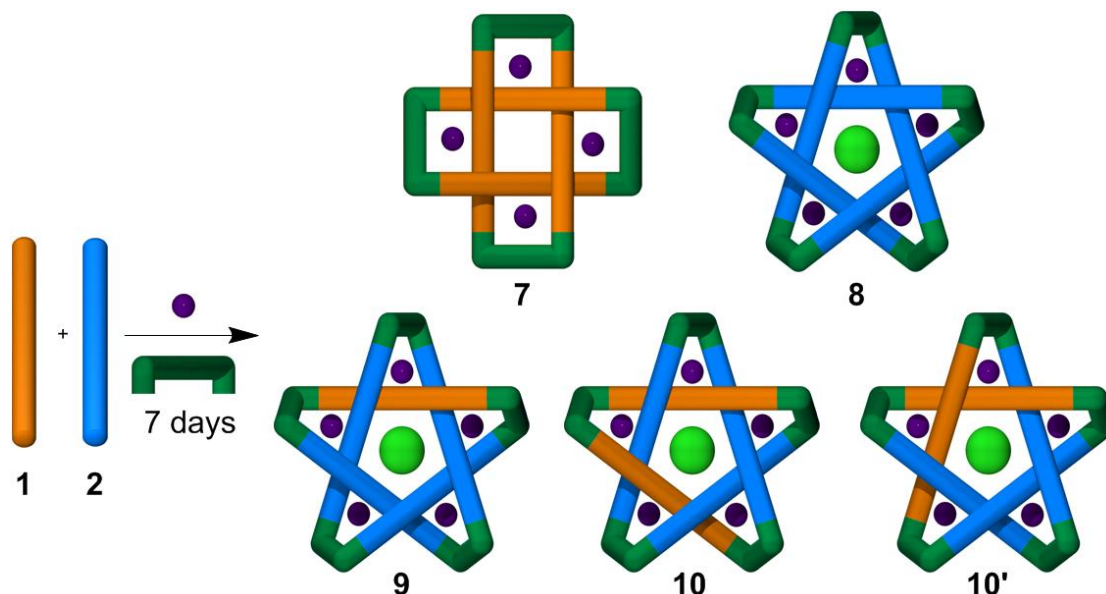


Figure 12. ^1H NMR (CD_3CN , 500 MHz) analysis after work up of the samples from Figures S6 and S7. **4** (orange) and **5** (blue) (a) solution C, (b) solution D.

4.5.2. Closed Systems

4.5.2.1. Experimental Procedure for the Self-Sorting of Solomon Link 7 and Pentafoil Knot 8



Scheme 6. Mixing experiments conducted with aldehyde **1** (orange) and aldehyde **2** (blue) with iron(II) (purple) and 2,2'-(ethylenedioxy)bis(ethylamine) (green) to form Solomon link **7** and pentafoil knots **8**, **9** and **10**.

To two separate solutions of **1** (1.1 mg, 2.4 μmol , in 0.5 mL) and **2** (1.0 mg, 2.4 μmol in 0.5 mL) was added a solution of anhydrous FeCl_2 (25 μL of a 0.104 M stock solution, 2.6 μmol). The two purple solutions were mixed thoroughly to ensure complete dissolution of both aldehydes. The solutions were combined together in a clean NMR tube before addition of a solution of 2,2'-(ethylenedioxy)bis(ethylamine) (50 μL of a 0.10 M stock solution, 2.6 μmol). The resulting mixture was heated for 7d at 60 $^\circ\text{C}$ before being allowed to cool to RT. The reaction mixture was precipitated using an excess saturated aqueous KPF_6 . The resulting purple powder was collected on Celite and washed with water, a small amount of EtOH and finally Et_2O . The product mixture was dissolved in CH_3CN and the solvent removed in vacuo to give a mixture of **6**, **7**, **8** and **9** as a purple powder which was analyzed by ^1H NMR (Figure

2), LR-ESI (Figure 13), HR-ESI (Figures 14 and 15), COSY (Figure 16) and ROESY (Figures 17 and 18) spectroscopy.

4.5.2.1.1. Characterization of Closed Topologies 7, 8, 9 and 10

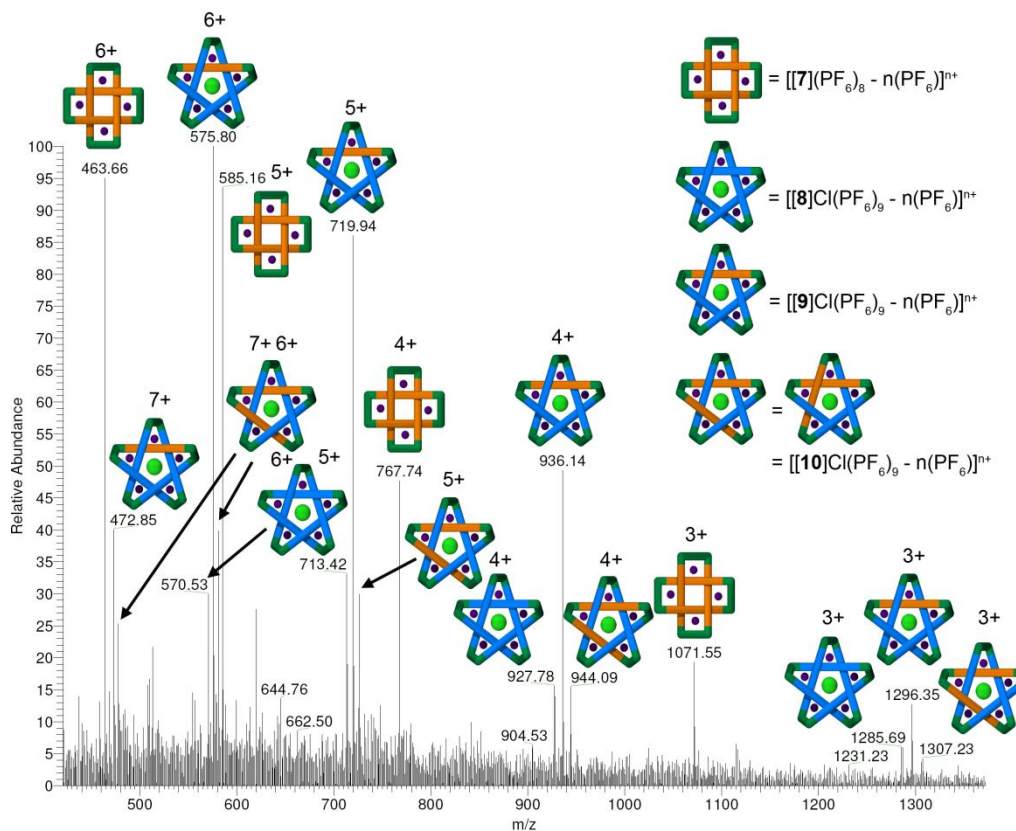


Figure 13. LRESI-MS analysis of the mixture of 7, 8, 9 and 10.

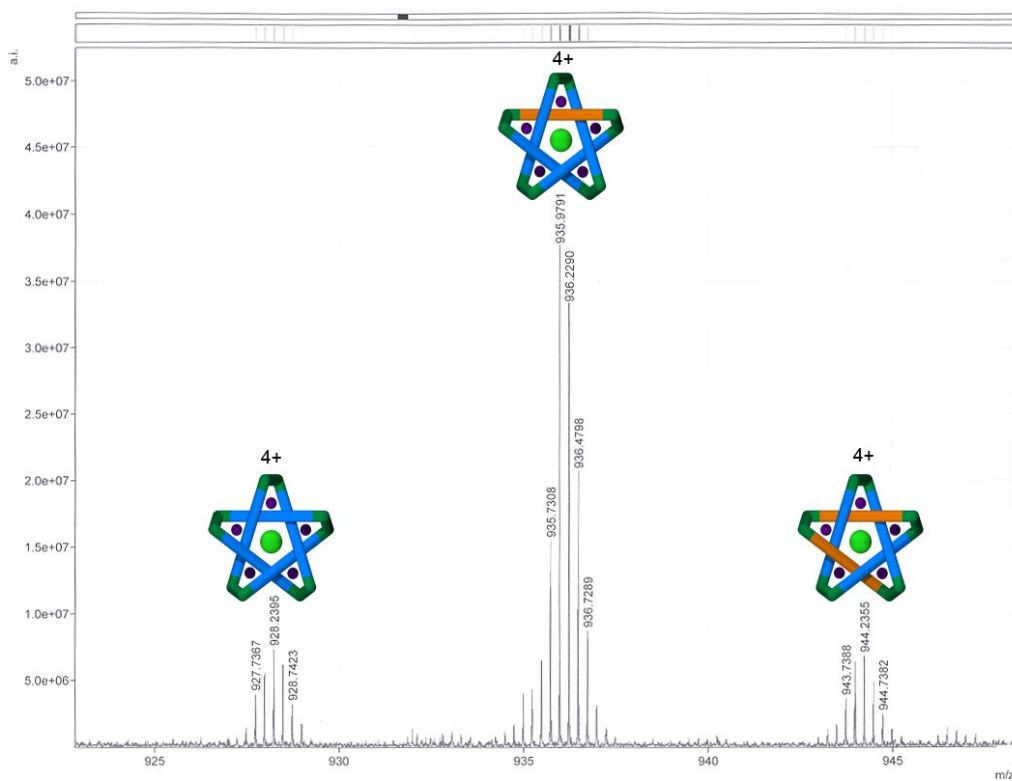


Figure 14. HRESI-MS highlighting pentafoil knots 7, 8 and 9.

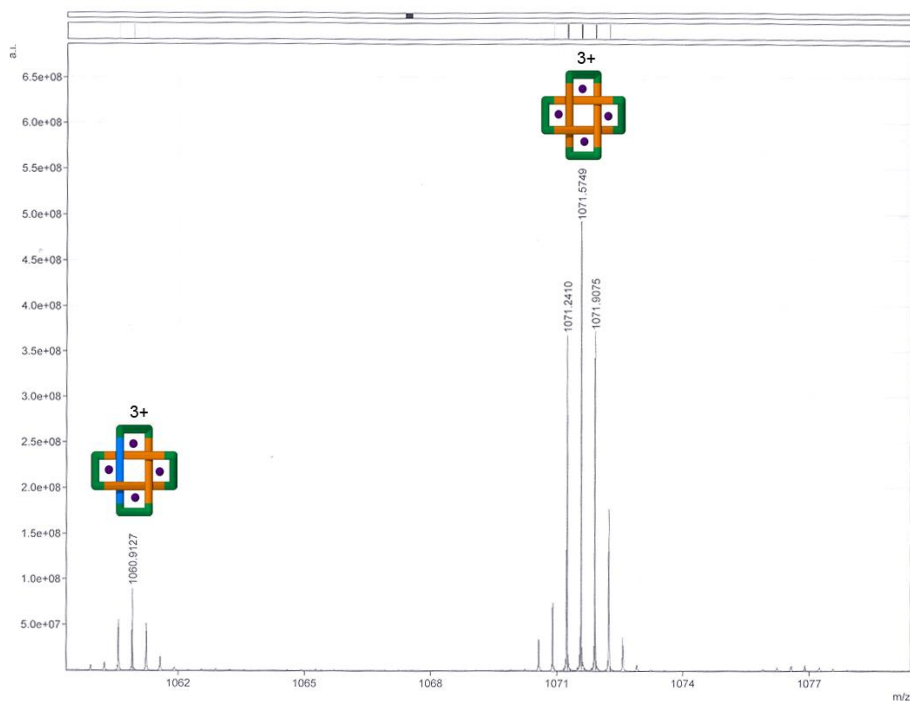


Figure 15. HRESI-MS highlighting Solomon link 4 and a mixed Solomon link incorporating one alternative component 2.

4.5.2.1.2. 2D NMR Characterisation of Mixed-Ligand Pentafoil Knot 9

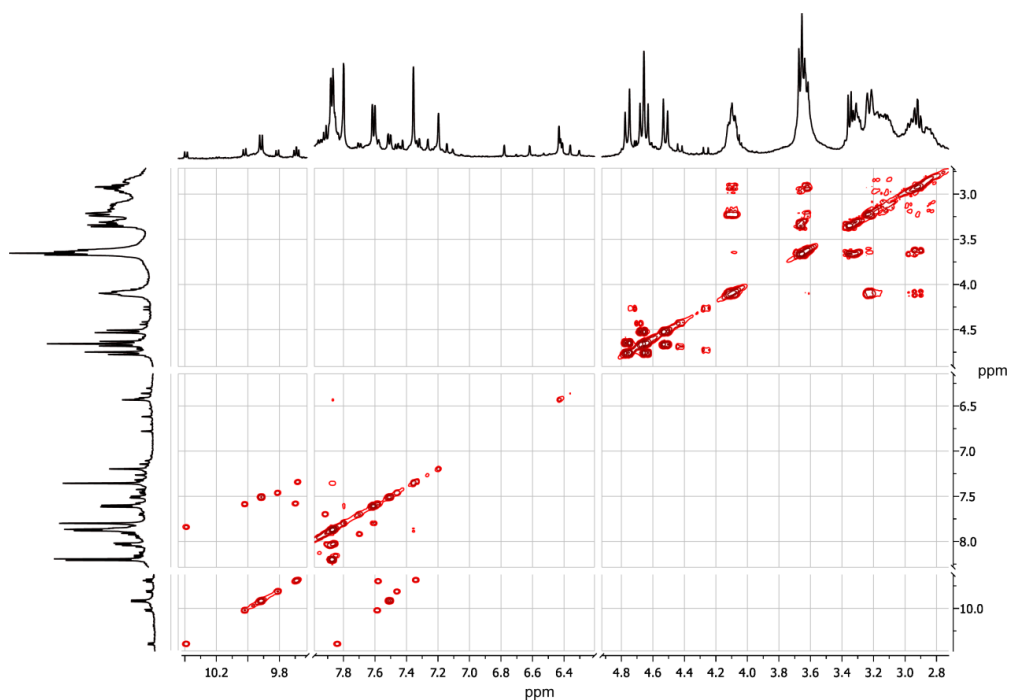


Figure 16. COSY NMR spectrum (500 MHz, CD₃CN) of a mixture of **7**, **8**, **9** and **10**, confirming no coupling between the non-equivalent signals for proton H^A.

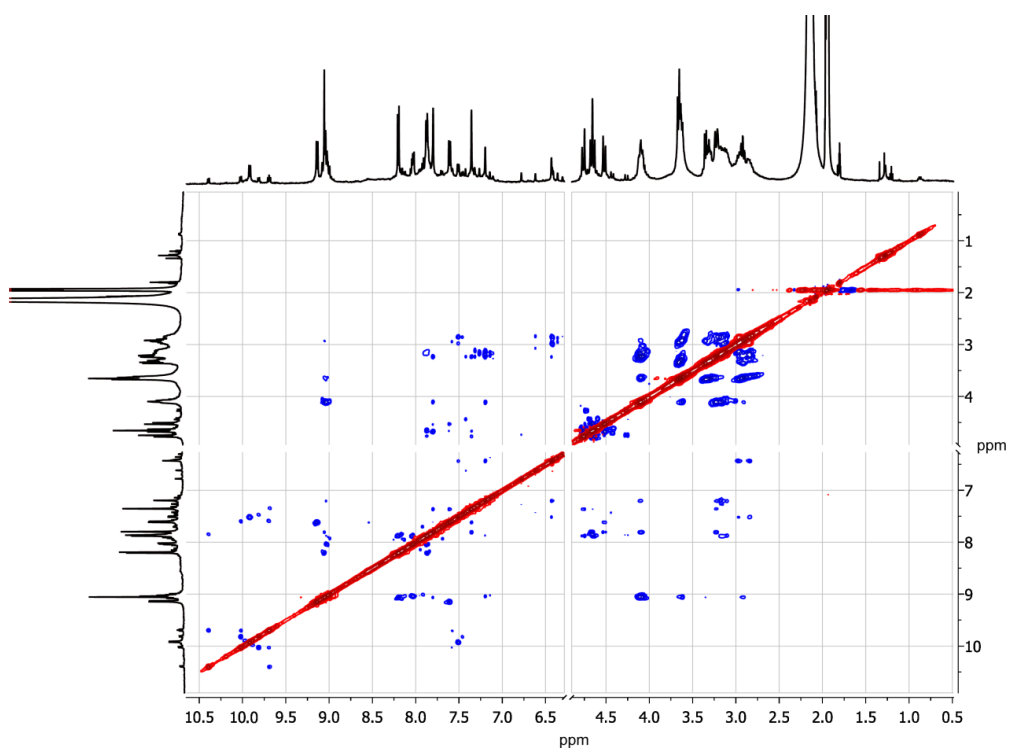


Figure 17. ROESY NMR spectrum (500 MHz, CD₃CN) of a mixture of **7**, **8**, **9** and **10**.

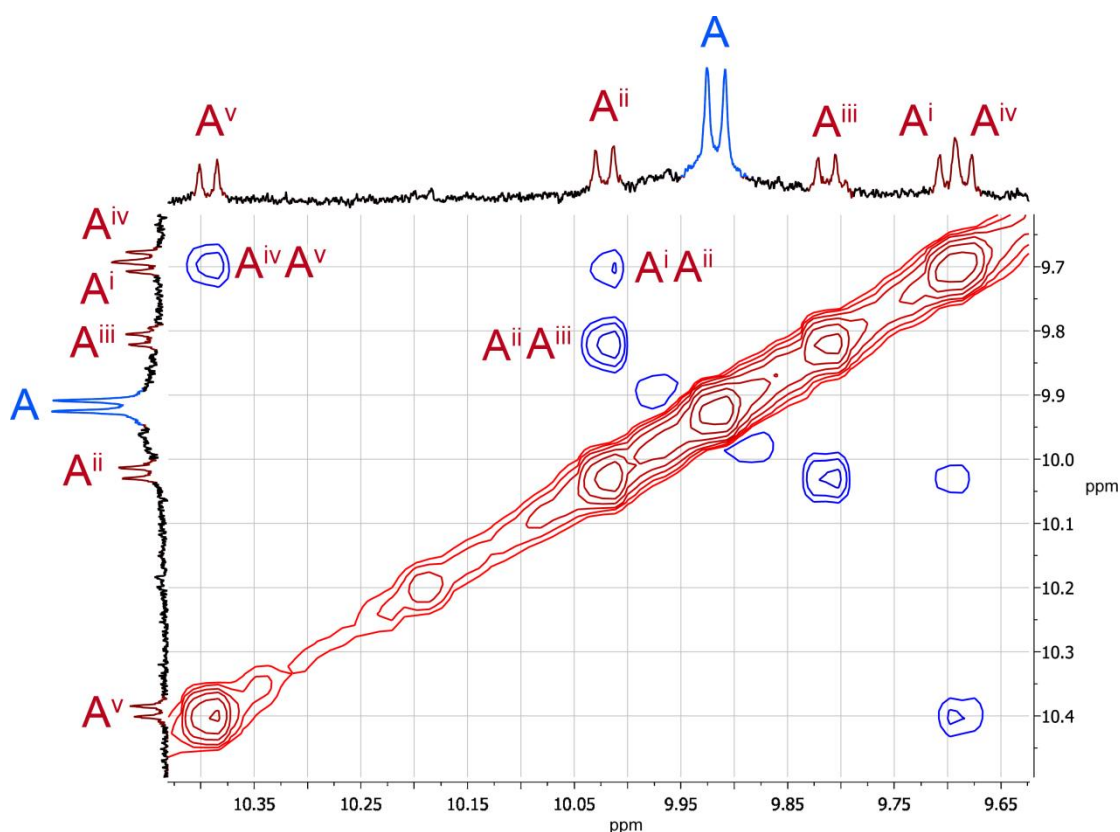
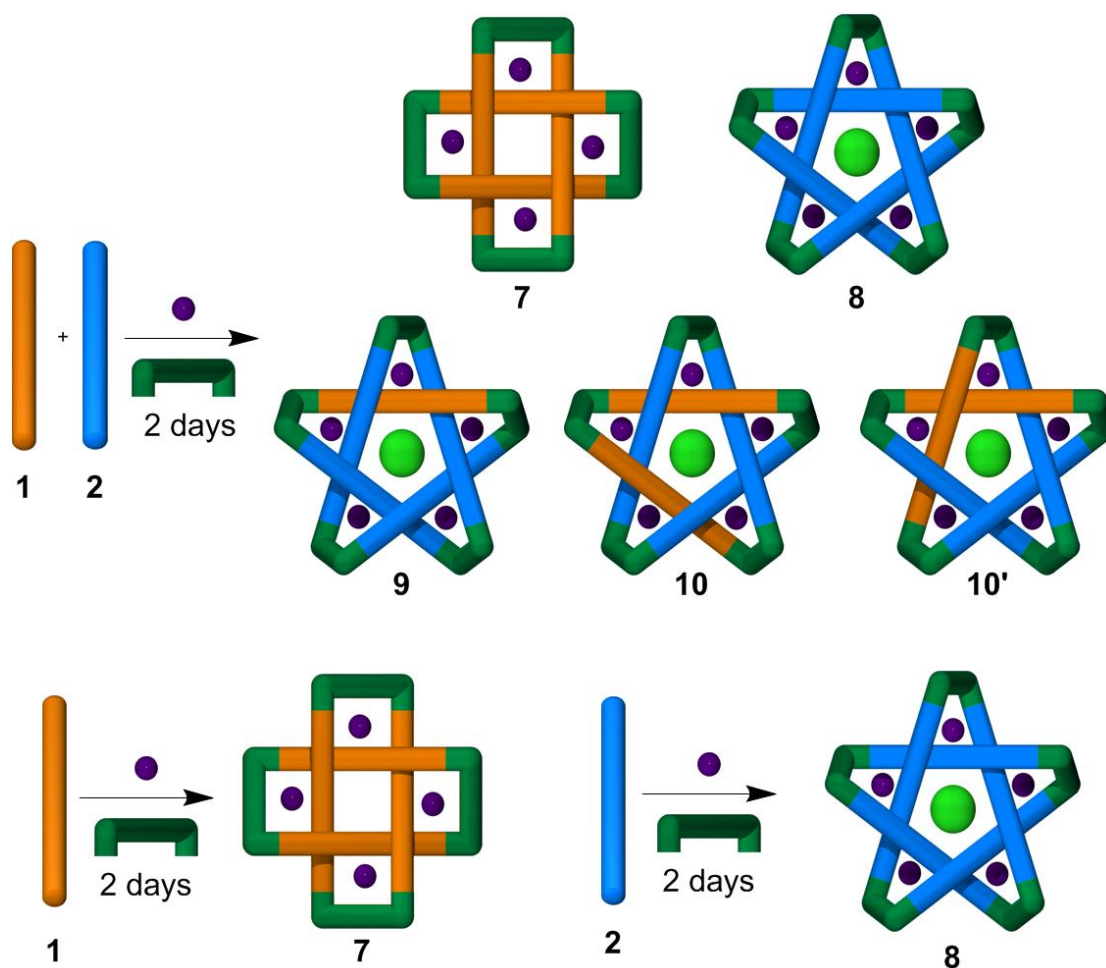


Figure 18. Zoom of ROESY NMR spectrum (500 MHz, CD_3CN) of a mixture of **7**, **8**, **9** and **10** highlighting the region between 9.60 and 10.40 ppm. Cross peaks from mixed-ligand pentamer **9** are shown, consistent with the proposed structure.

4.5.2.2. Experimental Procedure to Determine the Effects of Mixing on the Relative Yields of Solomon Link **7** and Pentafoil Knot **8**

To two separate $\text{DMSO-}d_6$ solutions of **1** (2.1 mg, 4.7 μmol , in 1.0 mL) and **2** (2.0 mg, 4.7 μmol in 1.0 mL) was added FeCl_2 (50 μL of a 0.10 M stock solution, 5.2 μmol). The two purple solutions were mixed thoroughly to ensure complete dissolution of both aldehydes. A 0.5 mL aliquot of **1**. FeCl_2 was mixed with a 0.5 mL aliquot of **2**. FeCl_2 in a clean NMR tube before addition of 2,2'-(ethylenedioxy)bis(ethylamine) **6** (50 μL of a 0.10 M stock solution, 5.2 μmol). The remaining 0.5 mL aliquots of **1**+ FeCl_2 and **2**+ FeCl_2 were separately reacted with 2,2'-(ethylenedioxy)bis(ethylamine) **6** (25 μL of a 0.10 M stock solution, 2.6 μmol , for each reaction). The three solutions were heated for 4d at 60 $^\circ\text{C}$ before being allowed to

cool. The following purification procedure was applied to each sample individually: The reaction mixture was precipitated using KPF_6 (saturated aqueous solution). The resulting purple powder was collected on Celite and washed with water, a small amount of EtOH and finally Et₂O. The product mixture was dissolved in CH₃CN and the solvent removed in vacuo. The three samples were dissolved in 0.5 mL of CD₃CN and compared by ¹H NMR (Figure 19).



Scheme 7. Self-sorting experiments conducted to determine the effect of mixing on the relative yields of **7** and **8**. Reactions were carried out using stock solutions of aldehydes **1** and **2** under identical conditions.

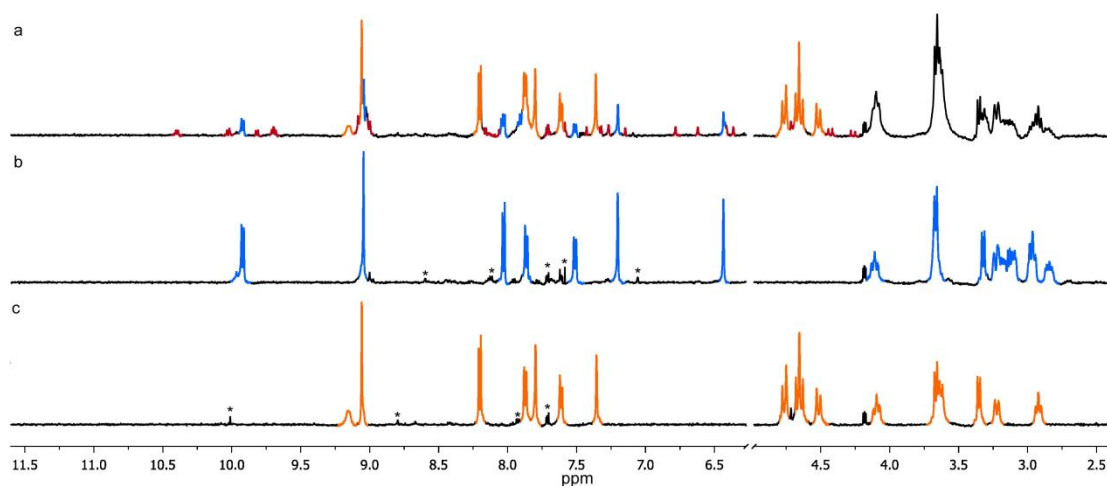


Figure 19. Effect of mixing on the yield of formation for closed topologies **6** and **7**. ^1H NMR (500 MHz, CD_3CN), (a) mixture of **6** (orange), **7** (blue), **8** (red) and **9** (not detected by ^1H NMR, see section 4.3.), (b) **7** only, (c) **6** only. * indicates peaks corresponding to aldehyde **1** or **2** resulting from hydrolysis of the respective helicate. Reactions were run at the same concentration with aldehydes taken from a stock solution. As can be seen the yield of formation of Solomon link **6** is unaffected by the presence of **7** whereas the yield of **7** is drastically reduced with the presence of mix species **8** clearly visible. The total yield of pentafoil knot formation (**7** + **8** + **9**) remains comparable with the yield of **7** in spectrum (b).

4.5.2.3. Experimental Procedure to Determine the Effects of Concentration on the Self-Sorting of Closed Topologies **7**, **8** and **10**

To two separate $\text{DMSO}-d_6$ solutions of **1** (2.0 mg, 4.7 μmol , in 1.7 mL) and **2** (2.1 mg, 4.7 μmol in 1.7 mL) was added FeCl_2 (25 μL of a 0.2 M stock solution, 5.2 μmol). The two purple solutions were mixed thoroughly to ensure complete dissolution of both aldehydes. Three mixed samples were analyzed differing in the concentration of the reaction mixture.

Sample 4, concentration 5.9 mM:

A 0.5 mL aliquot of **1**+ FeCl_2 (1.2 μmol of **1**) was mixed with a 0.5 mL aliquot of **2**+ FeCl_2 (1.2 μmol of **2**) in a clean NMR tube before addition of 2,2'-(ethylenedioxy)bis(ethylamine), **6**, (20 μL of a 0.12 M stock solution, 2.4 μmol).

0.5 mL aliquots of **1**+FeCl₂ and **2**+FeCl₂ were separately reacted with 2,2'-(ethylenedioxy)bis(ethylamine) **6** (10 μL of a 0.12 M stock solution, 1.2 μmol, for each reaction).

Sample 5, concentration 4.7 mM:

A 0.5 mL aliquot of **1**+FeCl₂ was mixed with a 0.5 mL aliquot of **2**+FeCl₂ in a clean NMR tube before addition of DMSO-*d*₆ (0.5 mL) then 2,2'-(ethylenedioxy)bis(ethylamine) **6** (20 μL of a 0.12 M stock solution, 2.4 μmol).

0.5 mL aliquots of **1**+FeCl₂ and **2**+FeCl₂ were separately diluted with DMSO-*d*₆ (0.25 mL) then reacted with 2,2'-(ethylenedioxy)bis(ethylamine) **6** (10 μL of a 0.12 M stock solution, 1.2 μmol, for each reaction).

Sample 6, concentration 2.4 mM:

A 0.5 mL aliquot of **1**+FeCl₂ was mixed with a 0.5 mL aliquot of **2**+FeCl₂ in a clean NMR tube before addition of DMSO-*d*₆ (1.0 mL) then 2,2'-(ethylenedioxy)bis(ethylamine) **6** (20 μL of a 0.12 M stock solution, 2.4 μmol).

0.5 mL aliquots of **1**+FeCl₂ and **2**+FeCl₂ were separately diluted with DMSO-*d*₆ (0.5 mL) then reacted with 2,2'-(ethylenedioxy)bis(ethylamine) **6** (10 μL of a 0.12 M stock solution, 1.2 μmol, for each reaction).

All nine reactions were heated for 2d at 60 °C before being allowed to cool. The following purification procedure was applied to each sample individually: The reaction mixture was precipitated using KPF₆ (saturated aqueous solution). The resulting purple powder was collected on Celite and washed with water, a small amount of EtOH and finally Et₂O. The product mixture was dissolved in CH₃CN and the solvent removed in vacuo. The nine

samples were dissolved in 0.5 mL of CD_3CN and compared by ^1H NMR (Sample 4, Figure 20. Sample 5, Figure 21. Sample 6, Figure 22).

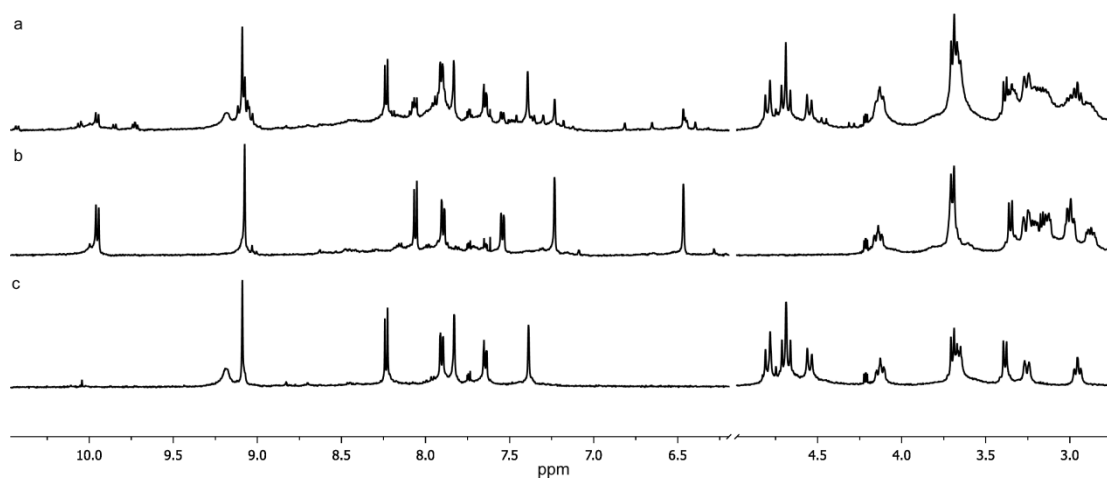


Figure 20. ^1H NMR (CD_3CN , 500 MHz) of sample 4 reaction concentration; 5.9 mM. (a) a mixture of **7**, **8**, **9** and **10** (b) **8** and (c) **7**.

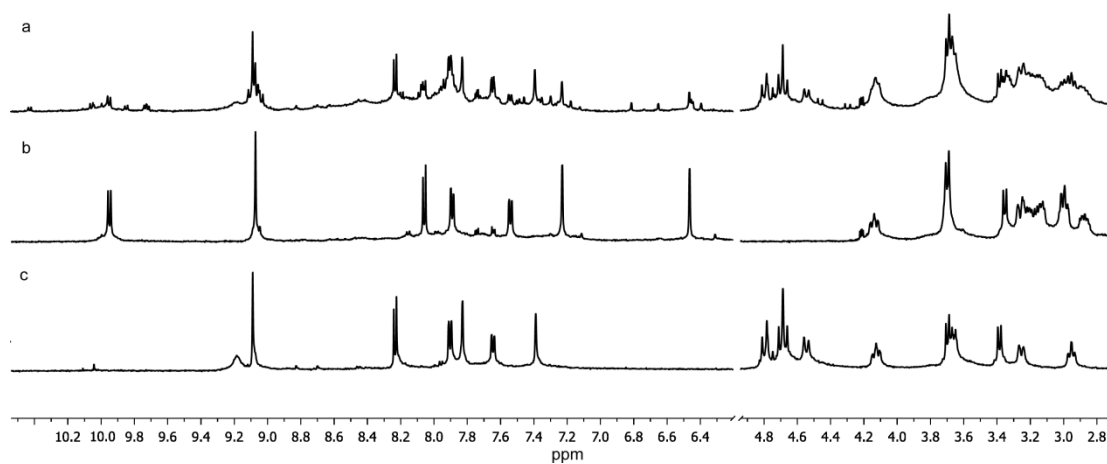


Figure 21. ^1H NMR (CD_3CN , 500 MHz) of sample 5 reaction concentration; 4.7 mM. (a) a mixture of **7**, **8**, **9** and **10** (b) **8** and (c) **7**.

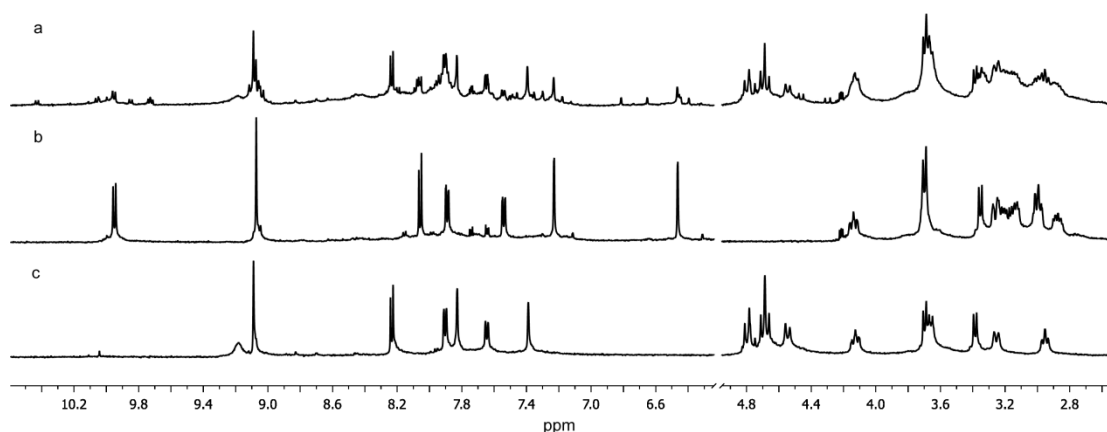


Figure 22. ^1H NMR (CD_3CN , 500 MHz) of sample 6 reaction concentration; 2.4 mM. (a) a mixture of **7**, **8**, **9** and **10** (b) **8** and (c) **7**,

4.5.2.4. Experimental Procedure For the Thermodynamic Investigations of the Self-Sorting of Closed Topologies **7**, **8**, **9** and **10**

See section 4.3. for further details.

To two separate $\text{DMSO-}d_6$ solutions of **1** (2.1 mg, 4.7 μmol , in 1.0 mL) and **2** (2.0 mg, 4.7 μmol in 1.0 mL) was added FeCl_2 (50 μL of a 0.10 M stock solution, 5.2 μmol). The two purple solutions were mixed thoroughly to ensure complete dissolution of both aldehydes. A 0.5 mL aliquot of **1**+ FeCl_2 was mixed with a 0.5 mL aliquot of **2**+ FeCl_2 in a clean NMR tube before addition of 2,2'-(ethylenedioxy)bis(ethylamine) **6** (50 μL of a 0.10 M stock solution, 5.2 μmol). The remaining 0.5 mL aliquots of **1**+ FeCl_2 and **2**+ FeCl_2 were separately reacted with 2,2'-(ethylenedioxy)bis(ethylamine) **6** (25 μL of a 0.10 M stock solution, 2.6 μmol , for each reaction). The three solutions were heated for 1d at 60 $^\circ\text{C}$. The solutions of **1**+ FeCl_2 +**6** and **2**+ FeCl_2 +**6** were combined in a clean NMR tube and thoroughly mixed before being heated at 60 $^\circ\text{C}$ for a further 7 days. Both samples were monitored over time (Figures S19 and S20). The two samples were allowed to cool and the following purification procedure was applied to each sample individually: The reaction mixture was precipitated using KPF_6 (saturated aqueous solution). The resulting purple powder was collected on Celite and

washed with water, a small amount of EtOH and finally Et₂O. The product mixture was dissolved in CH₃CN and the solvent removed in vacuo. Both samples were dissolved in 0.5 mL of CD₃CN and compared by ¹H NMR (Figure 3).

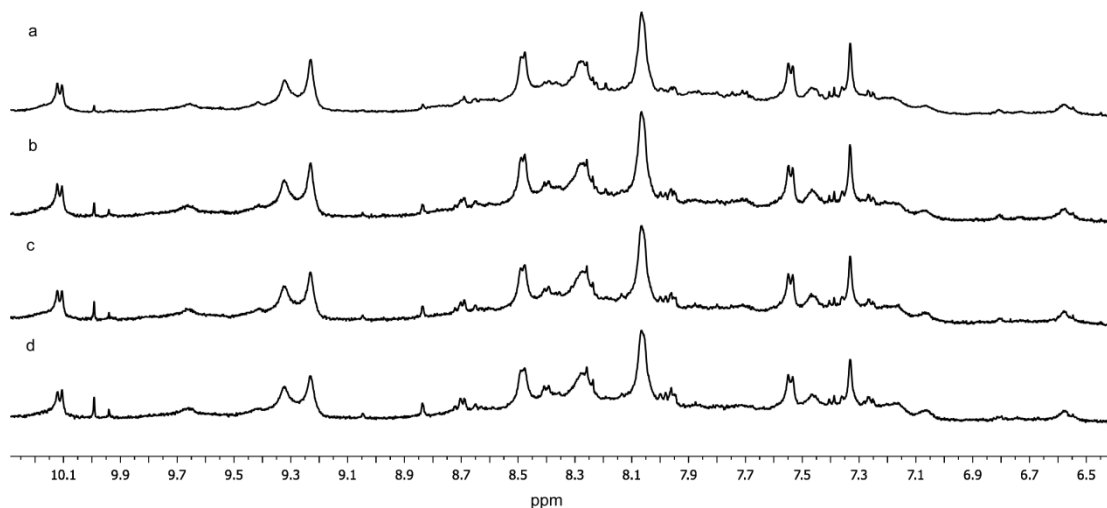


Figure 23. ¹H NMR (DMSO-*d*₆, 500 MHz) of sample A over time, spectra were recorded after heating for (a) 1 days, (b) 2 days, (c) 3 days and (d) 7 days.

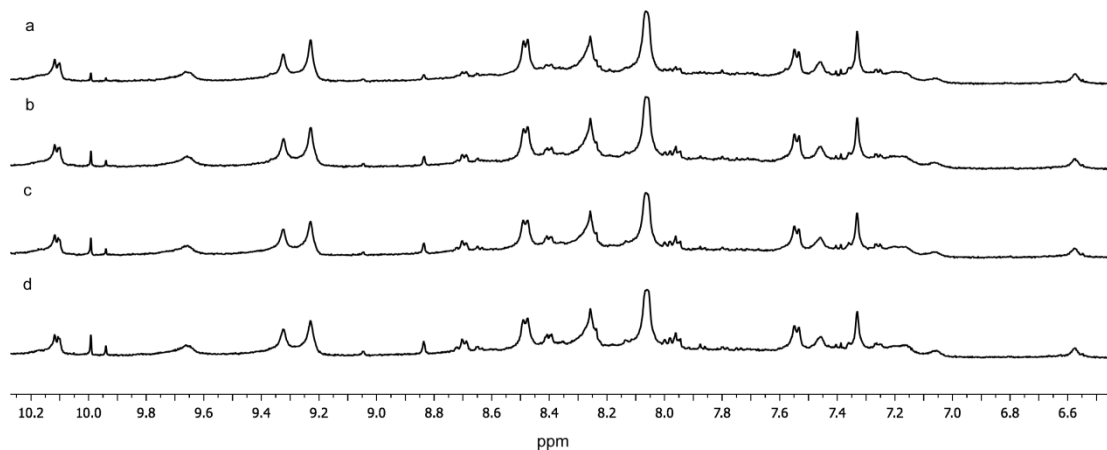


Figure 24. ¹H NMR (DMSO-*d*₆, 500 MHz) of sample B over time, spectra were recorded after mixing then heating for (a) 1 days, (b) 2 days, (c) 3 days and (d) 7 days.

4.6. Notes and references

- (a) S. J. Rowan, D. G. Hamilton, P. A. Brady, J. K. M. Sanders, *J. Am. Chem. Soc.*, **1997**, *119*, 2578–2579; (b) A. Wu, L. Isaacs, *J. Am. Chem. Soc.*, **2003**, *125*, 4831–4835; (c) M. M. Safont-Sempere, G. Fernández, F. Würthner, *Chem. Rev.*, **2011**, *111*, 5784–5814; (d) K. Osowska, O. Š. Miljanić, *Synlett* **2011**, 1643–1648; (e) M. Lal Saha, M. Schmittel, *Org. Biomol. Chem.*, **2012**, *10*, 4651–4684.
- (a) M. Edidin, *Nat. Rev. Mol. Cell Biol.*, **2003**, *4*, 414–418; (b) N. A. Campbell, J. B. Reece, M. R. Taylor, E. J. Simon, J. L. Dickey, *Biology: Concepts and Connections*, 6th ed., Benjamin/Cummings Publishing Company, San Francisco, CA, 2008.
- P. Mukhopadhyay, A. Wu, L. Isaacs, *J. Org. Chem.*, **2004**, *69*, 6157–6164.
- For recent examples of self-sorting based on hydrogen bonding, see (a) M. R. Molla, A. Das, S. Ghosh, *Chem. Eur. J.*, **2010**, *16*, 10084–10093; (b) L.-P. Cao, J.-G. Wang, J.-Y. Ding, A.-X. Wu, L. Isaacs, *Chem. Commun.*, **2011**, *47*, 8548–8550; (c) A. S. Singh, S.-S. Sun, *Chem. Commun.*, **2012**, *48*, 7392–7394; (d) M. L. Pellizzaro, K. A. Houton, A. J. Wilson, *Chem. Sci.*, **2013**, *4*, 1825–1829; for recent examples of self-sorting involving hydrophobic interactions, see (e) H. Gan, B. C. Gibb, *Chem. Commun.*, **2012**, *48*, 1656–1658; (f) Z. Huang, L. Yang, Y. Liu, Z. Wang, O. A. Scherman, X. Zhang, *Angew. Chem.*, **2014**, *126*, 5455–5459; *Angew. Chem. Int. Ed.*, **2014**, *53*, 5351–5355; for recent examples of self-sorting through π - π interactions, see (g) N.-T. Lin, A. Vargas Jentsch, L. Guénée, J.-M. Neudörfl, S. Aziz, A. Berkessel, E. Orentas, N. Sakai, S. Matile, *Chem. Sci.*, **2012**, *3*, 1121–1127; (h) Z. Xie, V. Stepanenko, K. Radacki, F. Würthner, *Chem. Eur. J.*, **2012**, *18*, 7060–7070; (i) K. Osowska, O. Š. Miljanić, *J. Am. Chem. Soc.*, **2011**, *133*, 724–727; (j) K. Osowska, O. Š. Miljanić, *Angew. Chem.*, **2011**, *123*, 8495–8499; *Angew. Chem. Int. Ed.*, **2011**, *50*, 8345–8349; (k) R. C. Lirag, K. Osowska, O. Š. Miljanić, *Org. Biomol. Chem.*, **2012**, *10*, 4847–4850.
- (a) R. Kramer, J.-M. Lehn, A. Marquis-Rigault, *Proc. Natl. Acad. Sci. USA* **1993**, *90*, 5394–5398; (b) J.-M. Lehn, *Science*, **2002**, *295*, 2400–2403.
- For examples of self-sorting involving differing numbers of metal-ion binding sites, see Ref. [5] and (a) R. Stiller, J.-M. Lehn, *Eur. J. Inorg. Chem.*, **1998**, 977–982; (b) P. N. Taylor, H. L. Anderson, *J. Am. Chem. Soc.*, **1999**, *121*, 11538–11545; for examples of

- self-sorting involving different types of metal-ion binding sites, see* (c) D. Schultz, J. R. Nitschke, *Angew. Chem.*, **2006**, *118*, 2513–2516; *Angew. Chem. Int. Ed.*, **2006**, *45*, 2453–2456; (d) K. Mahata, M. Schmittel, *J. Am. Chem. Soc.*, **2009**, *131*, 16544–16554; (e) K. Mahata, M. L. Saha, M. Schmittel, *J. Am. Chem. Soc.*, **2010**, *132*, 15933–15935; *for examples of self-sorting based on metal-ion size, see* (f) M. Barboiu, E. Petit, A. van der Lee, G. Vaughan, *Inorg. Chem.*, **2006**, *45*, 484–486; *for the use of steric constraints to control self-sorting, see* (g) L. Zhao, B. H. Northrop, Y.-R. Zheng, H.-B. Yang, H. J. Lee, Y. M. Lee, J. Y. Park, K.-W. Chi, P. J. Stang, *J. Org. Chem.*, **2008**, *73*, 6580–6586; *for the use of oxidation state to control self-sorting, see* (h) K. Parimal, E. H. Witlicki, A. H. Flood, *Angew. Chem.*, **2010**, *122*, 4732–4736; *Angew. Chem. Int. Ed.*, **2010**, *49*, 4628–4632.
7. *For examples of self-sorting through metal-ion binding sites separated by rigid linkers with various geometries, see* (a) D. L. Caulder, K. N. Raymond, *Angew. Chem.*, **1997**, *109*, 1508–1510; *Angew. Chem. Int. Ed. Engl.*, **1997**, *36*, 1440–1442; (b) R. Pinalli, V. Cristini, V. Sottili, S. Geremia, M. Campagnolo, A. Caneschi, E. Dalcanale, *J. Am. Chem. Soc.*, **2004**, *126*, 6516–6517; (c) H.-B. Yang, K. Ghosh, B. H. Northrop, P. J. Stang, *Org. Lett.*, **2007**, *9*, 1561–1564; (d) Y.-R. Zheng, H.-B. Yang, B. H. Northrop, K. Ghosh, P. J. Stang, *Inorg. Chem.*, **2008**, *47*, 4706–4711; (e) B. H. Northrop, Y.-R. Zheng, K.-W. Chi, P. J. Stang, *Acc. Chem. Res.*, **2009**, *42*, 1554–1563; (f) Y.-R. Zheng, H.-B. Yang, K. Ghosh, L. Zhao, P. J. Stang, *Chem. Eur. J.*, **2009**, *15*, 7203–7214; (g) M. M. J. Smulders, A. Jiménez, J. R. Nitschke, *Angew. Chem.*, **2012**, *124*, 6785–6789; *Angew. Chem. Int. Ed.*, **2012**, *51*, 6681–6685; (h) A. Jiménez, R. A. Bilbeisi, T. K. Ronson, S. Zarra, C. Woodhead, J. R. Nitschke, *Angew. Chem.*, **2014**, *126*, 4644–4648; *Angew. Chem. Int. Ed.*, **2014**, *53*, 4556–4560; *for examples of self-sorting involving metal-ion binding sites separated by flexible linkers, see* (i) E. J. Enemark, T. D. P. Stack, *Angew. Chem.*, **1998**, *110*, 977–981; *Angew. Chem. Int. Ed.*, **1998**, *37*, 932–935; (j) M. Albrecht, M. Schneider, H. Röttele, *Angew. Chem.*, **1999**, *111*, 512–515; *Angew. Chem. Int. Ed.*, **1999**, *38*, 557–559; (k) M. Albrecht, O. Blau, R. Fröhlich, *Proc. Natl. Acad. Sci. USA*, **2002**, *99*, 4867–4872; (l) A. Marquis, V. Smith, J. Harrowfield, J.-M. Lehn, H. Herschbach, R. Sanvito, E. Leize-Wagner, A. Van Dorsselaer, *Chem. Eur. J.*, **2006**, *12*, 5632–5641.

8. J. E. Beves, C. J. Campbell, D. A. Leigh, R. G. Pritchard, *Angew. Chem.*, **2013**, 125, 6592–6595; *Angew. Chem. Int. Ed.*, **2013**, 52, 6464–6467.
9. (a) J. F. Nierengarten, C. O. Dietrich-Buchecker, J. P. Sauvage, *J. Am. Chem. Soc.*, **1994**, 116, 375–376; (b) C. Dietrich-Buchecker, E. Leize, J.-F. Nierengarten, J.-P. Sauvage, A. Van Dorsselaer, *J. Chem. Soc. Chem. Commun.*, **1994**, 2257–2258; (c) C. Dietrich-Buchecker, J.-P. Sauvage, *Chem. Commun.*, **1999**, 615–616; (d) F. Ibukuro, M. Fujita, K. Yamaguchi, J.-P. Sauvage, *J. Am. Chem. Soc.*, **1999**, 121, 11014–11015; (e) C. P. McArdle, J. J. Vittal, R. J. Puddephatt, *Angew. Chem.*, **2000**, 112, 3977–3980; *Angew. Chem. Int. Ed.*, **2000**, 39, 3819–3822; (f) C. P. McArdle, M. C. Jennings, J. J. Vittal, R. J. Puddephatt, *Chem. Eur. J.*, **2001**, 7, 3572–3583; (g) C. D. Pentecost, K. S. Chichak, A. J. Peters, G. W. V. Cave, S. J. Cantrill, J. F. Stoddart, *Angew. Chem.*, **2007**, 119, 222–226; *Angew. Chem. Int. Ed.*, **2007**, 46, 218–222; (h) C. D. Meyer, R. S. Forgan, K. S. Chichak, A. J. Peters, N. Tangchaivang, G. W. V. Cave, S. I. Khan, S. J. Cantrill, J. F. Stoddart, *Chem. Eur. J.*, **2010**, 16, 12570–12581; (i) C. Peinador, V. Blanco, J. M. Quintela, *J. Am. Chem. Soc.*, **2009**, 131, 920–921; (j) T. Ciengshin, R. Sha, N. C. Seeman, *Angew. Chem.*, **2011**, 123, 4511–4514; *Angew. Chem. Int. Ed.*, **2011**, 50, 4419–4422; (k) T. Prakasam, M. Lusi, M. Elhabiri, C. Platas-Iglesias, J.-C. Olsen, Z. Asfari, S. Cianfèrani-Sanglier, F. Debaene, L. J. Charbonnière, A. Trabolsi, *Angew. Chem.*, **2013**, 125, 10140–10144; *Angew. Chem. Int. Ed.*, **2013**, 52, 9956–9960; for the assembly of a related “Solomon cube” topology, see (l) T. K. Ronson, J. Fisher, L. P. Harding, P. J. Rizkallah, J. E. Warren, M. J. Hardie, *Nat. Chem.*, **2009**, 1, 212–216.
10. (a) J.-F. Ayme, J. E. Beves, D. A. Leigh, R. T. McBurney, K. Rissanen, D. Schultz, *Nat. Chem.*, **2012**, 4, 15–20; (b) M. J. Hardie, *Nat. Chem.*, **2012**, 4, 7–8; (c) J.-F. Ayme, J. E. Beves, D. A. Leigh, R. T. McBurney, K. Rissanen, D. Schultz, *J. Am. Chem. Soc.*, **2012**, 134, 9488–9497.
11. (a) E. E. Fenlon, *Eur. J. Org. Chem.*, **2008**, 5023–5035; (b) J. E. Beves, B. A. Blight, C. J. Campbell, D. A. Leigh, R. T. McBurney, *Angew. Chem.*, **2011**, 123, 9428–9499; *Angew. Chem. Int. Ed.*, **2011**, 50, 9260–9327; (c) R. S. Forgan, J.-P. Sauvage, J. F. Stoddart, *Chem. Rev.*, **2011**, 111, 5434–5464; (d) D. B. Amabilino, J.-P. Sauvage, *Top. Curr. Chem.*, **2012**, 323, 107–126; (e) J.-F. Ayme, J. E. Beves, C. J. Campbell, D. A. Leigh, *Chem. Soc. Rev.*, **2013**, 42, 1700–1712.

12. *Trace amounts of a Solomon link incorporating one strand of dialdehyde 2 was observed by high-resolution ESIMS (see Figure 15 in the Experimental Section).*
13. *The asymmetry of 9 results in distinct signals for each ligand strand, each one appearing at one-fifth the intensity of the corresponding signal of 8.*
14. *Preliminary experiments by Lehn and co-workers in the mid-1990s indicated that self-sorting to form open circular helicates also occurs with the original Lehn ligand sets; personal communication, J.-M. Lehn.*
15. (a) B. Hasenknopf, J.-M. Lehn, B. O. Kneisel, G. Baum, D. Fenske, *Angew. Chem.*, **1996**, *108*, 1987–1990; *Angew. Chem. Int. Ed. Engl.*, **1996**, *35*, 1838–1840; (b) B. Hasenknopf, J.-M. Lehn, N. Boumediene, A. Dupont-Gervais, A. Van Dorsselaer, B. Kneisel, D. Fenske, *J. Am. Chem. Soc.*, **1997**, *119*, 10956–10962.
16. *For a discussion of the kinetic stability of products formed under thermodynamic control, see S. Sato, Y. Ishido, M. Fujita, J. Am. Chem. Soc.*, **2009**, *131*, 6064–6065.

Chapter V: "Probing the Dynamics of Pentameric Circular Helicates and Pentafoil Knots"

To be published as "Probing the Dynamics of Pentameric Circular Helicates and Pentafoil Knots", J.-F. Ayme, J. E. Beves, C. J. Campbell and D. A. Leigh

Acknowledgements

Dr. C. J. Campbell is gratefully acknowledged for his contribution to this chapter: C. J. C. synthesised ligand **1-D₈** and performed the amines exchange experiments. C.J.C. was also the first person to obtain the helicate **2-D₄₀** and the knot **6-D₄₀**. The rest of the presented work was a joint effort between the authors.

5.1. Synopsis

Self-assembled molecular systems based on reversible reactions often afford the most thermodynamically stable product out of a large distribution of theoretical products, but this concept can be an over simplified description of reality. In this chapter, the dynamic nature of pentameric circular helicates and a pentafoil knot derived from the reaction of iron(II) chloride with a bis(formylpyridine)bipyridyl building block and either a mono- or bis-amine is investigated. Experiments were conducted to monitor the exchange of amine residues on the periphery of a pentameric helicate. A deuterium labelled aldehyde ligand was used to study the exchange of the ligands of a pentameric helicate and pentafoil knot. Mixing labelled and non-labeled analogues enabled the observation of full aldehyde exchange in DMSO at 60°C over two weeks for hexylamine derived open helicates but the rate of exchange is significantly slower for the closed system pentafoil knot. These results indicate that the present systems are self-assembled under full thermodynamic control when given long enough reaction times (>14 days), significantly longer than the optimal reaction conditions of two days, hinting at kinetic factors leading to successful syntheses of these complexes.

5.2. Introduction

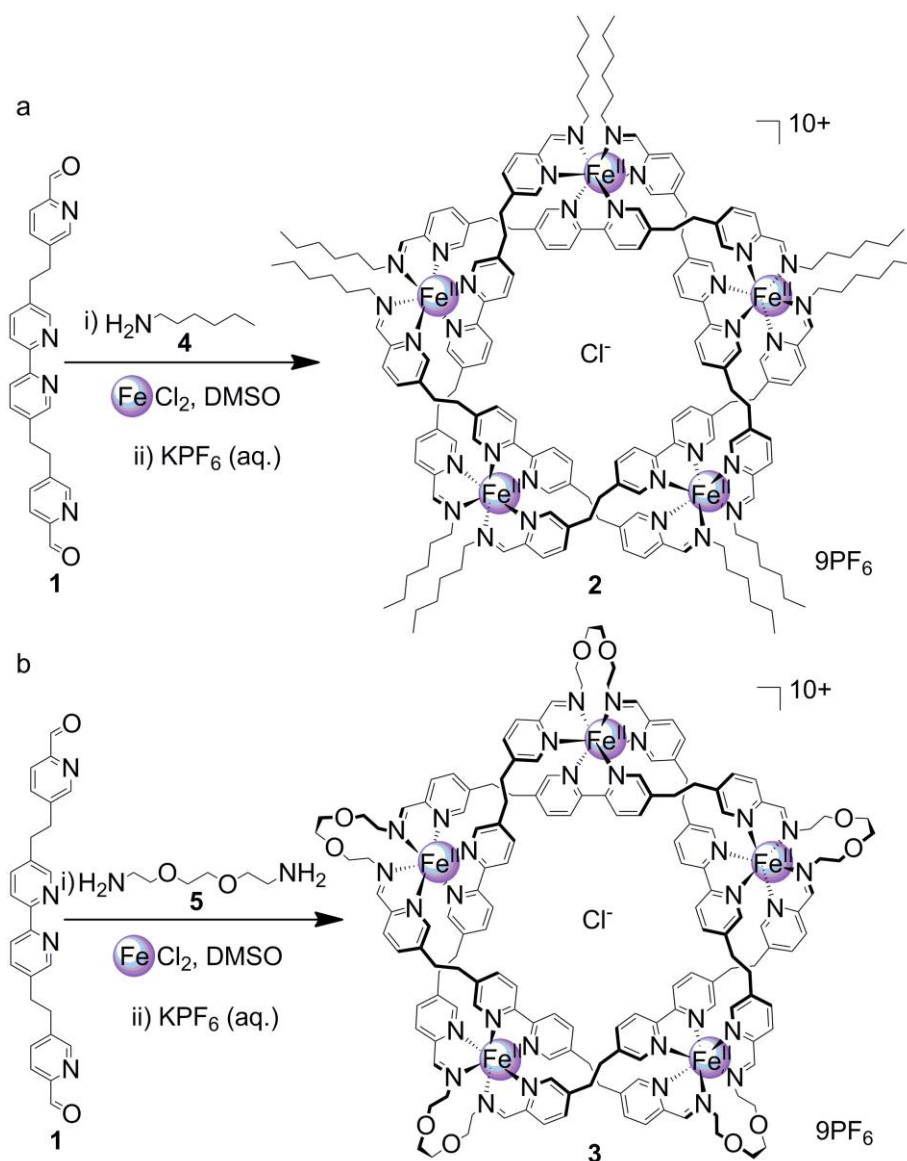
Molecular architectures self-assembled from reversible reactions are often the most thermodynamically stable structures formed from a wide distribution of theoretical product outcomes.¹ The inherent dynamic² nature of the interactions involved allows these systems to adapt to changes in conditions³ that alter the thermodynamic minimum of a given process.⁴ Introduction of specific chemical effectors such as templates⁵ or reagents⁶ can lead to drastic alterations of the product distribution of a reaction.⁷ Of these, metal templates⁸ continue to be a prominent tool for the construction of stable, complex supramolecular structures with increasingly impressive applications.⁹ The dynamic nature of the structure formation is usually credited with providing a means of error correction and allowing the thermodynamically preferred species to be selected from the landscape of possible alternatives. Despite it being acknowledged,^{1f} that "self-assembly under thermodynamic control" can be an overly-simplified description for many of these complicated multi-component processes, few have been studied in great detail. Likewise, there have been far fewer reports of self-assembly under non-equilibrium kinetic control,¹⁰ an essential process utilized by Nature.¹¹

5.3. Results and Discussion

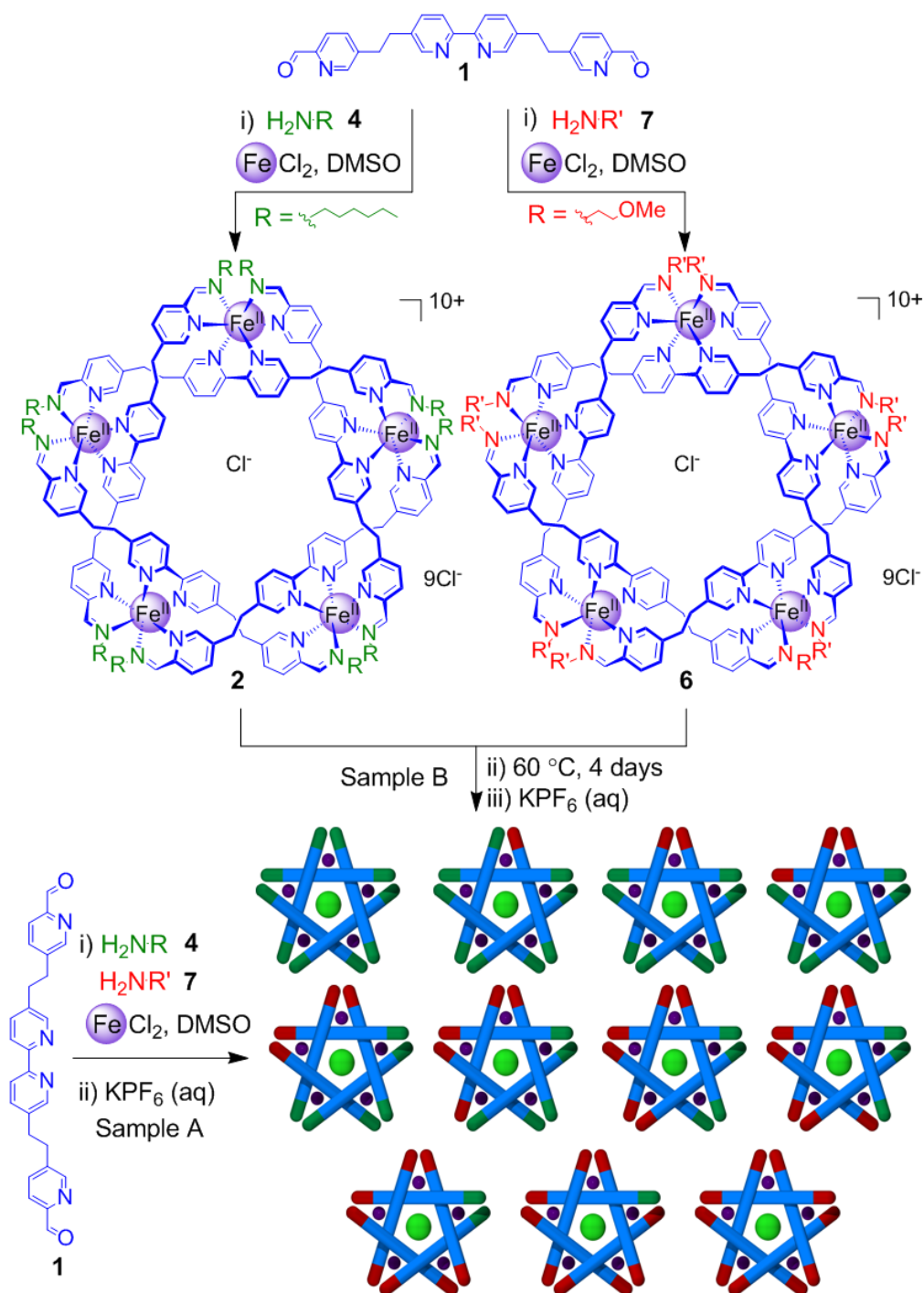
As an illustrative example, the use of aldehyde **1** in the self-assembly of pentameric circular helicates (such as complex **2**) and a molecular pentafoil knot (**3**)^{12,13} (Scheme 1) was rigorously analyzed and revealed some unexpected restrictions on the supramolecular formation processes. The assembly of these structures occurs spontaneously from 21 separate components (16 for knot **1**) when dialdehyde **3**, amine **4** (or diamine **5**) and FeCl₂

are combined in an appropriate stoichiometry in DMSO and heated for 24-48 hours at 60 °C.^{13,12} A two pronged approach was undertaken to investigate the reversibility and dynamic nature of the system. Firstly, the rate of imine exchange¹⁴ was investigated by conducting the reaction of dialdehyde **1** and FeCl₂ with similar amines. Secondly, the exchange of the central aldehyde residues¹⁵ was investigated by the use of a deuterium labeled derivative of aldehyde **1**, (**1-D₈**).

Scheme 1. Synthesis of (a) pentafoil knot **1 and (b) open helicate derivative **2**.**



Scheme 2. Exchange of amine residues on a pentameric circular helicate.



It has previously been noted that the addition of an excess of a primary amine to pentameric cyclic helicate **2** lead to partial decomposition of the complex,¹³ limiting the information about exchange processes which could be gathered. However, by mixing two preformed pentameric helicates derived from differing, but similar, amines (that is, helicates

2 and 6, Scheme 2) the exchange could be studied without requiring the use of an overall excess of amine.

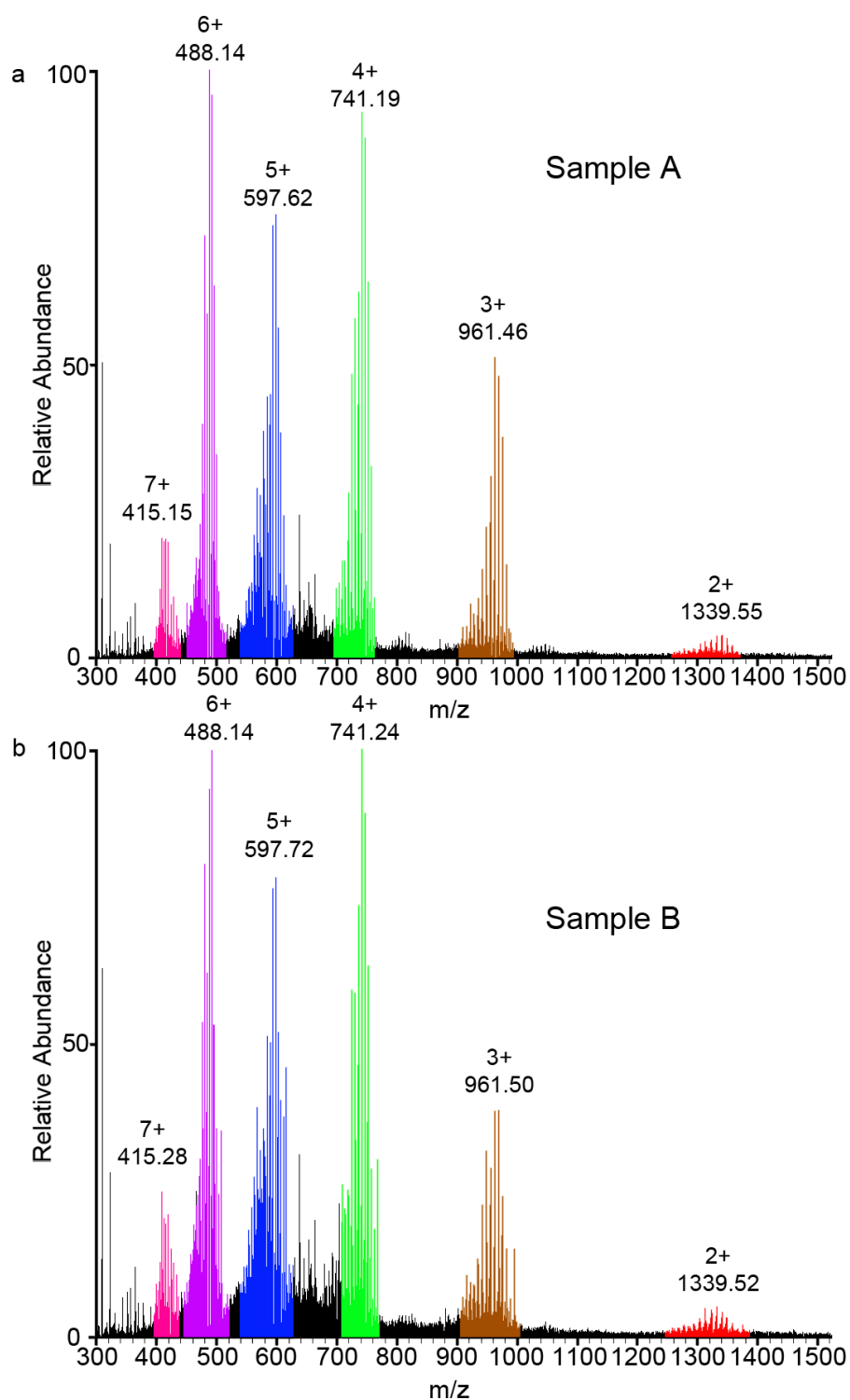


Figure 1. Low resolution electrospray ionization mass spectrometry analysis after anion exchange purification (a) sample A, a control sample, where amines 4 and 7 were mixed prior to addition to the reaction mixture, (b) sample B, where amines 4 and 7 were reacted separately

with aldehyde **1** to generate helicates **2** and **6** which were subsequently mixed and heated for 4 days at 60 °C. Peaks corresponding to helicates bearing n hexylamine residues and $(10 - n)$ 2-methoxyethyl amine residues (for $n = 0 - 10$) with varying numbers of PF_6^- counter-ions are evident.

To follow the exchange processes two reactions (Samples A and B, Scheme 2) were monitored. Firstly, a control reaction (Sample A) was performed using a 1:1 ratio of hexylamine **4** and methoxyethylamine **7** for the reaction with dialdehyde **1** and FeCl_2 , to ensure no thermodynamic bias between the two resulting structures (see Experimental Section for experimental details). After anion exchange with aqueous potassium hexafluorophosphate and dissolving in acetonitrile, the sample was analyzed by ^1H NMR and electrospray ionization mass spectrometry (ESI-MS). The ^1H NMR spectrum showed broad peaks indicative of the formation of a large number of similar species (Figure 4 and 6a) and ESI-MS (Figure 1a) confirmed the expected statistical distribution of 11 (not including regional isomers) pentameric circular helicates was formed bearing n hexylamine residues and $(10 - n)$ 2-methoxyethyl amine residues (for $n = 0 - 10$). This experiment confirms there is no significant thermodynamic preference between these two closely related helicates rendering them suitable for comparison.

The second reaction (Sample B, Scheme 2) was carried out where homoamine helicates **2** and **6** were preformed prior to mixing to investigate the amine exchange process. Aldehyde **1** was reacted with 2.2 equivalents of hexylamine under the standard reaction conditions.¹³ In a similar fashion aldehyde **1** was also reacted with 2.2 equivalents of 2-methoxyethyl amine under identical reaction conditions. After 1 day of heating these two reaction mixtures separately they were combined and heated for a further 4 days. Over time the two sets of signals in the ^1H NMR spectrum corresponding to homoamine helicates **2** and **6** were

observed to merge together to form broad signals indicative of the formation of mixed amine helicates (Figure 5). After 4 days no further changes to the ^1H NMR spectrum could be detected. The sample was precipitated by addition of aqueous KPF_6 , collected, washed and dissolved in CD_3CN . Comparison with control Sample A indicated that full scrambling of the amine residues had occurred: ^1H NMR (Figure 6) and ESI MS (Figure 1b) spectra for the two samples are identical, indicating the exchange of amines via imine hydrolysis is dynamic under the experimental conditions used and results in a thermodynamic distribution of amines about the helicate.

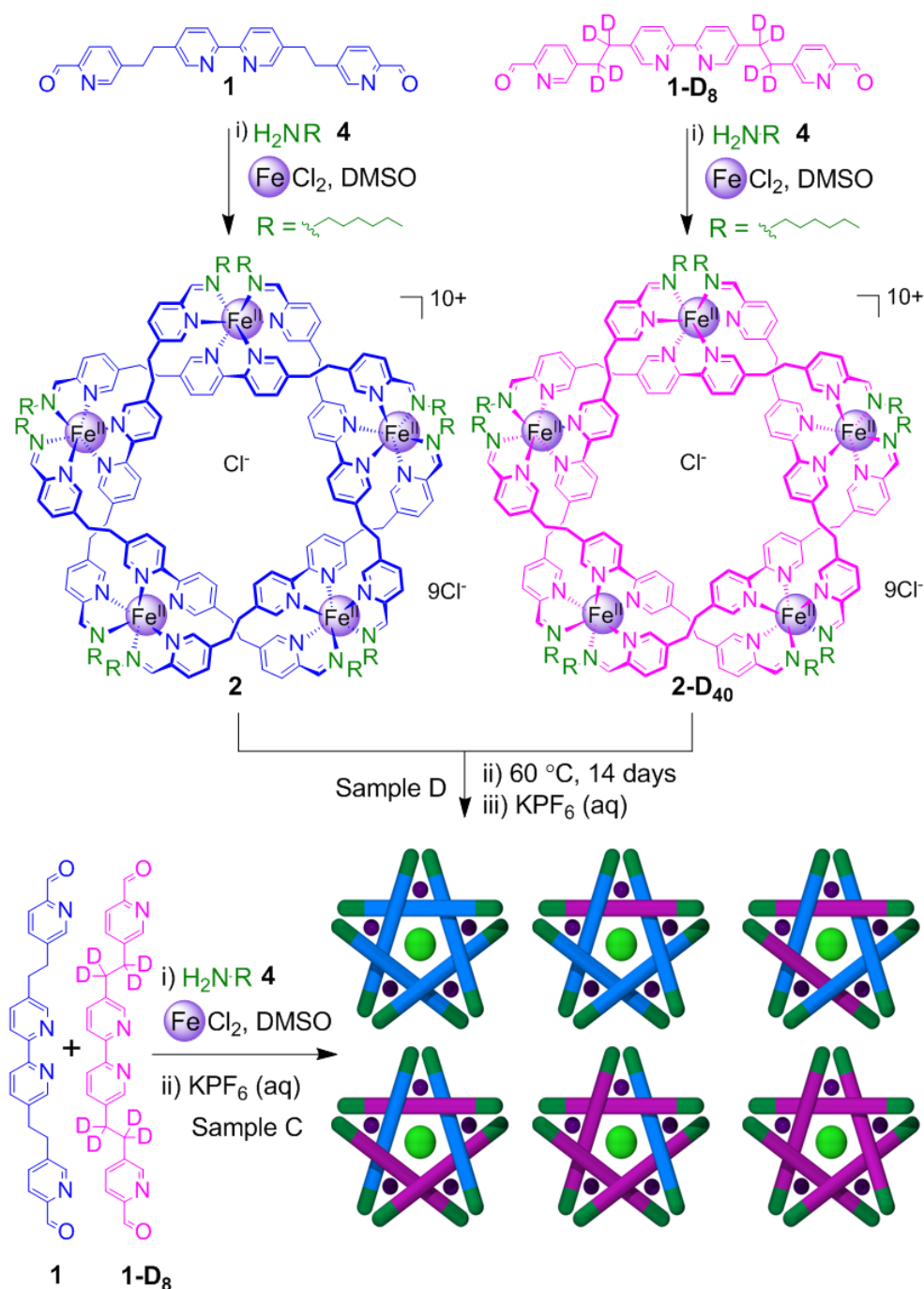
Having established the dynamic nature of the imine bonds of the helicates, the exchange of the core aldehyde residues, integral to overall structure of the helicate, was examined to investigate if the complete system is under thermodynamic control. Unlike imine exchange, the exchange of the central aldehyde requires a major structural re-arrangement, this is in contrast the type of exchange processes which have been typically reported for complex metallocsupramolecular assemblies¹⁶ wherein the exchange of each component is not detrimental to the overall structure, which essentially remains intact throughout the process and results in a very high degree of overall kinetic stability. A deuterated analogue of aldehyde **1** (**1-D₈**) was synthesized by modification of the synthesis of **1** (Scheme 7). As expected, aldehyde **1-D₈** was shown to behave in an exactly analogous fashion to aldehyde **1**.¹⁷ Using deuterium-labeled and non-labeled aldehydes it was possible to probe the dynamics of two different classes of reactions, namely those forming "open" pentameric circular helicates and those forming "closed" pentafoil knots.

The self-assembly of pentameric circular helicate **2** was investigated (Scheme 3) by a time-dependent mixing experiment. A control sample (Sample C), formed by reaction of 0.5

equivalents of aldehyde **1**, 0.5 equivalents of aldehyde **1-D₈**, 2.2 equivalents of hexylamine **4** and 1.1 equivalents of FeCl₂ in DMSO-*d*₆ was monitored over 14 days. ¹H NMR analysis of the mixture was consistent with any combination of the helicates depicted in Scheme 3. ESI-MS gave conclusive proof that the expected 1:5:10:10:5:1 statistical distribution of mixed aldehyde products (**2:2-D₈:2-D₁₆:2-D₂₄:2-D₃₂:2-D₄₀**) had been formed (Figure 2a) after 48 hours. This distribution of helicates remained constant when heating was continued for a further 12 days.

To monitor the exchange of aldehyde components between labeled and non-labeled helicates, aldehyde **1** was reacted with FeCl₂ and hexylamine **4** under the standard conditions for 1 day. Aldehyde **1-D₈** was reacted under identical conditions in a separate reaction. These two mixtures were combined and the resulting reaction (Sample D, Scheme 3) was heated at 60 °C and monitored over the course of 13 days by ESI-MS. After 1 day of heating predominately two species, homoaldehyde helicates **2** and **2-D₄₀**, were present. Samples taken after 3 and 6 days of heating indicate increasing quantities of mixed-aldehyde-derived products (Figure 2b-e). After 13 days of heating a nearly fully scrambled, statistical distribution was observed. ¹H NMR analysis of the sample after 13 days of heating exactly matched the spectrum of control sample, and showed the helicates to be fully intact, indicating heating for an extended period has not damaged the system (Figure 8).

Scheme 3. Exchange of aldehyde residues within a pentameric circular helicate.



The self-assembly of pentafoil knots was next investigated (Scheme 4). The experiment was conducted in an analogous method to that describe above replacing 2.2 equiv. of hexylamine **4** with 1.1 equiv. of diamine **5**. A control sample (Sample E) was formed by reaction of 0.5 equivalents of aldehyde **1** and 0.5 equivalents of aldehyde **1-D₈** with 1.1 equivalents of diamine **5** and FeCl_2 in DMSO. The ^1H NMR spectrum of the mixture was

consistent with the formation of mixed aldehyde species, however ESI-MS gave conclusive evidence of the expected formation of a 1:5:10:10:5:1 statistical distribution of mixed aldehyde pentafoil knots (**3:3-D₈:3-D₁₆:3-D₂₄:3-D₃₂:3-D₄₀**) (Figure 3a). This distribution of helicates remained constant throughout the entire experiment with no evidence of changes in composition.

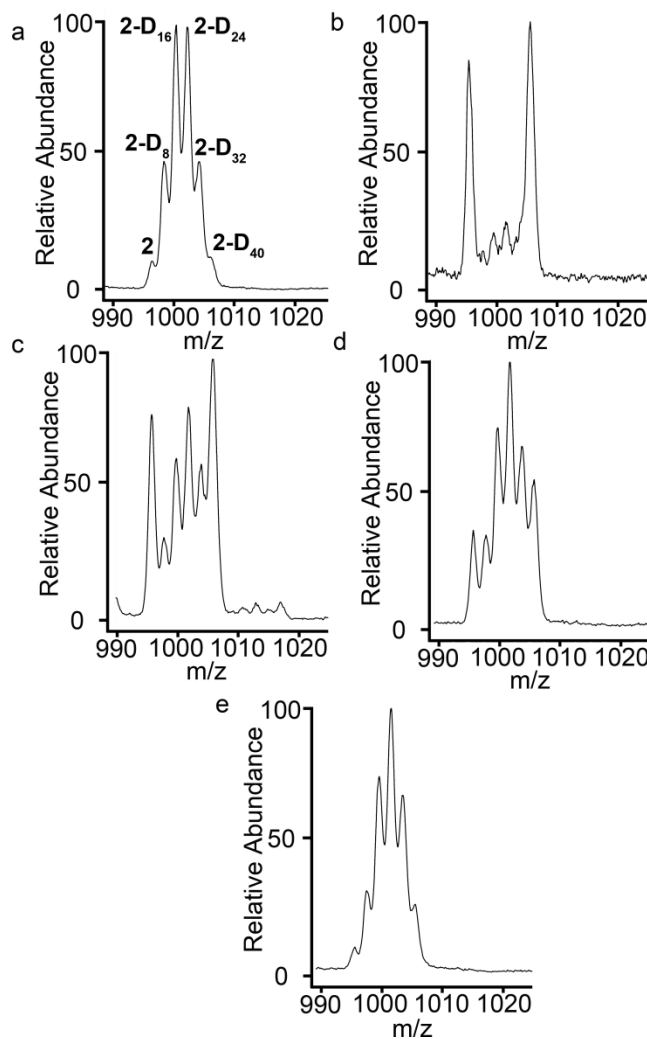
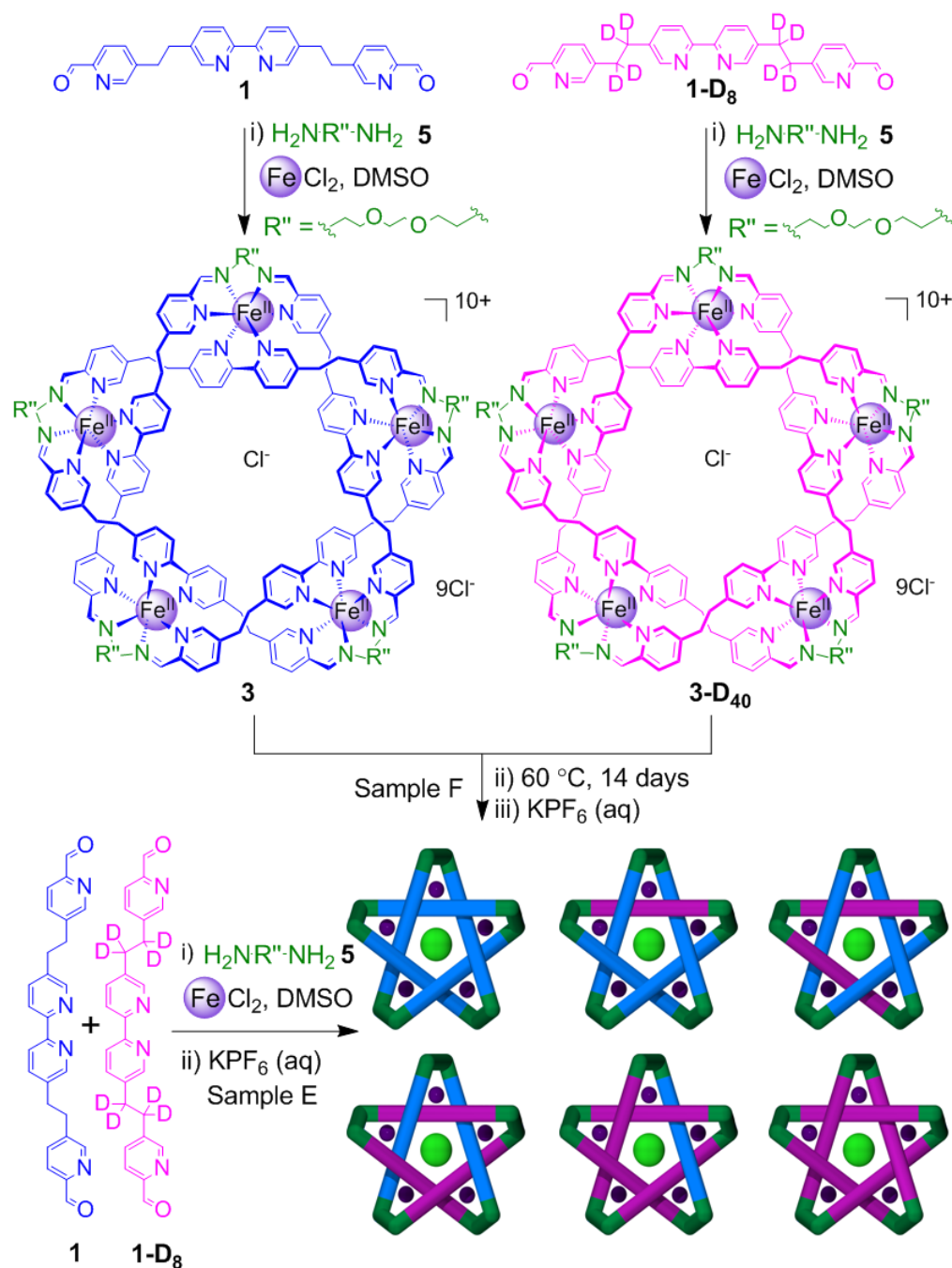


Figure 2. Low resolution electrospray ionization mass spectrometry analysis after anion exchange purification (a) sample C, a control sample, where aldehydes 1 and 1-D₈ were mixed prior to the addition of amine 4. Sample D, where aldehydes 1 and 1-D₈ were reacted separately with amine 4 to partially generate helicates 2 and 2-D₄₀ which were subsequently mixed and heated at 60 °C for (b) 1 day, (c) 3 days, (d) 6 days and (e) 13 days.

Scheme 4. Exchange of aldehyde residues within a pentafoil knot.



In order to observe the exchange of aldehyde residues between labeled and non-labeled pentafoil knots, aldehyde **1** was reacted with FeCl₂ and diamine **5** for 1 day at 60 °C. Likewise aldehyde **1-D₈** was reacted under identical conditions. These two reaction mixtures were combined and the resulting reaction (Sample F, Scheme 4) was maintained at 60 °C and monitored by ESI-MS over the course of 13 days. After 1 day of heating ESI-MS showed

predominately the presence of two species homoaldehyde pentafoil knots **3** and **3-D₄₀** (Figure 3b). Samples taken from the mixture after 3 and 6 days of heating indicate that pentafoil knots **3** and **3-D₄₀** are still dominant however small quantities of mixed aldehyde products are evident (Figure 3c and d).

After 13 days of heating significant scrambling has taken place although the distribution is far from statistical (Figure 3e) and no significant degradation was observed (Figure 10). Prolonged reaction times in excess of two weeks led to eventual degradation of the pentafoil knot system, possibly due to oxidation effects, however it would appear that if the reaction could be continued that full scrambling would be observed.

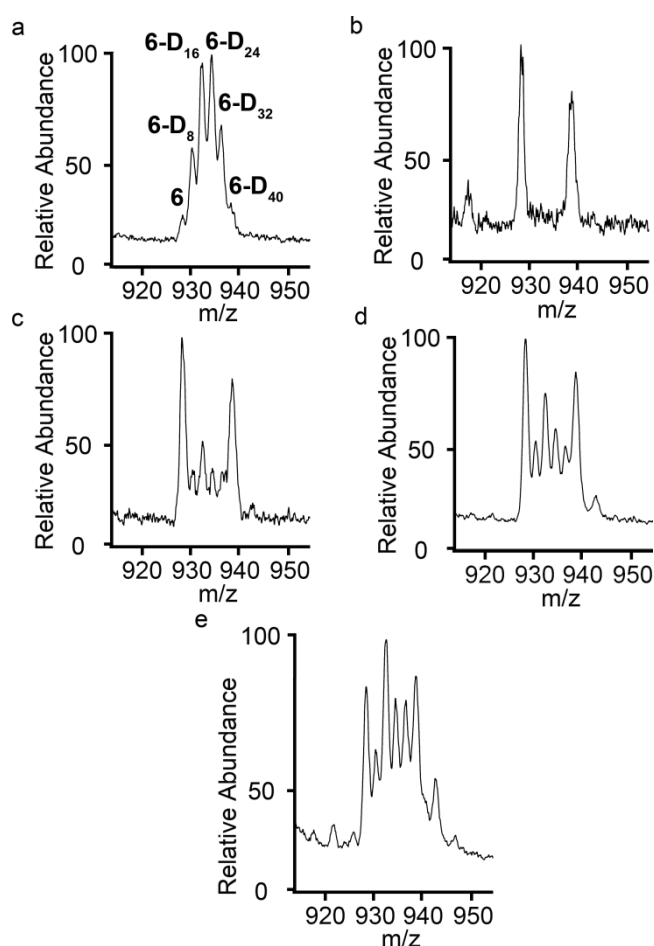


Figure 3. Low resolution electrospray ionization mass spectrometry analysis after anion exchange purification (a) sample E, a control sample, where aldehydes 1 and 1-D₈ were mixed prior to the addition of diamine 5. Sample F, where aldehydes 1 and 1-D₈ were reacted

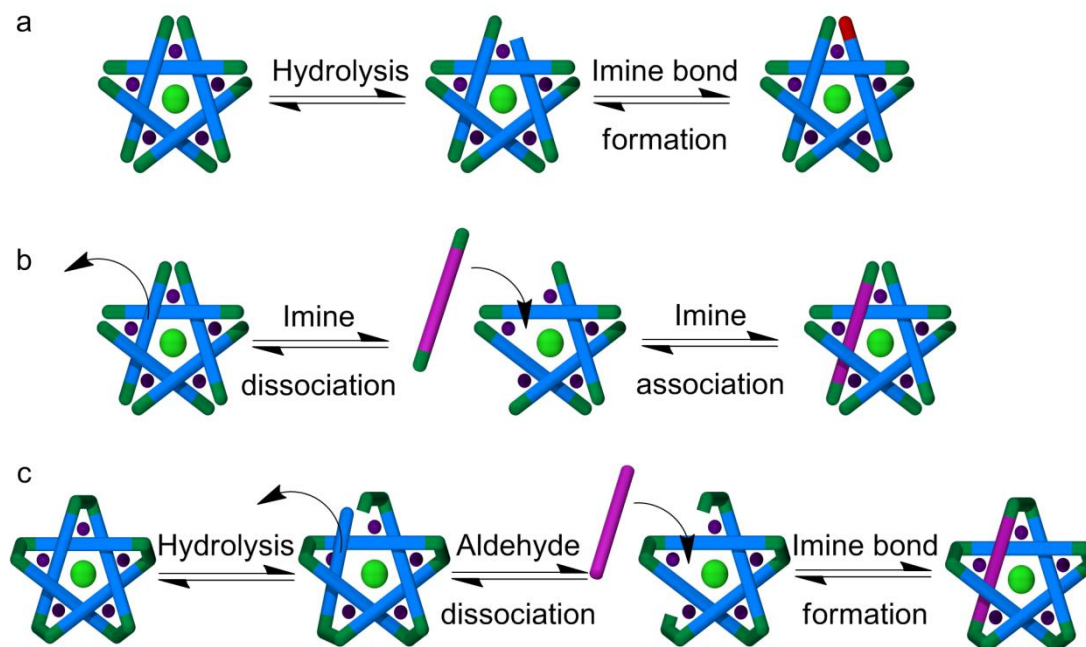
separately with diamine **5** to partially generate pentafoil knots **3** and **3-D₄₀** which were subsequently mixed and heated at 60 °C for (b) 1 day, (c) 3 days, (d) 6 days and (e) 13 days.

5.4. Conclusion

By carrying out three separate, but similar experiments it was possible to simply and fully probe the dynamic nature of this system. The exchange reactions of the peripheral amine residues of the helicates were established to be dynamic and the internal aldehyde residues of the helicate were also demonstrated to undergo exchange, albeit on a much longer timescale. This increase in reaction time can be rationalized in that amine exchange can take place without the degradation of the helicate structure (Scheme 5a). Hydrolysis of the imine bond and dissociation of the amine are the only requisites of efficient amine exchange. The remaining aldehyde unit is still able to coordinate the iron(II) centers and exchange requires the removal of the whole ligand by breaking two Fe-N(imine) and four Fe-N(pyridine) bonds (Scheme 5b)—a far more energetically demanding process. However over the course of ~14 days both processes must occur and the system is therefore under thermodynamic control under these conditions, as all elements of the system are in dynamic exchange.

By comparison far slower exchange dynamics are observed for the pentafoil knot **3**. This is easily rationalized by considering one potential mechanism of exchange highlighted in Scheme 5c. Unlike for the 'open' systems, for the 'closed' systems the only mechanism for exchange of the dialdehyde component is the hydrolysis¹⁸ of both the imine bonds.

Scheme 5. Schematic representation of possible amine (a) and aldehyde exchange mechanisms (b and c) within 'open' pentameric cyclic helicates (a and b) and 'closed' pentafoil knots (c).

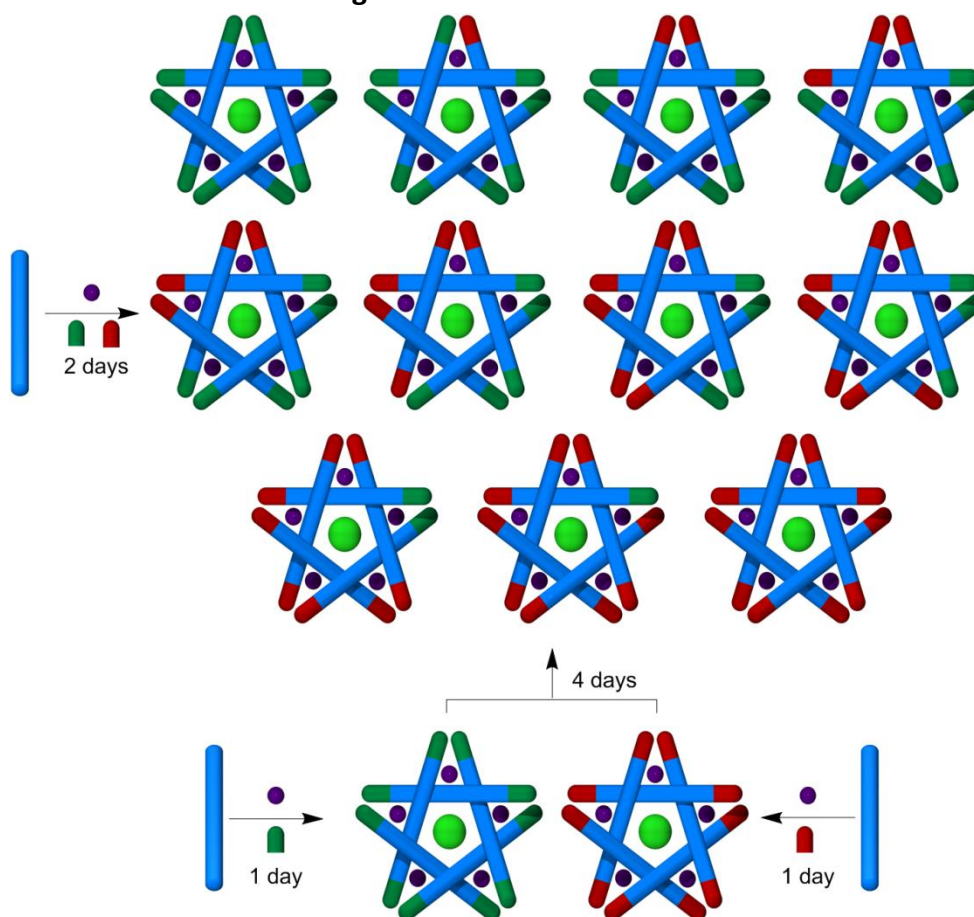


This coupling of imine bond hydrolysis and aldehyde removal greatly slows the overall exchange process leading to far longer exchange times, such that potentially only over the course of many months will full exchange occur and the self-assembly of all the structures presented in this study be under true thermodynamic control. It is proposed, therefore, that certain kinetic factors must be responsible for the initial assembly of these species leading to high yields of products after a reaction time of only 2 days. This key finding clearly demonstrates the pitfalls associated with the analysis of self-assembly processes and in so doing, highlights the potential for systems self-assembled under thermodynamic control to be greatly accelerated by kinetically irreversible processes and to deliver the type of non-equilibrium systems necessary to more closely mimic Nature's mastery of self-assembly processes.

5.5. Experimental Section

5.5.1. Amine Exchange on Pentameric Circular Helicates

5.5.1.1. Experimental Procedure for the Thermodynamic Investigations of Amine Scrambling



Scheme 6. Schematic diagram showing the synthesis of mixed amine pentameric cyclic helicates. Mixing the two amines (hexylamine **3**, green; 2-methoxyethylamine **4**, red) at the start of the reaction gives a statistical distribution of mixed amine helicates (only one positional isomer is shown where appropriate). Whereas two preformed homoamine helicates, when mixed, undergo exchange generating the same distribution of mixed species as above over the course of 4 days.

To two separate DMSO- d_6 solutions of **1** (4 mg, 9.5 μmol , in 2.0 mL) was added FeCl_2 (100 μL of a 0.10 M stock solution, 10.5 μmol). The purple solution was mixed thoroughly to ensure complete dissolution of the aldehyde. To a 1.0 mL aliquot of **1**+ FeCl_2 was added hexylamine

3 (25 μL of a 0.20 M stock solution, 5.2 μmol) and 2-methoxyethylamine **4** (25 μL of a 0.20 M stock solution, 5.2 μmol) (sample A). To a 0.5 mL aliquot of **1**+FeCl₂ was added hexylamine **3** (25 μL of a 0.20 M stock solution, 5.2 μmol) only. To the remaining 0.5 mL aliquot of **1**+FeCl₂ was added 2-methoxyethylamine **4** (25 μL of a 0.20 M stock solution, 5.2 μmol) only. The three solutions were heated for 1d at 60 °C. The solutions of **1**+FeCl₂+**3** and **1**+FeCl₂+**4** were combined in a clean NMR tube and thoroughly mixed (sample B) before being heated at 60 °C for a further 4 days. Both samples (A and B) were monitored over time (Figures S1 and S2). The two samples (A and B) were allowed to cool and the following purification procedure was applied to each sample individually: The reaction mixture was precipitated using KPF₆ (saturated aqueous solution). The resulting purple powder was collected on celite and washed with water, EtOH, CH₂Cl₂ and finally Et₂O. The product mixture was dissolved in CH₃CN and the solvent removed in vacuo. Both samples were dissolved in 0.5 mL of CD₃CN and compared by ¹H NMR (Figure 6) and LRESI-MS (see Figure 1).

5.5.1.2. ^1H NMR Analysis for the Thermodynamic Investigations of Amine Scrambling

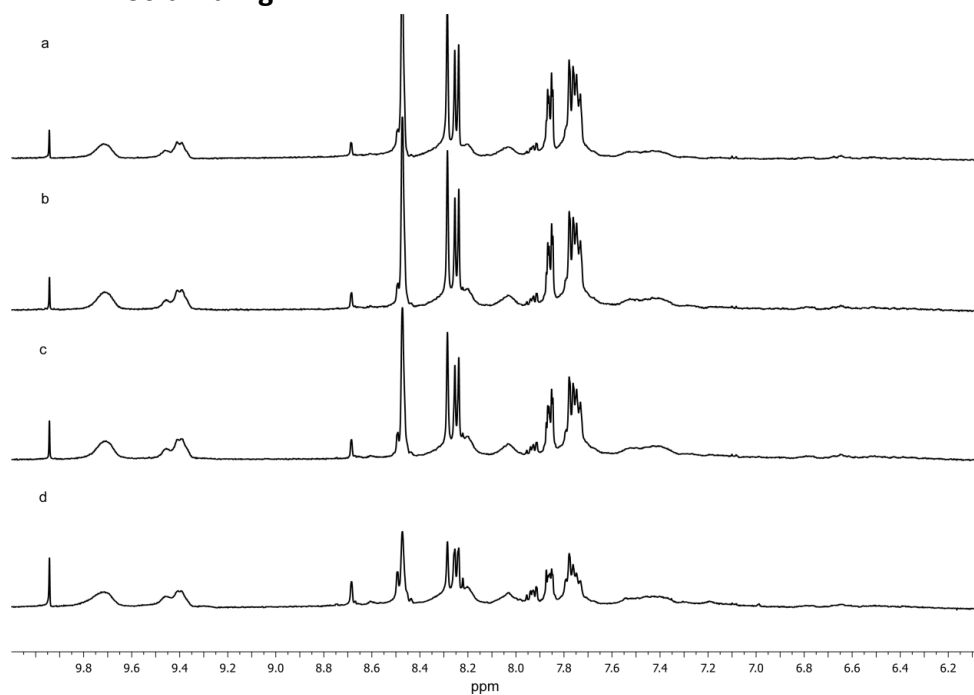


Figure 4. ^1H NMR (CD_3SOCD_3 , 500 MHz) analysis of the crude mixture of sample A after heating at 60 °C for; (a) 1 day, (b) 2 days, (c) 3 days, (d) 4 days.

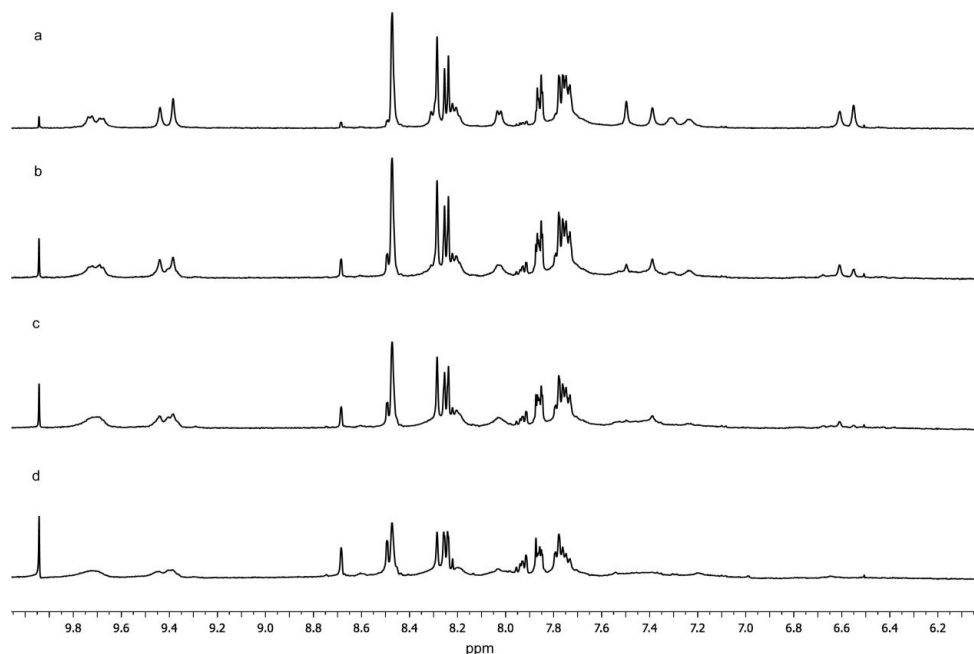


Figure 5. ^1H NMR (CD_3SOCD_3 , 500 MHz) analysis of the crude mixture of sample B after heating at 60 °C for; (a) 1 day, (b) 2 days, (c) 3 days, (d) 4 days.

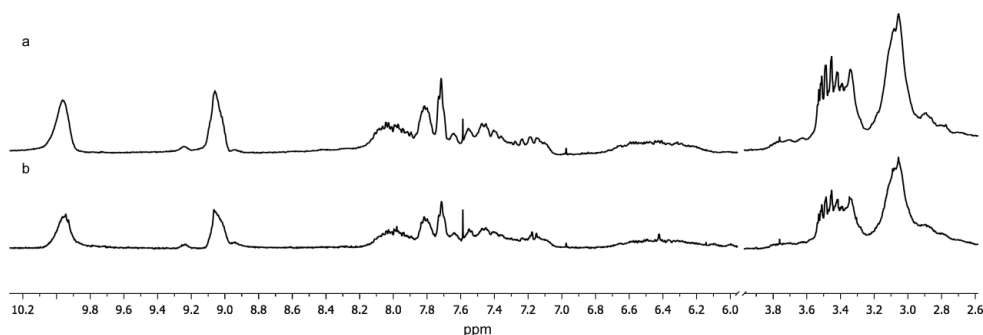
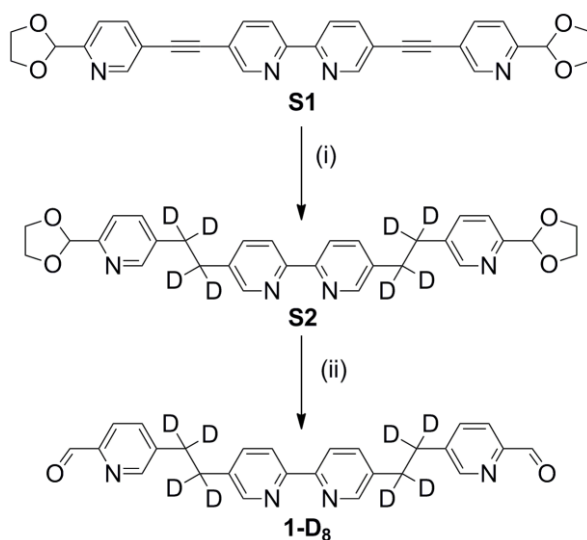


Figure 6. ^1H NMR (CD_3CN , 500 MHz) analysis after purification; (a) Sample A (b) Sample B.

5.5.2. Aldehyde Exchange on Pentameric Circular Helicate 2

5.5.2.1. Synthesis of labeled aldehyde 1-D_8



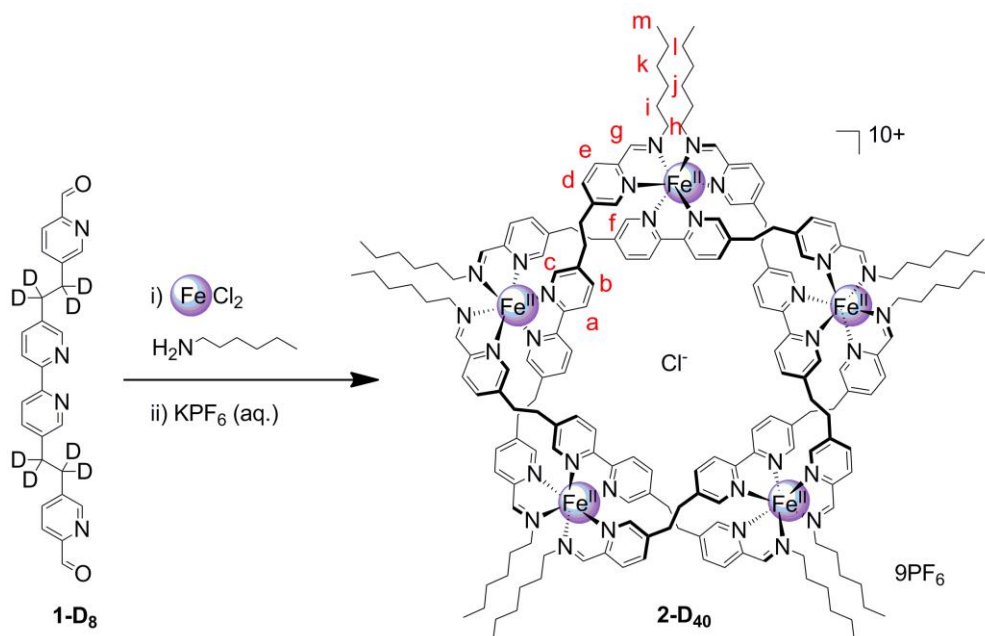
Scheme 7. Preparation of dialdehyde 1-D_8 . Reagents and conditions: (i) D_2 , $\text{Pd}(\text{OH})_2/\text{C}$, MeOH-d_4 , THF, 2d, quant. (ii) HCl, reflux, 1 h, quant.

S1¹² (200 mg, 0.40 mmol) was suspended in THF: MeOD-d_4 2:1 (30 mL) and 20 % w/w $\text{Pd}(\text{OH})_2/\text{C}$ (51 mg) was added. The mixture was stirred under an atmosphere of D_2 for 48 h. The mixture was filtered under gravity and washed with CH_2Cl_2 (20 mL). The solvent was

removed under reduced pressure to give **S2** an off white solid which was used in the subsequent step without further purification.

S2 was dissolved in 10 % aqueous HCl (25 mL) and heated under reflux for 1 h. Once the reaction mixture had cooled to room temperature it was neutralized by slow addition of NaHCO₃ (saturated aqueous solution). The aqueous mixture was extracted with CH₂Cl₂ (2 × 20 mL). The organic layer was washed with water (2 × 30 mL) then brine (30 mL), dried (MgSO₄), filtered under gravity and the solvent removed under reduced pressure. Flash chromatography (CH₂Cl₂ to CH₂Cl₂:EtOAc 1:4) followed by precipitation from CH₂Cl₂ by addition of pentane gave dialdehyde **1-D₈** as a white solid (150 mg, 0.35 mmol, 87 % yield from **S1**) ¹H NMR (400 MHz, CDCl₃) δ 10.05 (s, 2H), 8.58 (dd, J = 2.1, 0.7 Hz, 2H), 8.45 (d, J = 1.7 Hz, 2H), 8.32 (d, J = 7.7 Hz, 2H), 7.89 (dd, J = 7.9, 0.7 Hz, 2H), 7.61 (m, 4H), ¹³C NMR (126 MHz, CDCl₃) δ = 193.2, 154.0, 151.5, 150.6, 149.1, 141.1, 137.5, 137.1, 135.8, 121.8, 121.1, 34.2 – 32.7 (m, 4 carbons).

5.5.2.2. Experimental Procedure for the Synthesis of Helicate **2-D₄₀**



Scheme 8. Preparation of deuterated cyclic helicate **2-D₄₀**. Reagents and conditions: (i) 60 °C, DMSO-*d*₆, 1d. (ii) Precipitation by addition of an aqueous solution of KPF₆. Overall yield, 61%.

To a solution of dialdehyde **1-D₈** (2.0 mg, 4.6 μmol , 1.0 eq.) in DMSO- d_6 (1.0 mL) was added a solution of anhydrous FeCl_2 (50 μL of a 0.1 M DMSO- d_6 solution, 5.1 μmol , 1.1 eq.) followed by a DMSO- d_6 solution of hexylamine (50 μL , 0.2 M, 10.1 μmol , 2.2 eq.). The resulting dark purple reaction was thoroughly mixed and heated at 60 $^\circ\text{C}$ for one day. After cooling to room temperature, excess saturated aqueous KPF_6 was added (5.0 mL). A fine suspension of a purple material formed which was collected on celite, thoroughly washed with water, EtOH, CH_2Cl_2 and diethylether. The purple solid was dissolved in acetonitrile and concentrated under reduced pressure to give **2-D₄₀** as a purple powder (2.6 mg, 61 %). ^1H NMR (500 MHz, CD_3CN) δ 9.94 (d, $J = 8.3$ Hz, 10H, H^a), 9.06 (s, 10H, H^g), 7.98 (d, $J = 8.0$ Hz, 10H, H^e), 7.82 (d, $J = 8.0$ Hz, 10H, H^d), 7.53 (d, $J = 8.5$ Hz, 10H, H^b), 7.17 (s, 10H, H^c), 6.42 (s, 10H, H^f), 3.35 (m, 10H, H^h), 3.05 (m, 10H, H^i), 1.62–1.39 (m, 20H, H^j), 1.19 (m, 20H, H^k), 1.15–1.03 (m, 40H, H^k and H^l), 0.84 (t, $J = 7.2$, 30H, H^m).

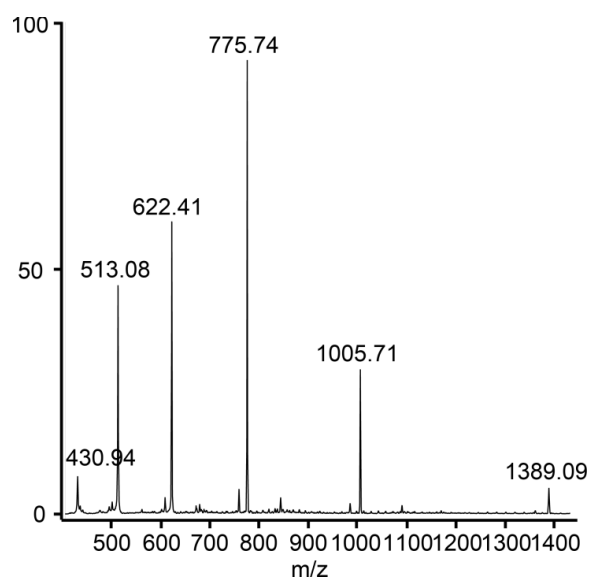
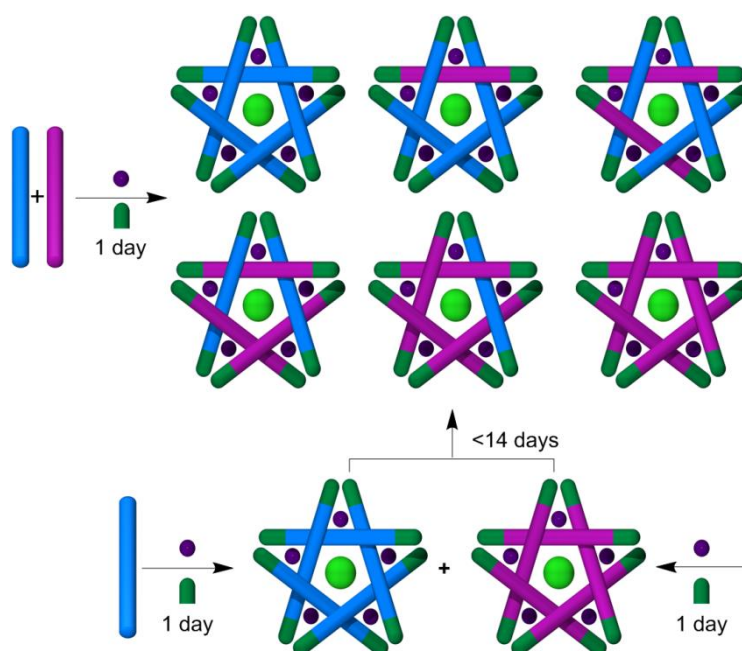


Figure 7. LRESI MS analysis after purification of cyclic helicate **2-D₄₀**. Peaks indicate sequential loss of PF_6^- counter-ions.

5.5.2.3. Experimental Procedure for the Thermodynamic Investigations of Aldehyde Scrambling on Helicates **2** and **2-D₄₀**



Scheme 9. Schematic diagram showing the synthesis of mixed aldehyde pentameric cyclic helicates. Mixing the two aldehydes (**1**, blue; **1-D₈**, pink) at the start of the reaction gives a statistical distribution of mixed aldehyde helicates (only one positional isomer is shown where appropriate). Whereas two preformed homoaldehyde helicates, when mixed, undergo exchange generating a similar distribution of mixed species as above over the course of 13 days.

To two separate DMSO-*d*₆ solutions of **1** (1.9 mg, 4.6 μmol, in 1.0 mL) and **1-D₈** (2.0 mg, 4.6 μmol in 1.0 mL) was added FeCl₂ (50 μL of a 0.10 M stock solution, 5.1 μmol). The two purple solutions were mixed thoroughly to ensure complete dissolution of both aldehydes. A 0.5 mL aliquot of **1**+FeCl₂ was mixed with a 0.5 mL aliquot of **1-D₈**+FeCl₂ in a clean NMR tube before addition of hexylamine **3** (50 μL of a 0.21 M stock solution, 10.2 μmol) (Sample C). The remaining 0.5 mL aliquots of **1**+FeCl₂ and **1-D₈**+FeCl₂ were separately reacted with hexylamine **3** (25 μL of a 0.21 mM stock solution, 2.6 μmol, for each reaction). The three solutions were heated for 1d at 60 °C. The solutions of **1**+FeCl₂+**3** and **1-D₈**+FeCl₂+**3** were combined in a clean NMR tube and thoroughly mixed (Sample D) before being heated at 60

°C for a further 13 days. Both samples were monitored over time (Figure 2). At each time point (1, 3, 6 and 13 days) a small sample (0.2 mL) was removed from each reaction mixture, allowed to cool and the following purification procedure was applied to each sample individually: The reaction mixture was precipitated using KPF_6 (saturated aqueous solution). The resulting purple powder was collected on celite and washed with water, EtOH, CH_2Cl_2 and finally Et_2O . The product mixture was dissolved in CH_3CN and the solvent removed in vacuo. Both samples were dissolved in 0.5 mL of CH_3CN and compared by LRESI MS (see Figure 2).

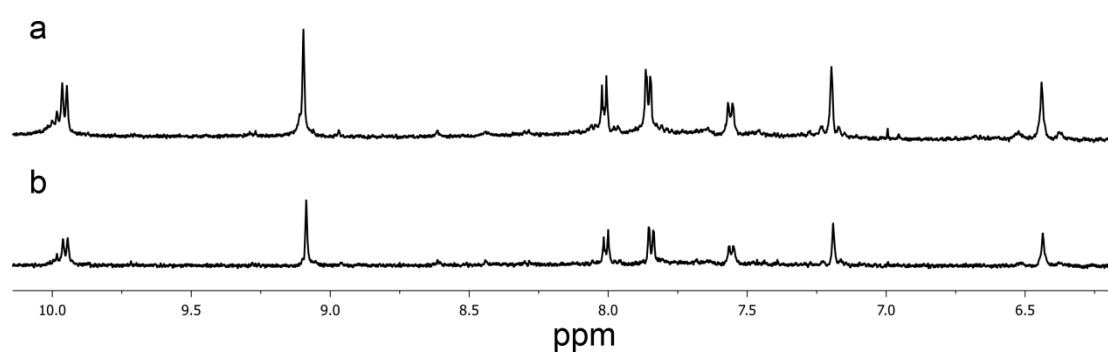
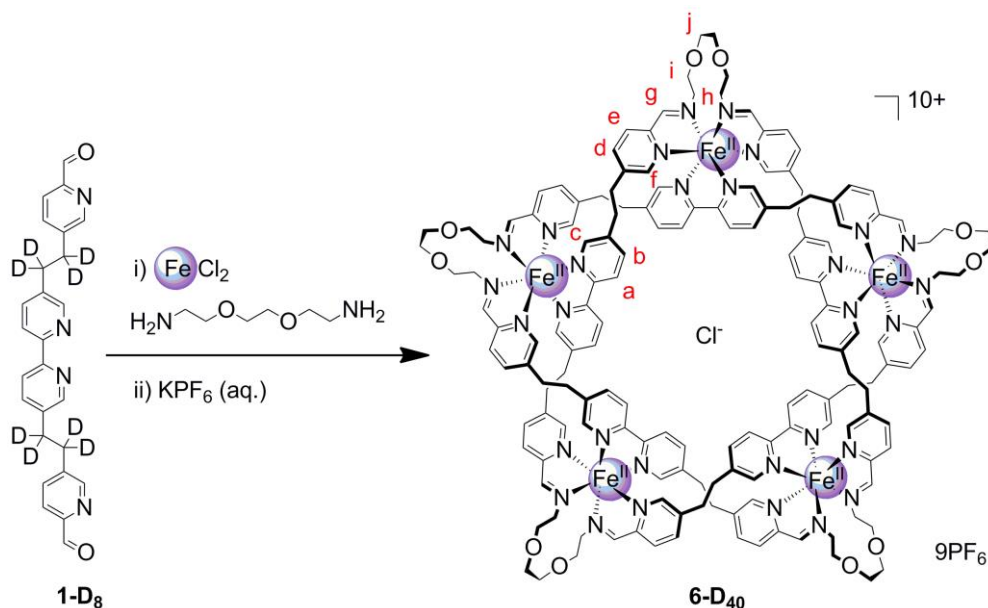


Figure 8. ^1H NMR (CD_3CN , 500 MHz) analysis of (a) Sample C and (b) Sample D after 13 days of heating at 60 °C followed by purification.

5.5.3. Aldehyde Exchange on Pentafoil Knot 6

5.5.3.1. Experimental Procedure for the Synthesis of Pentafoil Knot 6-D₄₀

Scheme 10. Preparation of deuterated pentafoil knot **6-D₄₀**. Reagents and conditions: (i) 60 °C, DMSO-*d*₆, 2d. (ii) Precipitation by addition of an aqueous solution of KPF₆. Overall yield, 39%.

To a solution of dialdehyde **1-D₈** (2.0 mg, 4.6 μmol, 1.0 eq.) in DMSO-*d*₆ (1.0 mL) was added a solution of anhydrous FeCl₂ (50 μL of a 0.10 mM DMSO-*d*₆ solution, 5.1 μmol, 1.1 eq.) followed by a DMSO-*d*₆ solution of 2,2'-(ethylenedioxy)bis(ethylamine) (50 μL, 0.10 M, 5.1 μmol, 1.1 eq.). The resulting dark purple reaction was thoroughly mixed and heated at 60 °C for 24 h. After cooling to room temperature, excess saturated aqueous KPF₆ was added (5.0 mL). A fine suspension of a purple material formed which was collected on celite, thoroughly washed with water, EtOH, CH₂Cl₂ and diethylether. The purple solid was dissolved in acetonitrile and concentrated under reduced pressure to give **6-D₄₀** as a purple powder (1.6 mg, 39 %). ¹H NMR (500 MHz, CD₃CN) δ 9.92 (d, *J* = 8.3 Hz, 10H, H^a), 9.04 (s, 10H, H^b), 8.03 (d, *J* = 8.1 Hz, 10H, H^c), 7.86 (d, *J* = 8.1 Hz, 10H, H^d), 7.51 (d, *J* = 8.0 Hz, 10H,

H^b), 7.19 (s, 10H, H^c), 6.43 (s, 10H, H^f), 4.11 (m, 10H, H^h), 3.67 (d, $J = 10.0$ Hz, 20H, H^i and H^j), 3.32 (d, $J = 9.8$ Hz, 10H, H^j), 3.23 (d, $J = 11.3$ Hz, 10H, H^h), 2.96 (m, 10H, H^i).

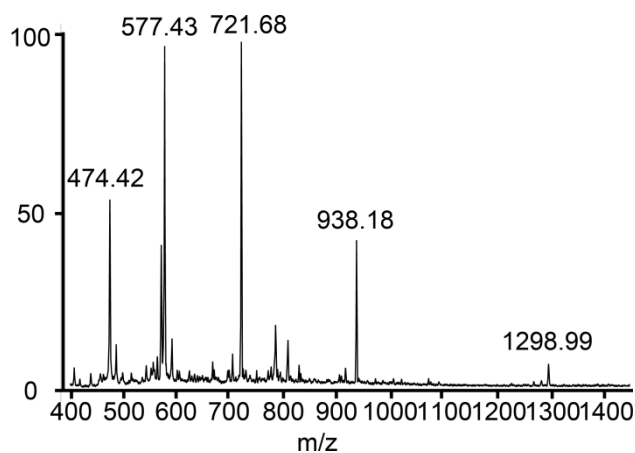
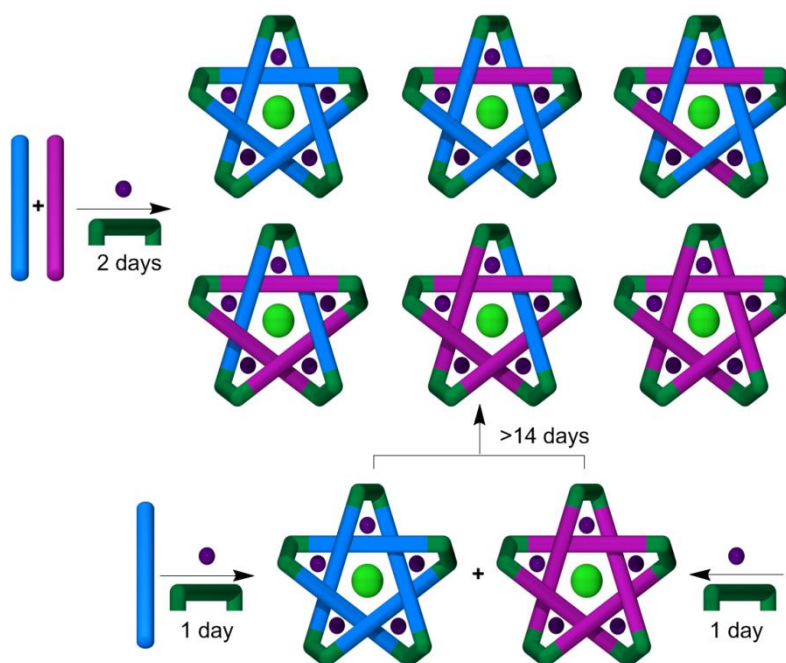


Figure 9. LRESI MS analysis after purification of cyclic helicate **6-D₄₀**. Peaks indicate sequential loss of PF_6^- counter-ions.

5.1.1.1. Experimental Procedure for the Thermodynamic Investigations of Aldehyde Scrambling on Pentafoil Knots **6** and **6-D₄₀**



Scheme 11. Schematic diagram showing the synthesis of mixed aldehyde pentafoil knots. Mixing the two aldehydes (**1**, blue; **1-D₈**, pink) at the start of the reaction gives a statistical distribution

of mixed aldehyde pentafoil knots (only one positional isomer is shown where appropriate). Whereas two preformed homoaldehyde helicates, when mixed, undergo slow exchange.

To two separate DMSO- d_6 solutions of **1** (1.9 mg, 4.6 μmol , in 1.0 mL) and **1-D₈** (2.0 mg, 4.6 μmol in 1.0 mL) was added FeCl₂ (50 μL of a 0.10 M stock solution, 5.1 μmol). The two purple solutions were mixed thoroughly to ensure complete dissolution of both aldehydes. A 0.5 mL aliquot of **1**+FeCl₂ was mixed with a 0.5 mL aliquot of **1-D₈**+FeCl₂ in a clean NMR tube before addition of 2,2'-(ethylenedioxy)bis(ethylamine) **7** (50 μL of a 0.10 mM stock solution, 5.1 μmol) (Sample E). The remaining 0.5 mL aliquots of **1**+FeCl₂ and **1-D₈**+FeCl₂ were separately reacted with 2,2'-(ethylenedioxy)bis(ethylamine) **7** (25 μL of a 0.10 mM stock solution, 2.6 μmol , for each reaction). The three solutions were heated for 1d at 60 °C. The solutions of **1**+FeCl₂+**7** and **1-D₈**+FeCl₂+**7** were combined in a clean NMR tube and thoroughly mixed (Sample F) before being heated at 60 °C for a further 13 days. Both samples were monitored over time (Figure 3). At each time point (1, 3, 6 and 13 days) a small sample (0.2 mL) was removed from each reaction mixture, allowed to cool and the following purification procedure was applied to each sample individually: The reaction mixture was precipitated using KPF₆ (saturated aqueous solution). The resulting purple powder was collected on celite and washed with water, EtOH, CH₂Cl₂ and finally Et₂O. The product mixture was dissolved in CH₃CN and the solvent removed in vacuo. Both samples were dissolved in 0.5 mL of CH₃CN and compared by LRESI MS (see Figure 3).

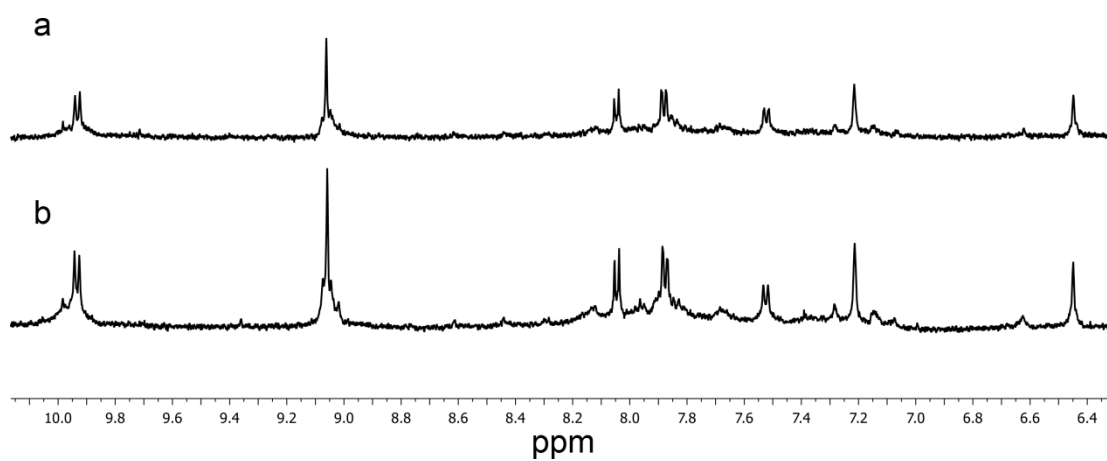


Figure 10. ¹H NMR (CD₃CN, 500 MHz) analysis of (a) Sample E and (b) Sample F after 13 days of heating at 60 °C followed by purification.

5.6. Notes and References

1. (a) Zeckert, K.; Hamacek, J.; Rivera, J.-P.; Floquet, S.; Pinto, A.; Borkovec, M.; Piguet, C. *J. Am. Chem. Soc.* **2004**, *126*, 11589-11601; (b) Hamacek, J.; Borkovec, M.; Piguet, C. *Chem.-Eur. J.* **2005**, *11*, 5227-5237; (c) Piguet, C.; Borkovec, M.; Hamacek, J.; Zeckert, K. *Coord. Chem. Rev.* **2005**, *249*, 705-726; (d) Hamacek, J.; Borkovec, M.; Piguet, C. *Dalton Trans.* **2006**, 1473-1490; (e) Riis-Johannessen, T.; Dalla Favera, N.; Todorova, T. K.; Huber, S. M.; Gagliardi, L.; Piguet, C. *Chem. Eur. J.* **2009**, *15*, 12702-12718; (f) Piguet, C. *Chem. Commun.* **2010**, *46*, 6209-6231; (g) Aboshyan-Sorgho, L.; Cantuel, M.; Bernardinelli, G.; Piguet, C. *Dalton Trans.* **2012**, *41*, 7218-7226.
2. (a) Lehn, J.-M. *Chem. Eur. J.* **1999**, *5*, 2455-2463; (b) Rowan, S. J.; Cantrill, S. J.; Cousins, G. R. L.; Sanders, J. K. M.; Stoddart, J. F. *Angew. Chem., Int. Ed.* **2002**, *41*, 898-952; (c) Corbett, P. T.; Leclaire, J.; Vial, L.; West, K. R.; Wietor, J.-L.; Sanders, J. K. M.; Otto, S. *Chem. Rev.* **2006**, *106*, 3652-3711; (d) Hunt, R. A. R.; Otto, S. *Chem. Commun.* **2011**, *47*, 847-858; (e) Moulin, E.; Cormos, G.; Giuseppone, N. *Chem. Soc. Rev.* **2012**, *41*, 1031-1049.
3. (a) Furlan, R. L. E.; Otto, S.; Sanders, J. K. M. *Proc. Natl Acad. Sci. U. S. A.* **2002**, *99*, 4801-4804; (b) Mirtschin, S.; Slabon-Turski, A.; Scopelliti, R.; Velders, A. H.; Severin, K. *J. Am. Chem. Soc.* **2010**, *132*, 14004-14005; (c) Hafezi, N.; Lehn, J.-M. *J. Am. Chem. Soc.* **2012**, *134*, 12861-12868.
4. Barrell, M. J.; Campaña, A. G.; von Delius, M.; Geertsema, E. M.; Leigh, D. A. *Angew. Chem., Int. Ed.* **2011**, *50*, 285-290.
5. (a) Chichak, K. S.; Cantrill, S. J.; Pease, A. R.; Chiu, S.-H.; Cave, G. W. V.; Atwood, J. L.; Stoddart, J. F. *Science* **2004**, *304*, 1308-1312; (b) Lam, R. T. S.; Belenguer, A.; Roberts, S. L.; Naumann, C.; Jarrosson, T.; Otto, S.; Sanders, J. K. M. *Science* **2005**, *308*, 667-669; (c) Fujii, S.; Lehn, J.-M. *Angew. Chem., Int. Ed.* **2009**, *48*, 7635-7638; (d) Bhat, V. T.; Caniard, A. M.; Luksch, T.; Brenk, R.; Campopiano, D. J.; Greaney, M. F. *Nature Chem.* **2010**, *2*, 490-497.
6. Campbell, V. E.; de, H. X.; Delsuc, N.; Kauffmann, B.; Huc, I.; Nitschke, J. R. *Nature Chem.* **2010**, *2*, 684-687.
7. (a) Giuseppone, N.; Lehn, J.-M. *Angew. Chem., Int. Ed.* **2006**, *45*, 4619-4624; (b) Giuseppone, N.; Lehn, J.-M. *Chem.-Eur. J.* **2006**, *12*, 1715-1722; (c) Suzuki, K.;

- Kawano, M.; Fujita, M. *Angew. Chem., Int. Ed.* **2007**, *46*, 2819-2822; (d) Ingerman, L. A.; Waters, M. L. *J. Org. Chem.* **2008**, *74*, 111-117; (e) Betancourt, J. E.; Martín-Hidalgo, M.; Gubala, V.; Rivera, J. M. *J. Am. Chem. Soc.* **2009**, *131*, 3186-3188; (f) Kilbas, B.; Mirtschin, S.; Scopelliti, R.; Severin, K. *Chem. Sci.* **2012**, *3*, 701-704.
8. Beves, J. E.; Blight, B. A.; Campbell, C. J.; Leigh, D. A.; McBurney, R. T. *Angew. Chem., Int. Ed.* **2011**, *50*, 9260-9327.
9. (a) Pluth, M. D.; Bergman, R. G.; Raymond, K. N. *Science* **2007**, *316*, 85-88; (b) Mal, P.; Breiner, B.; Rissanen, K.; Nitschke, J. R. *Science* **2009**, *324*, 1697-1699; (c) Sun, Q.-F.; Iwasa, J.; Ogawa, D.; Ishido, Y.; Sato, S.; Ozeki, T.; Sei, Y.; Yamaguchi, K.; Fujita, M. *Science* **2010**, *328*, 1144-1147; (d) Breiner, B.; Clegg, J. K.; Nitschke, J. R. *Chem. Sci.* **2011**, *2*, 51-56; (e) Brown, C. J.; Miller, G. M.; Johnson, M. W.; Bergman, R. G.; Raymond, K. N. *J. Am. Chem. Soc.* **2011**, *133*, 11964-11966; (f) de Hatten, X.; Bell, N.; Yufa, N.; Christmann, G.; Nitschke, J. R. *J. Am. Chem. Soc.* **2011**, *133*, 3158-3164; (g) Inokuma, Y.; Kawano, M.; Fujita, M. *Nature Chem.* **2011**, *3*, 349-358; (h) Freye, S.; Hey, J.; Torras-Galán, A.; Stalke, D.; Herbst-Irmer, R.; John, M.; Clever, G. H. *Angew. Chem., Int. Ed.* **2012**, *51*, 2191-2194; (i) Riddell, I. A.; Smulders, M. M. J.; Clegg, J. K.; Hristova, Y. R.; Breiner, B.; Thoburn, J. D.; Nitschke, J. R. *Nature Chem.* **2012**, *4*, 751-756; (j) Sun, Q.-F.; Sato, S.; Fujita, M. *Nature Chem.* **2012**, *4*, 330-333; (k) Wang, Z. J.; Clary, K. N.; Bergman, R. G.; Raymond, K. N.; Toste, F. D. *Nature Chem.* **2013**, *5*, 100-103.
10. (a) Fujita, M.; Nagao, S.; Ogura, K. *J. Am. Chem. Soc.* **1995**, *117*, 1649-1650; (b) Hasenknopf, B.; Lehn, J.-M.; Boumediene, N.; Leize, E.; Van, D. A. *Angew. Chem., Int. Ed.* **1998**, *37*, 3265-3268; (c) Takeda, N.; Umemoto, K.; Yamaguchi, K.; Fujita, M. *Nature* **1999**, *398*, 794-796; (d) Paraschiv, V.; Crego-Calama, M.; Ishi-i, T.; Padberg, C. J.; Timmerman, P.; Reinhoudt, D. N. *J. Am. Chem. Soc.* **2002**, *124*, 7638; (e) Tashiro, S.; Tominaga, M.; Kusukawa, T.; Kawano, M.; Sakamoto, S.; Yamaguchi, K.; Fujita, M. *Angew. Chem. Int. Ed.* **2003**, *42*, 3267-3270; (f) Davis, J. T.; Kaucher, M. S.; Kotch, F. W.; Iezzi, M. A.; Clover, B. C.; Mullaugh, K. M. *Org. Lett.* **2004**, *6*, 4265-4268; (g) Hori, A.; Yamashita, K.; Fujita, M. *Angew. Chem., Int. Ed.* **2004**, *43*, 5016-5019; (h) Albrecht, M.; Dehn, S.; Fröhlich, R. *Angew. Chem. Int. Ed.* **2006**, *45*, 2792-2794; (i) Pentecost, C. D.; Chichak, K. S.; Peters, A. J.; Cave, G. W. V.; Cantrill, S. J.; Stoddart, J. F. *Angew. Chem. Int. Ed.* **2007**, *46*, 218-222; (j) Cangelosi, V. M.; Carter, T. G.;

- Zakharov, L. N.; Johnson, D. W. *Chem. Commun.* **2009**, 5606-5608; (k) Beves, J. E.; Leigh, D. A. *Nature Chem.* **2010**, *2*, 708-710; (l) Hasell, T.; Wu, X.; Jones-James, T. A.; Bacsa, J.; Steiner, A.; Mitra, T.; Trewin, A.; Adams, D. J.; Cooper, A. I. *Nature Chem.* **2010**, *2*, 750-755; (m) Chepelin, O.; Ujma, J.; Barran, P. E.; Lusby, P. J. *Angew. Chem., Int. Ed.* **2012**, *51*, 4194-4197; (n) Gan, Q.; Ferrand, Y.; Chandramouli, N.; Kauffmann, B.; Aube, C.; Dubreuil, D.; Huc, I. *J. Am. Chem. Soc.* **2012**, *134*, 15656-15659.
11. (a) Jennings, P. A.; Wright, P. E. *Science* **1993**, *262*, 892-896; (b) Pellarin, R.; Schuetz, P.; Guarnera, E.; Caflisch, A. *J. Am. Chem. Soc.* **2010**, *132*, 14960-14970.
12. Ayme, J.-F.; Beves, J. E.; Leigh, D. A.; McBurney, R. T.; Rissanen, K.; Schultz, D. *Nature Chem.* **2012**, *4*, 15-20.
13. Ayme, J.-F.; Beves, J. E.; Leigh, D. A.; McBurney, R. T.; Rissanen, K.; Schultz, D. *J. Am. Chem. Soc.* **2012**, *134*, 9488-9497.
14. (a) Rowan, S. J.; Stoddart, J. F. *Org. Lett.* **1999**, *1*, 1913; (b) Ro, S.; Rowan, S. J.; Pease, A. R.; Cram, D. J.; Stoddart, J. F. *Org. Lett.* **2000**, *2*, 2411-2414.
15. Chichak, K. S.; Cantrill, S. J.; Stoddart, J. F. *Chem. Commun.* **2005**, 3391-3393.
16. (a) Ziegler, M.; Davis, A. V.; Johnson, D. W.; Raymond, K. N. *Angew. Chem., Int. Ed.* **2003**, *42*, 665-668; (b) Sato, S.; Ishido, Y.; Fujita, M. *J. Am. Chem. Soc.* **2009**, *131*, 6064-6065.
17. (17) Synthesis of labeled versions of hexylamine helicate 2-D40 and pentafoil knot 6-D40 were carried out following standard procedures and gave products in comparative yields to their non-labeled derivatives (see Experimental Section for details)
18. (18) (a) Hogg, L.; Leigh, D. A.; Lusby, P. J.; Morelli, A.; Parsons, S.; Wong, J. K. Y. *Angew. Chem. Int. Ed.* **2004**, *43*, 1218-1221; (b) Leung, K. C.-F.; Wong, W.-Y.; Arico, F.; Haussmann, P. C.; Stoddart, J. F. *Org. Biomol. Chem.* **2010**, *8*, 83-89; (c) Hasell, T.; Schmidtman, M.; Stone, C. A.; Smith, M. W.; Cooper, A. I. *Chem. Commun.* **2012**, *48*, 4689-4691.

Chapter VI: "Strong and Selective Anion Binding within the Central Cavity of Molecular Knots and Links"

Manuscript submitted as "Strong and Selective Anion Binding within the Central Cavity of Molecular Knots and Links ", J.-F. Ayme, J. E. Beves, C. J. Campbell, G. Gil-Ramírez, D. A. Leigh and A. J. Stephens

Acknowledgements

C.J.C. is gratefully acknowledged for his synthesis of the ligand used to obtain Solomon link **[1]**(PF₆)₈. A.J.S. is gratefully acknowledged for his synthesis of the Star of David **[3]**(PF₆)₁₂. J.F.A. realised the titrations presented in this chapter along with the synthesis of the compounds used. The design and analysis of the titrations was a joint effort between J.F.A, J.E.B., C.J.C. and G.G.R.

6.1. Synopsis

Knots and links (catenanes) are important structural features of circular DNA and some proteins. However, few synthetic molecular knots have been prepared to date and their properties remain largely unexplored. In this chapter, we show that a synthetic molecular knot and doubly- and triply-entwined [2]catenanes based on circular Fe(II)-double-helicate scaffolds can bind a single halide anion in their central cavities through electrostatic and $\text{CH}\cdots\text{X}^-$ hydrogen bonding interactions. Study of the X-ray crystal structures of the salts of each of the knot and these links shows that the metal ions not only provide long range attractive electrostatic interactions to any electron-rich moiety in the central cavity but also preorganize the cavity and inductively activate protons pointing inside it as hydrogen bond donors. By studying the sizes and shapes of the three different central cavities and by comparing them with the affinity of entanglement for halides, it is possible to establish a correlation between the strength and selectivity of the halide binding and the size of the cavity, the number of hydrogen bonds and the number of metals ions involved. The binding is up to $3.6\pm 0.2\cdot 10^{10} \text{ M}^{-1}$ in acetonitrile (for pentafoil knot $[\mathbf{2}\cdot\text{Cl}](\text{PF}_6)_9$), making these topologically complex molecules some of the strongest synthetic noncovalent binders of halide anions reported to date, comparable in chloride ion affinity to silver salts.

6.2. Introduction

In a classic series of experiments in the mid-1990s, Lehn and co-workers found that Fe(II) salts and tris(bipyridine) ligands with short spacers between the chelating groups assemble into double-stranded circular metal helicates.¹ The size of the circular helicate produced was often influenced by the counterion of the metal salt employed: for example, the use of FeCl₂ led to a pentameric cyclic helicate with a chloride anion at the center of the structure in the solid state.^{1a} Unlike the other counterions, this clearly strongly bound chloride ion was reported not to be exchanged upon washing with a saturated solution of hexafluorophosphate or triflate salts.^{1a} However, the strength and selectivity of the anion binding of these circular helicates was never quantified, perhaps because of the perceived difficulty of analyzing the substitution of one anion for another in the presence of other counterions.

We recently described the synthesis of a series of molecular knots² and links³ using different sized circular helicate scaffolds to control the number of crossings in the closed-loop ligand strand. Solomon link **[1]**(PF₆)₈ (a doubly-entwined [2]catenane) and pentafoil knot **[2•Cl]**(PF₆)₉ are derived from tetrameric and pentameric circular helicates, respectively,^{4,5} and are assembled through reversible imine chemistry (Figure 1).⁶ The Star of David 6₁² link **[3]**(PF₆)₁₂ (a triply-entwined [2]catenane) is based on a hexameric circular helicate prepared from tris(bipyridine) ligands with the entwined complex covalently captured by olefin metathesis.⁷ Here we report on the binding affinities of the central cavities of knots and links **[1]**(PF₆)₈, **[2]**(PF₆)₁₀ and **[3]**(PF₆)₁₂ (Figure 1) for various halide anions.⁸

6.3. Results and Discussion

Well-ordered anions are found associated with the central cavity in the X-ray crystal structures of salts of each of these links and knot: two PF_6^- anions in $[\mathbf{1}](\text{PF}_6)_8$;⁴ one Cl^- anion in $[\mathbf{2}\cdot\text{Cl}](\text{PF}_6)_9$ ⁵ and one PF_6^- anion in $[\mathbf{3}\cdot\text{PF}_6](\text{Ph}_4\text{B})_{11}$.⁷ The solid state structures (Figure 2) show that in each case the H^1 aromatic protons (see Figure 1 for numbering scheme) line the walls of the inner cavities of the circular helicates. The metal ions not only provide long range attractive electrostatic interactions to any electron-rich moiety in the central cavity (the overall charge of the complex is, of course, neutral because of the other counterions) but also preorganize the binding pocket (through formation of the relatively rigid circular double helicate) and inductively activate the C-H^1 protons as hydrogen bond donors for a second sphere of coordination¹⁰ to electron-rich species.¹¹⁻¹³

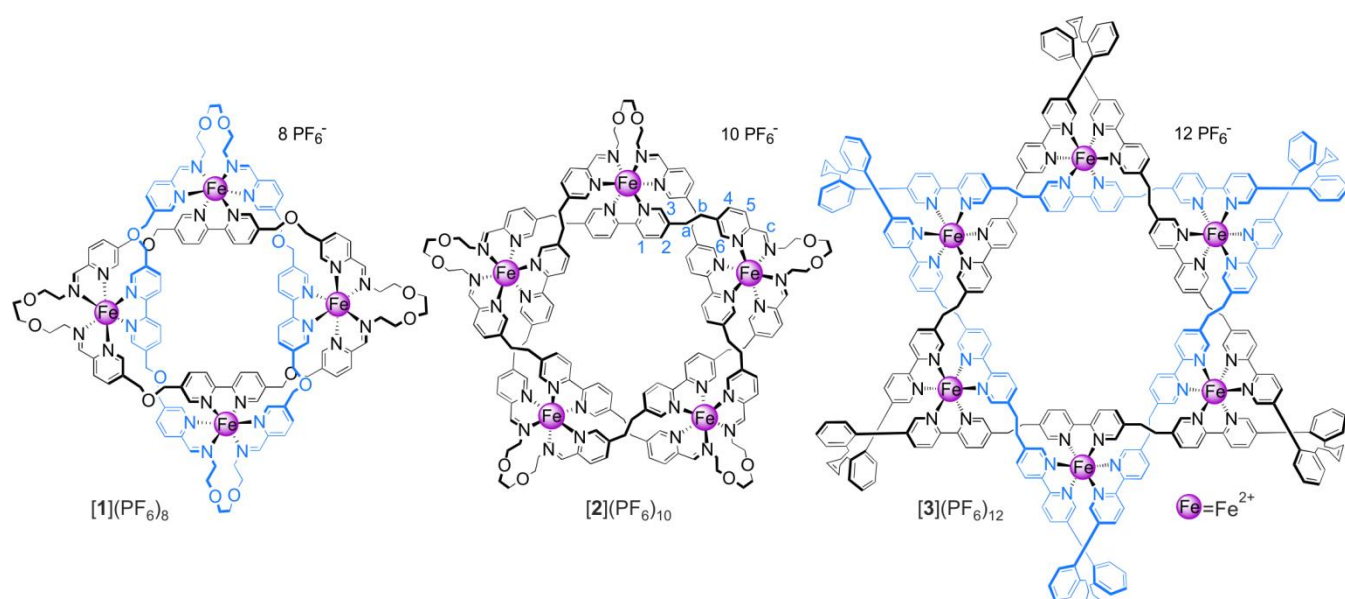


Figure 1. Chemical structures of Solomon link $[\mathbf{1}]$,⁴ pentafoil knot $[\mathbf{2}]$,⁵ and Star of David $[\mathbf{3}]$,⁷ shown as their PF_6^- salts.

The all- PF_6^- complexes of the Solomon link and Star of David catenane, $[\mathbf{1}](\text{PF}_6)_8$ and $[\mathbf{3}](\text{PF}_6)_{12}$, respectively, were isolated from the reactions used to form the interlocked

architectures by washing with aqueous KPF_6 .^{4,7} We found that the chloride anion could be removed from $[\mathbf{2} \cdot \text{Cl}](\text{PF}_6)_9$ by a two-stage procedure of salt metathesis,¹⁴ first using aqueous NH_4BF_4 and then aqueous NH_4PF_6 (see SI).¹⁵ Exchange of the chloride ion is accompanied by a ~ 1.4 ppm upfield shift in the H^1 protons as a consequence of their no longer being involved in strong $\text{CH} \cdots \text{Cl}^-$ hydrogen bonding (Figure 3e). Addition of up to one equivalent Bu_4NCl ¹⁶ to the 'empty'¹⁷ pentafoil knot ($[\mathbf{2}](\text{PF}_6)_{10}$) replaces just one of the ten PF_6^- anions (electrospray ionization mass spectrometry (ESI-MS) shows a series of m/z fragments corresponding to $[\mathbf{2}(\text{PF}_6)_n\text{Cl}]^{(9-n)+}$ but no evidence for complexes with more than one Cl^- anion). ^1H NMR Spectroscopy (Figure 3c) confirms that the chloride anion is bound within the central cavity of the knot in solution (H^1 , and to a lesser extent H^6 ,¹⁸ are significantly shifted compared to $[\mathbf{2}](\text{PF}_6)_{10}$; Figure 3c cf Figure 3e). Addition of less than one equivalent of Bu_4NCl to $[\mathbf{2}](\text{PF}_6)_{10}$ gives two distinct species in the ^1H NMR spectrum (Figure 3d), $[\mathbf{2}](\text{PF}_6)_{10}$ and $[\mathbf{2} \cdot \text{Cl}](\text{PF}_6)_9$, indicating that the Cl^- anion bound in the cavity of the knot only undergoes slow exchange on the NMR timescale with others in bulk solution.¹⁹

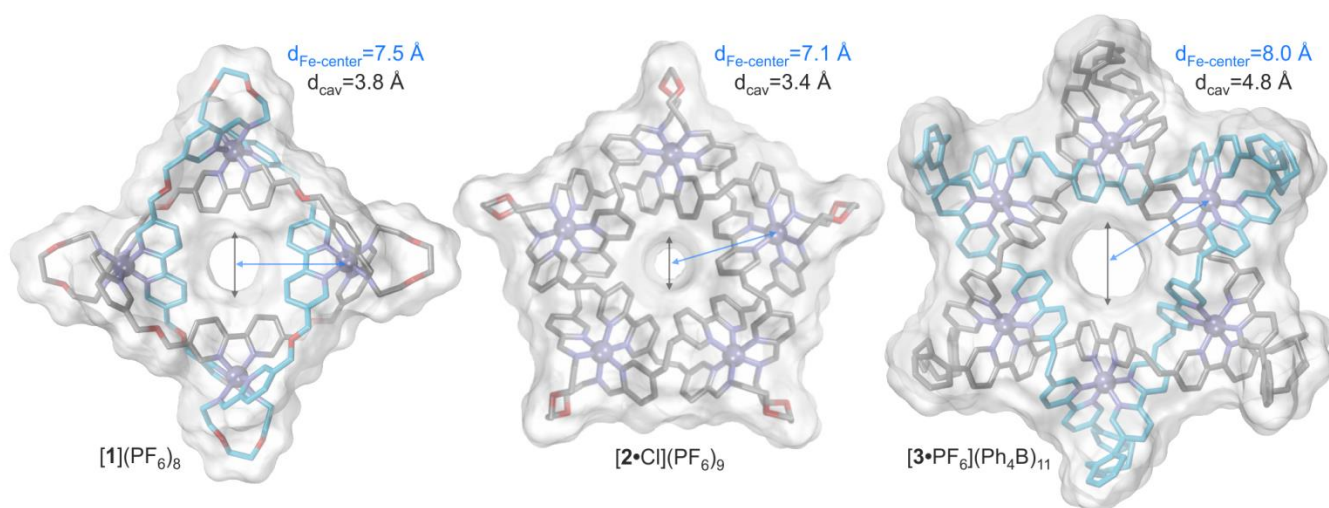


Figure 2. Single crystal X-ray structures of Solomon link $[\mathbf{1}](\text{PF}_6)_8$,⁴ pentafoil knot $[\mathbf{2} \cdot \text{Cl}](\text{PF}_6)_9$,⁵ and Star of David [2]catenane $[\mathbf{3} \cdot \text{PF}_6](\text{Ph}_4\text{B})_{11}$.⁷ Solvent molecules, hydrogen atoms and counterions have been omitted for clarity. The solvent-accessible isosurface is shown as a semi-transparent white surface. The distances between the centers of the inner binding pockets and the metal ions are shown by the blue double-headed arrows and the diameters of the pockets

(H^1 radius 1 Å, the typical value for hydrogen bonding hydrogen atoms⁹) are indicated by the black double-headed arrows.

With all three of the all- PF_6^- complexes (**[1]**(PF_6)₈, **[2]**(PF_6)₁₀ and **[3]**(PF_6)₁₂) in hand, we measured the equilibrium constant (effectively a binding constant) for the exchange of one of the PF_6^- anions for a single halide anion in acetonitrile²⁰ (Scheme 1; Table 1). In every case (with the exception of Cl^- or Br^- with **[3]**)²¹: (i) ESI-MS showed the exchange of only one halide for a PF_6^- anion (i.e. no complexes with more than one halide) during addition of up to one equivalent of the tetrabutylammonium salt;¹⁶ and (ii) 1H NMR indicated halide binding only within the central cavity of the circular helicates (significant shifts in H^1 compared to the rest of the 1H NMR spectrum, e.g. Figure 3).²² These results confirmed that the displacement of the first PF_6^- anion, by a halide that binds within the central cavity, occurs in a very different binding strength regime to the exchange of the other PF_6^- counterions.

The strength of binding of each knot/link with iodide was sufficiently modest in acetonitrile that it could be measured by 1H NMR titration experiments (see SI). In contrast, the affinity of the pentafoil knot for Cl^- or Br^- was so strong, even in acetonitrile, that it was determined by comparison with the affinity of $AgPF_6$ for the halide (see SI). The other binding constants were measured by competition experiments with a calix[4]bipyrrole derivative for which (strong) halide binding constants had previously been determined (see SI).²³

The anion exchange experiments (Table 1) show that the links and knot each bind halide ions strongly in the central cavity in acetonitrile. The K_1 values given in Table 1 denote the preference for halide binding over PF_6^- association by the circular helicate and indicate that

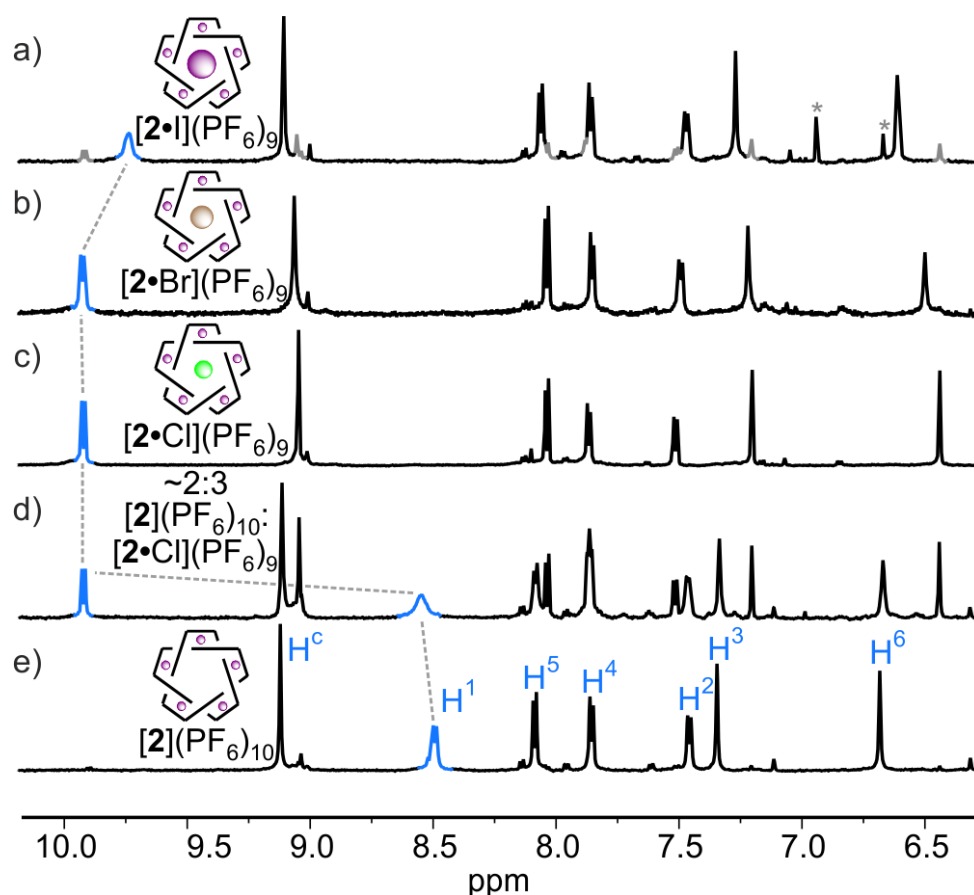
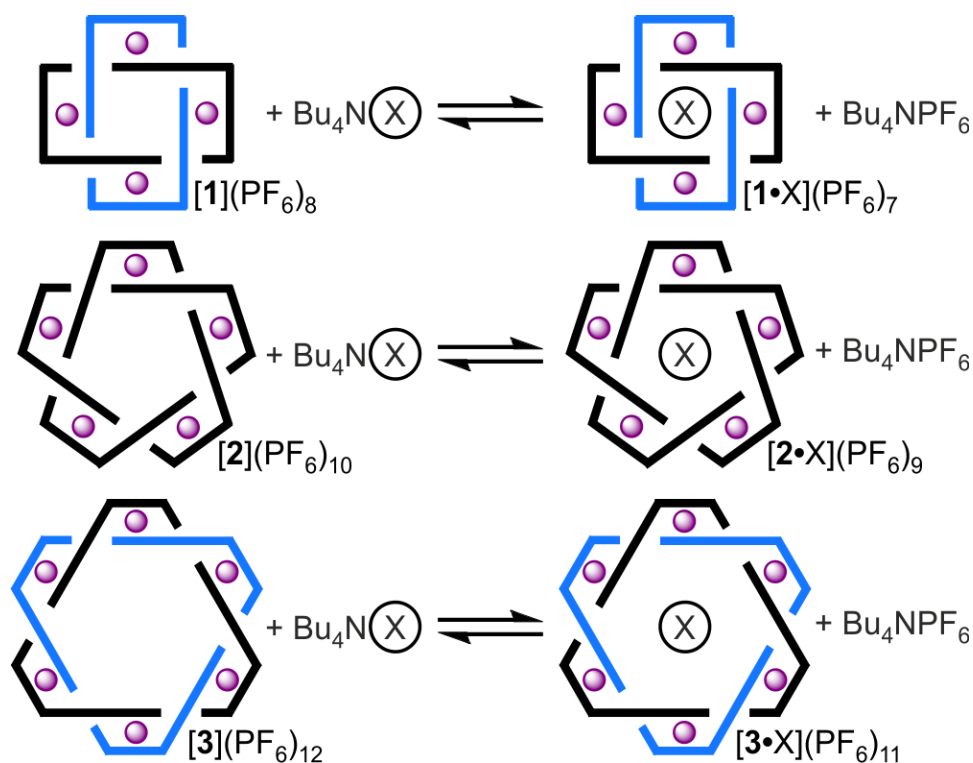


Figure 3. Partial ^1H NMR spectra (600 MHz, CD_3CN , 298 K) of the halide-complexed and 'empty'¹⁷ pentafoil knot: a) iodide-complexed pentafoil knot $[\mathbf{2}\cdot\text{I}](\text{PF}_6)_9$; b) bromide-complexed pentafoil knot $[\mathbf{2}\cdot\text{Br}](\text{PF}_6)_9$; c) chloride-complexed pentafoil knot $[\mathbf{2}\cdot\text{Cl}](\text{PF}_6)_9$; d) $\sim 2:3$ mixture of $[\mathbf{2}](\text{PF}_6)_{10}$ and chloride-complexed pentafoil knot $[\mathbf{2}\cdot\text{Cl}](\text{PF}_6)_9$ showing that the bound halide is not in fast exchange; e) $[\mathbf{2}](\text{PF}_6)_{10}$. Note the large upfield shift in H^1 of $[\mathbf{2}](\text{PF}_6)_{10}$ compared to the other complexes in which H^1 is involved in $\text{CH}\cdots\text{X}^-$ hydrogen bonding within the central cavity. The proton assignments correspond to that shown in Figure 1. The signals shown in grey are due to $[\mathbf{2}\cdot\text{Cl}](\text{PF}_6)_9$ formed during the experiment. * impurity.

even the weakest halide host, Star of David catenane $[\mathbf{3}]$, binds I^- $>10,000\times$ stronger in the central cavity than it does PF_6^- . Pentafoil knot $[\mathbf{2}]$ binds a single Cl^- or Br^- ion with extremely high affinity ($>10^{10} \text{ M}^{-1}$), five orders of magnitude stronger than I^- . To put this into context, 450 equivalents²⁴ of AgPF_6 are required to remove all of the chloride ions from $[\mathbf{2}\cdot\text{Cl}](\text{PF}_6)_9$ in acetonitrile (see SI).²⁵ Unless in the presence of excess AgPF_6 , pentafoil knot $[\mathbf{2}](\text{PF}_6)_{10}$

readily sequesters traces of Cl^- from its environment, including solvents and glassware, reforming $[\mathbf{2}\cdot\text{Cl}](\text{PF}_6)_9$.



Scheme 1. Exchange of a single PF_6^- anion for a halide (X^-) in the formation of $[\mathbf{1}\cdot\text{X}](\text{PF}_6)_7$, $[\mathbf{2}\cdot\text{X}](\text{PF}_6)_9$ and $[\mathbf{3}\cdot\text{X}](\text{PF}_6)_{11}$ from the corresponding knot or link all- PF_6^- salts with tetrabutylammonium halides (Bu_4NX , $\text{X}^- = \text{Cl}^-$, Br^- or I^-) in acetonitrile (298 K).

Solomon link $[\mathbf{1}]$ also binds the two smaller halide anions strongly (Cl^- : $K_1 = 3.0 \pm 2.5 \cdot 10^8 \text{ M}^{-1}$; Br^- : $K_1 = 1.0 \pm 0.5 \cdot 10^7 \text{ M}^{-1}$), although notably weaker than the pentafoil knot. The Star of David $[\mathbf{2}]$ catenane $[\mathbf{3}]$ binds the first I^- ion exchanged for PF_6^- selectively within the catenane's central cavity ($K_1 = 1.2 \pm 0.1 \cdot 10^4 \text{ M}^{-1}$) in the manner observed for the smaller host molecules with each of the halides. However, unlike the other systems, a single PF_6^- anion is not exchanged for one Cl^- or Br^- ion preferentially before all of the others,²¹ nor are the Cl^- or Br^- ions bound exclusively within the central cavity (the resonances of several ligand protons, not just H^1 , shift in the ^1H NMR spectrum). With each of the circular helicates, non-spherical anions did not show selective binding of solely a single exchanged anion.

Table 1. Equilibrium constants (K_d , M^{-1}) for the exchange of one PF_6^- anion for one halide anion for complexes of molecular knot and links [1], [2] and [3] (CD_3CN , 295 K).^a

	Cl^- $d = 3.6 \text{ \AA}^{26}$	Br^- $d = 3.9 \text{ \AA}^{26}$	I^- $d = 4.4 \text{ \AA}^{26}$
[1](PF_6) ₈	$3.0 \pm 2.5 \cdot 10^8$ ^{b,c}	$1.0 \pm 0.5 \cdot 10^7$ ^{b,c}	$2.1 \pm 0.2 \cdot 10^5$ ^d
[2](PF_6) ₅	$3.6 \pm 0.2 \cdot 10^{10}$ ^e	$1.7 \pm 0.2 \cdot 10^{10}$ ^e	$5.8 \pm 1.3 \cdot 10^5$ ^d
[3](PF_6) ₄	- ^f	- ^f	$1.2 \pm 0.1 \cdot 10^4$ ^d

^a Equilibrium constants are the average of several experiments (titrations or competition experiments). The errors given are intrinsic limits of the method or twice the standard deviation of the experimental data. ^b Determined by competitive binding against a calix[4]bipyrrole derivative.²³ ^c Determined by competitive binding against [2](PF_6)₁₀. ^d Determined by ¹H NMR titration. ^e Determined by competitive binding with $AgPF_6$. ^f A single halide anion is not bound selectively within the central cavity.²¹

The strength and binding preferences within the central cavities of the knot and links can be rationalized through consideration of the solid state structures shown in Figure 2. The smallest cavity is actually that of the pentafoil knot [2], a circular pentameric helicate, which has a size (diameter $\sim 3.4 \text{ \AA}$ at its narrowest) and hourglass cylindrical topography that allows the spherical Cl^- (3.6 \AA diameter²⁶) and Br^- (3.9 \AA diameter²⁶) anions to bind effectively to the inner ring of electron-poor H^1 protons. The Solomon link cavity is slightly larger ($\sim 3.8 \text{ \AA}$ at its narrowest) despite being based on a circular tetramer helicate, as a result of the ligand strand having extra oxygen atoms either side of the bipyridine groups. The weaker halide affinity of the Solomon link is consistent with halide binding in the central cavity being based on eight $CH \cdots X^-$ hydrogen bonds and slightly longer range ($Fe(II) \cdots X^-$ 7.5

Å) electrostatic interactions with four Fe(II) ions, compared to ten CH \cdots X $^-$ hydrogen bonds and five (Fe(II) \cdots X $^-$ 7.1 Å) Fe(II)-X $^-$ ion interactions in the pentafoil knot complexes.

The Star of David [2]catenane, based on a hexameric circular helicate, has a significantly larger diameter central cavity (\sim 4.8 Å at its narrowest) than the other two host molecules studied. This is close to the diameter of an I $^-$ anion (4.4 Å²⁶), with which it forms a 1:1 complex (Table 1), but is too large for the other halide anions to be able to simultaneously form hydrogen bonds with all of the H¹ protons, which may account for why Cl $^-$ and Br $^-$ are not solely bound within the cavity.

6.4. Conclusion

In conclusion, molecular knots and links derived from circular metal double helicate scaffolds of different sizes bind a single halide anion within their central cavities through multiple CH \cdots X $^-$ hydrogen bonds and long range Fe(II) \cdots X $^-$ electrostatic interactions. The size of the cavity, and the number of hydrogen bonds and metal ions involved, determines the strength and selectivity of halide binding. Pentafoil knot [2] is one of the strongest noncovalent binding synthetic hosts for Cl $^-$ known, with a chloride:hexafluorophosphate binding preference of $>10^{10}$:1 in acetonitrile and a chloride affinity comparable to that of silver salts.

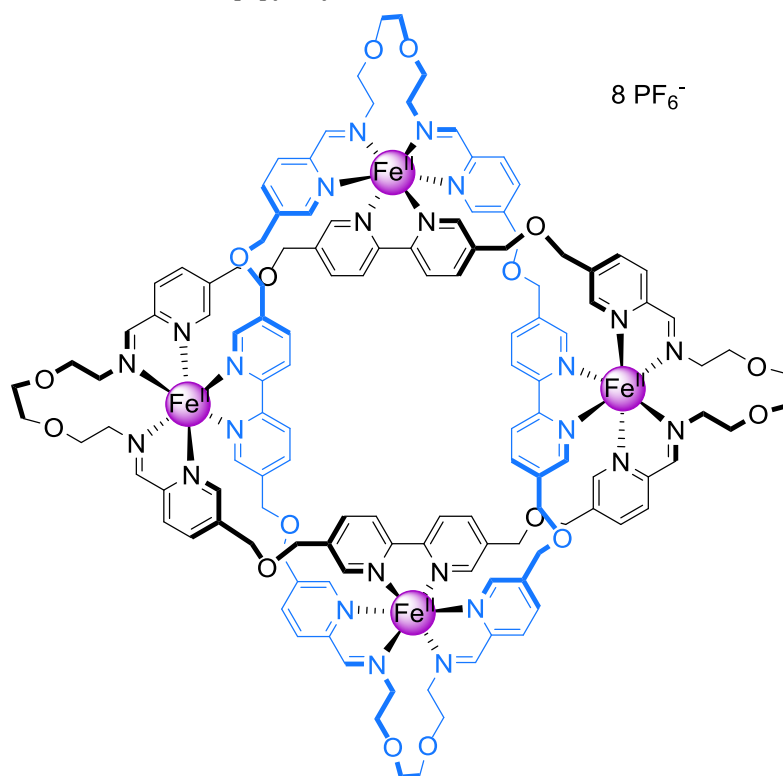
The physical manifestation of knots and links at various length scales is increasingly being recognized in contexts as disparate as biopolymers,²⁷ colloidal clusters,²⁸ liquid crystals²⁹ and soap films³⁰. The exceptional strength and selectivity of the anion binding of [1], [2] and [3], and the fact that their binding pockets are intrinsically topologically chiral, make

metalated molecular knots and links an intriguing new class of host architectures for anion binding and recognition processes.

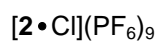
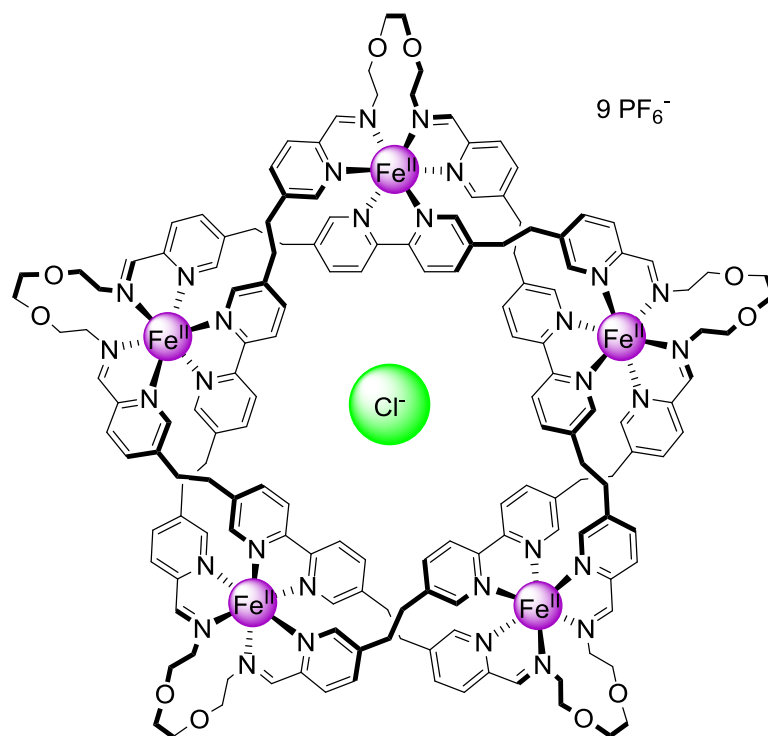
6.5. Experimental Section

6.5.1. Synthetic Procedures and Characterization Data

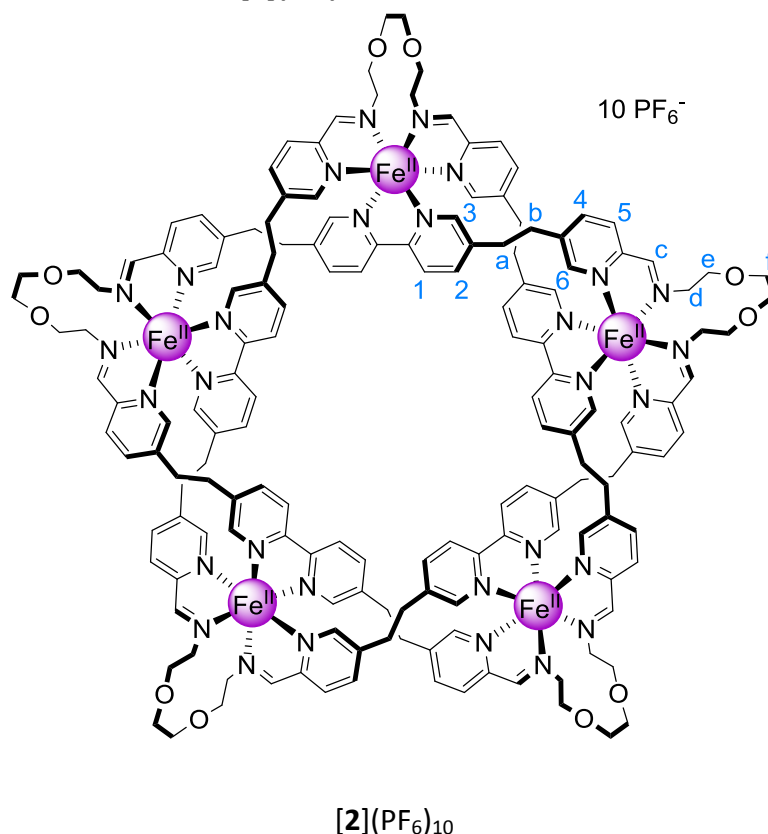
6.5.1.1. Solomon link [1](PF₆)₈



Solomon link [1](PF₆)₈ was prepared according to a literature procedure.⁴ The characterization data for [1](PF₆)₈ was in accordance with that previously reported.

6.5.1.2. Pentafoil knot $[2 \cdot \text{Cl}](\text{PF}_6)_9$ 

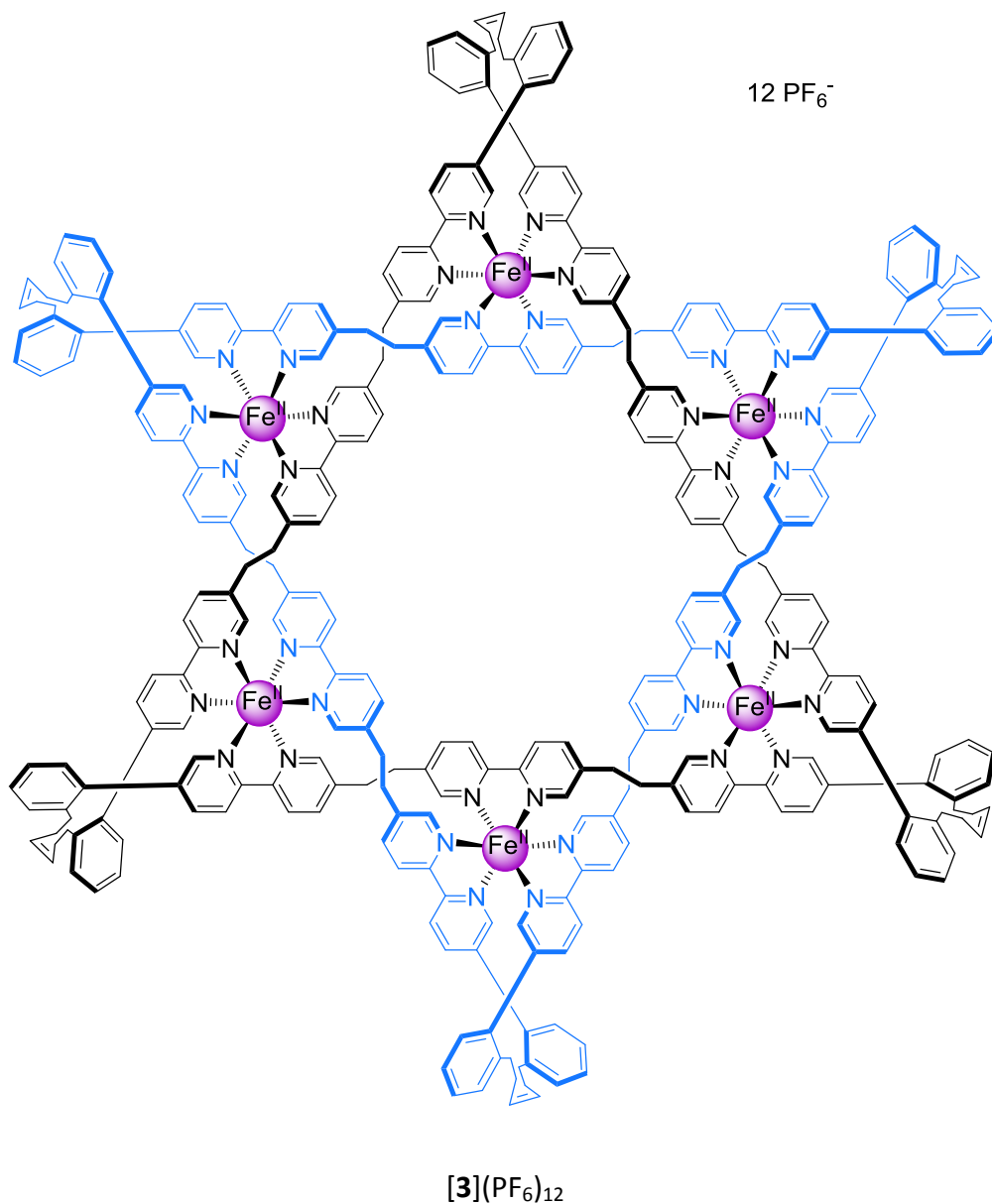
Pentafoil knot $[2 \cdot \text{Cl}](\text{PF}_6)_9$ was prepared according to a literature procedure.⁵ The characterization data for $[2 \cdot \text{Cl}](\text{PF}_6)_9$ was in accordance with that previously reported.

6.5.1.3. Pentafoil knot **[2](PF₆)₁₀**

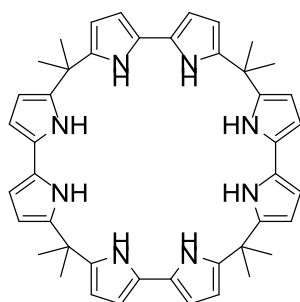
Pentafoil knot **[2•Cl](PF₆)₉** (10 mg, 2.3 μmol) was dissolved in 1 mL of acetonitrile. The resulting solution was treated with 2 mL of a saturated aqueous solution of NH_4BF_4 . A fine suspension of a purple material was collected on Celite, thoroughly washed with water, EtOH, CH_2Cl_2 and diethylether. The purple solid was dissolved in acetonitrile (2 mL) and collected under reduced pressure before being treated with a saturated aqueous solution of NH_4PF_6 (2 mL). A fine suspension of a purple material was collected on Celite, thoroughly washed with water, EtOH, CH_2Cl_2 and diethylether. The purple solid was dissolved in acetonitrile and concentrated under reduced pressure to give **[2](PF₆)₁₀** as a purple powder (5.4 mg, 1.2 μmol , 54%). Note 99.999% minimum purity NH_4BF_4 and 99.99% minimum purity NH_4PF_6 salts must be used.

^1H NMR (600 MHz, Acetonitrile- d_3) δ 9.11 (s, 10H, H^c), 8.48 (d, J = 8.5 Hz, 10H, H¹), 8.07 (d, J = 8.1 Hz, 10H, H⁵), 7.84 (d, J = 7.9 Hz, 10H, H⁴), 7.45 (d, J = 8.2 Hz, 10H, H²), 7.33 (s, 10H, H³),

6.67 (s, 10H, H^g), 4.14 – 4.07 (m, 10H, H^d), 3.74 – 3.66 (m, 20H, H^e+ H^f), 3.35 (d, $J = 9.3$ Hz, 10H, H^f), 3.27 – 3.15 (m, 20H, H^b+ H^d), 3.13 – 3.05 (m, 10H, H^a), 3.02 (t, $J = 9.6$ Hz, 20H, H^e+ H^a) 2.87 – 2.79 (m, 10H, H^b).

6.5.1.4. Star of David catenane $[3](PF_6)_{12}$ 

Star of David catenane $[3](PF_6)_{12}$ was prepared according to a literature procedure.⁷ The characterization data for $[3](PF_6)_{12}$ was in accordance with that previously reported.

6.5.1.5. Calix[4]bipyrrole S1**S1**

Calix[4]bipyrrole **S1** was prepared according to a literature procedure.²³ The characterization data of **S1** was in accordance with that previously reported.

6.5.2. Derivation of the expressions used to determine K_1

6.5.2.1. Derivation of the equation for competitive binding studies of pentafoil knot [2] for Cl^- using AgPF_6

Considering the following equilibrium between a host helicate Hel and a guest halide X that can form a host-guest complex HelX:



The equilibrium constant for this binding event is defined as:

$$K_1 = \frac{[\text{HelX}]}{[\text{Hel}][\text{X}]} \quad (\text{Eq.2})$$

The mass balance for the helicate Hel is given by:

$$[\text{Hel}]_0 = [\text{Hel}] + [\text{HelX}] \quad (\text{Eq.3})$$

By rearranging Eq.3 the concentration of Hel can be determined as:

$$[\text{Hel}] = [\text{Hel}]_0 - [\text{HelX}] \quad (\text{Eq.4})$$

The solubility product constant K_{sp} of AgX is defined as:

$$K_{\text{sp}} = [\text{X}][\text{Ag}^+] \quad (\text{Eq.5})$$

By rearranging Eq.2 the concentration of halide X can be expressed as:

$$[\text{X}] = \frac{[\text{HelX}]}{K_1[\text{Hel}]} \quad (\text{Eq.6})$$

Combining Eq.5 and Eq.6 yields:

$$K_{\text{sp}} = \frac{[\text{HelX}][\text{Ag}^+]}{K_1[\text{Hel}]} \quad (\text{Eq.7})$$

Furthermore, from Eq.7 and Eq.4 the solubility product constant K_{sp} is equal to:

$$K_{\text{sp}} = \frac{[\text{HelX}][\text{Ag}^+]}{K_1([\text{Hel}]_0 - [\text{HelX}])} \quad (\text{Eq.8})$$

Rearranging Eq.8 gives:

$$K_1[\text{Hel}]_0 - K[\text{HelX}] = \frac{1}{K_{\text{sp}}}[\text{HelX}][\text{Ag}^I] \quad (\text{Eq.9})$$

$$K_1[\text{Hel}]_0 = \frac{1}{K_{\text{sp}}}[\text{HelX}][\text{Ag}^I] + K[\text{HelX}] \quad (\text{Eq.10})$$

$$K_1[\text{Hel}]_0 = \left(\frac{[\text{Ag}^I]}{K_{\text{sp}}} + K \right) [\text{HelX}] \quad (\text{Eq.11})$$

$$[\text{HelX}] = \frac{K[\text{Hel}]_0}{\left(\frac{[\text{Ag}^I]}{K_{\text{sp}}} + K \right)} \quad (\text{Eq.12})$$

If the change on the integral of proton in the ^1H NMR of the helicate ΔI_{obs} is defined as:

$$\Delta I_{\text{obs}} = I_0 - I_{\text{obs}} \quad (\text{Eq.13})$$

I_{obs} is a function of the molar fraction of $[\text{HelX}]$ therefore ΔI_{obs} can be expressed as:

$$\Delta I_{\text{obs}} = I_0 - I_0 \frac{[\text{HelX}]}{[\text{Hel}]_0} \quad (\text{Eq.14})$$

Substituting Eq.12 in Eq.14 yields:

$$\Delta I_{\text{obs}} = I_0 - I_0 \frac{K_1[\text{Hel}]_0}{[\text{Hel}]_0 \left(\frac{[\text{Ag}^I]}{K_{\text{sp}}} + K_1 \right)} \quad (\text{Eq.15})$$

$$\Delta I_{\text{obs}} = I_0 - I_0 \frac{K_1}{\left(\frac{[\text{Ag}^I]}{K_{\text{sp}}} + K_1 \right)} \quad (\text{Eq.16})$$

The mass balance for silver Ag is given by:

$$[\text{Ag}^I]_0 = [\text{Ag}^I] + [\text{AgX}] \quad (\text{Eq.17})$$

As the amount of silver added $[\text{Ag}]$ is very large in comparison with the amount of AgX formed it can be assumed that:

$$[\text{Ag}^I] \approx [\text{Ag}^I]_0 \quad (\text{Eq.18})$$

Combining Eq.17 and Eq.18:

$$\Delta I_{\text{obs}} = I_0 - I_0 \frac{K_1}{\left(\frac{[Ag^+]_0}{K_{sp}} + K_1\right)} \quad (\text{Eq.19})$$

Equation Eq.19 was used to fit the binding data to a 1:1 model using OriginPro.³¹

6.5.2.2. Derivation of the fraction of occupied host as a function of total guest concentration via ¹H NMR integrals in the case of the 1:1 binding at [2] + I⁻ in slow exchange

As it was not possible to integrate precisely the signal of both free and bound host only the appearance of the bound species was followed. The appearing signal of the host was integrated against a signal of the host which remained unchanged upon complexation.

Considering the following equilibrium between a host helicate Hel and a guest halide X that can form a host-guest complex HelX:



The equilibrium constant for this binding event is defined as:

$$K_1 = \frac{[\text{HelX}]}{[\text{Hel}][\text{X}]} \quad (\text{Eq.2})$$

The mass balance for the helicate Hel and for the guest X are respectively given by:

$$[\text{Hel}]_0 = [\text{Hel}] + [\text{HelX}] \quad (\text{Eq.3})$$

$$[\text{X}]_0 = [\text{X}] + [\text{HelX}] \quad (\text{Eq.20})$$

Combining Eq.2, Eq.3 and Eq.20 yields:

$$[\text{HelX}] = \left(\frac{1}{2K_1}\right) \left[(K_1[\text{X}]_0 + K_1[\text{Hel}]_0 + 1) - \sqrt{(K_1[\text{X}]_0 + K_1[\text{Hel}]_0 + 1)^2 - 4K_1^2[\text{Hel}]_0[\text{X}]_0} \right] \quad (\text{Eq.21})$$

The integral value I_{obs} observed for an NMR signal of the complex HelX is a function of the molar fraction χ_{HelX} of the complex and the integral value I_0 of the complex:

$$I_{\text{obs}} = \chi_{\text{HelX}} I_0 \quad (\text{Eq.22})$$

By developing the expression of the molar fraction χ_{HelX} the integral value I can be expressed as a function of the total concentration of host $[\text{Hel}]_0$ and the concentration of the host-guest complex $[\text{HelX}]$:

$$I_{\text{obs}} = \frac{[\text{HelX}]}{[\text{Hel}]_0} I_0 \quad (\text{Eq.23})$$

By combining Eq.21 and Eq.23:

$$I_{\text{obs}} = \left(\frac{I_0}{2K_1[\text{Hel}]_0} \right) \left[(K_1[\text{X}]_0 + K_1[\text{Hel}]_0 + 1) - \sqrt{(K_1[\text{X}]_0 + K_1[\text{Hel}]_0 + 1)^2 - 4K_1^2[\text{Hel}]_0[\text{X}]_0} \right] \quad (\text{Eq.24})$$

Equation Eq.24 was used to fit the binding data to a 1:1 model using OriginPro.³¹

6.5.2.3. Derivation of the fraction of occupied host as a function of total guest concentration via NMR chemical shift in the case of a 1:1 binding event in fast exchange

Equation Eq.25 has been used in the literature³² to fit ¹H NMR data to a 1:1 binding stoichiometry and therefore it was used to fit the binding data using OriginPro.³¹

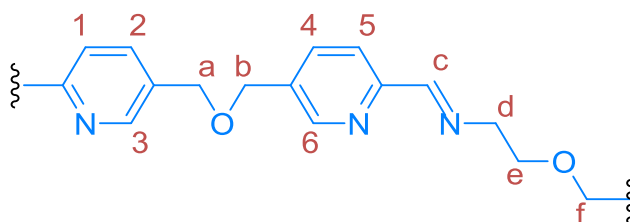
$$\delta = \delta_0 + \frac{\Delta\delta}{2K_1[\text{Hel}]_0} \left((K_1([\text{Hel}]_0 + [\text{X}]_0) + 1) - \sqrt{((K_1([\text{Hel}]_0 + [\text{X}]_0) + 1)^2 - 4K_1^2[\text{Hel}]_0[\text{X}]_0)} \right) \quad (\text{Eq.25})$$

Where

- δ the measured chemical shift
- δ_0 the chemical shift of empty host solution
- $\Delta\delta$ the maximal change in chemical shift
- K_1 the binding constant
- $[\text{Hel}]_0$ the total host concentration
- $[\text{X}]_0$ the total guest concentration

6.5.3. Binding studies

6.5.3.1. Solomon link $[1](PF_6)_8$



6.5.3.1.1. Determination of K_1 for Solomon link $[1](PF_6)_8$ with Cl^- by competition against calix[4]bipyrrole **S1** and knot $[2\bullet Cl](PF_6)_9$

The strength of the interaction between Solomon link $[1](PF_6)_8$ and Cl^- was assessed by competitive binding titrations. Receptor **S1** and pentafoil knot $[2](PF_6)_{10}$ were used as competitive hosts for Cl^- . The association constant between **S1** and Cl^- has previously been reported²³ as $K_1 = 2\,940\,000\,M^{-1}$ (MeCN) and the association constant between pentafoil knot $[2](PF_6)_{10}$ and Cl^- was determined in section 6.5.5.2.1 as $K_1 = (3.6 \pm 0.2) \times 10^{10}\,M^{-1}$ (MeCN).

A $1.4 \times 10^{-4}\,M$ 1:1 mixture of Solomon link $[1](PF_6)_8$ and calix[4]bipyrrole **S1** in MeCN was titrated with TBACl. Negligible changes in the 1H NMR signals of **S1** were observed upon addition of Cl^- (up to 1 eq. relative to $[1](PF_6)_8$) whereas signals characteristic of the formation of $[1\bullet Cl](PF_6)_8$ were observed (see Figure S9). This indicates that the affinity of the Solomon link $[1](PF_6)_8$ for Cl^- should be at least two orders of magnitude higher³³ than that of receptor **S1**, and hence $K_1 \geq 3 \cdot 10^8\,M^{-1}$. Because of the limitations regarding the precise determination of the quantity of calix[4]bipyrrole bound $[S1\bullet Cl]$ present, no greater accuracy can be claimed for the measurement of the Solomon link K_1 with Cl^- .

Similarly, a $7.5 \times 10^{-5}\,M$ solution of pentafoil knot $[2\bullet Cl](PF_6)_{10}$ in MeCN was titrated with a solution of Solomon link $[1](PF_6)_8$ (up to 1 eq. relative to $[2\bullet Cl](PF_6)_9$). No changes were

observed in the ^1H NMR signals of either interlocked species during the titration. This result indicates that the affinity of the Solomon link $[\mathbf{1}](\text{PF}_6)_8$ for Cl^- must be at least two orders of magnitude lower^{S7} than that of knot $[\mathbf{2}\bullet\text{Cl}](\text{PF}_6)_9$, therefore $K_1 \leq 3 \cdot 10^8 \text{ M}^{-1}$.

The combination of both of these experiments allows the association constant of Solomon link $[\mathbf{1}](\text{PF}_6)_8$ with Cl^- to be estimated at $K_1 \approx (3 \pm 2.5) \cdot 10^8 \text{ M}^{-1}$ (MeCN).

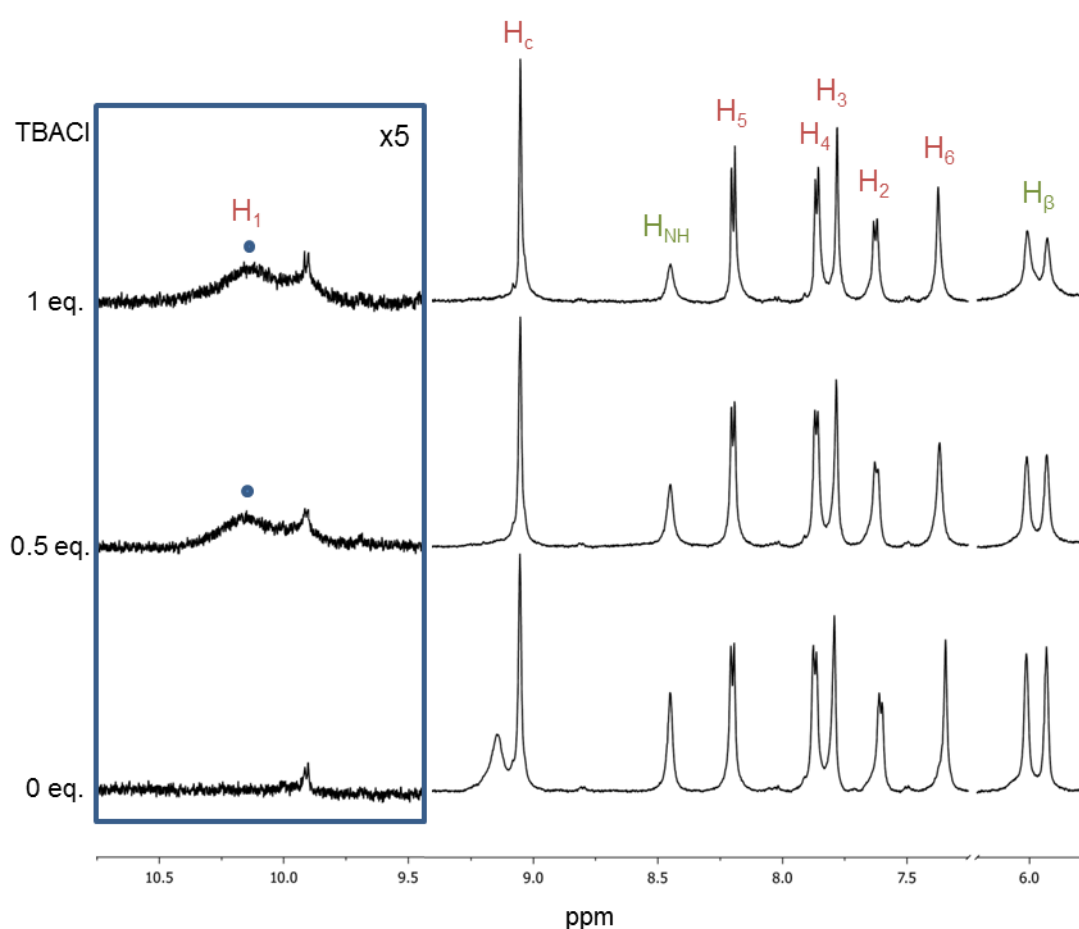


Figure S1. Partial ^1H NMR (600 MHz, CD_3CN , 298 K) of a $1.4 \times 10^{-4} \text{ M}$ 1:1 mixture of Solomon Link $[\mathbf{1}](\text{PF}_6)_8$ and calix[4]bipyrrole $\mathbf{51}$ in the presence of increasing amounts of TBACl (tetrabutylammonium chloride) at 298 K. The insert shows the signals of protons H^1 with a 5-fold increased intensity in comparison with the rest of the spectra. The blue rectangle shows the position of the H^1 protons pointing towards the central cavity of the link. The pyrrole NH and beta protons are annotated as H^{NH} and H^β , respectively. The amount of TBACl added is given as equivalents relative to $[\mathbf{1}](\text{PF}_6)_8$.

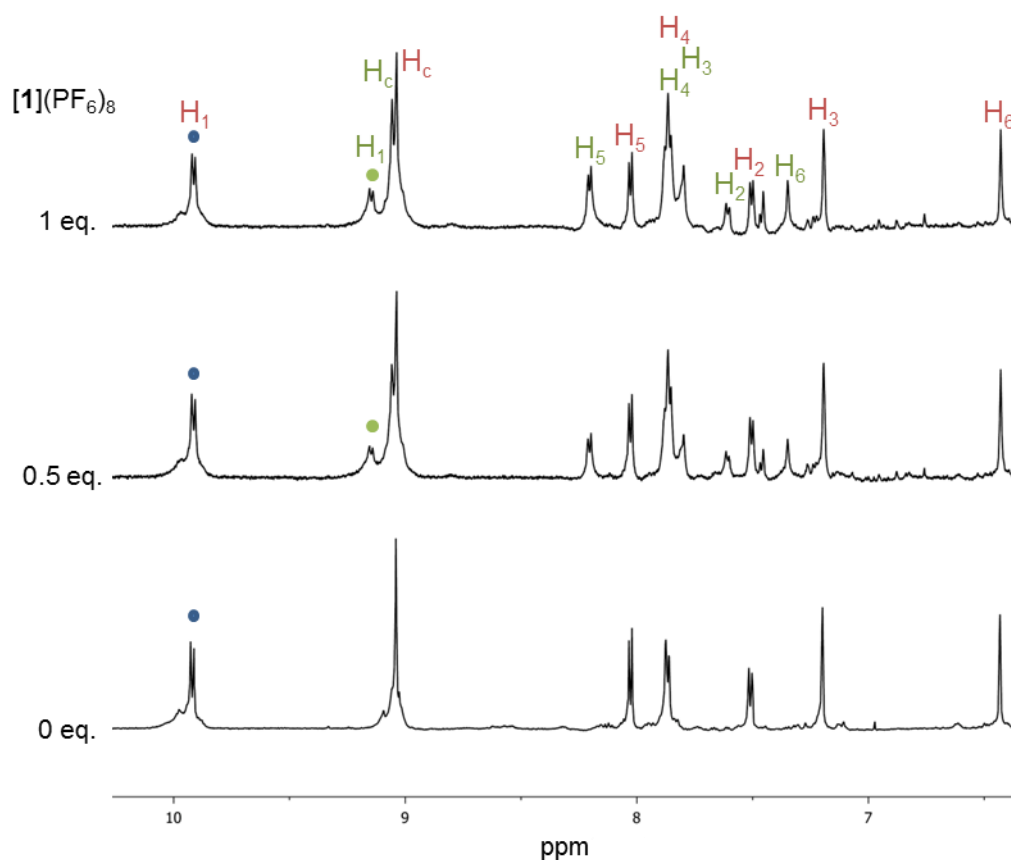


Figure S2. Partial ^1H NMR (600 MHz, CD_3CN , 298 K) of a 7.5×10^{-5} M solution the pentafoil knot $[\mathbf{2}\cdot\text{Cl}](\text{PF}_6)_9$ in the presence of an increasing amount of the Solomon Link $[\mathbf{1}](\text{PF}_6)_8$ at 298 K. The H1 protons, pointing towards the central cavity of the helicate, corresponding to the knot $[\mathbf{2}\cdot\text{Cl}](\text{PF}_6)_9$ are labelled with a blue dot and the analogous H1 protons in the link $[\mathbf{1}](\text{PF}_6)_8$ are labelled with a green dot. The color of the proton labels indicates the helicate they correspond to: red for the knot $[\mathbf{2}\cdot\text{Cl}](\text{PF}_6)_9$ and green for the link $[\mathbf{1}](\text{PF}_6)_8$. The amount of link $[\mathbf{1}](\text{PF}_6)_8$ added is given in equivalents relative to $[\mathbf{2}\cdot\text{Cl}](\text{PF}_6)_9$.

6.5.3.1.2. Determination of K_1 for Solomon link $[1](PF_6)_8$ with Br^- by competition against calix[4]bipyrrole **S1**

The strength of the interaction between Solomon link $[1](PF_6)_8$ and Br^- was assessed by competitive binding titrations. Receptor **S1** and pentafoil knot $[2](PF_6)_{10}$ were used as competitive hosts for Br^- . The association constant between **S1** and Br^- has previously been reported²³ as $K_1 = 112\,000\ M^{-1}$ (MeCN) and the association constant between pentafoil knot $[2](PF_6)_{10}$ and Br^- has been determined in section 3.2.2 as $K_1 = (1.7 \pm 0.2) \times 10^{10}\ M^{-1}$ (MeCN).

A $1.4 \times 10^{-4}\ M$ 1:1 mixture of Solomon link $[1](PF_6)_8$ and calix[4]bipyrrole **S1** in MeCN was titrated with TBABr. Negligible changes were observed in the 1H NMR signals of **S1** upon addition of Br^- (up to 1 eq. relative to $[1](PF_6)_8$) whereas signals characteristic of the formation of $[1 \bullet Br](PF_6)_8$ were observed (see Figure S11). This indicates that the affinity of the Solomon link $[1](PF_6)_8$ for Br^- should be at least two orders of magnitude higher³³ than that of receptor **S1**, and hence $K_1 \geq 10^7\ M^{-1}$. Because of the limitations regarding the precise determination of the quantity of calix[4]bipyrrole-bound $[S1 \bullet Br]$ no greater accuracy can be claimed for the measurement of the Solomon link K_1 with Br^- .

Similarly, a $7.5 \times 10^{-5}\ M$ solution of pentafoil knot $[2 \bullet Br](PF_6)_{10}$ in MeCN was titrated with a solution of Solomon link $[1](PF_6)_8$ (up to 1 eq. relative to $[2 \bullet Br](PF_6)_{10}$). No changes were observed in the 1H NMR signals of either interlocked species during the titration. This result indicates that the affinity of the Solomon link $[1](PF_6)_8$ for Br^- must be at least two orders of magnitude lower³³ than that of knot $[2 \bullet Br](PF_6)_{10}$, therefore $K_1 \leq 10^8\ M^{-1}$.

The combination of these experiments allows the association constant of Solomon link $[1](PF_6)_8$ with Br^- to be estimated at $K_1 \approx (1 \pm 0.5) \times 10^7\ M^{-1}$ (MeCN)

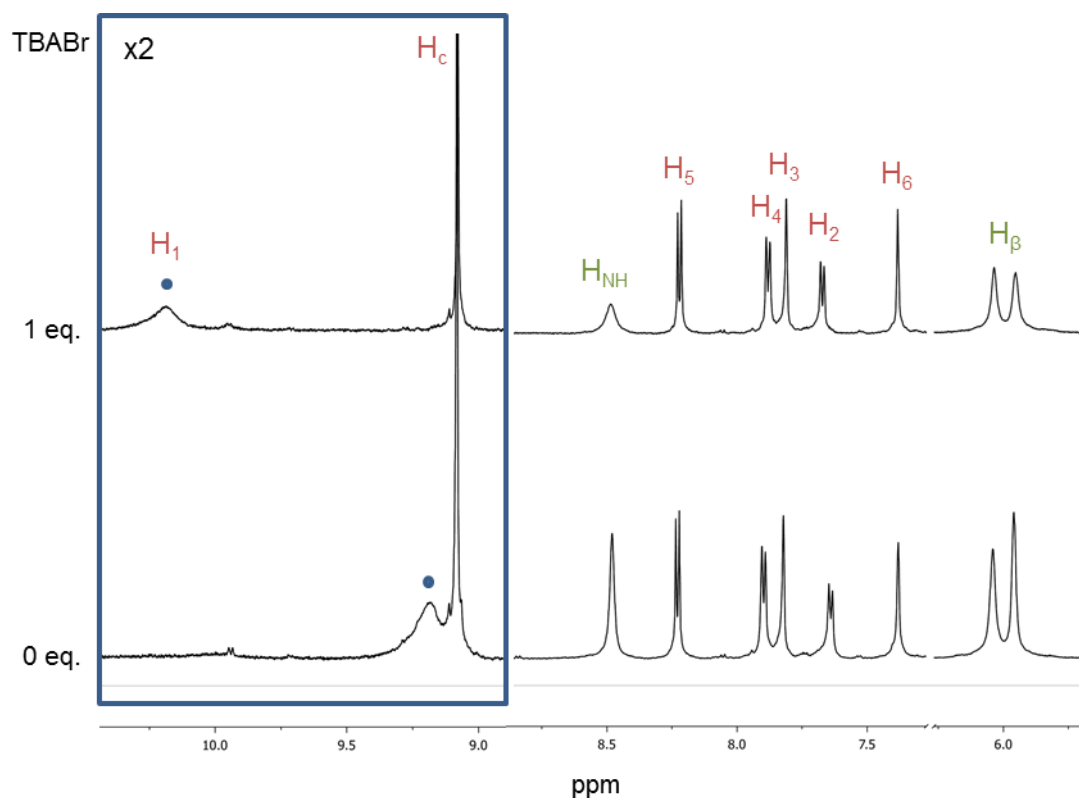


Figure S3. Partial ^1H NMR (600 MHz, CD_3CN , 298 K) of a 1.4×10^{-4} M 1:1 mixture of Solomon Link $[\mathbf{1}](\text{PF}_6)_8$ and calix[4]bipyrrole $\mathbf{S1}$ in the presence of an increasing amount of TBABr at 298 K. The insert shows the signals of protons H^1 with a 2-fold increased intensity in comparison with the rest of the spectra. The H^1 protons pointing towards the central cavity of the link are labelled with a blue dot. The pyrrole NH and beta protons are annotated as H^{NH} and H^β , respectively. The amount of TBABr added is given as equivalents relative to $[\mathbf{1}](\text{PF}_6)_8$.

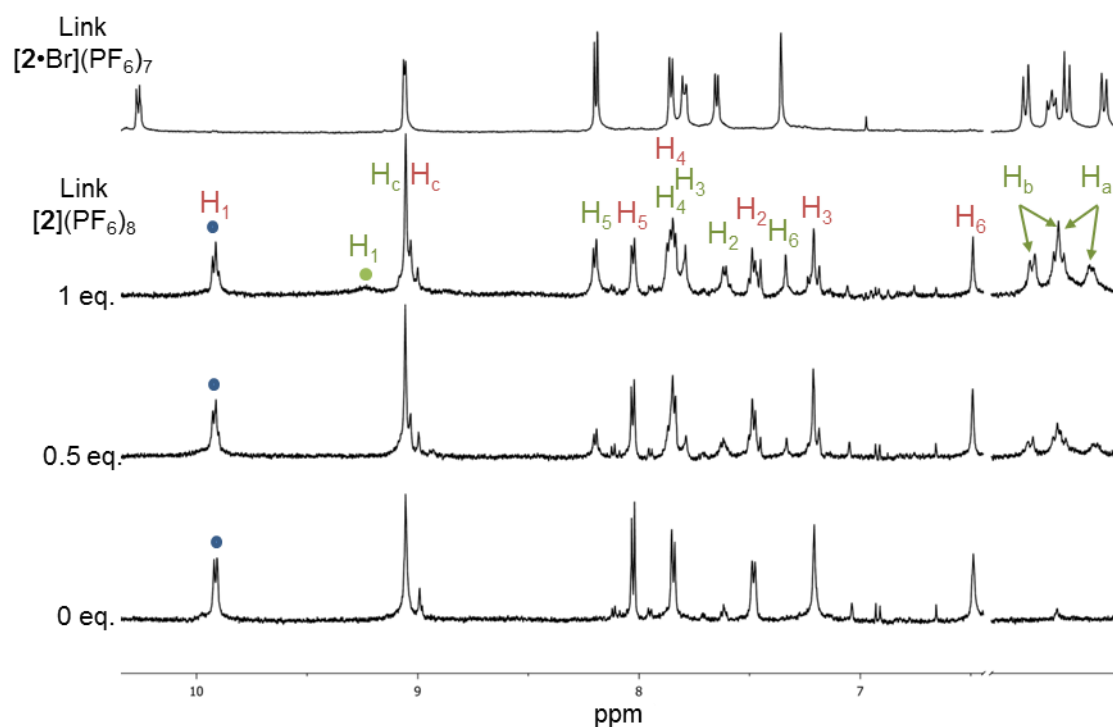


Figure S4. Partial ^1H NMR (600 MHz, CD_3CN , 298 K) of a 7.5×10^{-5} M solution of the pentafoil knot $[\mathbf{2}\cdot\text{Br}](\text{PF}_6)_9$ in the presence of an increasing amount of the Solomon Link $[\mathbf{1}](\text{PF}_6)_8$ at 298 K. The blue circle indicates the H^1 protons of the knot $[\mathbf{2}\cdot\text{Br}](\text{PF}_6)_9$ and the green circle indicates the position of the analogous proton in the link $[\mathbf{1}](\text{PF}_6)_8$. The colour of the proton labels indicates the helicate they correspond to: red for knot $[\mathbf{2}\cdot\text{Br}](\text{PF}_6)_9$ and green for link $[\mathbf{1}](\text{PF}_6)_8$. The amount of link $[\mathbf{1}](\text{PF}_6)_8$ added is shown in equivalents relative to $[\mathbf{2}\cdot\text{Br}](\text{PF}_6)_9$. Due to the broadness of the proton H^1 of $[\mathbf{1}](\text{PF}_6)_8$, protons H^a and H^b of the link were used to quantify the formation of $[\mathbf{1}\cdot\text{Br}](\text{PF}_6)_8$. When one equivalent of link was added to the knot the splitting of the protons H^a and H^b characteristic of $[\mathbf{1}\cdot\text{Br}](\text{PF}_6)_7$ was not observed, demonstrating that the affinity of $[\mathbf{2}](\text{PF}_6)_{10}$ for Br^- is greater than that of $[\mathbf{1}](\text{PF}_6)_8$.

6.5.3.1.3. Determination of K_1 for Solomon link $[1](PF_6)_8$ with I^- by direct titration with tetrabutylammonium iodide

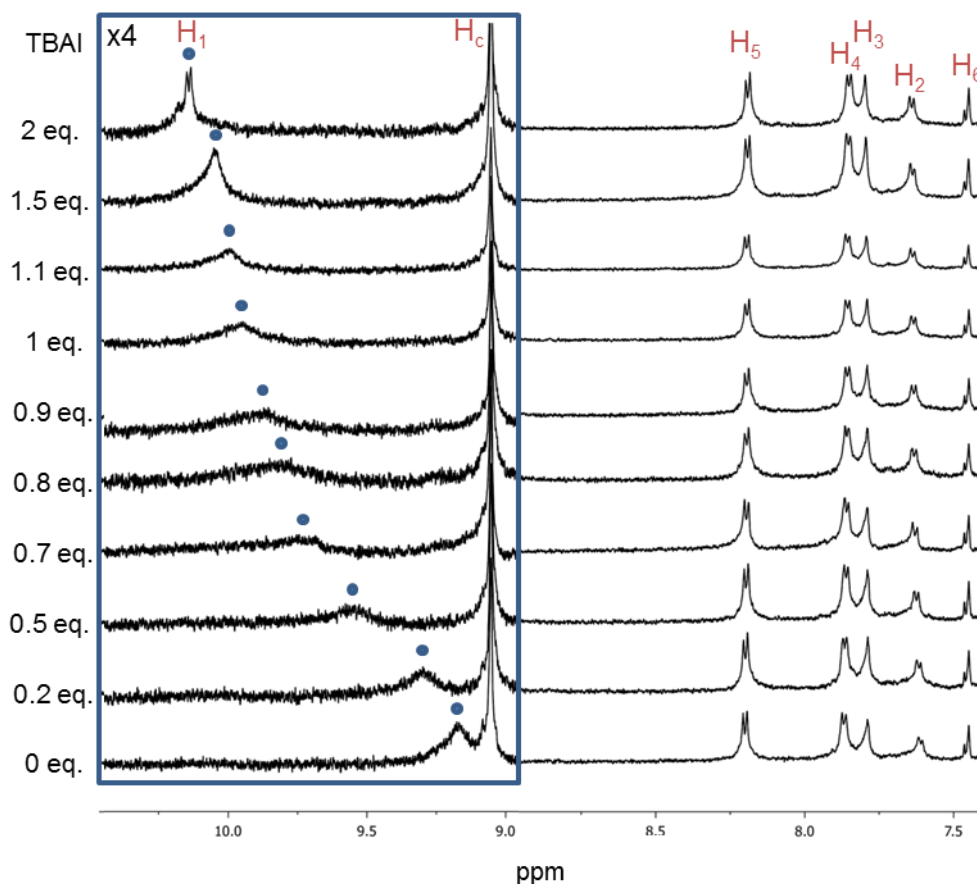


Figure S5. Partial 1H NMR (600 MHz, CD_3CN , 298 K) of a 7.1×10^{-5} M solution of Solomon link $[1](PF_6)_8$ in CD_3CN at 298 K in the presence of an increasing amount of TBAI. The insert shows the signals of protons H^1 and H^c with a 4-fold increased intensity in comparison with the rest of the spectra. The blue rectangle shows the position of the H^1 protons of $[1](PF_6)_8$. The amount of TBAI added is given as equivalents relative to $[1](PF_6)_8$.

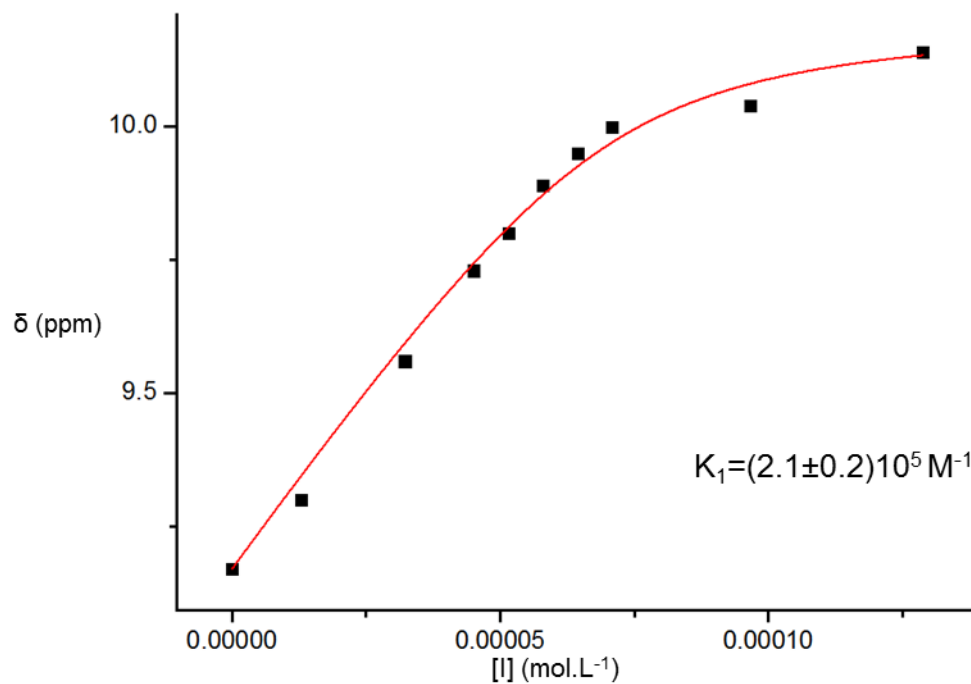


Figure S6. Binding isotherm derived from the ¹H NMR spectroscopic titration of a 7.1×10^{-5} M solution of Solomon link **[1]**(PF₆)₈ with TBAI in CD₃CN at 298 K. The red line shows the fitting to a 1:1 model obtained using eq. 25 in OriginPro.³¹

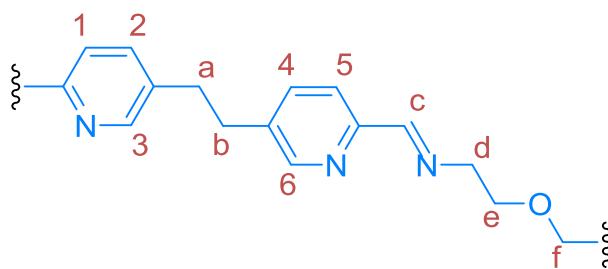
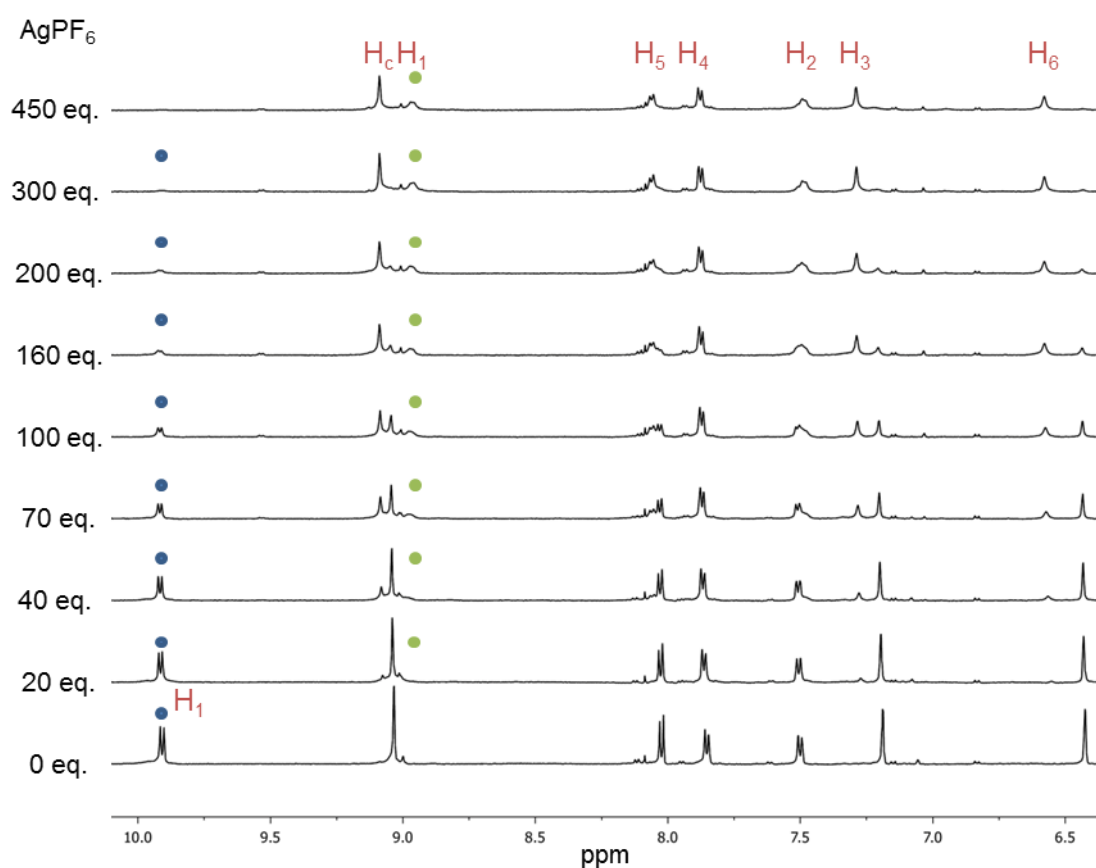
6.5.3.2. Pentafoil knot $[2](PF_6)_{10}$ 6.5.3.2.1. Determination of K_1 for pentafoil knot $[2](PF_6)_{10}$ with Cl^- by competitivebinding with $AgPF_6$ 

Figure S7. Partial 1H NMR (600 MHz, CD_3CN , 298 K) of a 1.4×10^{-4} M solution of pentafoil knot $[2 \bullet Cl](PF_6)_9$ in CD_3CN at 298 K in the presence of an increasing amount of $AgPF_6$. The blue circle indicates the H^1 protons of knot $[2 \bullet Cl](PF_6)_9$ and the green circle indicates the analogous H^1 proton of the 'empty' knot $[2](PF_6)_{10}$. The amount of $AgPF_6$ added is shown in equivalents relative to $[2 \bullet Cl](PF_6)_9$.

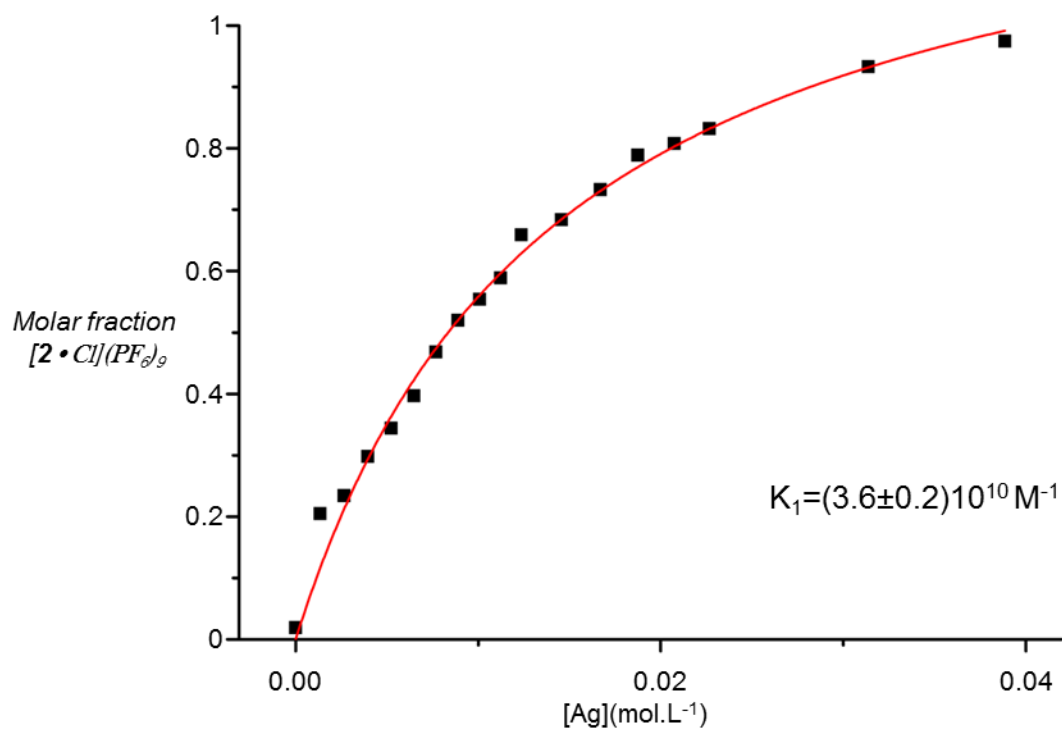


Figure S8. Binding isotherm derived from the 1H NMR spectroscopic titration of pentafoil knot $[2 \cdot Cl](PF_6)_9$ ($1.4 \times 10^{-4} M$) with $AgPF_6$ in CD_3CN at 298 K. The red line shows the fitting to a 1:1 model obtained using eq. 19 in OriginPro.³¹ The solubility product constant K_{sp} of $AgCl$ has previously been reported³⁴ as $K_{sp} = 10^{-12.4} M^2$ (MeCN).

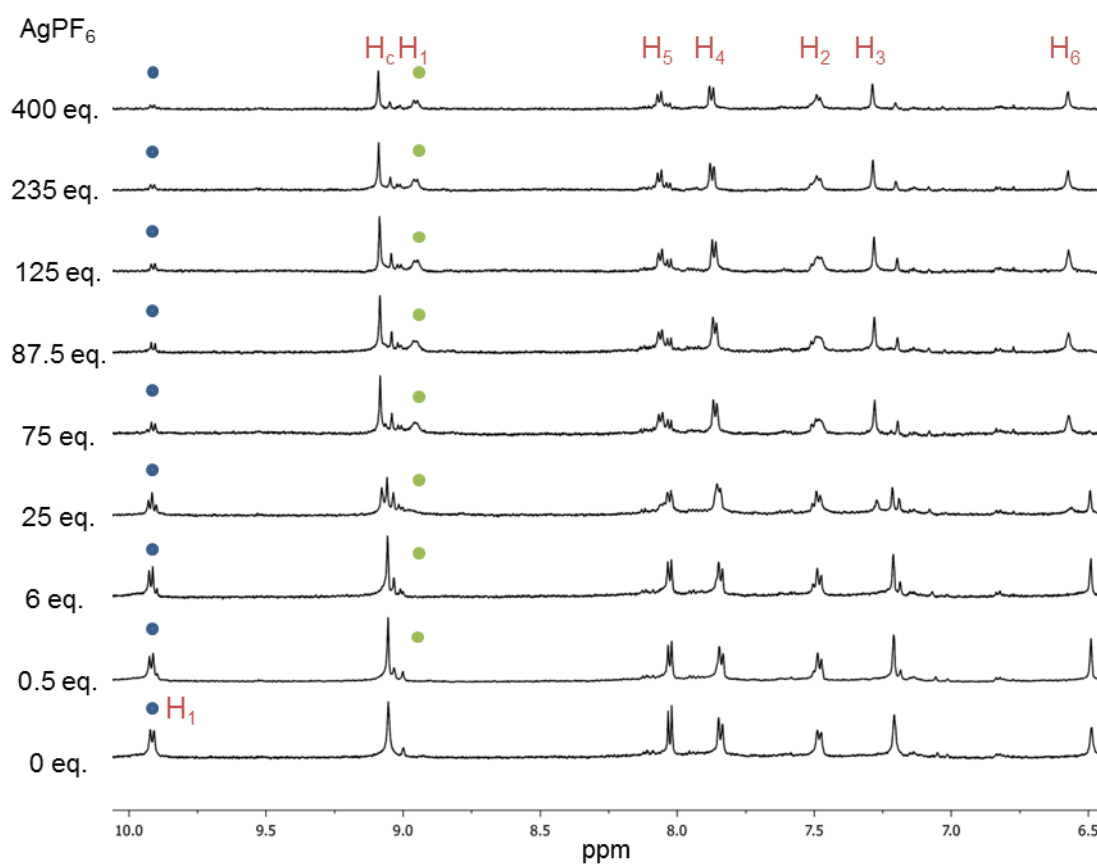
6.5.3.2.2. Determination of K_1 for pentafoil knot $[2](PF_6)_{10}$ with Br^- by competitivebinding against $AgPF_6$ 

Figure S9. Partial 1H NMR (600 MHz, CD_3CN , 298 K) of a 6.0×10^{-5} M 1:1 mixture of pentafoil knot $[2](PF_6)_{10}$ and TBABr (tetrabutylammonium bromide) in CD_3CN at 298 K in the presence of an increasing amount of $AgPF_6$. The blue circle indicates the H^1 protons of knot $[2\bullet Br](PF_6)_9$ and the green circle indicates the analogous H^1 protons of the 'empty' knot $[2](PF_6)_{10}$. The amount of $AgPF_6$ added is shown in equivalents relative to $[2](PF_6)_{10}$.

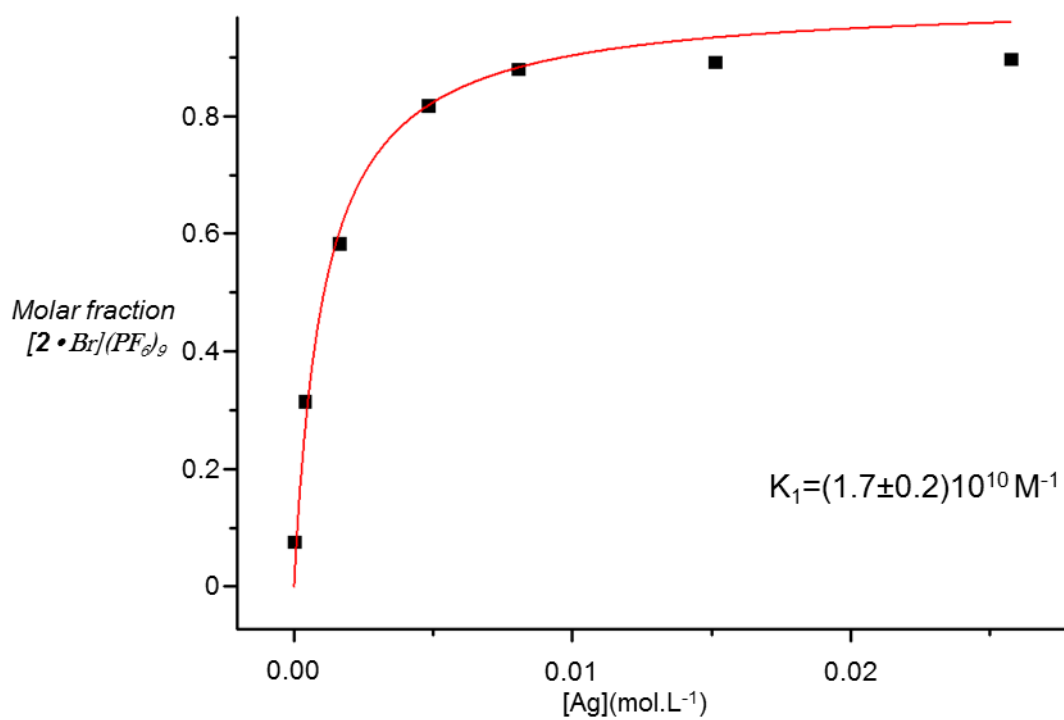


Figure S10. Binding isotherm derived from the ¹H NMR spectroscopic titration of a 6.0 × 10⁻⁵ M 1:1 mixture of pentafoil knot [2](PF₆)₁₀ and TBABr with AgPF6 in CD₃CN at 298 K. The red line shows the fitting to a 1:1 model obtained using eq. 19 for OriginPro.³¹ The solubility product constant *K*_{sp} of AgBr has previously been reported³⁴ as *K*_{sp} = 10^{-13.2} M² (MeCN).

6.5.3.2.3. LRESI-MS of a 1:1:1 mixture of [2•Cl](PF₆)₉:TBABr:S1

In order to probe the relative affinities of pentafoil knot [2](PF₆)₁₀ for Cl⁻ and Br⁻ a 1:1:1 mixture of [2•Cl](PF₆)₉:TBABr:S1 was analysed by ESI-MS. The ¹H NMR titration predicts that the two binding constants are similar (with K_1 pentafoil knot [2](PF₆)₁₀ for Br⁻ slightly smaller). Calix[4]bipyrrole S1 was used to bind the excess halide in the mixture and minimize the formation of knot containing two or more halides (e.g. [2•Cl](Br)(PF₆)₈).

Electrospray ionization mass spectrometry (ESI-MS) confirmed the presence of m/z peaks corresponding to multiply charged (e.g., +5, +6 or +7) knot [2](PF₆)₁₀ complexes with chloride or bromide (Figure S11). This result indicates that the chloride anion present in the starting [2•Cl](PF₆)₉ material gets exchanged by bromide, consistent with the affinity of knot 2 for chloride and bromide being similar.

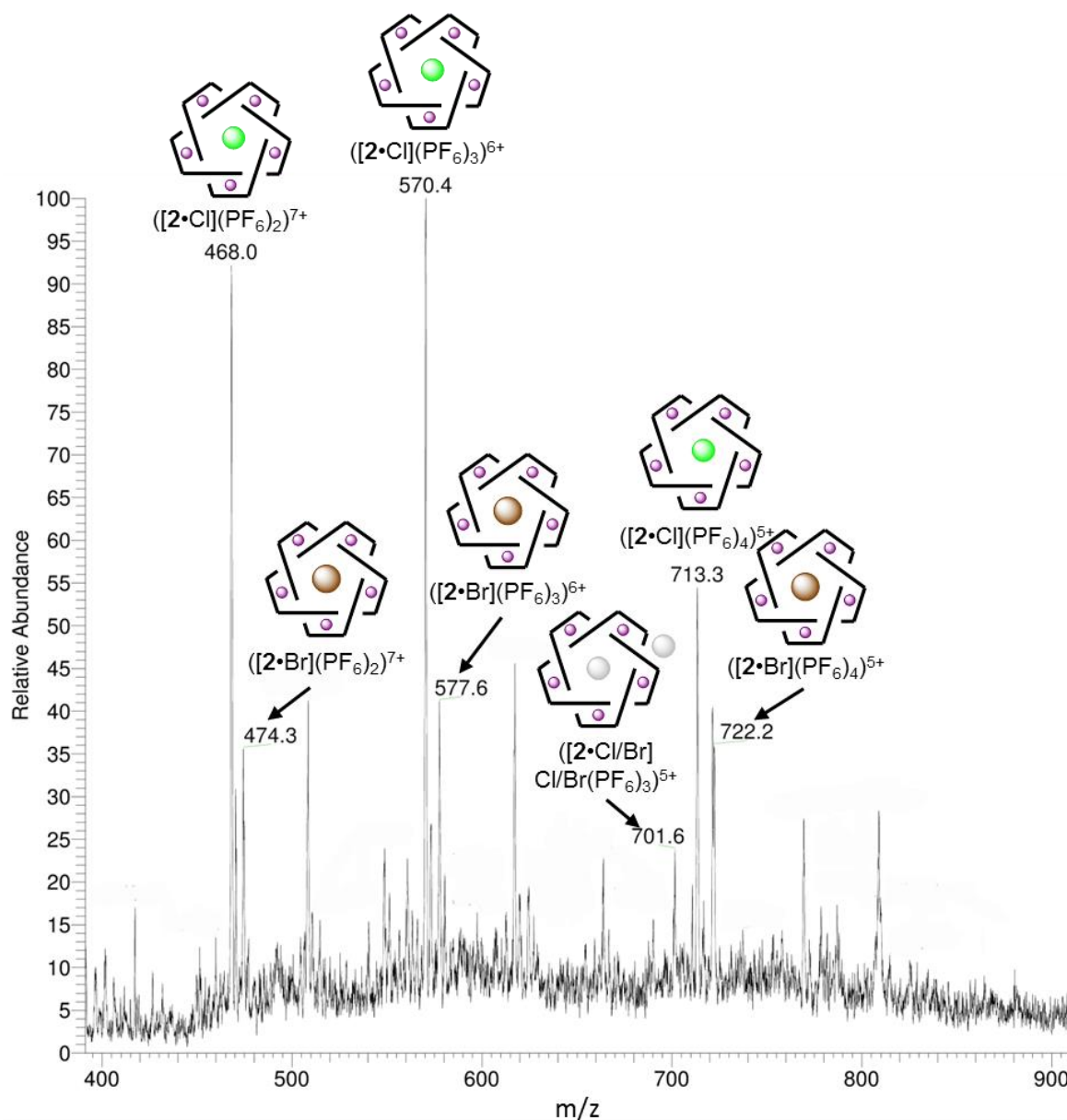


Figure S11. Partial LRESI-MS spectra of a 1:1:1 mixture of $[2 \bullet \text{Cl}](\text{PF}_6)_9$:TBABr:S1

6.5.3.2.4. Determination of K_1 for pentafoil knot $[2](PF_6)_{10}$ with I⁻ by 1H NMR

direct titration

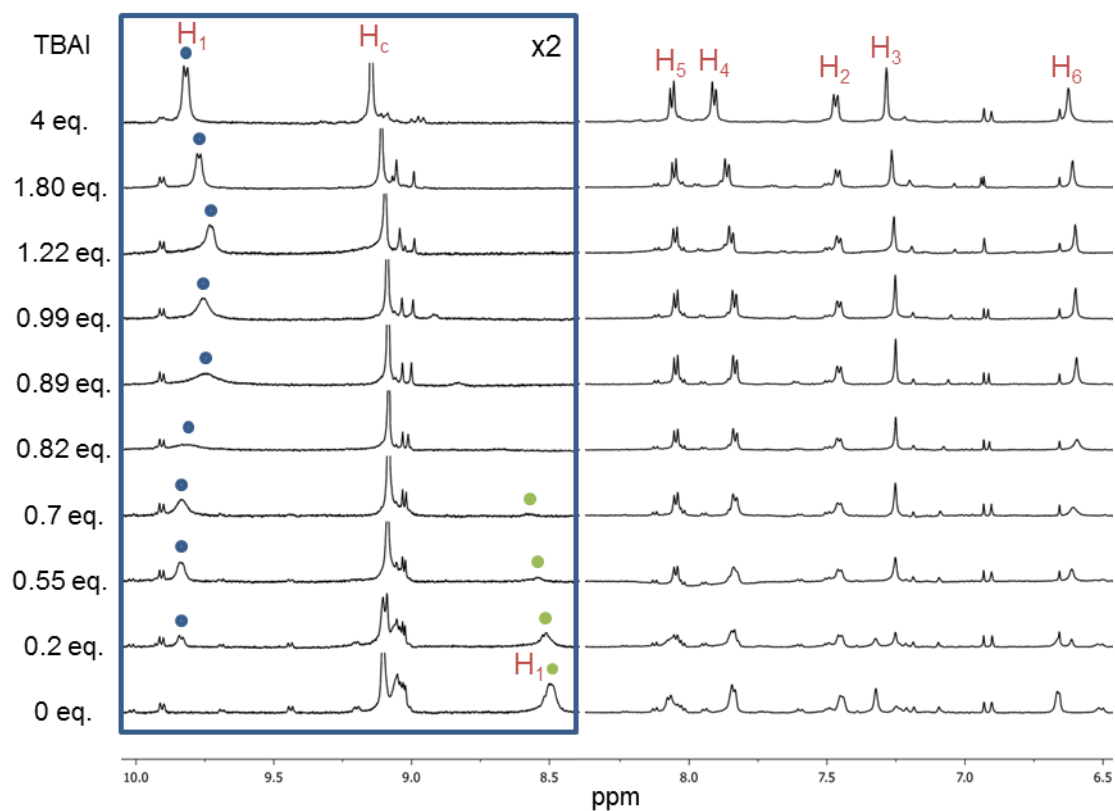


Figure S12. Partial 1H NMR (600 MHz, CD_3CN , 298 K) of a 6.56×10^{-5} M solution of 'empty' pentafoil knot $[2](PF_6)_{10}$ in CD_3CN at 298 K in the presence of an increasing amount of TBAI (tetrabutylammonium iodide). The blue circle indicates the H^1 protons of knot $[2 \bullet I](PF_6)_9$ and the green circle indicates the analogous H^1 protons in the 'empty' knot $[2](PF_6)_{10}$. The amount of TBAI added is given as equivalents relative to $[2](PF_6)_{10}$.

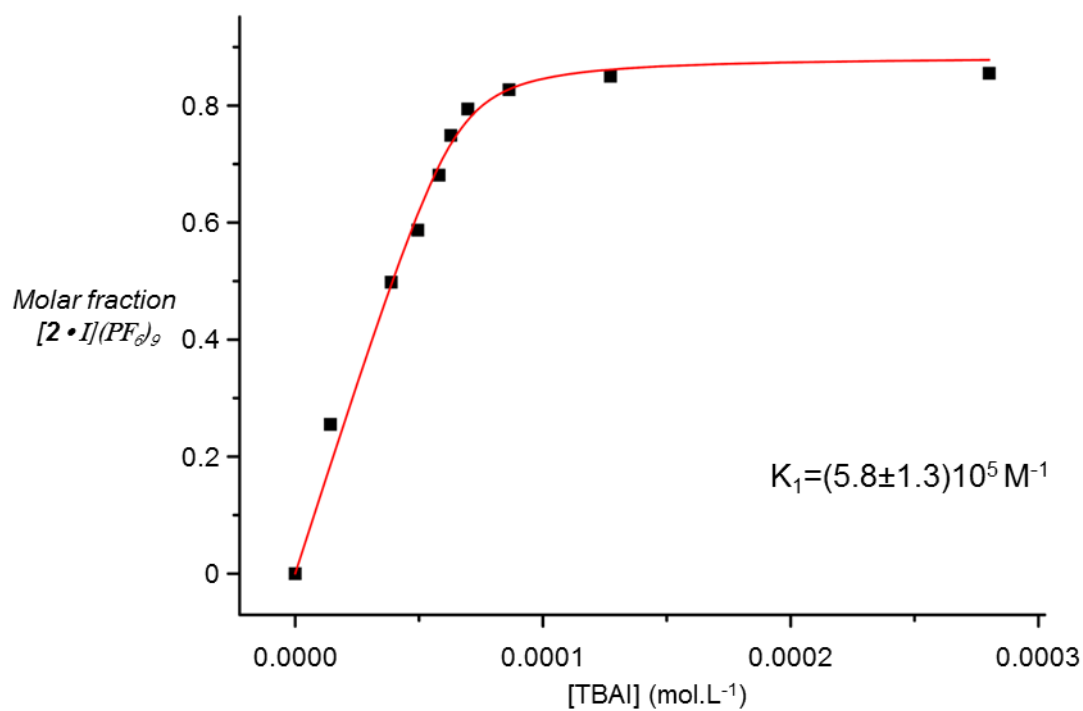
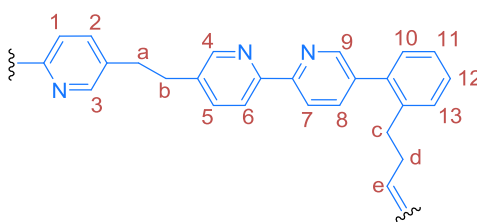


Figure S13. Binding isotherm derived from the ¹H NMR spectroscopic titration of a 6.56×10^{-5} M mixture of pentafoil knot [2](PF₆)₁₀ with TBAI in CD₃CN at 298 K. The red line shows the fitting to a 1:1 model obtained using eq. 24 in OriginPro.³¹

6.5.3.3. Star of David catenane **[3](PF₆)₁₂**



6.5.3.3.1. Determination of K_1 for Star of David catenane **[3](PF₆)₁₂** with Cl⁻ by competitive binding against calix[4]bipyrrole **S1**

The strength of the interaction between the Star of David catenane **[3](PF₆)₁₂** and Cl⁻ was assessed by competitive binding titrations. Receptor **S1** was used as a competitive host for Cl⁻. The association constant between **S1** and Cl⁻ has previously been reported²³ as $K_1 = 2\,940\,000\text{ M}^{-1}$ in MeCN.

A 1:1 mixture of Star of David catenane **[3](PF₆)₁₂** and TBACl in CD₃CN was titrated by ¹H NMR with a solution of calix[4]bipyrrole **S1** in CD₃CN. Two equivalents of the calix[4]bipyrrole **S1** were necessary to remove all the Cl⁻ from **[3•Cl](PF₆)₁₁** and restore the ¹H NMR spectrum characteristic of **[3](PF₆)₁₂**. This indicates that the affinity of the Star of David catenane **[3](PF₆)₁₂** for chloride is less³³ than that of receptor **S1** and therefore the upper boundary for the association constant of the Star of David catenane **[3](PF₆)₁₂** with Cl⁻ is $K_1 \sim 10^5\text{ M}^{-1}$ (MeCN). The addition of TBACl to the Star of David **[3](PF₆)₁₂** produced significant changes in the chemical shift of protons H¹ (the inner helicate protons) and H⁷ (which point towards the outside of the helicate) indicating that chloride does not preferentially bind in the inner cavity of **[3]**.

The combination of both of these experiments allows an upper limit for the helicate association constant of $K_1 \leq 10^5\text{ M}^{-1}$ (MeCN). However the lack of selectivity for the inner binding pocket prevents any direct comparison with the other systems presented.

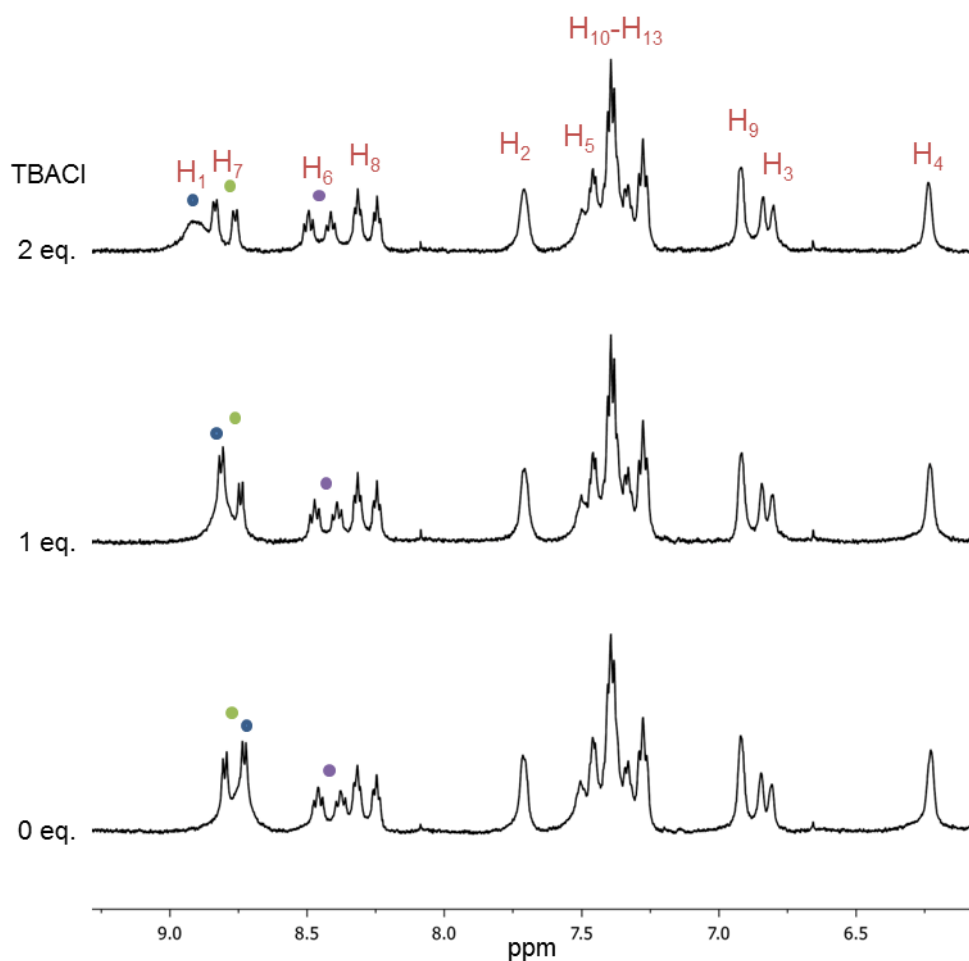


Figure S15. Partial ^1H NMR (600 MHz, CD_3CN , 298 K) of a 6.4×10^{-5} M solution of Star of David catenane $[\mathbf{3}](\text{PF}_6)_{12}$ in CD_3CN at 298 K in the presence of an increasing amount of TBACl. The blue circle indicates the H^1 protons of link $[\mathbf{3}](\text{PF}_6)_{12}$. The green and purple circles indicate the pyridyl protons H^6 and H^7 of $[\mathbf{3}](\text{PF}_6)_{12}$ which are protons pointing towards the outside of the helicate. The amount of TBACl added is shown in equivalents relative to $[\mathbf{3}](\text{PF}_6)_{12}$.

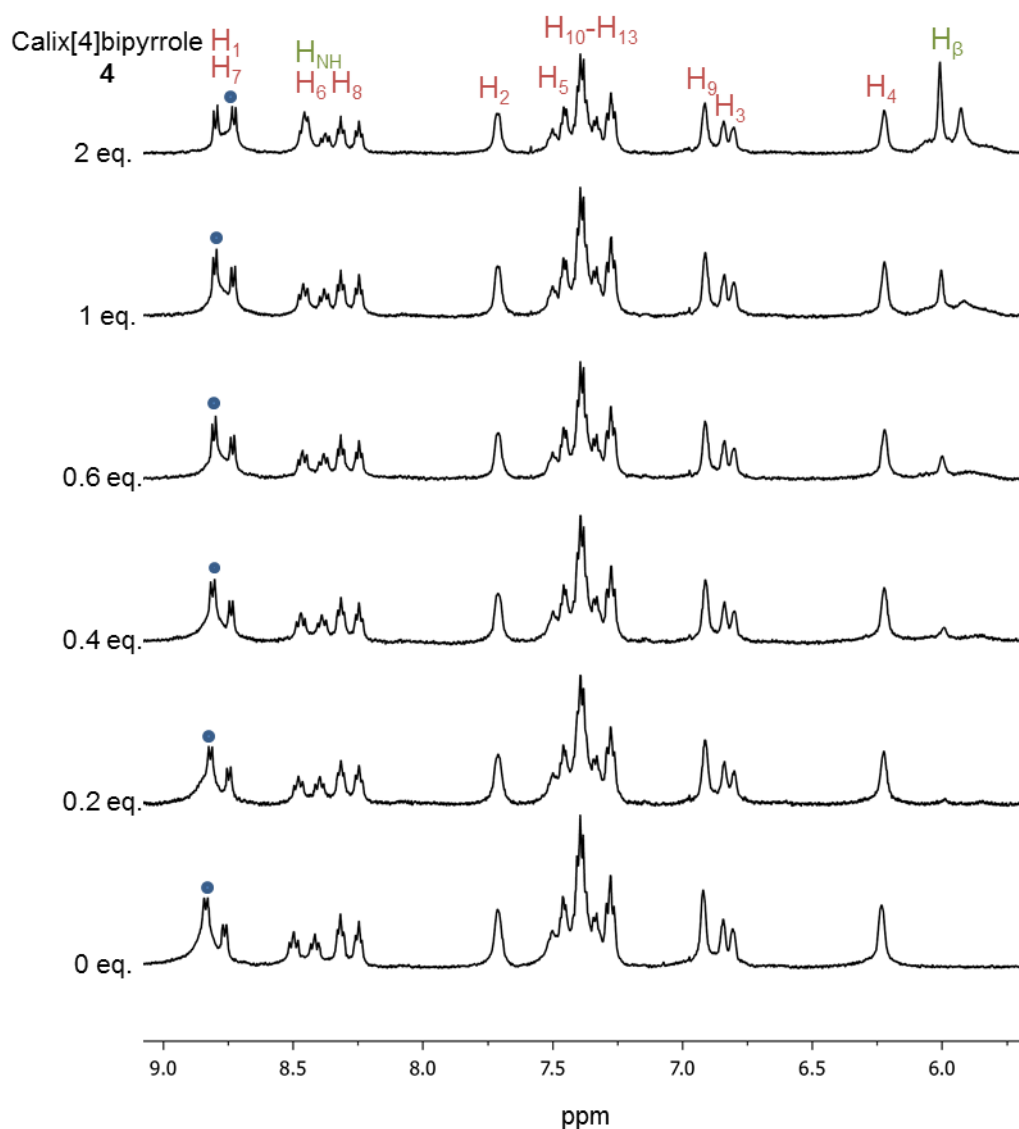


Figure S16. Partial ^1H NMR (600 MHz, CD_3CN , 298 K) of a 9.4×10^{-5} M 1:1 mixture solution of Star of David catenane **[3]**(PF_6)₁₂ and TBACl in CD_3CN at 298 K in the presence of an increasing amount of calix[4]bipyrrole **S1**. The blue circle indicates the H^1 protons of link **[3]**(PF_6)₁₂. The pyrrole NH and beta protons are annotated as H^{NH} and H^β . The amount of calix[4]bipyrrole **S1** added is shown in equivalents relative to **[3]**(PF_6)₁₂.

6.5.3.3.2. Determination of K_1 for Star of David catenane $[3](PF_6)_{12}$ with***Br⁻ by competitive binding versus calix[4]bipyrrole S1***

The strength of the interaction between the Star of David catenane $[3](PF_6)_{12}$ and Br^- was assessed by competitive binding titrations by 1H NMR. Receptor **S1** was used as a competitive host for Br^- . The association constant between **S1** and Br^- has been previously reported²³ as $K_1 = 112\ 000\ M^{-1}$.

A 1:1 mixture of Star of David catenane $[3](PF_6)_{12}$ and TBABr in CD_3CN was titrated with a solution of calix[4]bipyrrole **S1** in CD_3CN . Two equivalents of the calix[4]bipyrrole **S1** were necessary to remove all the Br^- from $[3\bullet Br](PF_6)_{11}$ and restore the 1H NMR spectrum characteristic of $[3](PF_6)_{12}$. This indicates that the affinity of the Star of David catenane for bromide is less³³ than that of receptor **S1** and therefore the upper boundary for the association constant of the Star of David catenane with Br^- is $K_1 \sim 10^4\ M^{-1}$ in MeCN. The addition of TBABr to the Star of David catenane $[3](PF_6)_{12}$ produced significant changes in the chemical shift of protons H^1 (which point inside the inner binding pocket) and protons H^7 (which point towards the outside of the helicate) indicating that bromide does not preferentially bind in the inner binding pocket of **[3]**.

The combination of both of these experiments allows an upper limit to be set for the link $[3](PF_6)_{12}$ association constant of $K_1 \leq 10^4\ M^{-1}$ in MeCN. However the lack of selectivity for the inner binding pocket prevents any direct comparison with the other systems presented.

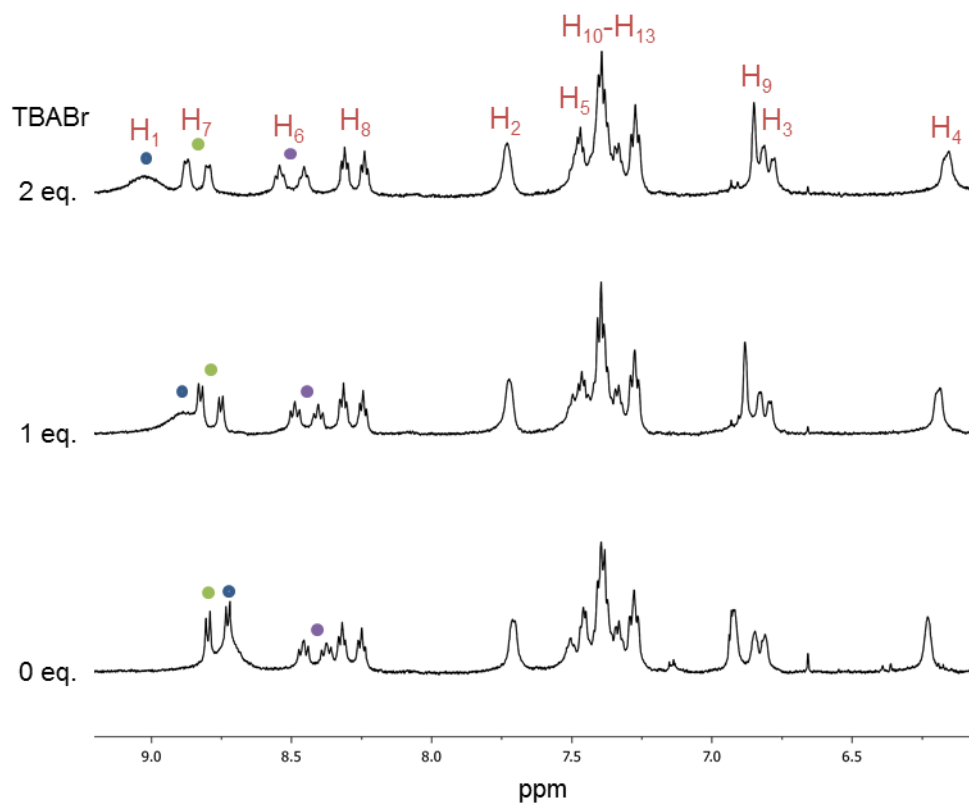


Figure S17. Partial ^1H NMR (600 MHz, CD_3CN , 298 K) of a 6.4×10^{-5} M solution of Star of David catenane $[\mathbf{3}](\text{PF}_6)_{12}$ in CD_3CN at 298 K in the presence of an increasing amount of TBABr. The blue circle indicates the H^1 protons of link $[\mathbf{3}](\text{PF}_6)_{12}$. The green and purple circles indicate the positions of the pyridyl protons H^6 and H^7 of $[\mathbf{3}](\text{PF}_6)_{12}$ which are protons pointing towards the outside of the helicate. The amount of TBABr added is shown in equivalents relative to $[\mathbf{3}](\text{PF}_6)_{12}$.

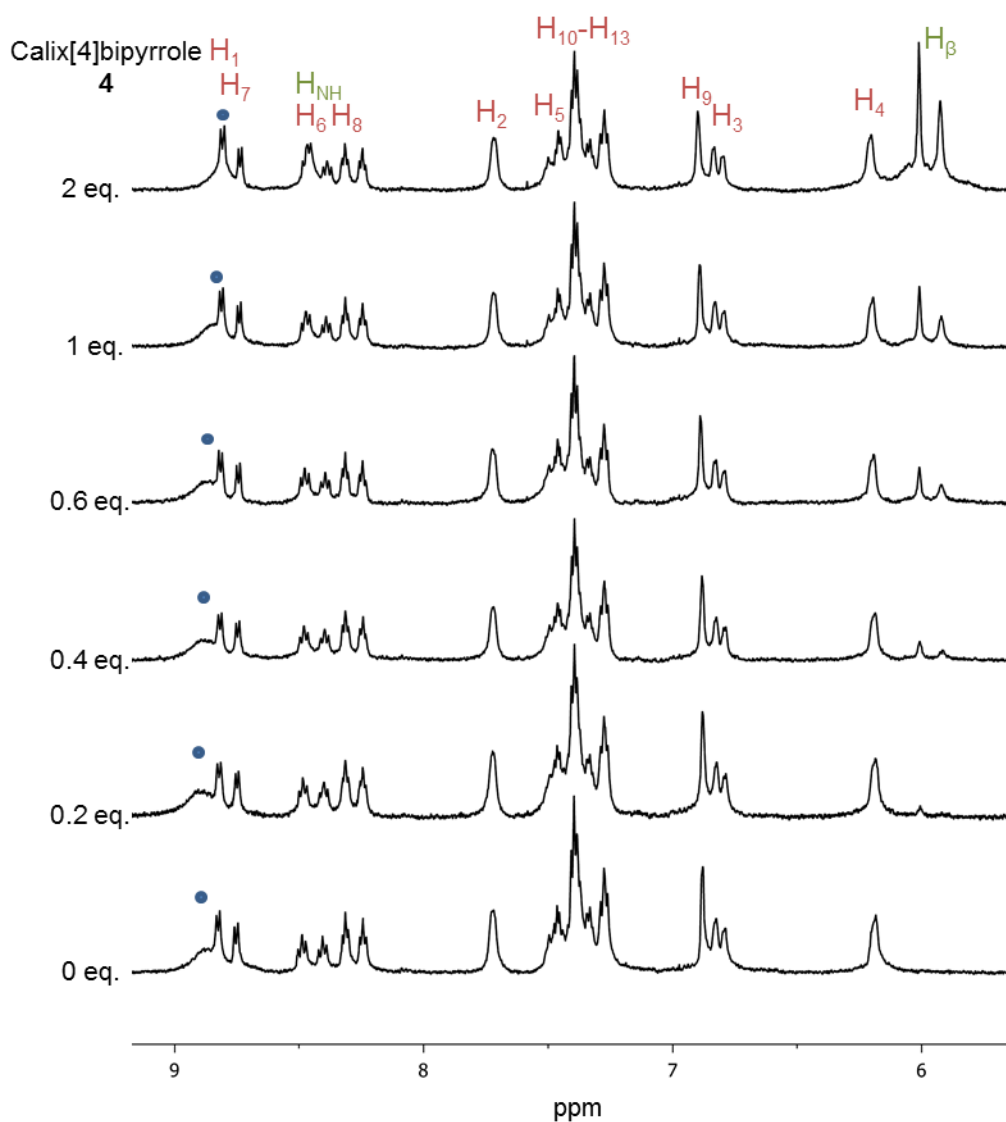


Figure S19. Partial ^1H NMR (600 MHz, CD_3CN , 298 K) of a 9.4×10^{-5} M 1:1 mixture solution of Star of David catenane $[\mathbf{3}](\text{PF}_6)_{12}$ and TBABr in CD_3CN at 298 K in the presence of an increasing amount of calix[4]pyrrole $\mathbf{1}$. The blue circle highlights the position of the H^1 protons of link $[\mathbf{3}](\text{PF}_6)_{12}$. The pyrrole NH and beta protons are annotated as H^{NH} and H^β . The amount of calix[4]pyrrole $\mathbf{1}$ added is shown in equivalents relative to $[\mathbf{3}](\text{PF}_6)_{12}$.

6.5.3.3.3. Determination of K_1 for Star of David catenane $[3](PF_6)_{12}$ with I^-

by direct titration against tetrabutylammonium iodide

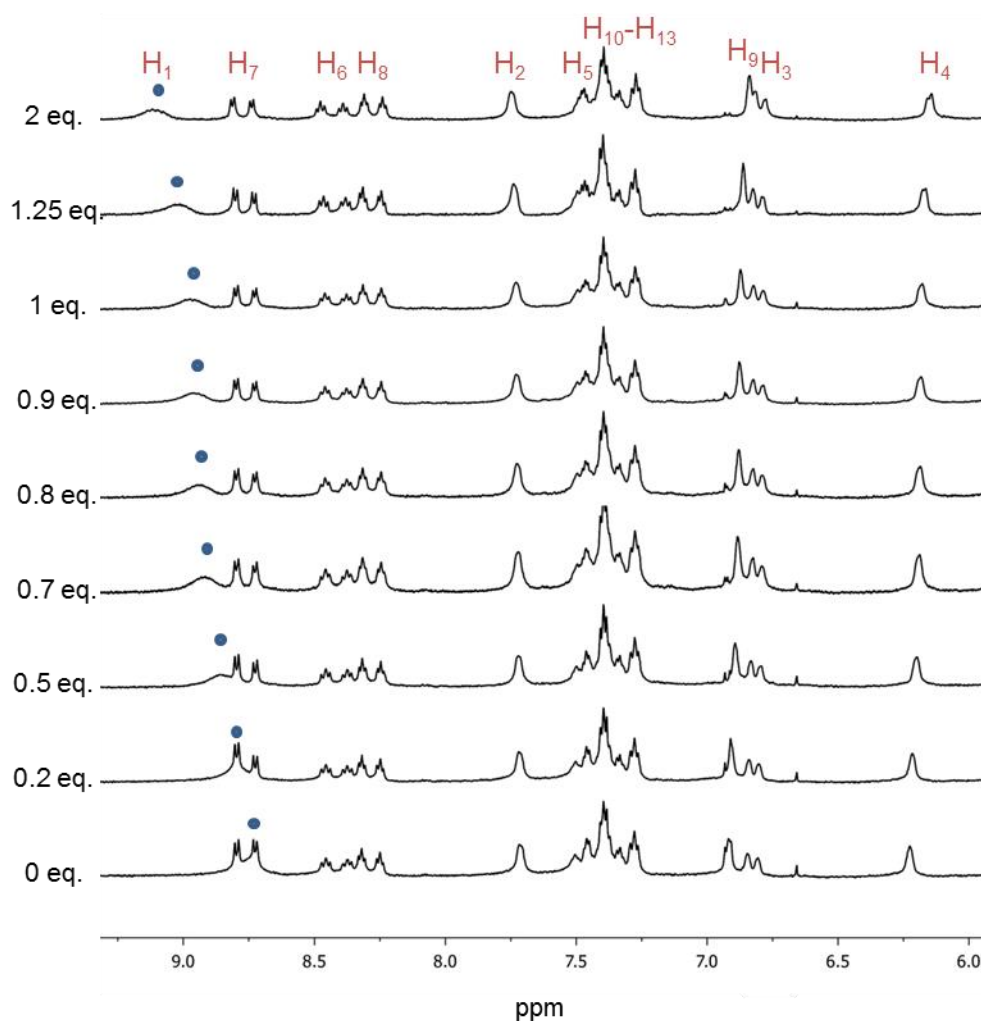


Figure S20. Partial 1H NMR (600 MHz, CD_3CN , 298 K) of a 6.3×10^{-5} M solution of Star of David catenane $[3](PF_6)_{12}$ in CD_3CN at 298 K in the presence of an increasing amount of TBAI. The blue circles indicate the position of the H^1 protons of link $[3](PF_6)_{12}$. The amount of TBAI added is shown in equivalents relative to $[3](PF_6)_{12}$.

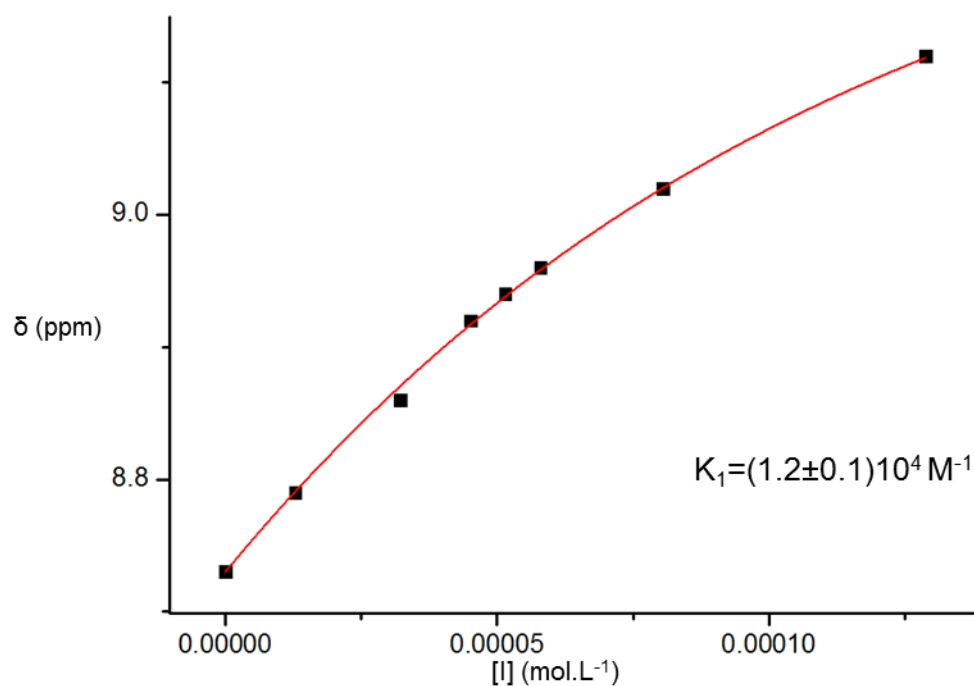


Figure S21. Binding isotherm derived from the ¹H NMR spectroscopic titration of a 6.3×10^{-5} M mixture of Star of David catenane **[3]**(PF₆)₁₂ with TBAI in CD₃CN at 298 K. The red line shows the fitting to a 1:1 model obtained using eq. 25 in OriginPro.³¹

6.6. Notes and References

1. (a) Hasenknopf, B.; Lehn, J.-M.; Kneisel, B. O.; Baum, G.; Fenske, D. *Angew. Chem., Int. Ed.* **1996**, *35*, 1838–1840. (b) Hasenknopf, B.; Lehn, J.-M.; Boumediene, N.; Dupont-Gervais, A.; Van Dorsselaer, A.; Kneisel, B.; Fenske, D. *J. Am. Chem. Soc.* **1997**, *119*, 10956–10962. (c) Hasenknopf, B.; Lehn, J.-M.; Boumediene, N.; Leize, E.; Van Dorsselaer, A. *Angew. Chem., Int. Ed.* **1998**, *37*, 3265–3268.
2. For reviews on the synthesis of molecular knots, see: (a) Dietrich-Buchecker, C. Colasson, B. X. Sauvage, J.-P. *Top. Curr. Chem.* **2005**, *249*, 261–283. (b) Lukin, O.; Vögtle, F. *Angew. Chem., Int. Ed.* **2005**, *44*, 1456–1477. (c) Fenlon, E. E. *Eur. J. Org. Chem.* **2008**, 5023–5035; (d) Beves, J. E.; Blight, B. A.; Campbell, C. J.; Leigh, D. A.; McBurney, R. T. *Angew. Chem., Int. Ed.* **2011**, *50*, 9260–9327. (e) Forgan, R. S.; Sauvage, J.-P.; Stoddart, J. F. *Chem. Rev.* **2011**, *111*, 5434–5464. (f) Amabilino, D. B.; Sauvage, J.-P. *Top. Curr. Chem.* **2012**, *323*, 107–126. (g) Ayme, J.-F.; Beves, J. E.; Campbell, C. J.; Leigh, D. A. *Chem. Soc. Rev.* **2013**, *42*, 1700–1712.
3. Gil-Ramírez, G.; Leigh, D. A.; Stephens, A. J. *Angew. Chem., Int. Ed.* **2015**, *54*, 6110–6150.
4. Beves, J. E.; Campbell, C. J.; Leigh, D. A.; Pritchard, R. G. *Angew. Chem., Int. Ed.* **2013**, *52*, 6464–6467.
5. Ayme, J.-F.; Beves, J. E.; Leigh, D. A.; McBurney, R. T.; Rissanen, K.; Schultz, D. *Nat. Chem.* **2012**, *4*, 15–20.
6. The circular helicates obtained using iminopyridine-terminated tris(bidentate) ligand strands (e.g. [1] and [2]) do not always parallel the chemistry of Lehn's tris(bipyridine) systems [Ayme, J.-F.; Beves, J. E.; Leigh, D. A.; McBurney, R. T.; Rissanen, K.; Schultz, D. *J. Am. Chem. Soc.* **2012**, *134*, 9488–9497].
7. Leigh, D. A.; Pritchard, R. G.; Stephens, A. J. *Nat. Chem.* **2014**, *6*, 978–982.
8. For reviews on metal-assembled anion receptors, see: (a) Rice, C. R. *Coord. Chem. Rev.* **2006**, *250*, 3190–3199. (b) Steed, J. W. *Chem. Soc. Rev.* **2009**, *38*, 506–519. (c) Amouri, H.; Desmarests, C.; Moussa, J. *Chem. Rev.* **2012**, *112*, 2015–2041. For anions bound within molecular capsules, see: (d) Ballester, P. *Chem. Soc. Rev.* **2010**, *39*, 3810–3830.
9. Klein, R. A. *Chem. Phys. Lett.* **2006**, *425*, 128–133.

10. Mercer, D. J.; Loeb, S. J. *Chem. Soc. Rev.* **2010**, *39*, 3612–3620.
11. For examples of anions bound in linear helicates by interactions that include CH...anion hydrogen bonds, see: (a) Goetz, S.; Kruger, P. E. *Dalton Trans.* **2006**, 1277–1284. (b) Cui, F.; Li, S.; Jia, C.; Mathieson, J. S.; Cronin, L.; Yang, X.-J.; Wu, B. *Inorg. Chem.* **2012**, *51*, 179–187.
12. For examples of anions bound in cages by interactions that include CH...anion hydrogen bonds, see: (a) Yoon, J.; Kim, S. K.; Singh, N. J.; Kim, K. S. *Chem. Soc. Rev.* **2006**, *35*, 355–360. (b) Amendola, V.; Boiocchi, M.; Colasson, B.; Fabbri, L.; Rodriguez Douton, M.-J.; Ugozzoli, F. *Angew. Chem., Int. Ed.* **2006**, *45*, 6920–6924. (c) Riddell, I. A.; Smulders, M. M. J.; Clegg, J. K.; Hristova, Y. R.; Breiner, B.; Thoburn, J. D.; Nitschke, J. R. *Nat. Chem.* **2012**, *4*, 751–756. (d) Riddell, I. A.; Ronson, T. K.; Clegg, J. K.; Wood, C. S.; Bilbeisi, R. A.; Nitschke, J. R. *J. Am. Chem. Soc.* **2014**, *136*, 9491–9498.
13. For other examples of anion receptors that include CH...anion hydrogen bonds, see: (a) Lee, C. H.; Na, H. K.; Yoon, D. W.; Won, D. H.; Cho, W. S.; Lynch, V. M.; Shevchuk, S. V.; Sessler, J. L. *J. Am. Chem. Soc.* **2003**, *125*, 7301–7306. (b) Chen, Q. Y.; Chen, C. F. *Tetrahedron Lett.* **2004**, *45*, 6493–6496. (c) Chmielewski, M. J.; Charon, M.; Jurczak, J. *Org. Lett.* **2004**, *6*, 3501–3504. (d) Kang, S. O.; VanderVelde, D.; Powell, D.; Bowman-James, K. *J. Am. Chem. Soc.* **2004**, *126*, 12272–12273. (e) Ilioudis, C. A.; Tocher, D. A.; Steed, J. W. *J. Am. Chem. Soc.* **2004**, *126*, 12395–12402. (f) Kwon, J. Y.; Jang, Y. J.; Kim, S. K.; Lee, K. H.; Kim, J. S.; Yoon, J. Y. *J. Org. Chem.* **2004**, *69*, 5155–5157. (g) Maeda, H.; Kusunose, Y. *Chem.–Eur. J.* **2005**, *11*, 5661–5666. (h) Vega, I. E.; Gale, P. A.; Light, M. E.; Loeb, S. J. *Chem. Commun.* **2005**, 4913–4915. (i) Fujimoto, C.; Kusunose, Y.; Maeda, H. *J. Org. Chem.* **2006**, *71*, 2389–2394. (j) Nishiyabu, R.; Palacios, M. A.; Dehaen, W.; Anzenbacher, P. *J. Am. Chem. Soc.* **2006**, *128*, 11496–11504. (k) Zielinski, T.; Kedziorek, M.; Jurczak, J. *Chem.–Eur. J.* **2008**, *14*, 838–846. (l) Li, Y.; Flood, A. H. *Angew. Chem., Int. Ed.* **2008**, *47*, 2649–2652. (m) Yoon, D.-W.; Gross, D. E.; Lynch, V. M.; Sessler, J. L.; Hay, B. P.; Lee, C.-H. *Angew. Chem., Int. Ed.* **2008**, *47*, 5038–5042. (n) Li, Y.; Flood, A. H. *J. Am. Chem. Soc.* **2008**, *130*, 12111–12122. (o) Hua, Y.; Flood, A. H. *Chem. Soc. Rev.* **2010**, *39*, 1262–1271. (p) Lee, S.; Chen, C.-H.; Flood, A. H. *Nat. Chem.* **2013**, *5*, 704–710. (q) Shi, G.; Gadhe, C. G.; Park, S.-W.; Kim, K. S.; Kang, J.; Seema, H.; Singh, N. J.; Cho, S. J. *Org. Lett.* **2014**, *16*, 334–337. (r) Hirsch, B. E. Lee, S.; Qiao, B.;

Chen, C.-H.; McDonald, K. P.; Tait, S. L.; Flood, A. H., *Chem. Commun.* **2014**, *69*, 9827–9830. (s) Zapata, F.; Gonzalez, L.; Caballero, A.; Alkorta, I.; Elguero, J.; Molina, P. *Chem.–Eur. J.* **2015**, *21*, published online 1 June 2015. DOI: 10.1002/chem.201500231.

14. Use of high purity NH_4BF_4 (e.g. 99.999 % trace metal basis, Sigma-Aldrich, product number 541893 Aldrich) and NH_4PF_6 (e.g. 99.99 % trace metal basis, Sigma-Aldrich, product number 216593 Aldrich) is necessary to obtain a chloride-free product. Attempts with salts of lower guaranteed purity failed to remove the last traces of chloride ion from samples of the knot.
15. Salt metathesis of $[\mathbf{2}\cdot\text{Cl}](\text{PF}_6)_9$ with NH_4PF_6 does not exchange all of the Cl^- ions, even after exhaustive washings. It is necessary to first exchange all of the counterions of $[\mathbf{2}\cdot\text{Cl}](\text{PF}_6)_9$ for BF_4^- (with NH_4BF_4), forming $[\mathbf{2}](\text{BF}_4)_{10}$, and then exchange the BF_4^- counterions for PF_6^- (with NH_4PF_6). This may be because the centrally bound Cl^- is less strongly held in an intermediate $[\mathbf{2}\cdot\text{Cl}](\text{BF}_4)_9$ complex.
16. Tetrabutylammonium salts were employed to promote loose ion-pairing (de Namor, A. F. D.; Shehab, M. *J. Phys. Chem. B* **2003**, *107*, 6462–6468).
17. The central cavities of the ‘empty’ all- PF_6^- complexes of **1–3** are solvent and anion accessible (well-ordered PF_6^- anions are bound in the cavities of **[1]** and **[3]** in the X-ray crystal structures^{4,7}).
18. H^6 is in the shielding region of a pyridine ring (see Figure 2) and so is sensitive to minor structural changes in the circular helicates that occur upon binding.
19. The slow kinetics of exchange of all of the halides (Figure 3), even relatively weakly bound I^- , in complexes of the pentafoil knot, $[\mathbf{2}\cdot\text{X}](\text{PF}_6)_9$, suggests that the kinetic barrier to exchange may be due to slow release of a PF_6^- anion from $[\mathbf{2}](\text{PF}_6)_{10}$ (a putative intermediate in the exchange process). The corresponding Solomon link and Star of David catenane complexes are all in fast exchange.
20. In some solvents the halide- PF_6^- anion exchange experiments significantly changed the solubility of the knot/link complexes. Acetonitrile proved to be a solvent where the binding constants could be compared across the range of different sized knot and links with each halide ion.
21. The addition of Bu_4NCl or Bu_4NBr to $[\mathbf{3}](\text{PF}_6)_{12}$ also produced ions corresponding to more than one halide-for- PF_6^- substitution.

22. The bipyridyl CH protons on the outside of the circular helicates (H^4 and H^5) are also electron-poor as a result of metal coordination to the bipyridyl groups, and can also interact with anions. From the 1H NMR spectra and by competition with calix[4]bipyrrole these association constants are of the order $\sim 10^3 M^{-1}$ (I^-), $\sim 10^3 M^{-1}$ (Br^-) and $\sim 10^4 M^{-1}$ (Cl^-), typically several orders of magnitude less than halide binding associated with the central cavity of the knot or links.
23. (a) Sessler, J. L.; An, D.; Cho, W. S.; Lynch *Angew. Chem., Int. Ed.*, **2003**, *42*, 2278–2281. (b) Sessler, J. L.; An, D.; Cho, W. S.; Lynch, V.; Marquez M. *Chem. Commun.* **2005**, 540–542.
24. The value of 450 equivalents is a revision of the 90 equivalents of $AgPF_6$ stated to completely remove Cl^- from $[2 \bullet Cl](PF_6)_9$ in MeCN in ref (5). The amount of $AgPF_6$ required to remove Cl^- from the pentafoil knot is reduced when using older bottles of the reagent. We speculate that this may be due to the presence of traces of fluoride arising from the decomposition of PF_6^- .
25. The amount of $AgPF_6$ required to remove the chloride from $[2 \bullet Cl](PF_6)_9$ depends on the solubility product (K_{sp}) of $AgCl$ in the solvent used. Only 1.2 equivalents of $AgPF_6$ are required in d_6 -acetone ($AgCl$: $\log K_{sp} = -16.4$) compared to 450 equivalents of $AgPF_6$ in CD_3CN ($AgCl$: $\log K_{sp} = -12.4$). $AgCl$ solubility product values: Luehrs, D. C.; Iwamoto, R. T.; Kleinberg, J. *Inorg. Chem.* **1966**, *5*, 201–204.
26. Schmidtchen, F. P.; Berger, M. *Chem. Rev.* **1997**, *97*, 1609–1646.
27. Meluzzi, D.; Smith, D. E.; Arya, G. *Ann. Rev. Biophys.* **2010**, *39*, 349–366.
28. Farrell, J. D.; Lines, C.; Shepherd, J. J.; Chakrabarti, D.; Miller, M. A.; Wales, D. J. *Soft Matter* **2013**, *9*, 5407–5416.
29. Jampani, V. S. R.; Skarabot, M.; Ravnik, M.; Copar, S.; Zumer, S.; Musevic, I. *Phys. Rev. E* **2011**, *84*, 031703.
30. Goldstein, R. E.; Moffatt, H. K.; Pesci, A. I.; Ricca, R. L. *Proc. Natl. Acad. Sci. USA* **2010**, *107*, 21979–21984.
31. OriginPro 8.5.1 from OriginLab[®].
32. Hristova, Y. R.; Smulders, M. M. J.; Clegg, J. K.; Breinera, B.; Nitschke, J. R. *Chem. Sci.*, **2011**, *2*, 638–641.

33. Connors, K. A. Binding constants: the measurement of molecular complex stability; Wiley: New York, 1987.
34. Luehrs, D. C.; Iwamoto, R. T.; Kleinberg, J.; *Inorg. Chem.*, **1966**, *5*, 201-204.

Outlook

The molecular pentafoil knot presented in this thesis represents a significant advance in the field of molecular topology. In fact, in the thirty years prior to this work, only two other kind of knots– the unknot (a macrocycle) and trefoil knot–out of the six billion knots known to mathematics have been synthesized using small molecules.

Beside the complexity of the knot obtained, it is the strategy used to obtain it that represents a major leap forward in the field of molecular topology. The use of cyclic metal helicates and interwoven grids as templates and scaffolds for the synthesis of topologically complex targets brings many new higher order knots and links at the fingertips of small-molecule chemists.

In addition, the extensive study of the self-assembly processes yielding the pentafoil knots and its non-interlocked derivatives unravelled many weaknesses in our current understanding of these systems by showing among other things that templates can have a more complicated role than just holding building blocks in a desired spatial arrangement, that self-assemble systems are not exclusively under thermodynamic or kinetic control but more likely a mixed of both.

Finally, the last chapter of this thesis is a small step towards the next big target of topological chemistry: unravelling and exploiting the unique properties of entwined structures. With complicated topologically non trivial objects being more readily available and easier to make it should soon be possible to use them as catalysts or study their impact when included in polymeric strands.

